STUDY ON CORROSION BEHAVIOR AND CORROSION INHIBITION OF MAGNESIUM ALLOY ZE41
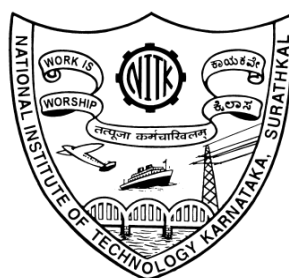
Thesis

Submitted in partial fulfillment of the requirements for the degree of

DOCTOR OF PHILOSOPHY

By

NANDINI K

DEPARTMENT OF CHEMISTRY

NATIONAL INSTITUTE OF TECHNOLOGY KARNATAKA,

SURATHKAL, MANGALORE – 575025.

APRIL, 2014

DECLARATION

I hereby *declare* that the Research Thesis entitled "STUDY ON CORROSION BEHAVIOR AND CORROSION INHIBITION OF MAGNESIUM ALLOY ZE41" which is being submitted to the **National Institute of Technology Karnataka, Surathkal**, in partial fulfillment of the requirements for the award of the Degree of **Doctor of Philosophy in Chemistry** is a *bonafide report of the research work carried out by me*. The material contained in this Research Thesis has not been submitted to any University or Institution for the award of any degree.

Nandini K

Register Number: 110639CY11F02

Department of Chemistry

Place: NITK – Surathkal

Date: 16th April 2014

CERTIFICATE

This is to *certify* that the Research Thesis entitled "STUDY ON CORROSION BEHAVIOR AND CORROSION INHIBITION OF MAGNESIUM ALLOY ZE41" submitted by **NANDINI K** (Register Number: 110639CY11F02) as the record of the research work carried out by her, is *accepted as the Research Thesis submission* in partial fulfillment of the requirements for the award of the Degree of **Doctor of Philosophy.**

(**Dr. A. Nityananda Shetty**)

Research Guide

Chairman – DRPC

ACKNOWLEDGEMENTS

ABSTRACT

The alloys of magnesium are in the spot-light lately. With applications that run the gamut from automobile parts to medical implants, this class of alloys truly deserve all the adulation coming their way. ZE41 is one such cast alloy, which is lighter than aluminium, can be cast or machined into variety of desired shapes and has good damping and shock absorption abilities. A very low resistance to corrosion puts the otherwise remarkable efficacy of ZE41 in jeopardy. Hence understanding the corrosion of ZE41 and developing the measures to combat the same are indispensable.

In the present thesis the corrosion of ZE41 and its mitigation were analyzed using techniques like potentiodynamic polarization and AC impedance, along with SEM and EDX analyses. Sodium sulfate and its mixture with sodium chloride were chosen as two corrosive media. The blank corrosion studies were performed at various medium concentrations, pH and temperatures. The results revealed a trend of higher corrosion rate associated with higher medium concentration, lower pH and higher temperature.

Five different long chain alkyl monocarboxylates namely stearate, palmitate, myristate, laurate and caprylate were synthesized and tested as corrosion inhibitors for ZE41. The calculated activation and thermodynamic parameters have been documented in the thesis. The carboxylates were predominantly physisorbed and adsorption was in accordance with Langmuir adsorption isotherm. The studied carboxylates were found to function as mixed-type inhibitors which predominantly suppressed anodic reaction. The carboxylates were more efficient at lower temperatures and in combined medium. At an optimum concentration the efficiencies of the carboxylates decreased in the order: stearate > palmitate > myristate > laurate > caprylate and this has been accredited to the reduction in aliphatic chain length. The proposed mechanism attributed the cathodic inhibition to the blockage of the reaction spots by chemisorbed carboxylates. The anodic inhibition resulted from the compaction of porous film by precipitated magnesium carboxylate salts.

Keywords: ZE41 alloy, Corrosion, Inhibitor, Alkyl carboxylates, Impedance.

CONTENTS

CHAPTER – 4: SUMMARY AND CONCLUSIONS

LIST OF FIGURES

LIST OF TABLES

NOMENCLATURE

ABBREVIATIONS

AC	Alternating current
A/C	Ratio of anodic area to cathodic area
ASTM	American Society for Testing and Materials
ATC	Aggregate transition concentration
CMC	Critical micelle concentration
CPE	Constant phase element
DC	Direct current
ECAP	Equal channel angular pressing
EDTA	Ethylenediamine tetraacetic acid
EDX	Electron dispersive x-ray analysis
EEC	Equivalent electrical circuit
EIS	Electrochemical impedance spectroscopy
EW	Equivalent weight of the corroding material
GDP	Gross domestic product
hf	High frequency
IUPAC	International Union of Pure and Applied Chemistry
lf	Low frequency
mf	Medium frequency
NACE	National Association of Corrosion Engineers
NDE	Negative difference effect
NLS	Sodium salts of N-lauroylsarcosine

NLT	N-lauroyl-N-methyltaurine
OCP	Open circuit potential
SBF	Simulated body fluid
SCC	Stress corrosion cracking
SCE	Saturated calomel electrode
SDBS	Sodium dodecylbenzenesulphonate
SDS	Sodium dodecylsulfate
SEM	Scanning electron microscopy
SKPFM	Scanning Kelvin probe force microscopy
SLS	Sodium lauryl sulfate
VPI	Vapor phase inhibitors

SYMBOLS

E_a	Activation energy
ω	Angular frequency
$\Delta H^{\#}$	Apparent enthalpy of activation
$\Delta S^{\#}$	Apparent entropy of activation
W_i	Atomic weight of alloying element
N	Avogadro's number
C_{dl}	Capacitance of electrical double layer
C_f	Capacitance of surface film
b_c	Cathodic Tafel slope

R_{ct}	Charge transfer resistance
C_{inh}	Concentration of inhibitor
Q_{diff}	Constant phase element associated with electrolyte diffusion
Y_0	Constant phase element constant
Q_{dl}	Constant phase element of double layer
Q_f	Constant phase element of surface film
i_{corr}	Corrosion current density
$i_{corr\,(b)}$	Corrosion current density in the absence of the inhibitor
$i_{corr\,(inh)}$	Corrosion current density in the presence of the inhibitor
E_{corr}	Corrosion potential
υ_{corr}	Corrosion rate
ρ	Density of the corroding material
W	Electrical work done
r_{oxd}	Equilibrium oxidation rate
r_{red}	Equilibrium reduction rate
i_o	Exchange current density
F	Faraday's constant
R_f	Film resistance
ω_{max}	Frequency at which the imaginary part of the impedance has a maximum
η_{max}	Highest inhibition efficiency at optimum concentration
Z''	Imaginary impedance
Z	Impedance
Z_{mod}	Impedance modulus

η	Inhibition efficiency
f	Inhibitor interaction parameter
R^2	Linear regression coefficient
ε	Local dielectric constant
C_{max}	Most economic concentration of carboxylates
n	Number of electrons in a reaction
χ	Number of water molecules replaced per molecule of adsorbed inhibitor
R_{hf}	Overall resistance associated with higher frequency capacitive loop
$R_{hf (b)}$	Overall resistance associated with higher frequency capacitive loop in the absence of the inhibitor
$R_{hf (inh)}$	Overall resistance associated with higher frequency capacitive loop in the presence of the inhibitor
$θ_{max}$	Phase maximum
ϕ	Phase shift
h	Planck's constant
R_p	Polarization resistance
E_{pzc}	Potential of zero charge
Z'	Real impedance
R_{dif}	Resistance associated with electrolyte diffusion
R_f	Resistance of surface film
E_o	Rest potential
E_t	Sinusoidal alternating potential
R_s	Solution resistance
$ΔH°_{ads}$	Standard enthalpy of adsorption

ΔS°_{ads}	Standard entropy of adsorption
ΔG°_{ads}	Standard free energy of adsorption
E^{o}	Standard reduction potential
E_{surf}	Surface charge on the metal
θ	Surface coverage
T	Temperature
d	Thickness of the electrical double layer or surface film
I_{t}	Time dependent current response
R	Universal gas constant
n_{i}	Valence of alloying element
f_{i}	Weight fraction of alloying element

1.1 HISTORICAL BACKGROUND OF CORROSION

The corrosion of metallic materials is prehistoric. The familiarity of the mankind towards such an undesirable phenomenon can be evidenced in several ancient and religious literatures. The Latin term *corrodere* which means 'gnawing to pieces' is the etymon of 'corrosion' in English. A glance at the early world history unveils the fact that the corrosion protection practices were quite popular at the ancient epoch. Some outstanding archetypes include, Indian archeological remains, mainly, the fifth century iron pillar in Delhi and the eleventh century Dhar pillar in Madhya Pradesh which have stood the test of time and remained rust-resistant. Furthermore the Greeks used lead coated copper nails to build lead-plastered decks in ships. The craftsmen of that era were probably aware of the differential metal corrosion. The Romans safeguarded the iron articles by coating them with bitumen and tar (Sastri et al. 2007).

In spite of recognition during antediluvian times, the corrosion was scientifically established only in nineteenth century. Some important historical milestones in corrosion science literature are enlisted below (Hackerman 1993):

- Pliny (AD 23–79) mentioned in his article 'Ferrum Corrumpitar', the corrosion damage of iron.
- Herodotus (fifth century BC) recommended the coat of tin for guarding iron.
- A publication by Robert Boyle (1675) named 'Of the mechanical origin of corrosiveness' discussed the causes of corrosion.
- Jacques Thenard (1819) described corrosion as an electrochemical event.
- Hall (1829) reported that the presence of oxygen is crucial for rusting of iron.
- Humphry Davy (1824) put forward the principles of cathodic and sacrificial anodic protection of iron.
- Michael Faraday (1834-1840) proposed a computable relation between chemical reaction and electric current. Faraday's laws today form the basis for assessment of metal corrosion rate.

- Evans, Uhlig and Fontana are considered as pioneers in contemporary understanding of corrosion.

1.2 CORROSION - DEFINITION AND AFTERMATH

Understanding corrosion begins with defining it. Uhlig (Uhlig and Revie 1991) defined corrosion as the destructive attack on a metal by chemical or electrochemical reaction with its environment. This definition is factually restricted to metals and alloys. However, in general, it holds good for other non-metallic materials of interest, like plastic, ceramic and rubber, all of which deteriorate in harsh surroundings.

The corrosion is inevitable. It is often regarded as an inherent attribute of metals. In spite of decades of research and innovation in the field, the metal corrosion continues unabated, as the process of corrosion is spontaneous and impelled by the diminution in system's free energy. The extractive metallurgy being endothermic, upon extraction from an ore, a metal is forced away from an energetically stable combined state. Such a susceptible metal returns to the combined form during corrosion, by reacting with various components of the prevailing environment. Hence combating corrosion is thermodynamically an uphill battle (Fontana 2005).

Even though the corrosion losses are regarded as matters which are primarily of economic concern, the repercussions of such damages torment the society. Some major corrosion consequences are summarized below (McCafferty 2010).

1.2.1 Capital losses

In an industrialized era which is profoundly dependent on metallic materials, the economy of any nation is vulnerable to capital losses caused by corrosion. The corrosion related economic losses are categorized into direct and indirect losses. Direct losses refer to the cost spent for overall maintenance and replacement of industrial and domestic metallic equipments. Indirect corrosion based losses transpire in the form of unexpected

plant shutdown which leads to drop in production profit, loss of valuable products due to leakage and costs spent for overdesign of the equipments to meet the future needs.

A leap-forward two year study published by the United States Federal Highway Administration in 2001 (Koch et al. 2001) appraised the annual direct cost of corrosion in the US to be $ 276 billion which is nearly 3.1 % of Gross Domestic Product (GDP). As of 2013 corrosion costs in the United States are expected to surpass a shocking $ 1 trillion (Jackson 2011). On implementation of suitable corrosion mitigation measures nearly 25-30 % of the cost could be economized.

1.2.2 Health and safety concerns

There are numerous ill-fated mishaps in the history which were caused by corrosion failure of aged infrastructures, like collapse of bridges and buildings, industrial boiler explosions and cracking of water reservoirs. Furthermore the corrosion of metallic bio-implants is intimidating from a healthcare point of view. From orthodontic braces to pacemakers for heart, the metal implant industry is vast and growing. Keeping in mind the corrosive nature of human body fluids, the corrosion failure of the implants and inflammations generated by corrosion products does raise genuine concerns.

1.2.3 Conservation issues

Metals are precious resources. Their production requires a combination of ample energy and human effort, all of which are blown apart by corrosion. Most of the times recycling of the metals from corrosion products is not economically viable. Hence the corroded junk is building up, where as the raw material ores are depleting day-by-day. In this sense controlling corrosion indirectly contributes to conservation of natural mineral resource. The corrosion is a menace to heritage as well. The ancient artifacts are valuable treasures which reflect the cultural history of any nation. The corrosion loss of such metal relics is irreplaceable. Hence the corrosion control of such archeological metal objects is vital and serves as a way to conserve the historical legacy.

1.2.4 Environmental concerns

The corrosion disasters pollute the environment beyond repair. The leakage of hazardous chemicals from corroded containers and pipelines is devastating. The marine oil spills, leakage of toxic gases, explosives and radioactive substances are some examples. Proper monitoring and much efficient corrosion combating measures are crucial from an ecological safety point of view.

1.2.5 Technological effects

The corrosion hinders in ways more than one, the development in technology. Most of the technological creations could have been much economical and accessible if corrosion was out of the picture. Many engineering innovations require the materials to withstand simultaneously, higher temperatures, elevated pressures and strong corrosives. In all such cases due to material corrosion the technologies fail to be lucrative.

1.3 ELECTROCHEMICAL THEORY OF CORROSION

With an exception of direct chemical oxidation, corrosion otherwise is invariably associated with electrochemical reactions. The electrochemical nature of corrosion is well established. As per electrochemical theory, the corrosion occurs either due to the formation of differential sites (anodic and cathodic) on the metal surface or on contact of dissimilar metals in a conducting electrolyte. The anodic sites generate electrons by metal oxidation and cathodic sites acts as 'electron sinks' which consume electrons to reduce the oxidizing species. Comparatively anodic reactions are simple and involve metal dissolution through oxidation. Oxidation proceeds in several stages for metals which exhibit multiple oxidation states. The electrons produced during oxidation make up corrosion current. The anodic and cathodic half-cell reactions of corrosion are coupled in such a way that the reactions proceed simultaneously at identical rates. Hence during corrosion electro-neutrality is maintained throughout and it is impossible for a corroding metal to build up electric charge on its own. The anodically generated metal ions and some anions produced at the cathode diffuse through the conducting electrolyte and

combine to form a corrosion product at someplace between the anode and cathode (Fontana 2005). An electrochemical cell established at a corroding metal surface is depicted in Fig. 1.1.
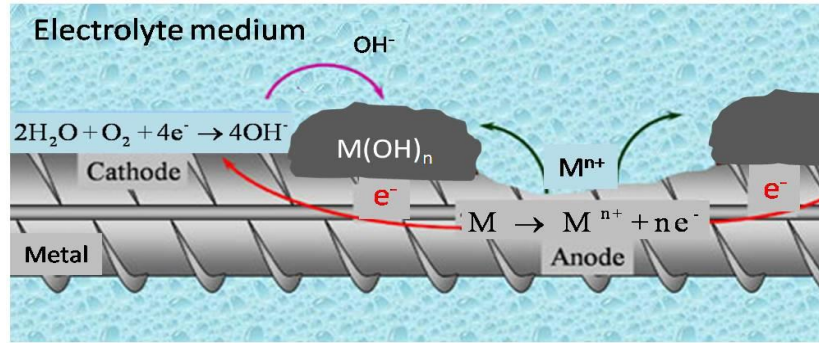
Fig. 1.1 An illustrative electrochemical cell formed at a corroding metal surface.

The half-cell reactions of corrosion are shown below.

Anodic oxidation reaction: Metal undergoes oxidation to produce metal ions and electrons. The number of electrons liberated corresponds to the valence of metal.

$$M \rightarrow M^{n+} + ne^- \tag{1.1}$$

Cathodic reduction reactions: The reduction reactions are relatively complicated and can be grouped into following four categories.

- **Hydrogen evolution:** These reactions are dependent upon pH of the medium and occur in the absence of oxygen. In acidic media protons are reduced and in neutral or alkaline media reduction of water takes place.

$$2H^+ + 2e^- \rightarrow H_2 \tag{1.2}$$

$$2H_2O + 2e^- \rightarrow 2OH^- + H_2 \tag{1.3}$$

- **Oxygen reduction:** At acidic pH oxygen is reduced to water, whereas at alkaline or neutral pH hydroxyl ion formation is favored.

$$4H^+ + O_2 + 4e^- \rightarrow 2H_2O \tag{1.4}$$

$$2H_2O + O_2 + 4e^- \rightarrow 4OH^- \tag{1.5}$$

- **Metal ion reduction:** Some impurity metal ions undergo reduction.

$$M^{3+} + e^- \rightarrow M^{2+} \tag{1.6}$$

- **Metal deposition:** Secondary metal ions get reduced and deposited at cathodic regions.

$$M^{3+} + 3e^- \rightarrow M \tag{1.7}$$

1.4 CLASSIFICATION OF CORROSION

There are several factors which constitute the basis for classification of corrosion. Some important factors are described below (Fontana 2005).

Table 1.1 General classification of corrosion.

Influencing Factor	Type of corrosion	Features
1. Nature of corrosive media	1. Wet corrosion	The media electrochemically attacks the metal in the presence of moisture
	2. Dry corrosion	Usually occurs at high temperatures, corrosive often in the form of gas chemically attacks the metal in the absence of moisture
2. Corrosion mechanism	1.Electrochemical corrosion	Electrolyte medium attacks the metal
	2. Chemical corrosion	Metal subjected to direct chemical oxidation
3.Appearance of corroded specimen	1. Uniform corrosion	Metal specimen corrodes at an uniform rate all over the surface
	2. Localized corrosion	Corrosion is restricted to certain areas on metal surface like crevices and pits.

For the purpose of convenience corrosion is categorized based on the form in which it manifests itself. Accordingly various forms are illustrated in following sub-sections. This classification is often accomplished through close visual examination of the corroded specimen.

1.4.1 Uniform corrosion

Uniform corrosion is regarded as the simplest form of corrosion and it is prevalent both industrially and domestically. The entire uncovered area of the metal is attacked and the metal dissolution occurs at a uniform rate throughout the exposed surface. The metal equipment ultimately fails due to substantial loss of metal. From an engineering point of view, even with significant metal loss, uniform corrosion is a trivial matter in the sense that the life of the equipment can be predicted with accuracy, which eliminates the possibilities of abrupt failures. Moreover, protecting a uniformly corroding surface is easier.

1.4.2 Galvanic corrosion

It is also termed as differential metal corrosion. Galvanic corrosion arises on contact of two different metallic materials in a common electrolyte. The potential difference existing between the galvanic couple propel the corrosion of the less noble (with lower standard electrode potential) material. The galvanic corrosion was observed in the Statue of Liberty in 1980s where the wrought iron body had corroded on contact with outer copper skin due to failure of resin insulation present in-between.

1.4.3 Crevice corrosion

It is a localized and insidious type of corrosion occurring within confined spaces where corrosive ingress is restricted. Such spots which are cut-off from electrolyte ingress are termed as crevices and are often formed at the region of metal-to-metal or metal-to-nonmetal contact. The gap defining a crevice should be large enough to ensnare a liquid yet too small for circulation to occur. Due to lack of circulation the electrolyte within the crevice will be famished of oxygen, hence the crevices become anodic. While

peripheral metal surface in contact with electrolyte having bountiful of oxygen, act as cathode. With a concentration cell established, metal dissolution occur uninterrupted within crevices, however external surface masks the rampant ongoing corrosion within the crevices by remaining damage free.

1.4.4 Pitting corrosion

At the regions of lattice imperfections, the metal dissolution will be fleetingly higher which in a course of time generates pits and facilitate localized corrosion. The pits once formed auto-accelerate to grow deeper and at times transpire as massive dents, which can cause structural failure. Due to practical difficulties, rate of pitting or the lifetime of concerned equipment remain inestimable. Hence even with negligible amount of metal loss pitting raise concerns as pitting related failures are unforeseen.

1.4.5 Intergranular corrosion

The grain boundaries are the lattice regions of crystallographic mismatch and are chemically more active than the grain area. During intergranular corrosion, corrosive attacks the metal along the grain boundaries which dissolve as anode and body of the grain remain protected as cathode. The intergranular attack accelerates with time because of significant disparity in surface area, where a minute anode is surrounded by large cathode.

1.4.6 Selective leaching

The exclusion of more susceptible metal from an alloy by corrosion is termed as selective leaching. Such preferential leaching turns a well-built alloy into feeble and porous deposit of its nobler metal. As a result, the applications that the alloy was built to fulfill remain underachieved. Dezincification is a classic example of selective leaching where zinc corrodes and seep out of brass and originally yellow alloy attains copper color. Graphitic corrosion is another case in point where iron in gray cast iron selectively corrodes.

1.4.7 Erosion corrosion

A deteriorative impact of a mechanical force is called erosion. When erosion accelerates metal corrosion, the combined attack is referred to as erosion corrosion. An aqueous or gaseous corrodent in motion which is swirling over the metal surface leads to erosion corrosion. The attack creates grooves, depressions, gullies or waves on metal surface, all of which often exhibit directionality. The cavitations seen in steam turbine blades are after-effects of erosion corrosion.

1.4.8 Stress corrosion cracking (SCC)

A metallic material under static tensile stress is more vulnerable to corrosion in contrast to its stress-free counterpart. This is because the atoms of metal under stress are relatively at higher energy states compared to those in stress free zones. SCC materializes upon conjoint action of specific corrosive and stress. SCC produces deep cracking in alloys. The cracks propagate along the stressed regions in a direction perpendicular to applied stress and the stress-free parts remain unaffected. The cracking can be intergranular or transgranular depending upon material structure. SCC of equipments operating at high temperature and pressure circumstances lead to devastating explosions.

1.4.9 Hydrogen damage

Metals deteriorate mechanically and physically on interaction with hydrogen. Though such hydrogen damages do not precisely qualify as corrosion, the consequences are equally disastrous. Metals readily absorb atomic hydrogen. Several circumstances prompt hydrogen introduction into metal lattice like electroplating, acid pickling, welding, heat treatments and corrosion. The hydrogen atoms after diffusion into metal lattice combine to produce molecular hydrogen at crystal voids. Unable to diffuse out, the molecular hydrogen builds up immense pressure within the body of the metal. Such internal pressures often in association with residual or applied stress result in mechanical deformation, internal flaking, cracking and blistering. Owing to hydrogen damage metal

becomes mechanically weak often accompanied with the loss of ductility and tensile strength.

1.4.10 Microbial corrosion

Some micro-organisms especially chemoautotrophs promote corrosion when present in the vicinity of the metal. For instance the sulfate-reducing bacteria produce hydrogen sulfide and the species of *Acidithiobaccillus* genus secrete sulfuric acid; both metabolites are potential corrosives. Moreover varieties of aerobic and anaerobic bacteria grow as discrete colonial patterns on metal surface; such a growth invariably facilitates galvanic corrosion (Sastri et al. 2007).

1.5 FACTORS INFLUENCING CORROSION RATE

Quite a lot of factors influence the rate of metal corrosion. For convenience these factors can be grouped under broad categories; metallic and environmental factors. (Gadag and Shetty 2010).

1.5.1 Metallic factors

In any corrosive medium the nature of metal or alloy plays a key role in deciding the rate and the mechanism of corrosion. Most of these factors are inherent. Some aspects of metal nature that have a noteworthy effect on metal corrosion rate are discussed as follows.

1.5.1.1 Purity of the metal

A very pure metal is more corrosion resistant than its commercial counterpart. Unfortunately highly pure metals are pricey and delicate with limited applications. Metals or alloys are manufactured uniquely to meet the commercial demands and when tailored to fulfill such applications the corrosion resistance of the pure metal is bound to be compromised. Many undesirable factors like impurities, precipitated phases, localized stress, and scratches develop in metal when subjected to mechanical design and all these factors initiate and accelerate corrosion.

1.5.1.2 Electrode potential of metal

The standard electrode potential of metals is the benchmark to compare their tendency to undergo corrosion. In general resistance to corrosion improves with increase in standard electrode potential. Thus metals like magnesium and zinc with low standard electrode potential are more susceptible to corrosion than noble metals like platinum and gold. However, aluminium comes across as an exception to this trend and this unusually high corrosion resistance of aluminium arises as a result of surface passivation.

1.5.1.3 Hydrogen overvoltage on metal surface

In simplified sense hydrogen overvoltage is the ease with which hydrogen is evolved over a metal surface. At instances where cathodic reaction is predominantly hydrogen evolution, the metal with lower hydrogen overvoltage is more susceptible to corrosion and vice versa. Enhancing the hydrogen overvoltage by surface modification is a means to control corrosion.

1.5.1.4 Nature of corrosion product

Once initiated the rate of further corrosion is principally dependent upon the nature of corrosion product. In case the corrosion product precipitates as stable surface film which is uniform, continuous and impervious, it protects the fresh metal surface from corrosive attack and hence corrosion is retarded. Instead when the developed corrosion product is unstable, soluble, non uniform and porous, then corrosion continues incessantly.

1.5.1.5 Relative areas of anodic and cathodic region

A smaller anode in electrical contact with a relatively larger cathode corrodes intensely as a large cathode offers faster means of consumption of anodically generated electrons. For practical purposes ratio of anodic area to cathodic area [A/C] is determined. Smaller the A/C ratio more severe is the metal corrosion.

1.5.2 Environmental factors

The nature of corrosive medium is equally significant as metallic factors. For a metal, the corrosion rates can be poles apart in two divergent media. Some prominent environmental factors are described below.

1.5.2.1 Temperature

Generally the rate of a given chemical reaction increases with rise in temperature and corrosion is no different as it fundamentally is a redox reaction. Hence the rate of corrosion increases with rise in temperature. At higher temperatures increased ionic mobility acts as a contributing factor. Even passivating metals are not spared at higher temperature as the rise in temperature shrinks the passive range, possibly due to increased dissolution of the passivating surface layer.

1.5.2.2 pH of medium

The type of cathodic reaction is chiefly reliant on medium pH. In general lower the pH of the medium higher is the rate of corrosion. Exception exists with some amphoteric metals like aluminium, lead and zinc which dissolve at pronounced rates in highly alkaline medium.

1.5.2.3 Humidity

Usually corrosion rate increases with increase in humidity of the environment. The moisture in air settles over metal surface, it acts as conducting electrolyte and directs the formation of concentration cells. Some examples are observed in everyday life, like metal equipments deployed in damp areas corrode severely in comparison with that in arid surroundings.

1.5.2.4 Presence of impurities

Presence of some impurities or atmospheric pollutants like sulfur dioxide contributes to enhanced metal corrosion. Sulfur dioxide combines with moisture in

environment forming sulfuric acid. Enhanced acidity often results in increased corrosion rate in most of the metals.

1.5.2.5 Electrical conductivity of medium

Corrosion rate increases with increase in conductivity of the medium. Higher conductivity boosts the ion migration between the cathodic and anodic regions and which consequently creates an electron surge. As overall result, the rate of corrosion is increased. It is due to the higher electrical conductivity that sea water is more corrosive than fresh water.

1.5.2.6 Presence of oxygen and oxidizers

The presence of oxidizers invariably enhances the rate of metal corrosion. Even noble metals are known to corrode in the presence oxidizing agents. Oxygen and oxidizers have a high tendency to undergo reduction at the cathode. Their presence, hence, provides more means of clearance of anodically generated electrons. Although for metals which exhibit active-passive transition, the moderate addition of oxidizers facilitates metal passivation.

1.5.2.7 Velocity of medium

Activation controlled processes are independent of corrosive velocity. The corrosion rate increases on agitation when cathodic reaction is under diffusion control. For passivated or coated metals an extremely high corrosive velocity mechanically damage protective films and such broken films often accelerates the corrosion.

1.5.2.8 Concentration of medium

The medium concentration corresponds to the amount of corrosive ions and hence rise in medium concentration magnifies corrosion. However, weak acids present an exception. At very high concentration due to reduced ionization, corrosion brought about by weak acids subsides.

1.5.2.9 Polarization of anode and cathode

The rate of corrosion suffers a significant reduction due to polarization of the electrodes. Polarization is reaction inertia. The electrochemical reactions polarize under the influence of one or more impeding chemical, physical or environmental factors. The rate of electron transfer always exceeds rate of ionic conduction. Hence the dissolved metal ions in vicinity of anode build-up with time and polarizes anode. The anodic polarization also results from passivation of anode. The cathodic reactions occurring in a sequence of steps at electrode/electrolyte interface are often under activation polarization. Concentration polarization too hinders cathodic reactions by retarding the diffusion of cathodic reactants and products.

1.6 THERMODYNAMICAL ASPECTS OF CORROSION

The study of corrosion from an energetics perspective offers deeper insight into overall process and mechanisms governing it. Thermodynamics is the science of energy changes and the concepts of thermodynamics are extensively used in understanding physical, chemical and electrical processes and corrosion is one amongst them. Following are some aspects of thermodynamics used in corrosion studies (Sastri et al. 2007).

1.6.1 Concept of free energy

The work capacity of any thermodynamic system corresponds to its free energy content. For electrical and electrochemical processes the work done ($-W$) by the system will be the product of charges moved and the potential difference (E) between the two half-cells of an electrochemical cell. The same is expressed in terms of free energy change (ΔG) per mole of reactants in the following expression.

$$\Delta G = -n\text{F}E \qquad\qquad (1.8)$$

where n is the number of electrons transferred in the cell reaction, F is Faraday's constant, and E is the cell potential or emf.

The spontaneous process leads the system to a thermodynamically stable energy state hence is invariably accompanied by decrease in free energy of the system. It follows from the equation 1.8 that for any electrochemical process to be spontaneous, the emf of the cell should be positive. The free energy change accompanying a process of corrosion can be expressed as follows.

$$\Delta G = -n\mathrm{F}[E_{(\mathrm{H}^+ / \mathrm{H}_2)} - E_{(\mathrm{M}^{n+} / \mathrm{M})}] \tag{1.9}$$

In the above expression, hydrogen evolution is assumed to be the cathodic reaction for the purpose of representation. It follows from the equation 1.9 that, metals with standard electrode potential ($E°$) more negative than that for cathodic process, will corrode spontaneously. The bottom line is that corrosion will not occur unless the reaction of anodic metal oxidation (metal dissolution) is spontaneous.

1.6.2 Application of thermodynamics to corrosion

A foremost application of thermodynamics to corrosion is construction of potential-pH plots or Pourbaix diagrams. Pourbaix diagrams are graphical representations which depicts the stability of a metal and its corrosion products as a function of the potential and pH of the aqueous solution. The potential is taken along the vertical axis and the horizontal axis shows the pH scale. The solubility data of metal compounds and Nernst equations for various reaction equilibria are considered while developing Pourbaix diagrams. In the diagram, the electron transfer equilibria which are pH independent are represented as horizontal lines. The vertical lines on the other hand stand for potential independent chemical equilibria. The electrochemical equilibria where both ions and electrons participate are shown as sloping lines. Pourbaix diagrams are of corrosion engineers' interest as they precisely portray the conditions which favor following metal behaviors.

- Immunity: The corrosion of an immune metal is thermodynamically impossible.
- Corrosion: Soluble corrosion products are formed and corrosion proceeds spontaneously.

- Passivity: Insoluble reaction products precipitate over metal surface to form a protective film which hinders further corrosion.

The Pourbaix diagram for pure magnesium-water system at 25 °C is shown in Fig. 1.2 (Pourbaix 1974). The diagram predicts the magnesium corrosion to spontaneously occur at conditions of potentials positive than -2.37 V ($E°$ of magnesium) and pH below 10.5. Magnesium remains immune to corrosion when its potential is held at values more negative than its $E°$. The corrosion product magnesium hydroxide ($Mg(OH)_2$) precipitation is shown to be favored in highly alkaline conditions with pH above 10.5. $Mg(OH)_2$ deposits to form surface film which is expected to passivate the underlying metal.
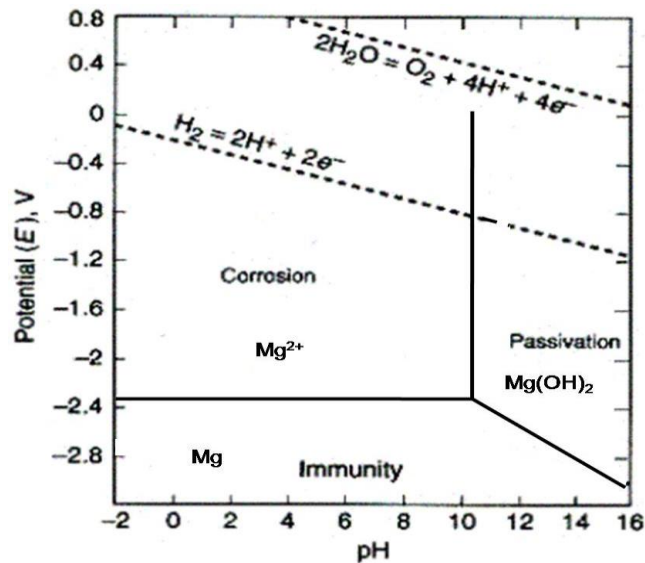
Fig. 1.2 Pourbaix diagram of magnesium and water system at 25 °C, showing the theoretical domains of corrosion, immunity and passivation (Pourbaix 1974).

Pourbaix diagrams can be used for:

- Predicting spontaneity of corrosion processes.
- Appraising the stability and composition of corrosion products.

- Speculating measures like alteration of environment which in all probability retards corrosion.

Some shortcomings of Pourbaix diagrams are given below.

- The information provided is based solely on thermodynamic data pertaining to various equilibria and kinetic aspects like rate of corrosion are not conveyed.
- Even though the occurrence of passivation is predicted accurately, the efficiency of such passive film remains obscure.
- All the information conveyed is pertaining to metal behavior in aqueous medium. The prevailing natural circumstances can be totally unalike.

1.7 CORROSION KINETICS

Thermodynamics observe corrosion from an equilibrium perspective. However, a perfect equilibrium is rarely observed in corroding systems. Apart from that major constraint thermodynamics fails to predict the rate of corrosion. Even a spontaneous corrosion could be a trivial matter if it progresses at a negligible rate. For all practical considerations, kinetics of corrosion are equally important. Hence the principles of electrode kinetics are applied to corrosion phenomenon to determine the rate of corrosion. Following are few such electrochemical kinetic concepts.

1.7.1 Polarization

Electrode polarization is defined as the extent of divergence of the electrode potential from an equilibrium value, resulting from a net current flowing from or to the electrode surface. Several chemical, physical or environmental factors tend to polarize the electrochemical reactions. Polarization is reaction inertia and it reduces the overall potential difference between the two half cells, hence, retards the electrochemical processes. The degree of polarization is called as overvoltage or overpotential given by the following equation:

$$\text{Overvoltage} = E - E_\circ \tag{1.10}$$

where E is the electrode potential for some condition of current flow and E_o is the electrode potential for zero current flow at equilibrium (also termed as the open-circuit potential (OCP), corrosion potential, rest potential) (McCafferty 2010).

1.7.1.1 Activation polarization

An electrochemical process is termed to be under activation polarization when its rate is controlled by the slowest step of reaction sequence taking place at the metal/electrolyte interface. Such a slowest step in order to commence often necessitates some activation energy to be supplied as an increment in potential.

The activation polarization of cathodic hydrogen evolution results when the rate of formation of H atoms is slower than the rate of supply of electrons to cathodic surface. The electron build-up at the metal side of cathode/solution interface deviate cathodic potential in negative direction. At anode, activation polarization becomes evident when the rate of metal oxidation is slow. The electrons leave the metal lattice faster than metal atoms. The potential of anode will be shifted in positive direction due to deficiency of electrons on metal side of the interface.

1.7.1.2 Concentration polarization

Concentration polarization refers to an electrochemical process controlled by the diffusion of electrode active species from or into the electrolyte bulk. At the cathode, concentration polarization comes into existence, when the diffusion of oxidizers from the bulk towards the cathode surface is slow. As a consequence, the electrons accumulate at the cathodic interface and hence the potential of the cathode become more negative. Concentration polarization at the anode arises due to the slow diffusion of metal ions from anode/solution interface into the electrolyte bulk. The potential of anode becomes more positive due to the metal ions accumulated at the interface. Any operation which tends to destroy the concentration gradient like agitation counteracts the concentration polarization and hence speeds up electrode reactions.

1.7.1.3 Ohmic polarization

The electrolyte solutions, no matter how conductive, always offer some degree of resistance to the flow of current. Ohmic polarization arises as a result of such potential drop (IR drop) due to the resistance of electrolyte solution. An electrochemical reaction dominated by ohmic polarization is referred as IR controlled. Apart from solution resistance, many other factors facilitate ohmic polarization like resistance of films, coatings and insulations present over the metal surface. Ohmic polarization is negligible for electrolytes with high conductivity like aqueous salt solutions, but become substantial for low-conductivity media like organic solutions, soli and concrete. In electrochemical measurements the IR drop resulting from solution resistance can be compensated by the use of reference electrodes with Luggin-Haber capillary. This allows the placement of reference electrode as close to the working electrode surface as practically possible.

1.7.2 Exchange current density

The exchange current is the steady state value of current for a particular half-cell reaction at zero overpotential. It can be understood as the background current to which the net current witnessed at other overpotentials is normalized. The exchange current density reflects the innate electron transfer rates between electrode and electroactive analyte. For any electrochemical equilibrium, the rates of half-cell reactions are related to exchange current density as follows.

$$r_{\mathrm{oxd}} = r_{\mathrm{red}} = \frac{i_\circ}{n\mathbf{F}} \tag{1.11}$$

where r_{oxd} and r_{red} are, respectively, rate of oxidation and reduction at equilibrium and $i_\mathbf{o}$ is exchange current density expressed in units A cm^{-2}.

The magnitude of exchange current density is strongly influenced by some factors mentioned below (Fontana 2005).

- The ratio of concentration of oxidized to reduced species at electrodes.

- Temperature of the medium. In general, i_o increases with the rise in temperature.
- The composition of the electrode surface. During a long term use, the electrode surface tends to change due to passivation or adsorption. In such cases i_o of the original and modified surfaces will be dissimilar.
- The roughness of the electrode surface. A rougher surface offers greater surface area and hence i_o will be higher. For instance a platinized platinum electrode has higher i_o for hydrogen evolution than bright platinum.

1.7.3 Mixed potential theory

As per the definition provided by the International Union of Pure and Applied Chemistry (IUPAC), mixed potential is the potential of an electrode (measured with respect to a suitable reference electrode, often the standard hydrogen electrode) when appreciable fraction of the anodic or cathodic current arises from species of two or more different redox couples, but when the total current on the electrode is zero. That is when more than one redox couple is considered, the electrode potential which arises upon simultaneous action of all the redox couples at zero net electrode current is termed as mixed potential.

Mixed potential theory was formally presented for the first time by Wagner and Traud in 1938. It is based on two postulates.

- Any electrochemical reaction is separated into two or more partial oxidation and reduction reactions.
- There can be no net accumulation of electric charge during an electrochemical process.

A corroding electrode as per mixed potential theory is viewed as a mixed electrode which is at a time in contact with two or more redox systems. A corroding metal hence can be considered as a combination of the non-corroding metal in a reversible equilibrium with the solution of its ions of unit activity and hydrogen electrode (as if non-corroding metal was saturated with H_2 gas at unit activity, at unit pressure). By the application of mixed

potential theory the influence of oxidizer addition, cathodic concentration polarization and galvanic coupling on corrosion rate of metal can be easily postulated. Mixed potential theory no doubt provides a modern approach to the understanding of classical concepts of corrosion (Fontana 2005).

1.8 ELECTROCHEMICAL CORROSION TESTING

Several standard tests are available to evaluate the rate of corrosion. Many of such test methods have been developed and documented by National Association of Corrosion Engineers (NACE) and American Society for Testing and Materials (ASTM). A suitable method is opted based on type of the metal and the prevalent form of corrosion. Given the electrochemical nature of corrosion, the electrochemical corrosion testing methods are precise and popular choices. The electrochemical attributes of corrosion is well established. Even the corrosion occurring under natural circumstances like metal corroding in open air or corrosion of steel rods in concrete reinforcements can be viewed from an electrochemical outlook. In both the cases the moisture in air and in wet concrete constitute the electrolyte. Electrochemical techniques for corrosion rate measurement are broadly categorized into two types.

- Direct current (DC) electrochemical corrosion monitoring techniques
- Alternating current (AC) electrochemical corrosion monitoring techniques

Both these practices often use three electrode systems where a corroding sample is made into a working electrode, the potential changes across the working electrode is supervised using a standard reference electrode having a stable and known electrode potential. Saturated calomel electrode (SCE) and silver chloride electrode (Ag/AgCl) are widely employed as standard reference electrodes. A counter or auxiliary electrode is introduced to complete the path of current flow and such an electrode acts as a current source and/or sink. Counter electrodes are often made of inert materials like platinum, gold and graphite and the platinum electrode is most frequently used. For practical electroanalytical tests a three electrode system is operated using an electronic hardware

called potentiostat. The potentiostat comprises of an electric circuit which functions based on Ohm's law. Here the potential of the working electrode is kept constant with respect to reference electrode by sensing the potential changes as variations in resistance and appropriately adjusting the current at counter electrode to balance the potential changes. A representative potentiostat layout is shown in Fig. 1.3. The potential across working electrode and reference electrode is measured by a high impedance voltmeter. The current across the auxiliary and working electrode is recorded by a low resistance ammeter.
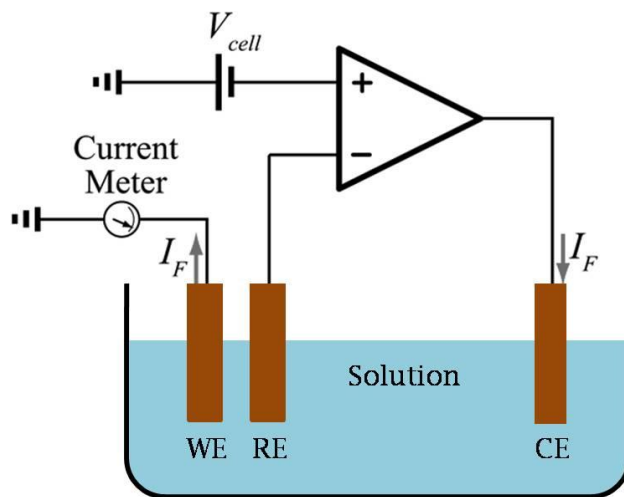
Fig. 1.3 A schematic potentiostat layout.

The old-fashioned potentiostats were independent in terms of result output. The results were retrieved as a physical data trace. The contemporary potentiostats however are devised to interface with personal computers and are operated through automated software (Barnartt 1977).

1.8.1 DC electrochemical corrosion monitoring techniques

This is a potentiodynamic corrosion monitoring technique. The working electrode sample is polarized by sweeping its potential away from the steady state potential. The polarization causes electrochemical changes at the working electrode surface. The electrode kinetics and diffusion rates of electroactive species control the magnitude of

current generated. The current generated in the cell as a response to potential drift is monitored as a function of time or potential (Thompson and Payer 1998).

1.8.1.1 Tafel extrapolation method

Wagner and Traud used Tafel extrapolation as a tool to verify the mixed-potential theory, where the extrapolation was utilized for corrosion rate deduction. In this practice the working electrode is initially allowed to stabilize and reach a steady state at which point of time the corrosion reactions possibly acquire a constant rate. This steady state electrode potential is OCP. Post the attainment of OCP the electrode is subjected to polarization both anodically and cathodically with respect to its OCP. A plot of logarithm of current density versus applied potential produces the results as Tafel plots. A representative Tafel plot is shown in Fig. 1.4, comprising of an anodic and a cathodic branches.
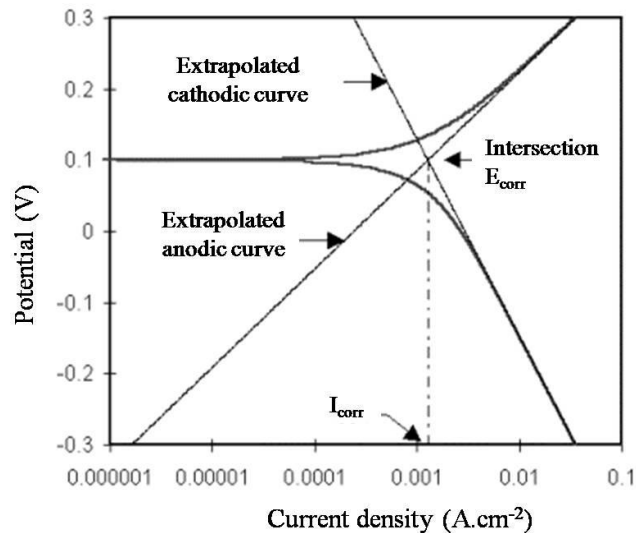
Fig. 1.4 A representative Tafel plot showing extrapolation.

The branches are nonlinear at potentials very close to OCP and linearity is exhibited at potentials widely differing from OCP. This linear portion of the polarization curves is termed as Tafel region. The Tafel regions are extrapolated back to meet at OCP. The point of intersection upon its projection to potential and current axis, respectively, gives the corrosion potential (E_{corr}) and the corrosion current density (i_{corr}). E_{corr} is an attribute

of the material. The i_{corr} is used for evaluation of corrosion rate by application of equation given below.

$$\upsilon_{corr} = \frac{K \times i_{corr} \times EW}{\rho}$$

(1.12)

where, K is a constant, the value of which defines the unit of corrosion rate. For υ_{corr} expressed in units mpy (mills per year), $\mu m/year$ and mm/year, the value of K, respectively, is 0.129, 3.27 and 0.00327, i_{corr} is the corrosion current density in $\mu A\ cm^{-2}$, ρ is the density of the corroding material in $g\ cm^{-3}$, EW is the equivalent weight of the corroding material.

A kinetically controlled electrochemical half-cell reaction obeys Tafel equation as shown below.

$$i = i_o\ e^{\,[\,2.3(E\text{-}E_o)/\beta\,)\,]}$$

(1.13)

where, i is the electrode current density of the reaction, i_o is exchange current density, E is the electrode potential, E_o is the equilibrium potential, β is the Tafel slope (constant for a given reaction expressed in units of volts/decade). This Tafel equation corresponds to one isolated half-cell reaction. The combination of the Tafel equations for both the anodic and cathodic reactions of a corroding system generates the Butler-Volmer Equation, as represented below.

$$i = i_a + i_c = i_{corr}\,[e^{\,[2.3(E\text{-}E_o)/\beta_a]} - e^{\,[-2.3(E\text{-}E_o)/\beta_c]}]$$

(1.14)

where β_a and β_c, respectively, are Tafel slopes for linear portion of anodic and cathodic Tafel branches. They are also termed as Tafel constants. The Tafel constants are related to electrode kinetic parameters and are helpful in assessment of polarization resistance (R_p) as described by the Stern-Geary equation.

$$R_p = \frac{\beta_a \times \beta_c}{2.3\ i_{corr}(\beta_a + \beta_c)}$$

(1.15)

Noteworthy benefits of Tafel extrapolation technique:

- In contrast to the conventional corrosion monitoring practices like weight loss method, Tafel extrapolation technique is highly rapid.
- It offers good accuracy even when the measured corrosion rates are exceptionally low.
- Some industrial processes necessitate a continuous corrosion monitoring to ensure the ultra high purity of the products and electrochemical methods like Tafel technique come in handy.

Prominent drawbacks of Tafel extrapolation method:

- Tafel extrapolation works best for the systems that are activation controlled. When concentration polarization arises, its interference is marked by a polarization curve vertical to current density axis, the extrapolation of which fails to yield accurate results. Since results are deduced by extrapolation, the Tafel region must spread over a current density range of at least one order of magnitude in order to achieve appreciable accuracy.
- The systems with multiple reductions present distorted Tafel regions and hence the Tafel technique will not be applicable for corrosion rate determination.

1.8.1.2 Linear polarization method

The linear polarization technique relies on electrode polarization for corrosion rate determination. This methodology stems from the phenomenon where the measured current density is found to linearly vary with applied potential when the specimen is polarized within ± 20 mV from the rest potential. It is further seen that the linear relation tends to cease at applied potentials beyond the above mentioned range, as shown in Fig. 1.5. The slope of such linear polarization curve ($\Delta E/\Delta i_{app}$) is inversely related to corrosion current as shown in the following equation.

$$\frac{\Delta E}{\Delta i} = \frac{\beta_a \times \beta_c}{2.3 \ i_{corr} \ (\beta_a + \beta_c)} \qquad (1.16)$$

where, $(\Delta E/\Delta i)$ is the slope of the linear portion of the polarization curve, β_a and β_c are the anodic and cathodic Tafel slopes, respectively and i_{corr} is the corrosion current density.
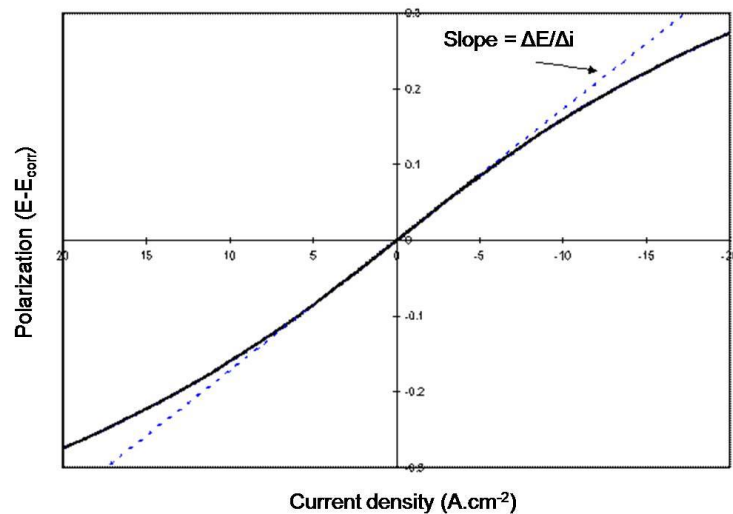
Fig. 1.5 A typical linear polarization plot.

The parameters like slope of the linear polarization curve and the Tafel slopes can be experimentally determined. The i_{corr} is computed by the application of equation 1.16. The corrosion rate eventually can be deduced from calculated values of the i_{corr}.

Some advantages of linear polarization method:

- Like the Tafel extrapolation method, linear polarization too enables rapid, precise and uninterrupted assessment of corrosion rates.
- The overvoltage applied on the metal being small, the technique is relatively non-destructive.

Notable limitations of linear polarization method:

- The practice is partially dependent on the Tafel extrapolation method. The values of the Tafel slopes, if unavailable from the literature, must be deduced using the Tafel extrapolation.

- The alteration of specimen surface often leads to variation in the slopes of linear polarization plots.

1.8.2 AC electrochemical corrosion monitoring techniques

1.8.2.1 Electrochemical impedance spectroscopy [EIS]

EIS is a versatile technique. The researchers of several disciplines benefit from EIS studies. Apart from corrosion, EIS applications today are well established in biosensor, battery and fuel cell development. As an astonishing fact EIS has also been used to check the freshness of fish (Niu and Lee 2000). The electrochemical interfaces are best understood when viewed from an impedance standpoint. The impedance studies of corroding systems help to characterize and analyze the complex interfaces. The impedance is the AC equivalent of DC resistance (R). It is the opposition put forward by a circuit to the flow of AC. In impedance tests a sinusoidal electrochemical (current or potential) perturbation considered with reference to a suitable DC condition is impressed on the system. Most corrosion investigations involve application of a small amplitude voltage excitation which is centered on the corrosion potential and which encompasses a wide range of frequencies. Such multiple frequency stimulation enables computation of electrode capacitance and rates of various electrochemical reactions. Small amplitude stimulation is preferred so as to achieve a linear or pseudo-linear response from the system. In a linear (or pseudo-linear) system, the output will be a current sinusoid at the same frequency but shifted in phase as shown in Fig. 1.6.

An expression similar to Ohm's law gives the impedance (Z) of the system as the ratio of potential to current both expressed as functions of time, as represented in equation 1.17.

$$Z = \frac{E_t}{I_t} = \frac{E_o (\sin \omega t)}{I_o (\sin \omega t + \phi)} = Z_o \frac{(\sin \omega t)}{(\sin \omega t + \phi)} \qquad (1.17)$$

where E_t and I_t are the potential and current at time t, E_o and I_o are the amplitude of potential and current signals, ω is the radial frequency, Z_o is the magnitude of the impedance and ϕ is the phase shift.
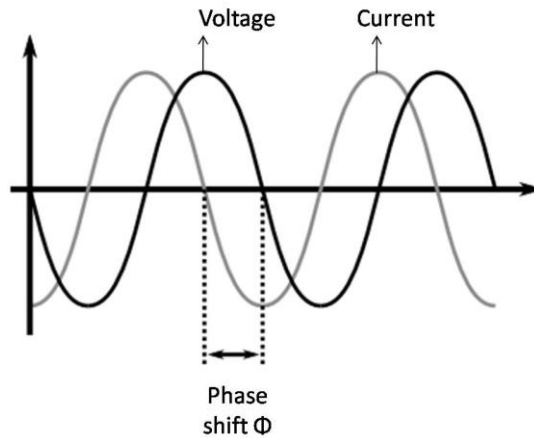
Fig. 1.6 A sinusoidal current response in a linear system.

However the impedance ($Z_{(\omega)}$) for practical convenience is expressed in terms of real Z^I (ω) and imaginary Z^{II} (ω) components in Cartesian coordinates as given in equation 1.18.

$$Z(\omega) = Z^I(\omega) + Z^{II}(\omega) \tag{1.18}$$

The impedance data are interpreted by developing different plots like Nyquist and Bode plots. On plotting Z^I along x-axis and Z^{II} along y-axis Nyquist plot will be generated. A plot of log (Z_o) along y-axis and log (f) (frequency in hertz) along x-axis yields Bode magnitude plot, whereas Bode phase angle plot is procured by plotting ϕ along y-axis against log (f) taken along x-axis. On a Nyquist Plot the impedance is symbolized as a vector, the length of which corresponds to the magnitude Z_o and the angle with which the vector remains inclined to x-axis is equivalent to ϕ. A foremost drawback of Nyquist plots is that the exact frequency at which any data point is recorded remains disguised. The Bode plots however compensate for this limitation. Representative impedance plots are shown in Fig. 1.7.
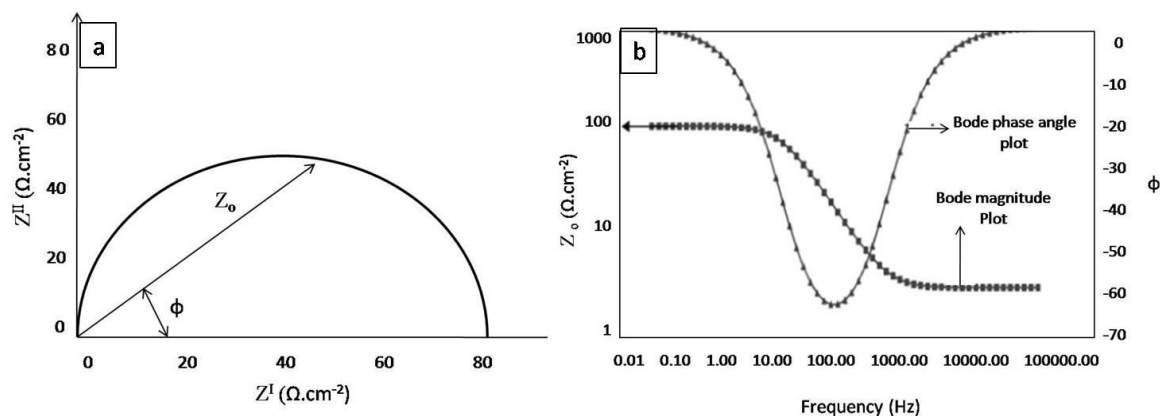
Fig. 1.7 Representative impedance plots (a) Nyquist plot (b) Bode plots.

The interpretation of impedance data is often achieved through simulation of the experimentally acquired impedance behavior with that of a suitable theoretical electrical circuit. Most of these equivalent electrical circuit models comprise of various combinations of common electrical elements like resistors, capacitors, and inductors. An equivalent electrical circuit chosen for fitment of impedance data should be such that a property related to physical electrochemistry of the system is reflected in each of the elements in the model.

It goes without saying that, EIS though effective, cannot give all the answers. It is a complementary technique and for complete understanding of interfacial processes the impedance data must be compared with other results (Mansfeld 1990, Lasia 1999).

EIS has the edge over DC methods as outlined in the following.

- Even extremely low corrosion rates in slowly changing systems can be evaluated.
- It is applicable to systems with low medium conductivity like organic liquids, soil and concrete.
- The quality of coatings on metal surface can be estimated precisely

Some shortcomings of EIS method are listed below.

- Interpretation of results is relatively tedious and complicated.
- It is a complementary technique and needs benchmarking with other corrosion monitoring practices.

1.9 CORROSION CONTROL

Combating corrosion is indeed a tough task. The corrosion manifests in several forms. The mechanisms and prevailing conditions are so diverse that not a single corrosion controlling method is universal in its application. Based on the type of metallic material, its design, rampant form of corrosion, and the nature of the existing environment, a suitable corrosion control technique is adopted. Some well-known measures to mitigate corrosion are explained below (Bradford 2001, Roberge 2008).

- **Material selection:** For any application the chosen material should be financially viable, with a superior corrosion resistance against the prevailing environment. In this context whenever practicable the pure metals or nonmetallics which are inherently more resistant to corrosion should be used as substitutes to commercial alloys without compromising the aspired productivity.
- **Alteration of environment:** Environment plays a pivotal role in material corrosion. Hence altering the same opens the door for unique and versatile ways to subside corrosion. Some frequently employed measures include, lowering the solution temperature, minimizing velocity, changing corrosive concentration and exclusion of cathodic depolarizers like oxygen and oxidizers. The use of corrosion inhibitors is also an environmental alteration measure.
- **Mechanical design:** A material design, if not done properly, might end up introducing undesirable factors in metal which initiate and accelerate corrosion. The designing should be such that the functional requirement is met and any scope for corrosion is held at bay. Some fundamental design rules include, avoiding heterogeneity, excess mechanical stress and sharp bends and edges.

- **Cathodic protection:** A cathode is intrinsically resistant to corrosion. A material can be protected by supplying electrons to its surface so that it remains cathodic to its surroundings. Cathodic protection can be accomplished through galvanic coupling with a more active metal which operates as a sacrificial anode. The impressed current method is another measure where external power supply is used to maintain required metal as a cathode with respect to an inert anode. The cathodic protection is most efficient as it doesn't merely suppress but completely eliminates corrosion.

- **Anodic protection:** The metals which exhibit a potential dependant active-passive transition phenomenon can be protected as anodes by inducing passivation. By employing a potentiostat, the potential of metal is held constant well within the range where passivity prevails.

- **Surface coatings:** A metal can be protected by isolating it from the corrosive. A coating on the surface insulates the metal and acts as a physical barrier. Depending on the requirement metallic, inorganic or organic coatings are developed. To be efficient, a coating must be uninterrupted, even, impervious, chemically inert to corrosive and preferably possessing a long shelf life.

1.10 CORROSION INHIBITORS

The addition of an inhibitor to minimize corrosion is an environmental alteration technique. A corrosion inhibitor by definition is a chemical substance which brings down the metallic corrosion rate in an environment, on its addition in minute amounts. For their efficiency exhibited at minuscule concentrations, the corrosion inhibitors are often deemed as retarding catalysts. The corrosion mitigation by inhibitor addition is an economic and easy approach, in contrast with other corrosion control measures. It would appear that the corrosion in any of its dreadful forms can be kept at bay with the employment of materials that are innately resistant to corrosion but it is the cost factor that outweighs all other considerations. Hence even with the development of new alloys, the cheap tried and tested alloys in combination with efficient corrosion control practices

continue to be popular in industrial circles. Besides cost-effectiveness, the possibility of *in situ* implementation and modification of the inhibitors without muddling with the process on the run, widen their spectrum of applications. To qualify as a good inhibitor any chemical must fulfill the following requisites.

- Possession of chemical inertness and thermal stability.
- High efficiency even when present in very small concentrations.
- Cost-effectiveness, easy availability and ecofriendly nature.

There are ample of commercial corrosion inhibitors available in market today. The inhibitors have been employed in several domains of industrial machinery and infrastructure like pipelines, heating systems, boilers, water cooling systems and metal extraction enginery. The inhibitors are also used for metal protection during its transportation and storage. The industries that are among the major consumers of chemical inhibitors include petroleum extraction and refinery industries, the chemical manufacturing industrial units, material manufacturing industries, water purification plants, automobile and aircraft manufacturers (Sastri 1998, Gräfen et al. 2000).

1.10.1 Classification of corrosion inhibitors

The class of corrosion inhibitors is vast and diverse. Several authors have categorized the corrosion inhibitors based on various factors and few of the most accepted bases for classification are given below (Schweitzer 2010).

- Chemical nature (organic or inorganic compounds).
- Inhibitor nature (oxidizing and non-oxidizing substances).
- Field of application under focus (pipeline networks, heating or cooling water systems, pickling and descaling).
- Mode of action (surface film formers, passivating agents, scavengers).

A complete classification of corrosion inhibitors is represented in Fig. 1.8.
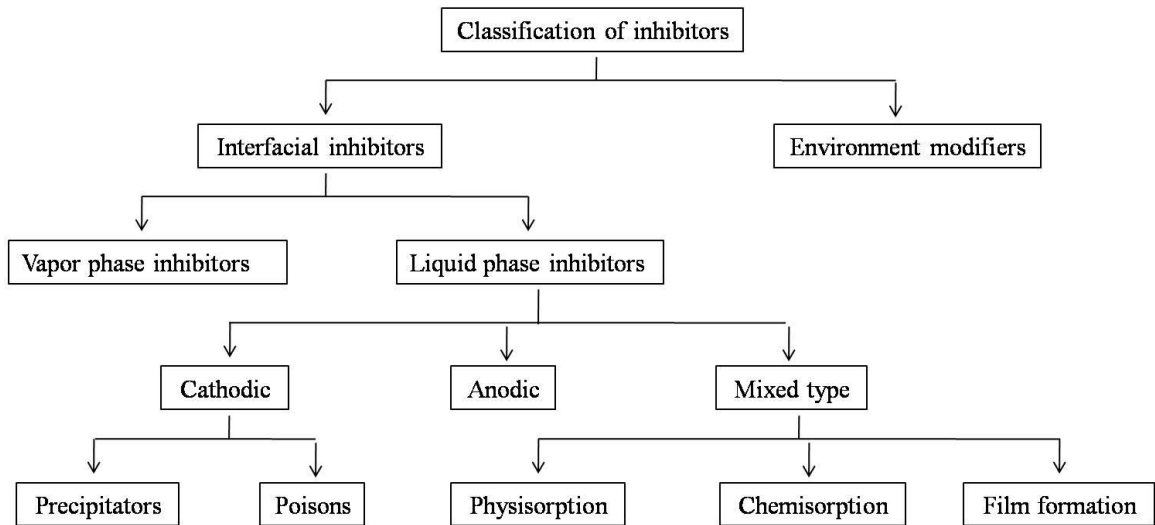
Fig. 1.8 A comprehensive classification of corrosion inhibitors.

This broad categorization takes into consideration the mechanism of inhibition and possibly all available inhibitors can be accounted as per this classification (Flick 1993, Papavinasam 2011, Sastri 2012).

1.10.1.1 Environment modifiers

These inhibitors bring down the aggressiveness of the environment. The presence of certain species imparts corrosiveness to the medium. The added inhibitor acts as a scavenger and eliminates the corrosive species from the environment. The oxygen scavengers like sodium sulphite and hydrazine are used as environment conditioners to control corrosion in neutral and alkaline solutions. In near- neutral media oxygen reduction being the predominant cathodic reaction and the removal of oxygen is bound to diminish the rate of cathodic reaction, which subsequently reduces corrosion. Sodium sulphite and hydrazine consume the dissolved oxygen as specified in the equations shown below.

$$2Na_2SO_3 + O_2 \rightarrow 2Na_2SO_4 \qquad (1.19)$$

$$N_2H_4 + O_2 \rightarrow N_2 + 2H_2O \qquad (1.20)$$

The biocides or antimicrobial agents are among other examples for environment conditioners, which combat microbial corrosion. Benzalkonium chloride is a widely employed biocide in oil field industry.

1.10.1.2 Interfacial inhibitors

These are also referred to as adsorption-type inhibitors, which, as the name suggests, bring about corrosion inhibition by adsorbing along the metal/electrolyte interface. A majority of corrosion inhibitors are interfacial in their action. The further grouping of interfacial inhibitors is briefed in the following.

a) Vapor phase inhibitors (VPIs): These are volatile compounds with low vapor pressures where the vapors exhibit corrosion inhibiting property. VPIs offer a short-term protection in closed systems, where they volatilize and the vapors condense all over the exposed metal surface. Amines vaporize in molecular form. On the contrary dicyclohexylamine nitrite reacts with moisture and dissociates to release amine and nitrous acid, which subsequently settle down on the metal surface. The vapors interact with metal surface through physisorption or chemisorption. VPIs can be directly placed in the vicinity of the metal or can even be infused into the wrapping sheets. VPIs are effective in safeguarding the materials during storage or transportation and they have also been used to guard electronic materials, for instance circuit boards.

b) Liquid phase inhibitors: These chemicals are added to the corrosive medium, where they interact with the surface in a solubilized form. Based on which half-cell reaction of corrosion is retarded in their presence, liquid phase inhibitors are further classified into anodic, cathodic and mixed-type as described below

Anodic inhibitors: These chemicals act in a selective way by inhibiting only anodic metal dissolution reaction in particular. Anodic inhibitors like oxyanions (chromates, molybdates and tungstates) react with metal ions at the anodic region. The metal salts of these inhibitors more often than not are sparingly soluble and hence precipitate over the anode as films. Such films when impervious and continuous bring about a barrier effect

and ultimately passivate the metal. In case of metals which inherently passivate, these added oxyanions help to patch up the defective surface film. A major shortcoming of use of anodic inhibitors is that the safety is rendered only in case when enough amount of inhibitor is added and on the contrary corrosion will be accelerated if the amount added is inadequate. The outcome of anodic inhibitor addition on the polarization curves is depicted in Fig.1.9 (a). The anodic polarization curve alone shifts to a region of more positive corrosion potential and lower current density, the latter of which symbolize minimized rate of anodic reaction or inhibition of corrosion in general.

Cathodic inhibitors: These compounds selectively hinder cathodic reaction of corrosion, which is hydrogen evolution or oxygen reduction. These can be cathodic poisons or precipitators as described below.

Cathodic poisons: Also referred to as hydrogen evolution poisons, which readily undergo reduction at the cathode and consequently deposit over the cathode as adherent metallic films. The oxides of arsenic, antimony, salts like sodium metarsenite have been promising cathodic poisons. The hydrogen overvoltage of these metals (arsenic and antimony) is high enough to suppress hydrogen evolution at the cathode.

Cathodic precipitators: These compounds precipitate selectively over the cathode to constitute impermeable films which block the cathodic reactants like H^+ ions and oxygen from getting reduced at the cathode. Urea, thiourea and mercaptans form films impervious to H^+ ions, where as zinc sulfate and magnesium sulfate deposit as their hydroxides which resist oxygen diffusion near the cathode.

The influence of cathodic inhibitor addition on the polarization curves is illustrated in Fig.1.9 (b). The cathodic polarization curve alone shifts to lower current density region at the same time corrosion potential become more negative.

Mixed-type inhibitors: As the name appropriately suggests these are classes of compounds which slow down both half-cell reactions of corrosion to different extent. Majority of organic molecules display this feature. The distribution of electron density in

these molecules is such that their adsorption is favored at cathodic as well as at anodic sites. The change brought about in polarization curves on introduction of mixed-type inhibitor is illustrated in Fig.1.9 (c). Both the polarization curves shift to lower current density region with a negligible change in corrosion potential.
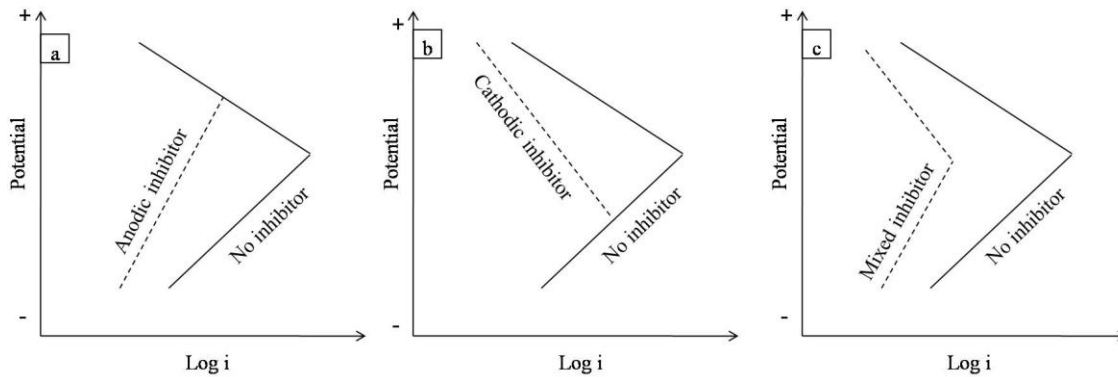
Fig. 1.9 Evans diagrams illustrating the result of addition of a) anodic inhibitor, b) cathodic inhibitor and c) mixed-type inhibitor.

The protection rendered by the mixed-type inhibitors could possibly be the outcome of one or more of the following phenomena.

a) Physical adsorption

b) Chemical adsorption

c) Film formation

a) Physical adsorption: The physisorption transpires when some weak electrostatic forces come into existence as means of anchoring of the inhibitor molecules to the metal surface. The metal in contact with an electrolyte instantaneously develops charged interface. This electric charge on the metal attracts inhibitor molecules that are oppositely charged ions or the dipoles. The process of physisorption is instantaneous or entails less activation energy. However the forces of interaction being weak, physisorbed inhibitors are vulnerable to desorption brought about by several factors, like the increase in

temperature. Hence the inhibition efficiency of physisorbed inhibitors tends to diminish at higher temperatures.

b) Chemical adsorption: During chemisorption, strong coordinate type chemical bonds are developed due to charge transfer interactions between inhibitor molecules and the metal surface. Such strong interactions make desorption less likely. The chemisorption is energetically more demanding in the sense that these processes are slow and progress with supply of comparatively higher activation energy. The established bonds strengthen with rise in temperature, hence chemisorbed inhibitors function more efficiently at higher temperatures. The chemisorption is highly specific, appearing only when the metal-inhibitor couple with an electron donor and acceptor combination gets established. In general chemisorption is favored between metals having vacant, low-energy electron orbitals and inhibitors with rather loosely bound electrons.

c) Film formation: The inhibitor adsorption in some cases might initiate surface reactions leading to development of surface films. The adherent, insoluble and impervious films will be promising as protective barrior layers and the inhibitors which grow into such films are bound be highly efficient.

1.11 FACTORS INFLUENCING INHIBITOR EFFICIENCY

The efficiency of any inhibitor is always specified for a particular metal and environment. A prominent variation in metallic or environmental factors might render an efficient inhibitor inactive. Hence the selection of an inhibitor has to be done systematically by taking into consideration following influential factors. (Knag 2006, Papavinasam 2011).

1.11.1 Molecular structure of the inhibitor

A typical organic inhibitor can be perceived as a combination of structural moieties like an anchoring group, a backbone and a supporting substituent group, the nature and structure of all the three entities play a salient role in deciding the inhibition efficiency.

a) Anchoring group: From an electron donor-acceptor interaction perspective the inhibitors act as Lewis bases and the functional groups of inhibitor molecules more often than not operate as anchoring groups. The electron density and polarizability of these anchoring groups will decide the strength of inhibitor-metal interaction. For a stronger interaction the anchoring groups with pi-bonds and hetero atoms bearing lone pair of electrons like N, O, S and P are preferred. For a homologous series of organic substances which differ only in terms of the heteroatom of the anchoring groups, the efficiency is expected to increase in the order; $O < N < S < P$ (Papavinasam 2011). Table 1.2 enlists a few common organic functional groups which capably act as potential anchoring groups.

Table 1.2 Common anchoring (functional) groups in organic inhibitors.

Structure	Name	Structure	Name
-OH	hydroxyl	-SH	thiol
-C≡C-	-yne	-S-	sulfide
-C-O-C-	ether	-S=O	sulfoxide
-COOH	carboxy	-C=S-	thio
-CONH$_2$	amide	-P=O	phosphonium
-NH$_2$	amino	-P-	phosphor
-C=NH	imino	-As-	arsano
-NO$_2$	nitro	-Se-	seleno

b) Backbone: The basic structural unit which bears the functional and substituent groups in an inhibitor molecule is regarded as the backbone. For simple organic molecules the aromatic rings with delocalized pi-electron cloud are preferable backbones. Such aromatic backbones even tend to augment the electron density of the anchoring groups attached to them. As for aliphatic molecules the long aliphatic hydrocarbon chain as the backbone is anticipated to offer enviable inhibition efficiency. Such aliphatic chains lower the solubility and hence promote inhibitor precipitation and film formation over metal surface. Such surface films rich in aliphatic hydrocarbons develop hydrophobicity which is desirable for metals corroding in aqueous media.

c) Substituent groups: The structural units attached to the backbone other than the anchoring groups are termed as the substituent groups. For superior inhibition efficiency the substituent groups should boost the electron density of the anchoring groups. When substituent groups are introduced into the backbone the steric effects become apparent, which is unfavorable. Hence in conclusion for finer inhibition efficiency the substituent groups of the inhibitor molecules should be positioned in such a way that the steric hindrance is minimized where as the electron density of the anchoring groups is maximized.

The correlation between the molecular structure and the corrosion inhibition efficiency has been extensively documented. The researchers have used both practical and theoretical quantum chemical approaches to authenticate the influence the molecular structure on inhibition efficiency (Abdennabi et al. 1998, Lukovits et al. 2001, Fang and Lie 2002, Kara et al. 2012, Aouniti et al. 2013, John and Joseph 2013).

1.11.2 Influence of temperature

The temperature effects are more or less dependent on the type of inhibitor-metal interactions. The physisorbed inhibitors with weak interactive forces undergo desorption and hence turn out to be less efficient with the rise in temperature. On the contrary, the increased temperature enhances the inhibition efficiency of chemisorbed inhibitors. The increase in temperature strengthens the coordinate bonds with which the inhibitors are anchored to metal surface. This trend for chemisorbed inhibitors is valid up to a certain critical temperature. An elevated temperature might prove to be detrimental irrespective of the type of adsorption as organic inhibitor molecules undergo decomposition at very high temperatures.

1.11.3 Surface charge on the metal

The electric charge on the metal surface plays a pivotal role during physisorption of the inhibitors. At the metal/electrolyte interface the electric field at the outer Helmholtz plane of the electrical double layer gives rise to surface charge. The surface

charge (E_{surf}) is defined as the difference of equilibrium potential of the metal (E_{corr}) and it's potential of zero charge (E_{PZC}), as shown in equation 1.21.

$$E_{surf} = E_{corr} - E_{PZC} \qquad\qquad (1.21)$$

E_{PZC} is the electrode potential at which metal surface has zero charge. In other words at E_{PZC} the electrical double layer ceases to exist and this is the virtual condition at which the metal surface has highest efficiency for adsorption. Once the electrical double layer gets established, the electric field draws the water molecules close to metal surface. Henceforth, the inhibitors, in order to adsorb should dislodge the previously adsorbed water molecules.

The type of the inhibitor suitable for a particular metal type can be predicted by knowing the values of E_{PZC} and E_{corr} for the metal. When E_{surf} is negative ($E_{PZC} > E_{corr}$) cationic inhibitors are attracted towards the metal surface and are subsequently physisorbed. On the other hand a positive E_{surf} ($E_{PZC} < E_{corr}$) preferentially aids the adsorption of anionic inhibitors. For nonionic inhibitors which adsorb as dipoles the E_{surf} controls the orientation of such dipoles at metal surface.

1.11.4 Intermolecular interactions among adsorbed molecules

The intermolecular interactions among the adsorbed inhibitor molecules become apparent at increased surface coverage. Such lateral interactions if attractive will be beneficial as these lead to improved surface coverage and hence superior inhibition efficiency is obvious. The inhibitors possessing long aliphatic chains have surprisingly high efficiency owing to the attractive van der Waals forces operating between the hydrocarbon chains. The lateral interactions could also be repulsive in nature. In such cases the imperfection in surface coverage leads to poor inhibition efficiency. The repulsive interactions are evident when inhibitors adsorb as dipoles.

1.11.5 Reactivity of surface adsorbed inhibitors

The primary inhibition is the inhibition brought about by the added compound in its native form. The chemical nature of the inhibitor however might vary with time and/or electrode potential. In some cases the adsorbed inhibitor undergoes additional reactions like reduction or polymerization or precipitation. The inhibition exhibited by such reaction products is termed as secondary inhibition and the nature of the reaction products decides the superiority or the otherwise of the secondary inhibition. For instance diphenyl sulfoxide post adsorption gets reduced to diphenyl sulfide, the latter is a more efficient inhibitor compared to its precursor. Quite the contrary is seen when thiourea or its alkyl derivatives undergo reduction to produce sulfhydryl ion (HS^-), which is a potential corrosive and accelerates the corrosion (Papavinasam 2011). The reduction leading to polymerization is common among certain unsaturated hydrocarbons like alkynes. The polymer products by the virtue of their structure offer better surface coverage and hence superior efficiency. The surfactants on adsorption are known to precipitate as their metal salts. The precipitates form a hydrophobic surface layer which augments the barrior effect (Schweitzer 2010).

1.11.6 Synergism and antagonism

A combination of one or more inhibitors can be fruitful or otherwise depending upon the mutual interactions among them. If the interactions are attractive the inhibition efficiency of the mixture will be greater than the sum of the individual efficiencies and this effect is termed as synergistic effect. For example a mixture of formaldehyde and furfuralimine shows synergism. In contrast certain combination of inhibitors like narcotine and thiourea, turn out to be a debacle, due to antagonistic effect where the mixture fails to exhibit the good efficiency as shown by both the components individually.

1.12 MECHANISMS OF CORROSION INHIBITION

The mechanisms of corrosion inhibition are diverse and complex. Different substances act at different stages of corrosion and impede the process. Some commonly observed mechanisms are discussed in the following (Saji 2010, Papavinasam 2011).

1.12.1 Interfacial inhibition by adsorption

In a corroding metal the metal/solution interface is a dynamic region where the corrosion reactions occur unabated. The adsorption is a surface phenomenon and the adsorbed inhibitor molecules line up at the metal/solution interface. As per the generally accepted model, the adsorption of the inhibitor at the interface occurs concurrently with the displacement of previously adsorbed water molecules. The adsorption thus appears to be a replacement reaction as shown below.

$$\text{Inh}_{(sol)} + \chi \, H_2O_{(ads)} \rightleftharpoons \text{Inh}_{(ads)} + \chi \, H_2O_{(sol)} \qquad (1.22)$$
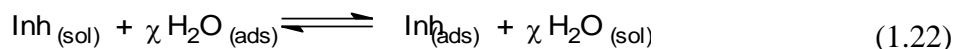
where, $\text{Inh}_{(sol)}$ and $\text{Inh}_{(ads)}$ are the free inhibitor molecules in the electrolyte solution and the adsorbed ones on the metal surface, respectively, $H_2O_{(ads)}$ is the water molecules adsorbed on the metal surface beforehand and χ is the size ratio corresponding to the number of water molecules dislodged during adsorption of one inhibitor molecule. As a result of adsorption the inhibitors accumulate at the interface and retard anodic and/or cathodic reactions depending upon the electrode on which their adsorption is favored. In any case, eventually the interfacial inhibitor adsorption impedes electrochemical corrosion.

1.12.2 Blocking of active reaction sites

The inhibitor adsorption brings along surface coverage. Such adsorbed inhibitors potentially cover the active reaction sites on the metal surface. The blocking of the active sites of reaction at anode or cathode impedes the rate of corresponding electrochemical reactions. Thus the rate of electrochemical corrosion diminishes proportionally with surface coverage generated by inhibitors. Usually the inhibitors operating this way do not

participate in electrode reactions nor do they change the mechanism of corrosion, hence this action can be precisely identified from the polarization curves, which on addition of this class of inhibitors assume a parallel shift with negligible change in Tafel slopes.

1.12.3 Formation of physical barrier film

The physical barrier effect becomes predominant when the surface adsorbed inhibitors precipitate as their sparingly soluble salts. The precipitates build up a film over the metal surface which subsequently insulates the metal and prevents the corrosive species from coming in contact with the surface. To be efficient as a physical barrier the film should resist the corrosive infiltration. Hence the efficient films are expected to be non-porous, sufficiently thick, and continuous, with appreciable stability and adherence.

1.12.4 Participation in electrode reactions

The electrochemical reactions occurring at the metal/solution interface are often multi-step processes. Some inhibitors involve and interfere with these sequences of reactions and divert the corrosion process so that it proceeds at a slower rate. The inhibition achieved through participation in electrode reactions can be pinpointed by the measurement of Tafel slopes which vary appreciably on the introduction of the inhibitors.

1.13 MODE OF INHIBITION IN NEAR-NEUTRAL SOLUTIONS

The corrosion of metal is pH dependent and so is the mechanism of inhibition. An inhibitor proved to be effective for the protection of a metal in acidic solutions might eventuate to be a disappointment in solutions of different pH, say in near-neutral media. In acidic media the metal surface is devoid of any oxide layer as strong acids dissolve the metal oxide film. Hence in acidic solutions inhibitor adsorption occurs over an oxide-free surface and hydrogen evolution will be the predominant cathodic reaction. On the contrary, in near-neutral solutions a corroding metal forms sparingly soluble corrosion products like metal-oxides and metal-hydroxides and oxygen is preferentially reduced at cathode. Usually the metal corrosion products deposit over the surface to form films which proffer some degree of safeguarding to the underlying metal. Thus for metal

protection in neutral solutions, the inhibitors are expected to possess an ability to adsorb over a pre-existent film (Turgoose 1990, Schweitzer 2010).

Inorganic anions like phosphates (Valcarce and Vázquez 2010, Yohai et al. 2011), carbonates (Dunn et al. 2004), silicates (Aramaki 2002) and oxidizing ions like chromates (Pokhmurskii et al. 2011) and nitrates (Lee et al. 2012, Ortíz et al. 2013) have been known to be efficient for inhibition in neutral solutions. The alternatives to inorganic ions are salts of organic acids like benzoate (Rammelt et al. 2008), cinnamate (Shi ei al. 2011), salicylate (Forsyth et al. 2002), etc. Some chelating agents have also been explored as corrosion inhibitors in neutral media like derivatives of sarcosine (Frignani et al. 1996), oximes (Senthilkumar et al. 2011), quinoline (Ebenso et al. 2010), etc.

1.14 MAGNESIUM AND ITS ALLOYS

The geochemical surveys confirm magnesium as the eighth most abundant element in the earth's continental crust (Railsback 2006). Magnesium in its elemental form possesses very high chemical reactivity and hence exists in its ores as magnesium compounds. Although magnesium occurs in over sixty minerals the most common and commercially viable ones include magnesite ($MgCO_3$), dolomite ($MgCO_3 \cdot CaCO_3$), carnallite ($KCl \cdot MgCl_2 \cdot 6H_2O$), brucite ($Mg(OH)_2$), etc. There is copious amount of magnesium dissolved in seawater, as a matter of fact, in seawater magnesium cation (Mg^{2+}) is the second most abundant cation next to sodium (Na^+). The availability of magnesium is so enormous that magnesium as a resource would seem imperishable. Magnesium in its metallic form is produced through the metallurgical extraction from its ores and by the electrolysis of molten magnesium chloride derived from seawater (Gupta and Sharon 2011).

Magnesium alloys were more often than not referred to as "elektron" in old literature. Elektron is the historic name coined by two employees Gustav Pistor and Wilhelm Moschel of the German company "Chemische Fabrik Griesheim – Elektron" in

the year 1908. Elektron is also a registered trade mark of magnesium alloys manufactured by Magnesium Elektron Limited; a British company (Wagner 2006).

Among structural metals magnesium is the lightest, with a density of 1.74 g/cm^3, which is nearly two-third that of aluminum. The exceptional alloying property of magnesium is exploited in the manufacturing of plenty of its alloys. Some common alloying elements blent in commercial magnesium alloys include Al, Zn, Li, Ce, Ag, Zr and Th. Magnesium alloys are often named after the synthetic method used for their manufacture, like cast alloys and wrought alloys. In spite of being the lightest, the utility of magnesium alloys in weight-sensitive applications remains a challenge owing to their vulnerability to corrosion, high-temperature creep and flammability. Over the years all these limitations have been overcome to some extent by new alloy development by means of inclusion of alloying elements that counteract these undesirable properties. The inclusion of scandium and gadolinium minimizes the high-temperature creep, the flammability is controlled by the addition of calcium and the corrosion resistance is improved by the introduction of cathodic poison like arsenic. Maintaining such precise elemental composition during alloy manufacturing is a tough task and it elevates the production costs, making the new alloys economically impractical (Dodson 2013). Hence cost-effective ways to combat magnesium corrosion and other unpleasant features continue to be the arena frequently explored.

Currently magnesium alloys are among the most sought-after structural alloys; their popularity is reflected in the astonishing growth of the global magnesium market (Brown 2000, Kramer 2013). Magnesium alloys showcase a desirable combination of physical and mechanical properties, like high strength-to-weight ratio, low density, superior damping characteristics, fine castability, recyclability and exceptional machinability. In addition, magnesium alloys are non-magnetic, possess relatively high thermal and electrical conductivity and excellent vibration and shock absorption ability, which makes their applications far-reaching (Froes et al. 1998, Agnew 2004).

1.14.1 Applications of magnesium alloys

The alloys of magnesium fetch a great demand as structural materials, especially in weight-critical applications. Some remarkable applications are briefed in the following.

1.14.1.1 Applications in transport industry

Several automobile parts are designed out of magnesium alloys like gearbox housing, steering wheels, fuel tank cover and even in interior parts like seat frame, driver's air bag housing. Even though first experimented in race cars, magnesium alloy parts have found their way into domestic automobiles as well. As of today almost all elite automobile manufacturers such as Audi, Volkswagen, Mercedes-Benz, Toyota, Ford, BMW, Jaguar, Fiat, Hyundai, etc, employ magnesium alloy parts in their merchandise (Luo 2002, Blawert et al. 2004, Rosen et al. 2005, Cole 2007, Logan 2007).

The research and development in the field of magnesium alloys benefits aviation industry as well. Apart from low density, the capability of magnesium alloys to tolerate elevated temperatures, exposure to ozone and bombardment of high-energy particles and small meteorites, makes them top contenders for applications in air-crafts. Magnesium based components of air-crafts include thrust reverser, gearbox, engines, and helicopter transmission casings (Wendt 2005).

1.14.1.2 Military applications

The technology in armed forces is not too far behind from exploiting the benefits of light-weight nature of magnesium alloys. The aircrafts fitted with magnesium alloy parts were employed during World War II. H-19 Chickasaw an US army helicopter built in 1951 had 17% (by weight) of magnesium, a highest during its time. Falcon GAR-1 a first air-to-air missile launched in 1956 had 90% of magnesium in its structure. Some other historically prominent examples for 'magnesium in military' include M-274 light cargo - personnel and weapon carrier, M-116 husky amphibious personnel carrier, military aircrafts like Eurofighter Typhoon, Tornado and F16 and intercontinental ballistic missiles like Titan, Agena and Atlas (Mathaudhu and Nyberg 2010).

1.14.1.3 Medical applications

Magnesium alloys are being explored as bio-implant materials. The density of magnesium alloys (1.7-2.0 $g.cm^{-3}$) is close to that of natural bone (1.8-2.1 $g.cm^{-3}$) and is lesser than that of close contenders; titanium alloys (4.4-4.5 $g.cm^{-3}$). The stress shielding effect appears to be minimized in the case of magnesium bio-implants as the elastic modulus of magnesium (41-45 GPa) is close to that of natural bone material. Magnesium alloys are mechanically strong when compared to ceramic or polymeric biomaterials and possess greater fracture toughness. Magnesium ion naturally takes part in human metabolism, it is the fourth most abundant cation in human body; hence magnesium is bio-compatible and nontoxic at moderate levels. The bio-corrosion of magnesium is favored at physiological conditions *in vivo*. This biodegradability of an implant material is desirable, as it wipes out the need of a supplementary surgery to extract the implant after its life time (Gu and Zheng 2010).

1.14.1.4 Applications in electronics

To be user friendly, portability is highly anticipated of the electronic gadgets. In comparison with the plastic electronic materials magnesium alloys are not only light-weight but also possess better heat transfer and the ability to shield interferences from electromagnetic and radio frequencies. Magnesium parts that are currently featuring in electronic devices include casings of cell phones, digital cameras, computers, laptops, digital projectors, media players. Appreciably good heat dissipation property of magnesium alloys is capitalized in developing magnesium based heat sinks in electronic goods.

1.14.1.5 Applications in sports

The popularity of magnesium alloys as structural materials for sports equipments is not surprising considering their enviable properties such as low density, easy machinability which aids to create complex shapes, good damping characteristics and appreciable shock and vibration absorption ability. The handles of archery bows, tennis

racquets, golf club head, chassis of in-line skates and frames of mountain biking bicycles are some notable examples of magnesium parts in sports equipments.

1.14.1.6 Other applications

Magnesium alloys find applications in consumer products which need to be light for easy portability. Some examples include spectacle frames, binocular parts and hand-held working tools for mechanical operations.

1.14.2 Magnesium alloy ZE41

ZE41 is a cast alloy of magnesium. The name ZE41 is derived from the two major alloying elements and their percentage composition (by weight) in the alloy; zinc (4 %) and rare earth elements (1 %). The rare earth elements include like Ce, La, Pr, Sr, and Nd.

The incorporation of Zn is known to enhance the mechanical strength of the alloy; moreover, Zn when added in conjunction with minute amounts of Ni and Fe as impurities diminishes the corrosion susceptibility of the alloy. Zr operates as a grain refiner when introduced into an alloy comprising Zn and rare earth elements (Ben-Hamu et al. 2007). Rare earth elements are expensive and their addition hence is confined to alloys for high profile applications. Alloying with rare earth elements improves the strength at elevated temperatures and the creep resistance (Rzychoń and Kiełbus 2006).

1.14.2.1 Properties of ZE41 alloy

The alloy ZE41, like metallic magnesium, is light weight. Apart from low density, ZE41 exhibit exceptionally good weldability, castability and machinability (Gupta and Sharon 2011). Some specific physical, thermal and mechanical properties of ZE41 are compared with that of aluminium as presented in Table 1.3.

Table 1.3 Physical, thermal and mechanical properties of ZE41 magnesium alloy in comparison with aluminium.

Parameter.	ZE41	Aluminium
Specific gravity	1.84	2.7
Melting range (K)	805 –911	933.5
Specific heat (J kg^{-1} K^{-1})	2.09	897
Thermal conductivity (W m^{-1} K^{-1})	24	237
Electrical resistivity (10^{-9} Ω m (20°C))	68	28.2 (at 20°C)
Modulus of elasticity (GPa)	44.13	70
Poisson ratio	0.35	0.34
Brinell hardness (HB)	55 – 70	15
Ultimate tensile strength (MPa)	217.87	214 (Al alloy 6061-T6)

1.15 LITERATURE REVIEW

1.15.1 Corrosion behavior of pure magnesium and magnesium alloys

The vulnerability of magnesium and its alloys towards corrosion has been well established. Pure magnesium has been perceived as a moderately passive metal under natural circumstances which tend to corrode extensively on exposure to pitting agents like chloride ions under non-oxidizing environments (Tunold et al. 1977). The anodic dissolution behavior of magnesium has often been referred as a strange phenomenon called as negative difference effect (NDE) and has been documented in detail. Four different mechanisms have been proposed in literature to explain NDE, like (a) univalent magnesium ion (Mg$^+$) model, according to which Mg$^+$ is believed to exist as a highly reactive intermediate (Greenblatt 1956, Lopez and Natta 2001, Song and Atrens 2003, Atrens and Dietzel 2007, Thomaz et al. 2010, Qiao et al. 2012, Shi et al. 2012b, Frankel et al. 2013), (b) undermining and falling away of cathodic secondary phase particles due to micro-galvanic corrosion (Makar and Kruger 1990), (c) hydride model, which predicts the formation of less stable magnesium hydride (MgH$_2$) during magnesium corrosion

(Gulbrandsen 1992), (d) partially protective film model, which predicts the existence of a partly protective surface film of corrosion products (Song et al. 1997b). A new mechanism of hydride dissolution has been suggested recently by Cao et al. (2013). The authors studied the corrosion of ultra pure magnesium in 3.5 % NaCl saturated with $Mg(OH)_2$ and accredited the difference between the corrosion rates measured through hydrogen evolution and weight loss studies to dissolution of cathodically evolved hydrogen in magnesium metal to form MgH_2. Thus formed MgH_2 is reported to dissolve and form corrosion products, keeping the overall reaction of magnesium corrosion the same as suggested in old literature.

The presence of a partially protective surface film over corroding magnesium is the most accepted mechanism of all. Several studies predict the corroding magnesium to invariably develop a partially protective film on the surface. A few of such studies have been briefed in the following. Pebere et al. (1990) conducted EIS measurements for magnesium exposed to aerated sodium sulfate solution. The augmentation of protection with increased immersion time has been attributed to growth of protective surface film of $Mg(OH)_2$ and/or MgO. Gulbrandsen et al. (1993) verified the passivity exhibited by magnesium in alkaline fluoride (NaF and NH_4F) solutions. As per the study, with increased fluoride amount a porous gel-like $Mg(OH)_2$ film transformed into more protective film comprised of MgF_2. Nordlien et al. (1997) reported a multilayer structure of surface film on corroding magnesium established by means of transmission electron microscopy (TEM). The surface film formed on exposure to water contained three layers; with inner cellular layer of $MgO-Mg(OH)_2$, an intermediate film of MgO found to be thin, dense and amorphous and an outer thick porous $Mg(OH)_2$ layer having a platelet-like morphology. The study related the corrosion characteristics of magnesium to the properties and the morphology of these surface layers. Song et al. (1997a) have inspected the corrosion of pure magnesium in NaCl at different medium pH. The study attributed the accelerated magnesium dissolution at higher anodic overvoltages to the breakdown of somewhat protective surface film. Baril and Pebere (2001) examined pure magnesium corrosion in aerated and deaerated sodium sulfate solutions by polarization and

impedance measurements. According to the results of the study, magnesium corroded at faster rate in aerated solutions which has been assigned to the presence of CO_2. It has been suggested that bicarbonate (HCO_3^-) formed from dissolution of CO_2 in water, caused the breakdown of $Mg(OH)_2$ surface film.

A wide variety of magnesium alloys have been developed to meet the demand in unique fields of application. The literature review highlights the emphasis which has been laid to comprehend the influence of the alloying elements and the microstructure of the alloys on the corrosion characteristics of magnesium and some of such prominent works have been discussed in the following. Baghni et al. (2004) reviewed the prominent works and presented a comparison between the corrosion performances of pure magnesium and few selected magnesium alloys in industrial and marine environments. The focus of the review was to underline the consequence of addition of alloying elements on the corrosion rate of magnesium. According to the review the elements like Zn, Cd, Ca, Ag exhibit a moderate accelerating effect, where as Mn, Na, Sn, Th, Be, Pr have negligible effect, however elements like Cu, Ni, Co, Fe being cathodic show severely deteriorating effect on the corrosion of magnesium. The deleterious effect of impurity iron on aluminium containing magnesium alloys has been reported by Matsubara et al. (2013). The alloying of magnesium with calcium has been reported to be beneficial (Liu et al. 2014, Mandal et al. 2014).

The effect of rare earth element addition has been documented in detail. Zucchi et al. (2006) studied the corrosion behavior of magnesium alloy WE43 containing rare-earth elements Y and Nd. The outcome of the study pointed out that the presence of Y and Nd enhanced the passivation tendency of magnesium even in strong electrolytes. The addition of rare earth element Ce to AZ91D magnesium alloy has been reported to be beneficial by Fan et al. (2006). Ce inclusion has been shown to improve not only the corrosion resistance but also the mechanical properties of the alloy. The study reported the formation of a more refined and continuous β-phase on introduction of Ce, which resulted in enhanced corrosion resistance. Furthermore the beneficial outcomes obtained

from the incorporation of rare earth elements into magnesium alloys have been focused in several studies (Rosalbino et al. 2006, Song 2007, Takenaka et al. 2007, Liu et al. 2009, Südholz et al. 2009, Sudholz et al. 2011, Arrabal et al. 2012).

Zirconium has been credited to function as a grain refiner when added in optimal concentrations to magnesium alloys (Qian et al. 2003, Peng et al. 2005, Prasad et al. 2012). The grain refinement of magnesium by Zr incorporation has shown to boost the corrosion resistance of the metal and its alloys. Song and StJohn (2002) examined the corrosion susceptibility of unrefined and Zr-refined microstructures of rare earth containing magnesium alloy MEZ. In the study Zr addition has shown to offer a handful of benefits, it removed iron impurity, stabilized magnesium matrix solid solution, delayed commencement of localized corrosion, lessened rates of both half-cell reactions of metal corrosion and passivated the precipitated particles. The amount of Zr added is vital during grain refinement. Sun et al. (2009) reported an optimum concentration of 0.42% of Zr for Mg-Gd-Y alloy, at which a best combination of corrosion resistance and mechanical properties were observed. The size and distribution of Zr-rich particles have been considered as the key factors in the study. Gandel et al. (2014) investigated sixteen different binary Mg-Zr alloys along with four commercial Zr containing alloys including ZE41 to underline the effect of concentration and distribution of zirconium on the corrosion of magnesium alloys. The study outlined the detrimental effect induced by zirconium when present both in metallic particle form and as a dissolved component in solid solution. The authors have suggested multiple element addition and post-manufacturing processing to bring down the unfavorable effect so as to meet the performance expected of the commercial magnesium alloys.

Zinc is one of the most commonly used additive for alloying magnesium. The addition of Zn has been reported to be beneficial, which improves the mechanical properties like tensile strength and yield strength of magnesium alloys (Yin et al. 2008, Yuan and Zheng 2014). Badawy et al. (2010) examined the electrochemical corrosion of Mg-Al-Zn and Mg-Al-Zn-Mn alloys in contrast with pure magnesium in aqueous

electrolytes. The alloys were learnt to be more corrosion resistant and the study attributed the diminished corrosion tendency to the presence of additive elements, mainly Zn. The alloys of Mg-Zn are mostly employed for biomedical applications as synthetic implants. Several studies have documented an enhanced corrosion resistance of Mg on inclusion of Zn in simulated body fluid (SBF) (Zhang et al. 2010, Cai et al. 2012). However, the deleterious effect of addition of zinc to magnesium has also been reported by many (Yamasaki et al. 2007, Song et al. 2012). Ha et al. (2013) showed that the addition of Zn in Mg-Zn binary alloys enhanced the protectiveness of the passive film as well as the rate of hydrogen evolution, the latter being predominant lead to an increase in overall rate of corrosion.

An alloy's microstructure immensely influences its behavior, the same holds good for magnesium alloys as well. Song et al. (1999) related the corrosion of AZ91D magnesium alloy to its microstructure. The investigation showed that the size and the distribution of intermetallic β-phase were crucial factors which decided the corrosion rate. A small particle size and uniformly distributed β-phase improved corrosion resistance, on the other hand an agglomerated β-phase with large particle size acted as cathode and promoted micro-galvanic corrosion. This peculiar influence of β-phase morphology has been documented in several other studies (Song et al. 1998, Mathieu et al. 2003, Zhao et al. 2008 a, Lyndon et al. 2013). Many metals incorporated as additives turn out to be cathodic to magnesium hence majority of the magnesium alloys are vulnerable to micro-galvanic corrosion, where the alloy microstructure plays a crucial role. There are several studies aimed at establishing this influential role of microstructure on corrosion of magnesium alloys (Ambat et al. 2000, Pardo et al. 2008, Zhang et al. 2008, Peng et al. 2009, Zhang et al. 2011b, Song and Xu 2012, Shi et al. 2013, Liu et al. 2014, Zeng et al. 2014, Zhao et al. 2014b).

Among the magnesium alloys AM (containing Al and Mn) and AZ (containing Al and Zn) alloy series have been studied extensively. The literature is packed with works aimed at understanding the corrosion behavior of these alloys (Mathieu et al. 2002,

Cheng et al. 2009, Pardo et al. 2010, Wang et al. 2010b, Liao et al. 2012, Shi et al. 2012a, Feliu et al. 2014, Song et al. 2014, Zhao et al. 2014b). In recent times the rare earth containing magnesium alloys are steadily gaining their due recognition, for instance ZE41 which is a magnesium alloy comprising of Zn, Zr and rare earth elements. The corrosion behavior of ZE41 under varying pH and chloride ion concentrations has been documented by Zhao et al. (2008b). The authors reported both pH and the chloride ion concentration as influential factors controlling ZE41 corrosion. As per the study the $Mg(OH)_2$ surface film regulated the rate of ZE41 dissolution, the circumstances like low pH and high chloride concentration destabilized the film hence accelerated ZE41 corrosion. Furthermore the study justified the existence of a difference between the corrosion rates deduced from electrochemical and hydrogen evolution measurements as a consequence of NDE. Neil et al. (2009) examined the influence of alloy microstructure on corrosion initiation and propagation in ZE41 in NaCl solution and reported the microstructure of ZE41 to consist of α-Mg grain along with secondary phases like Zr-rich β-phase particles and grain boundary T-phase (Mg_7Zn_3RE). The investigation concluded the Zr-rich β-phase particles to be potential cathodic sites which favored corrosion initiation and propagation. The study pointed out the susceptibility of ZE41 towards micro-galvanic corrosion and suggested β-particle size control as a micro-structural alteration measure to mitigate ZE41 corrosion. The cathodic nature of secondary micro-constituent phases which promote ZE41 alloy corrosion has been further established through a scanning Kelvin probe force microscopy (SKPFM) study conducted by Coy et al. (2010). The authors investigated four commercial rare earth containing magnesium alloys namely ZE41, WE54, cast WE43 and wrought WE43, out of which ZE41 showed highest susceptibility to corrosion in NaCl. The study confirmed the micro-galvanic corrosion of ZE41 promoted by the presence of cathodic precipitates of Zr_4Zn and cathodic Mg_7Zn_3RE phase. The impact of microstructure over ZE41corrosion has been further upheld by Neil et al. (2011) through a comparison study conducted on heat treated and sand-cast ZE41 alloys in borate buffer solution. The heat treatment altered the microstructure of sand-cast ZE41 alloy and corresponding variation in corrosion

morphology has been highlighted in the research work. Even though the microstructure is the predominant underlying cause for corrosion susceptibility of ZE41, the microstructural alteration need not always materialize into improved corrosion resistance as shown by Banerjee et al. (2013). The investigation involved surface modification of ZE41 alloy through laser application which resulted in a modification of alloy microstructure but the impact over corrosion resistance of the alloy was negligible. Apart from micro-galvanic corrosion, ZE41 has been reported to be susceptible to other prevalent forms of corrosion like stress corrosion cracking (Kannan et al. 2008) and pitting corrosion (Kannan et al. 2011).

1.15.2 Corrosion inhibitors for magnesium and magnesium alloys

Many chemical compounds have been investigated for their ability to inhibit magnesium corrosion in variety of media. This broad class of magnesium corrosion inhibitors includes both inorganic and organic chemicals and even the combination of the two. Some efficient magnesium inhibitors reported in literature along with certain essential details are listed in Table 1.4.

Table 1.4 Prominent corrosion inhibitors for magnesium and magnesium alloys.

Inhibitor used	Material	Medium	Reference
Sodium undecanoate	Mg-Zn-Al alloy	Aqueous salt solutions	Daloz et al. 1998
Potassium fluoride	Pure Mg	Ethylene glycol	Song and StJohn 2004
Potassium fluoride	AZ91D and AM-SC1	Commercial engine coolants	Song and StJohn 2005
Sodium decanoate and sodium heptanoate	Pure Mg	ASTM D1384-87	Mesbah et al. 2007
Cerium nitrate and lanthanum nitrate	AZ31 alloy	NaCl	Montemor and Ferreira 2008

Inhibitor used	Material	Medium	Reference
Sodium dodecylbenzenesulphonate (SDBS)	AZ31 alloy	NaCl	Li et al. 2009
Sodium dodecylsulfate (SDS), phytic acid, stearic acid, ethylenediamine tetraacetic acid(EDTA)	AZ61 alloy	Alkaline medium.	Yang et al. 2009
8-Hydroxyquinoline and SDBS	AZ91D alloy	ASTM D1384-87	Gao et al. 2010
1,2,4-Triazole, salts of F^- and Ce^{3+}	AZ31 alloy	NaCl	Karavai et al. 2010
Phosphate and chromate	Pure Mg	NaCl	Williams et al. 2010
Cerium nitrate	AZ91D alloy	Na_2SO_4	Correa et al. 2011
Sodium silicate	AZ91D alloy	ASTM D1384-87	Gao et al. 2011
Amino acid methionine	Mg-Al-Zn alloy	NaCl	Helal 2011
Amino acids	Mg–Al–Zn alloy	Chloride free neutral solutions	Helal and Badawy 2011
Sodium aminopropyltriethoxysilicate and zinc nitrate	GW 103	ASTM D1384-87	Hu et al. 2011
Sodium phosphate and SDBS	GW103 alloy	Ethylene glycol	Huang et al. 2011

Inhibitor used	Material	Medium	Reference
5-(3-Aminophenyl)-tetrazole	Mg-Mn alloy	NaCl	Sherif and Almajid 2011
Sodium lauryl sulfate (SLS), SDBS, sodium salts of N-lauroylsarcosine (NLS) and N-lauroyl-N-methyltaurine (NLT)	AZ31 alloy	Na_2SO_4 and NaCl	Frignani et al. 2012
Cerium nitrate	AM 60 alloy	NaCl	Heakal et al. 2012
Tetraphenylporphyrin	AZ91D alloy	NaCl	Hu et al. 2012
Sodium fluoride	Mg-Zr alloy	Aqueous alkaline solutions	Lambertin et al. 2012
2-Hydroxy-4-methoxy-acetophenone (paeanol)	AZ91D alloy	NaCl	Hu et al. 2013
Surperhydrophobic film of tetradecanoic acid	AZ31 alloy	NaCl	Zhao et al. 2014a

1.15.3 Corrosion protection of magnesium alloy ZE41

The literature reveals various attempts to combat ZE41 corrosion, however, the use of inhibitors seem to have been overlooked. This trend nevertheless is least surprising given the complications associated with the use of inhibitors for ZE41. The alloy microstructure is unique with cathodic micro-constituents promoting micro-galvanic corrosion (Neil et al. 2009) and hence the inhibitor is required to selectively interact with different phases of the alloy. The real world applications of ZE41 being mostly outdoor where the salts in polluted humid air and road splash act as potential corrosives, the

traditional concept of inhibitor addition to aggressive media, which in this case, is an open environment would seem pointless. Moreover a spontaneously developed corrosion product surface film (Zhao et al. 2008b) gets in the way of inhibitor interaction with the bare metal surface. Furthermore, not every electron donating molecule (Lewis base) is capable of impeding ZE41 corrosion, as the major micro-constituent phase of the alloy (α-Mg matrix) is pure Mg having inferior complexing ability (poor Lewis acid) due to the high energy of *3d* orbitals of Mg (Hu et al. 2012). Thus the adsorption-type inhibitors turn out to be ineffectual and so do the passivating inhibitors, given the inability of Mg to exhibit an inherent active-passive transition. Thus in the context of ZE41 all one is left to experiment with are precipitating inhibitors, as appropriately pointed out by Yang et al. (2009) who claimed the capacity of a molecule to precipitate as its Mg-salt in aqueous solutions as a prerequisite to function as efficient magnesium corrosion inhibitor. Some chelates and surfactants exhibit this ability. With this background it is intended in the present work to explore some selected surfactants as inhibitors for ZE41 alloy.

Currently various other alternative corrosion mitigation measures are being worked out for the protection of ZE41. Some imperative works in recent times are listed in Table 1.5.

Table 1.5 Strategies for corrosion control of ZE41 alloy.

Method opted	Outcome	Reference
Laser surface cladding with Al-Si powder	ZE41 microstructure homogenized on laser surface cladding leading to improvement of corrosion resistance	Volovitch et al. 2008
Equal channel angular pressing (ECAP)	ECAP resulted in grain refinement of ZE41 leading to betterment of corrosion resistance and mechanical properties	Jiang et al. 2009
Sealed anodized coatings	Immersion in E-coating bath amplified the alloy corrosion resistance of ZE41	Song 2009

Method opted	Outcome	Reference
Thermally sprayed Al and Al/SiCp composite coating	The improvement in corrosion resistance of coated ZE41 has been attributed to resistive nature of Al	Carboneras et al. 2010
Excimer laser surface melting treatment	A refined microstructure post laser treatment enhanced corrosion resistance and micro-hardness of ZE41	Khalfaoui et al. 2010
Sol–gel silica coating	The coating functioned as an efficient physical barrier and remained effective for more than seven days of immersion in corrosive	López et al. 2010
Alkaline pre-treatment prior to silane coating	A suitable pre-treatment with alkali improves the corrosion protection ability of silane surface coatings	Banerjee and Raman 2011
Vanadia-based protective surface coatings	The coating diminished ZE41 corrosion and imparted a self-healing functionality for pitting repair	Hamdy et al. 2012
Duplex plasma electrolytic oxidation/epoxy-silane coating	The hybrid coating augmented the corrosion resistance of ZE41 with negligible signs of corrosion for more than a month of immersion in corrosive	Ivanou et al. 2013

1.15.4 Surfactants as corrosion inhibitors

Surfactants are amphiphilic molecules comprising of both hydrophilic (head) and hydrophobic (tail) groups. True to their name surfactants are surface-active agents and exhibit a tendency to accumulate at interfaces. Metal corrosion being a surface phenomenon, this tendency of surfactants to aggregate at interfaces comes in handy while inhibiting corrosion. For convenience the surfactants are grouped on the basis of the chemical nature of the head group, as non-ionic (or molecular), cationic, anionic and

zwitter-ionic. The hydrophilic head of the surfactants is known to facilitate interaction with metal surface which leads to physical or chemical adsorption depending upon the charge of the hydrophilic group and that on the metal. The hydrophobic tail is credited for the water-repellent nature of inhibited metal surfaces which is an icing on the cake, considering so many other advantages of surfactants as corrosion inhibitors, like easy preparation, cost-effectiveness and low toxicity (Migahed and Al-Sabagh 2009, Malik et al 2011). There are more works in literature than one can quote, where the anti-corrosion property of the surfactants has been focused for various metal types. Among the magnesium inhibitors specified in Table 1.4, the following are surfactants; sodium undecanoate, sodium decanoate, sodium heptanoate, SDBS, SDS, stearic acid, sodium lauryl sulfate and sodium salts of N-lauroylsarcosine and N-lauroyl-N-methyltaurine. Some relevant, most prominent and recent works on surfactant mediated corrosion inhibition of metals other than magnesium are mentioned in Table 1.6.

Table 1.6 Surfactants as corrosion inhibitors.

Surfactant used	Material	Medium	Reference
Dodecanol, decanol and octanol	Mild steel	NaCl	Wang and Free 2004
Sodium octyl sulfate, sodium decyl sulfate, sodium dodecyl sulfate, sodium hexadecyl sulfate, SDBS	Aluminium	HCl	Elewady et al. 2008
Nonionic Schiff base amphiphiles of *p*-aminobenzoic acid	Aluminium	HCl	Negm and Zaki 2008
Schiff base-based cationic gemini surfactants	Carbon steel	HCl	Hegazy 2009
Sodium benzoate	nano-crystalline pure iron	NaCl + Na_2SO_4	Afshari and Dehghanian 2010

Surfactant used	Material	Medium	Reference
Alkyldimethylisopropylammonium hydroxide cationic surfactants	Carbon steel	HCl	Badawi et al. 2010
Sodium decanoate	AA 2024 Al alloy	Na_2SO_4	Boisier et al. 2010
12-Aminododecanoic acid	Carbon steel	HCl	Ghareba and Omanovic 2010
Non-ionic TRITON-X series	Iron	HCl	Amin et al. 2011
Gemini Surfactants of the series 1,2-alkane-bis-(ethyl ammonium bromide)	Mild steel	Acetic acid	Ansari and Quraishi 2011
Vanillin derived Schiff base surfactants	Carbon steel	HCl	Negm et al. 2011
Sodium salts of azelaic, sebacic, pelargonic and capric acid	Mild steel	Aerated neutral solutions	Rammelt et al. 2011
Gemini surfactants of the series hexanediyl-1,6-bis-(diethyl alkyl ammonium bromide)	Aluminium	HCl	Zhang et al. 2011a
Anionic surfactants based on cottonseed oil	Carbon steel	CO_2 saturated NaCl	Abd El-Lateef et al. 2012
Sulfated fatty acid potassium salt	Mild steel	CO_2 saturated NaCl	Abbasov et al. 2013
SLS, SDBS, sodium salts of NLS and NLT	AA2198 Al alloy	NaCl	Balbo et al. 2013

Surfactant used	Material	Medium	Reference
SDBS	Ferrous alloy	H_2SO_4	Kellou-Kerkouche et al. 2013
Ascorbyl palmitate	Carbon steel	Ethanol blended gasoline	Deyab 2014

1.16 SCOPE AND OBJECTIVES OF THE PRESENT WORK

1.16.1 Scope of the work

Magnesium alloys are in the limelight these days. This class of alloys rightfully deserves all the attention and adulation given their wide spectrum of applications in both domestic and industrial domains. Even in the automotive industry the use of magnesium alloy parts have escalated in recent times. In this era where fuel prices are skyrocketing, achieving superior fuel efficiency is undoubtedly the topmost goal of the transport industry. It is this aim which keeps the structural engineers busy in constant quest for light-weight materials like magnesium alloys because automobile weight reduction is the key to bring down fuel consumption and vehicular exhaust emission.

ZE41 is one among the elite magnesium alloys designed for structural and weight-sensitive applications. Currently ZE41 is a sought-after aerospace and automobile material. Despite a picture-perfect combination of mechanical properties ZE41 stumbles to be an ideal material owing to its vulnerability towards corrosion. This corrosion susceptibility restrains the complete utility of ZE41 and the same demands an extra attention from a research perspective. As clearly highlighted in the review of literature, the research conducted so far to boost the corrosion resistance of ZE41 have focused only on microstructural alterations and surface modification (chemical conversion coatings, anodizing, laser surface alloying, electroplating, organic coating and sol-gel coating). Unfortunately these techniques are associated with major drawbacks. The chemical conversion coatings and anodizing techniques make use of chromate-based solutions. The hexavalent chromium being carcinogenic these conversion coating techniques turn out to

be detrimental from a safety point of view. The surface coats or films (electroplated, organic and sol-gel) show mediocre adhesion to the alloy surface. At last the laser surface cladding, though efficient fails to be cost-effective due to the requirement of sophisticated instrumentation (Zhang and Wu. 2010). The inhibitor addition as an environmental alteration measure has been popular for other alloys as an effective and economic approach for corrosion mitigation. Regrettably, the employment of the inhibitors for ZE41 protection remains as the discipline seldom explored. It goes without saying that for any magnesium allied technology to be triumphant, the use of efficient, green and economic corrosion mitigation measures is indispensable. Hence the development of corrosion inhibitors for ZE41 which meet the above laid requirements is need of the hour.

1.16.2 Objectives

1. To study the corrosion behavior of magnesium alloy ZE41 specimen in a medium of sulfate at different medium concentrations and solution temperatures.

2. To investigate the effect of chloride ions on the corrosion of magnesium alloy ZE41 in a sulfate medium at different solution concentrations and temperatures.

3. To establish the influence of pH of sulfate medium on corrosion behavior of magnesium alloy ZE41.

4. To synthesize and use some organic corrosion inhibitors and investigate their corrosion inhibition performances on magnesium alloy ZE41 in sulfate medium and combined medium containing both sulfate and chloride.

5. To carry out corrosion inhibition experiments at different temperatures to evaluate the activation parameters for the corrosion process.

6. To evaluate the thermodynamic parameters for the adsorption of inhibitor and to propose an apt mechanism for the inhibition of ZE41 corrosion in sulfate medium and combined medium.

1.17 OUTLINE OF THE THESIS

The present thesis has been suitably divided into four chapters. The contents pertaining to each chapter has been discussed in detail.

The **chapter 1** introduces some of the fundamental aspects of corrosion and some measures to monitor and combat the same. This chapter also accentuates magnesium alloys as the futuristic structural materials for weight-sensitive applications. Furthermore, the appropriate works in the literature which focuses upon the corrosion and the inhibition of pure magnesium and its alloys; especially ZE41 have been reviewed. The chapter towards the end recognizes the scope of the present work, by stating the importance of ZE41 and by identifying the flaws in the currently employed corrosion mitigation measures. The chapter eventually lays down the objectives of the current work.

The **chapter 2** is comprised of descriptions about the experimentation part. The specific procedures adopted for the preparation of the test specimen and the electrolyte solutions has been elucidated. The chapter also presents the operational specifications related to the employed electrochemical techniques along with the calculations which have enabled the deduction of the numerical results of the current work.

The **chapter 3** gives a detailed account of the comprehensive results obtained in the study. This chapter also provides the interpretation of the graphical and the numerical results. This chapter basically is an attempt to explicate the electrochemical behavior and corrosion inhibition of ZE41 on the basis of the results of the study.

The brief summary of the overall work along with the major conclusions drawn from the study have been put together to constitute the concluding chapter; **chapter 4**.

2.1 MATERIALS

The investigation in the present study was focused on magnesium alloy ZE41. It is a cast alloy where magnesium is alloyed with zinc, zirconium and rare earth elements (Ce, La, Pr, Sr and Nd). The average elemental composition of the alloy is presented in Table 2.1.

Table 2.1 Chemical composition of ZE41 magnesium alloy.

Element	Wt (%)
Zinc	4.49
Cerium (RE)	1.05
Zirconium	0.7
Lanthanum (RE)	0.48
Praseodymium (RE)	0.12
Magnesium	Balance

The alloy was procured in an extruded rod form. With an intension to maintain a constant exposure area throughout the study, ZE41 alloy rod was metallographically mounted in a cold setting epoxy resin up to approximately 40 mm height as shown in Fig. 2.1.

Fig. 2.1 Alloy specimen mounted in epoxy resin.

The surface area of ZE41 alloy, exposed to medium in all the conducted experiments documented in this thesis was 0.732 cm^2. The standard metallographic practices were

employed for polishing of test specimen (ZE41 alloy mounted in resin), which included sequential procedure; belt grinding followed by abrading using emery papers (of grades in the range 600-2000) and lastly a mirror polish was achieved using abrasive legated alumina smeared over a polishing wheel. Post polishing, the test specimen was washed with double distilled water, degreased with acetone and thoroughly air-dried prior to immersion in the medium.

2.2 MEDIA

The experiments were conducted in two different media; sodium sulfate (Na_2SO_4) and mixture of sodium sulfate and sodium chloride (NaCl). For convenience the latter medium mixture will be referred to as the combined medium henceforth. The analyses were carried out at specific temperatures, 30 °C, 35 °C, 40 °C, 45 °C and 50 °C (± 0.5 °C) by means of a calibrated thermostat set up, under unstirred conditions.

2.2.1 Preparation of standard sodium sulfate solutions

The standard solution of sodium sulfate of 1.0 M concentration was initially prepared as the stock solution by dissolving analytical grade sodium sulfate salt in double distilled water both taken in appropriate amounts. The stock solution was subsequently diluted to obtain series of concentrations 0.2 M, 0.4 M, 0.6 M, and 0.8 M.

2.2.2 Preparation of combined media

The combined media containing both Na_2SO_4 and NaCl were prepared in total six different concentrations as mentioned below:

0.2 M Na_2SO_4 - 0.1 M NaCl, 0.2 M Na_2SO_4 - 1.0 M NaCl, 0.6 M Na_2SO_4 - 0.1 M NaCl, 0.6 M Na_2SO_4 - 1.0 M NaCl, 1.0 M Na_2SO_4 - 0.1 M NaCl and 1.0 M Na_2SO_4 − 1.0 M NaCl

These solutions were prepared by dissolving appropriate amounts of both analytical grade sodium sulfate and sodium chloride salts in double distilled water.

2.2.3 Preparation of sulfate media with varying solution pH

A part of the study dealt with understanding the influence of solution pH on corrosion of ZE41. For this particular investigation the sulfate media of concentrations 0.2 M, 0.6 M and 1.0 M were prepared by dissolving analytical grade sodium sulfate salt in double distilled water. The pH of the solutions were adjusted to desired value (pH = 2, 5, 7, 9, 12 for each sulfate concentration) with H_2SO_4 and NaOH, using a calibrated pH meter.

2.3 INHIBITORS

Five different anionic surfactants were prepared and tested for their inhibition effect. The studied inhibitors included stearate, palmitate, myristate, laurate and caprylate which, respectively, are conjugate bases of long chain monocarboxylic acids, stearic acid $(CH_3(CH_2)_{16}COOH)$, palmitic acid $(CH_3(CH_2)_{14}COOH)$, myristic acid $(CH_3(CH_2)_{12}COOH)$, lauric acid $(CH_3(CH_2)_{10}COOH)$ and caprylic acid $(CH_3(CH_2)_6COOH)$. The common molecular formula of the carboxylate inhibitors is shown in Fig. 2.2.
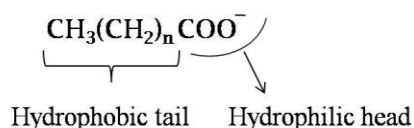
Fig. 2.2 Molecular formula of alkyl carboxylate inhibitors.

The inhibitors; stearate, palmitate, myristate, laurate and caprylate were prepared in aqueous solutions as dissolved sodium salts by neutralization of equimolar amounts of respective conjugate acids and NaOH. All the prepared carboxylates were tested for their ability to precipitate as magnesium salts in aqueous solutions; a criterion for precipitation-type magnesium inhibitors, by adding a solution of $MgCl_2$ to a part of formerly prepared sodium carboxylate solutions, both taken in equivalent amounts. All the alkyl carboxylates precipitated as magnesium carboxylates owing to sparingly soluble nature of the Mg-salts. The precipitated magnesium carboxylates were filtered, washed

with water, dried and finally verified through melting point (M.P) analysis. (M.P. of magnesium stearate = 132 - 133 ºC, magnesium palmitate = 120 - 121 ºC, magnesium myristate = 117 - 118 ºC, magnesium laurate = 148 - 149 ºC and magnesium caprylate = 104 - 105 ºC). The primarily prepared sodium carboxylate solutions were maintained as the stock solutions, from which the required inhibitor solutions of optimized concentrations were prepared through dilution with the required electrolyte medium.

2.4 METHODS

2.4.1 Electrochemical techniques

All the electrochemical investigations were conducted by means of electrochemical work station; Gill AC furnished with ACM instrument Version 5 software. A conventional arrangement of three-electrode compartment Pyrex glass cell was made use of. The ZE41 alloy specimen coupon was converted into the working electrode alongside a platinum counter electrode and a saturated calomel electrode (SCE) as reference. All the electrode potentials mentioned in this thesis should, therefore, be considered with respect to that of SCE. The working electrode on immersion into the electrolyte medium was allowed to establish a steady-state and the attainment of the steady-state was supervised by monitoring the change in potential of the working electrode with respect to time. Both polarization and impedance measurements were initiated only after the attainment of a steady-state with equilibrium electrode potential corresponding to the open circuit potential (OCP). The EIS studies and polarization studies were performed consecutively without subjecting the specimen to any additional surface treatment in-between. A minimum of three trials were carried out to ensure the reproducibility of the results and the average of the values were documented. The instrumentation set up employed for the electrochemical studies is shown in Fig. 2.3.

2.4.1.1 Potentiodynamic polarization method (Tafel extrapolation technique)

The specimen at a steady-state was polarized by drifting the potential -250 mV cathodically and +250 mV anodically relative to the OCP at a scan rate of 1 mV s^{-1}. The

instrument simultaneously developed the potentiodynamic current - potential curves (Tafel curves). The potentiodynamic parameters relevant in corrosion studies were deduced by the analysis of the Tafel plots.

Fig. 2.3 The instrumentation set up used for electrochemical studies.

2.4.1.2. Electrochemical impedance spectroscopy (EIS) studies

In impedance technique the measurements were performed at OCP. In this procedure a small amplitude (10 mV) sinusoidal ac voltage perturbation centered around the steady-state potential, in wide frequency range (100 kHz to 0.01 Hz) was applied to the system. The system generated Nyquist and Bode plots were interpreted to comprehend the corrosion behavior. The impedance data points were simulated with a suitable theoretical model corresponding to an equivalent electrical circuit using ZSimpWin software version 3.21. Such a simulation study yielded the impedance parameters.

2.4.2 Surface analysis

The morphology and composition of the specimen surface was examined by respectively, recording SEM images and EDX spectra of different samples using JEOL JSM-6380LA analytical scanning electron microscope.

2.5 CALCULATIONS

2.5.1 Computation of corrosion rate

The values of corrosion current density (i_{corr}) were deduced from the extrapolation of cathodic Tafel branches to the corrosion potential. The experimentally determined i_{corr} values were utilized in computation of the corrosion rate (v_{corr}) using the equation mentioned below (ASTM Standard G102 1999).

$$v_{corr} \ (\text{mm y}^{-1}) = \frac{K \ \times \ i_{corr} \ \times \ EW}{\rho} \tag{2.1}$$

where K is the constant which defines the unit of corrosion rate. For v_{corr} expressed in the unit mm y^{-1}, the constant takes up the value, $K = 0.00327$ mm g/μA cm y. Furthermore, i_{corr} is the corrosion current density expressed in μA cm^{-2}, ρ is the density of the corroding material, in the present instance, the density of ZE41 alloy which is equal to 1.84 g cm^{-3}, EW is the equivalent weight of the alloy, which was calculated using the following expression (ASTM Standard G102 1999).

$$EW = \frac{1}{\sum [\frac{n_i \times f_i}{W_i}]} \tag{2.2}$$

where f_i, W_i and n_i, respectively, are the weight fraction, atomic weight and valence of the ith element of the alloy. The values of f_i, W_i and n_i, of four major elements present in ZE41 are mentioned in Table 2.2.

The substitution of the values listed in Table 2.2 into Equation 2.2, gives the equivalent weight of the ZE41 alloy as shown in the calculation given below.

$$EW \text{ of ZE41} = \frac{1}{\left(\dfrac{0.937 \times 2}{24.305}\right) + \left(\dfrac{0.045 \times 2}{65.38}\right) + \left(\dfrac{0.011 \times 4}{140.116}\right) + \left(\dfrac{0.007 \times 4}{91.224}\right)} = 12.64 \tag{2.3}$$

Table 2.2 The valence, weight fraction and atomic weight of major elements present in ZE41 alloy.

Element	n_i	f_i	W_i
Mg	2	93.7	24.305
Zn	2	4.5	65.38
Ce (RE)	4	1.1	140.116
Zr	4	0.7	91.224

2.5.2 Calculation of inhibition efficiency

The inhibition efficiency (η) was evaluated as a function of surface coverage (θ) and the relation between the two is presented in the following equation.

$$\eta\ (\%) = \theta \times 100 \qquad (2.4)$$

The value of θ was deduced from the results of electrochemical measurements. The i_{corr} values obtained from the Tafel polarization studies and values of R_{hf} (overall resistance associated with higher frequency capacitive loop of the Nyquist plots) acquired from EIS measurements were used separately in evaluation of θ, as per the equations presented below.

$$\theta = \frac{i_{corr\ (b)} - i_{corr\ (inh)}}{i_{corr\ (b)}} \qquad (2.5)$$

$$\theta = \frac{R_{hf\ (inh)} - R_{hf\ (b)}}{R_{hf\ (inh)}} \qquad (2.6)$$

where $i_{corr\ (b)}$ and $R_{hf\ (b)}$, respectively, are the i_{corr} and R_{hf} values for the blank media in the absence of the inhibitor, whereas the same for the solutions containing the inhibitor are $i_{corr\ (inh)}$ and $R_{hf\ (inh)}$, respectively.

2.5.3 Evaluation of activation parameters

The activation parameters for the corrosion of ZE41 under various conditions were calculated. The estimated activation parameters included apparent activation energy (E_a), apparent enthalpy of activation ($\Delta H^{\#}$) and apparent entropy ($\Delta S^{\#}$) of activation. Arrhenius law equation (Eq.2.7) and transition state equation (Eq.2.8) were employed for the estimation as explained in the following.

Arrhenius law equation:

$$\upsilon_{\text{corr}} = A \, e^{-\frac{E_a}{RT}} \tag{2.7}$$

where A is proportionality constant which is dependent on the type of the metallic material, T is absolute temperature, R is the universal gas constant and υ_{corr} is corrosion rate. Arrhenius plots are typical plots of ln (υ_{corr}) versus reciprocal of absolute temperature ($1/T$) which yielded straight lines. The slope values of the straight lines were utilized in the deduction of E_a (slope = - E_a / R).

Transition state equation:

$$\upsilon_{\text{corr}} = \frac{RT}{Nh} \, e^{\frac{\Delta S^{\#}}{R}} \, e^{-\frac{\Delta H^{\#}}{RT}} \tag{2.8}$$

where h is Planck's constant and N is Avogadro's number. The parameters $\Delta H^{\#}$ and $\Delta S^{\#}$ were calculated, respectively, from the slope (slope = -$\Delta H^{\#}/R$) and intercept (intercept = ln (R/Nh) + $\Delta S^{\#}/R$) values of the straight lines obtained from the plots of ln (υ_{corr} /T) versus ($1/T$).

2.5.4 Calculation of thermodynamic parameters

The calculations of the thermodynamic parameters for the adsorption of inhibitor were based on a suitable adsorption isotherm model with which the system under the study showed best agreement. An adsorption isotherm is defined as a graphical

representation showing the variation of extent of adsorption with pressure at a given constant temperature. For the adsorption occurring at solution/solid interface, the concentration of the adsorbate (inhibitor) can be considered as the equivalent of pressure. The mathematical expression for the adsorption isotherms highlights an equilibrium relation between inhibitor concentrations on metal surface and that in bulk solution. Hence the adsorption isotherms are applicable to the systems where the inhibition is the consequence of surface coverage brought about by the inhibitor on adsorption. Some adsorption isotherms which are commonly verified to explain corrosion inhibition, their mathematical expressions and verification plots are presented in Table 2.3.

Table 2.3 List of adsorption isotherms

Name	Isotherm	Verification Plot
Langmuir	$\theta/(1-\theta) = \beta C$	(C/θ) vs. C
Frumkin	$[\theta/(1-\theta)]\ e^{f\theta} = \beta C$	θ vs. log C
Bockris-Swinkels	$\theta/(1-\theta)^n.[\ \theta + n(1-\theta)]^{n-1}/n^n =$ $C.e^{-\beta}/55.4$	$\theta/(1-\theta)$ vs. log C
Temkin	$\theta = (1/f) \ln KC$	θ vs. log C
Virial Parson	$\theta.e^{2f\theta} = \beta C$	θ vs. log(θ/C)
Flory Huggins	$\log(\theta/C) = \log \chi K + \chi \log (1-\theta)$	log (θ/C) vs. log$(1-\theta)$
El – Awady	$\log [\theta/(1-\theta)] = \log K + Y \log C$	log $[\theta/(1-\theta)]$ vs log C.

The parameters in the Table 2.3 include θ which is surface coverage, $\beta = \Delta G/2.303RT$, where ΔG is free energy change for adsorption, R is gas constant, T is temperature, C is inhibitor concentration in bulk electrolyte, χ is size ratio or the number of water molecules replaced per molecule of adsorbed inhibitor, f is inhibitor interaction parameter (0 implies no interaction; positive value implies attraction; negative value implies repulsion) and K and Y are constants.

The C and θ values from the current study involving alkyl carboxylates as inhibitors showed best agreement with the Langmuir adsorption isotherm. The standard

free energy of adsorption (ΔG°_{ads}) for the present system obeying Langmuir isotherm was computed as per the following expression which has been derived from the mathematical expression of Langmuir isotherm.

$$\Delta G^\circ_{ads} = -RT \ \ln \left[\frac{55.5 \times \theta}{C \ (1-\theta)} \right] \tag{2.9}$$

where C is the inhibitor concentration expressed in unit mol.dm^{-3} and 55.5 in mol dm^{-3} is the molar concentration of water in solution.

The standard enthalpy of adsorption (ΔH°_{ads}) and standard entropy of adsorption (ΔS°_{ads}) were evaluated by making use of a rearranged form of Gibbs-Helmholtz equation, as shown below.

$$\Delta G^\circ_{ads} = \Delta H^\circ_{ads} - T\Delta S^\circ_{ads} \tag{2.10}$$

As per the Equation 2.10, straight lines were obtained on graphically plotting the variation of ΔG°_{ads} with T. The slope and the intercept of the lines were, respectively, equal to ΔS°_{ads} and ΔH°_{ads}.

3.1 CORROSION BEHAVIOR OF ZE41 IN AQUEOUS SALT SOLUTIONS

3.1.1 Potentiodynamic polarization measurements

The corrosion behavior of the magnesium alloy ZE41 in blank aqueous salt solutions was established by exposing the alloy to conditions of varied temperature, ionic concentrations and medium pH, followed by the electrochemical monitoring. Fig. 3.1 (a), Fig. 3.1 (b) and Fig. 3.1 (c), respectively, represent the potentiodynamic polarization plots for the corrosion of ZE41 alloy at 30 °C, in sodium sulfate solutions of different concentrations, in 1.0 M Na_2SO_4 containing different concentrations of chloride and in 0.6 M Na_2SO_4 solution with gradually varying pH. All the plots chosen for illustration throughout this thesis are representative and henceforth it goes without saying that similar plots have been obtained at other respective conditions under consideration.

It is evidently seen from the Tafel plots in Fig. 3.1 that the polarization curves tend to shift towards the region of higher current density with the increase in the concentration of sulfate, chloride and with the diminution in medium pH. Such a shift is indicative of increased rate of alloy corrosion. Hence higher ionic concentration and lower pH tend to increase the dissolution of the ZE41 alloy. The anodic reaction of metal dissolution is represented in the Tafel plots by the anodic branches extending towards more positive potentials. Contrary to the expectations, the anodic branches of polarization curves are not linear, in terms that these branches exhibit two different slopes. Such an inflection in anodic curves appears at potentials more positive than corrosion potential (E_{corr}) and is thought to represent some sort of a kinetic barrier effect, probably the outcome of deposition of a surface film and its subsequent breakdown at higher anodic overvoltages due to rapid evolution of hydrogen. Such an asymmetry among the Tafel branches has been reported by Wang et al. (2010b) for Mg-Al-Pb alloy and by Zhao et al. (2008b) for ZE41 alloy. At potentials more negative than E_{corr} the cathodic reduction reaction predominates resulting in cathodic current as represented by cathodic branches

of the Tafel plots (Tamar and Mandler 2008). The linear nature of the cathodic Tafel branches is duly exploited in the deduction of the corrosion current density (i_{corr}) by cathodic Tafel extrapolation to corrosion potential.
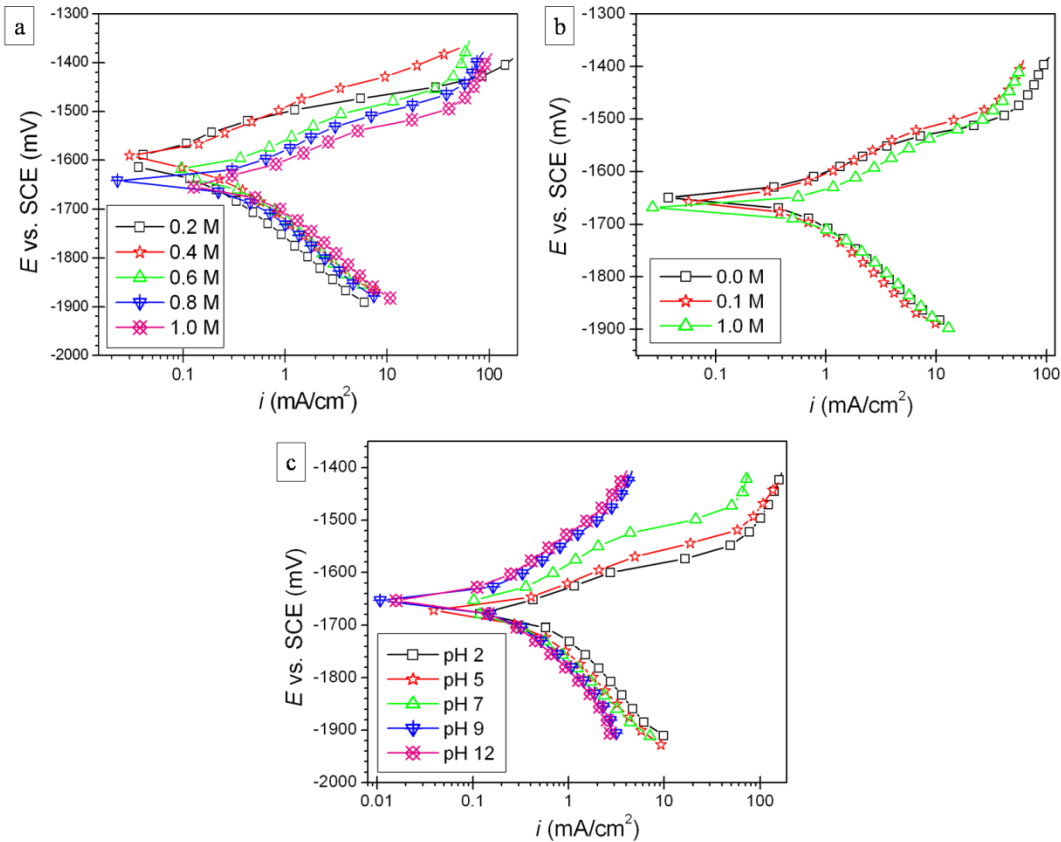
Fig. 3.1 The potentiodynamic polarization plots for the corrosion ZE41 alloy at 30 °C (a) in sodium sulfate solutions of different concentrations, (b) in 1.0 M Na$_2$SO$_4$ solution containing different concentrations of chloride and (c) in 0.6 M Na$_2$SO$_4$ solution with gradually varying pH.

Table 3.1 (a), Table 3.1 (b) and Table 3.1 (c), respectively, shows the deduced electrochemical polarization parameters like E_{corr}, i_{corr} and cathodic slope (b_c) for the corrosion of ZE41 alloy, in sodium sulfate media of different ionic concentrations at different temperatures, in combined media of different ionic concentrations at different temperatures and in sodium sulfate solutions with gradually varying pH and sulfate ion

concentrations at 30 ℃. The values of corrosion rate (v_{corr}) tabulated in Table 3.1 were evaluated as per Equation 2.1.

At any particular temperature the rate of ZE41 alloy corrosion (v_{corr}) as apparently seen from Table 3.1 (a) and Table 3.1 (b), increases with the increase in ionic concentration. A trend of higher corrosion rate associated with a higher sulfate ion concentration at each pH and with a lower pH at each sulfate ion concentration is seen from Table 3.1 (c). Furthermore, it can be collectively observed from Table 3.1 that an increase in v_{corr} is mostly associated with a cathodic shift of E_{corr} towards more active (more negative) potentials. Such a trend of higher v_{corr} accompanied by more negative E_{corr} though frequently observed for magnesium and its alloys (Baril and Pebere 2001, Zhao et al. 2008b) cannot be inferred as a characteristic phenomenon and remain ambiguous, as many studies have reported the contradictory results, where no such correlation between v_{corr} and E_{corr} has been seen. The response of the system towards changing ionic concentrations and pH is further reflected in slight but noticeable variations in cathodic slope (b_c) values. Such alterations in b_c values insinuate the impact these factors like ionic concentrations and pH have on the kinetics of cathodic reaction.

3.1.2 Electrochemical impedance spectroscopy studies

The impedance results were obtained as Nyquist plots for various conditions tested in the study. Fig. 3.2 (a), Fig. 3.2 (b) and Fig. 3.2 (c), respectively, correspond to the Nyquist plots for the corrosion of ZE41 alloy at 30 °C, in sodium sulfate solutions of different concentrations, in 0.6 M Na_2SO_4 with varying chloride concentrations and in 1.0 M Na_2SO_4 solution with gradually varying pH.

All the Nyquist plots display two depressed capacitive loops at the regions of higher and medium applied frequencies; former is comparatively much bigger than the later. The capacitive loops are followed by the beginning of an inductive loop at lower frequency region. The interpretation of such a frequency specific impedance behavior of magnesium alloys continues to be a subject of debate. A most common explanation

which is often cited in the literature attributes the higher frequency (*hf*) capacitive loop to the charge transfer of corrosion process and surface film effects. The medium frequency (*mf*) capacitive loop on the other hand is thought to be the consequence of mass transport (diffusion or electrolyte ingress) in solid phase through the corrosion product layer and finally the lower frequency (*lf*) inductive loop has been attributed to the relaxation of surface adsorbed intermediates like $Mg(OH)^+_{ads}$ and Mg^+_{ads} (Pebere et al. 1990, Baril and Pebere 2001, Mathieu et al. 2002, Zucchi et al. 2006, Ardelean et al. 2008, Frignani et al. 2012).
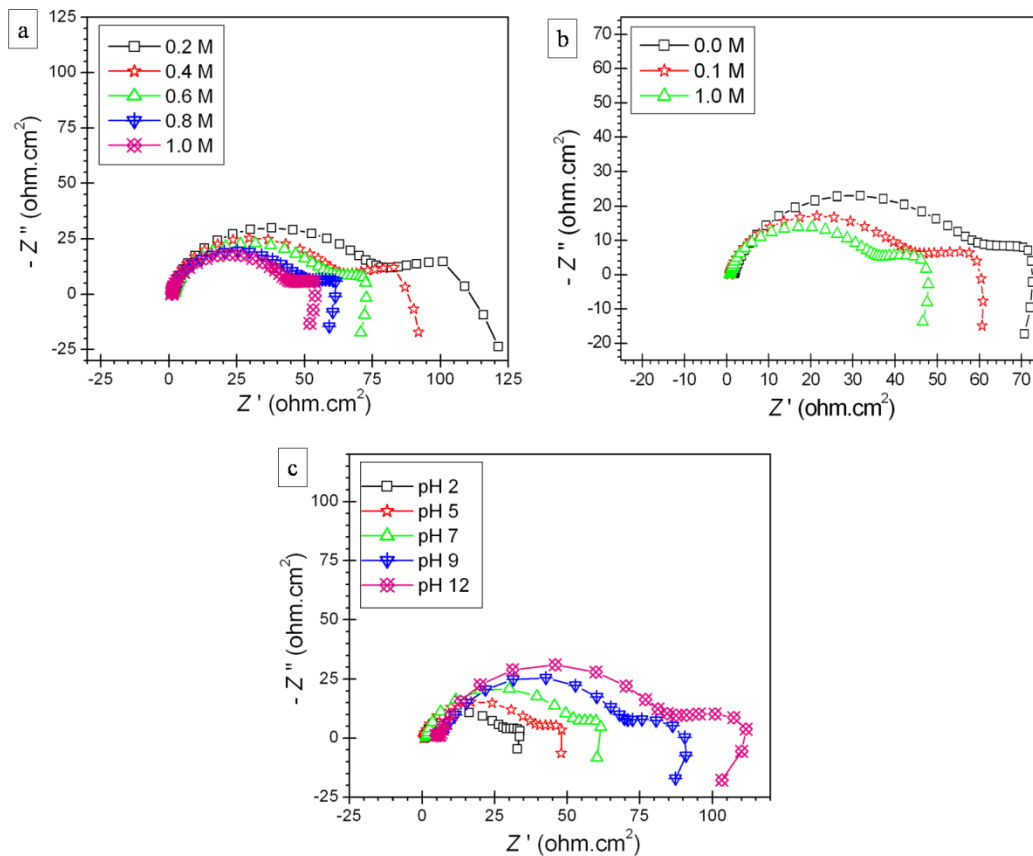
Fig. 3.2 The Nyquist plots for the corrosion ZE41 alloy at 30 °C (a) in sodium sulfate solutions of different concentrations, (b) in 0.6 M Na₂SO₄ solution containing different concentrations of chloride and (c) in 1.0 M Na₂SO₄ solution with gradually varying pH.

Among other impedance interpretations, Cheng et al. (2009) considered the appearance of the *lf* inductive loop as a consequence of partial protection offered by the surface film and the Nyquist plots for majority of aluminium containing alloys of magnesium are known to exhibit two capacitive loops at higher and lower frequencies, which have been described respectively, as the consequences of surface film formation and interfacial Faradaic charge transfer (Rosalbino et al. 2006, Badawy et al. 2010, Gao et al. 2010, Huang et al. 2011).

In general the diameter of the capacitive loops of the Nyquist plots symbolizes the corrosion resistance of the material and varies proportionally with it (Pebere. et al. 1990, Gao et al. 2010). As observed from the Fig. 3.2, the decrease in the medium pH and the increase in the concentrations of sulfate and chloride, cause the capacitive loops to increasingly shrink in diameter, suggesting a diminution in the corrosion resistance or in other words, the increase in the rate of the alloy corrosion.
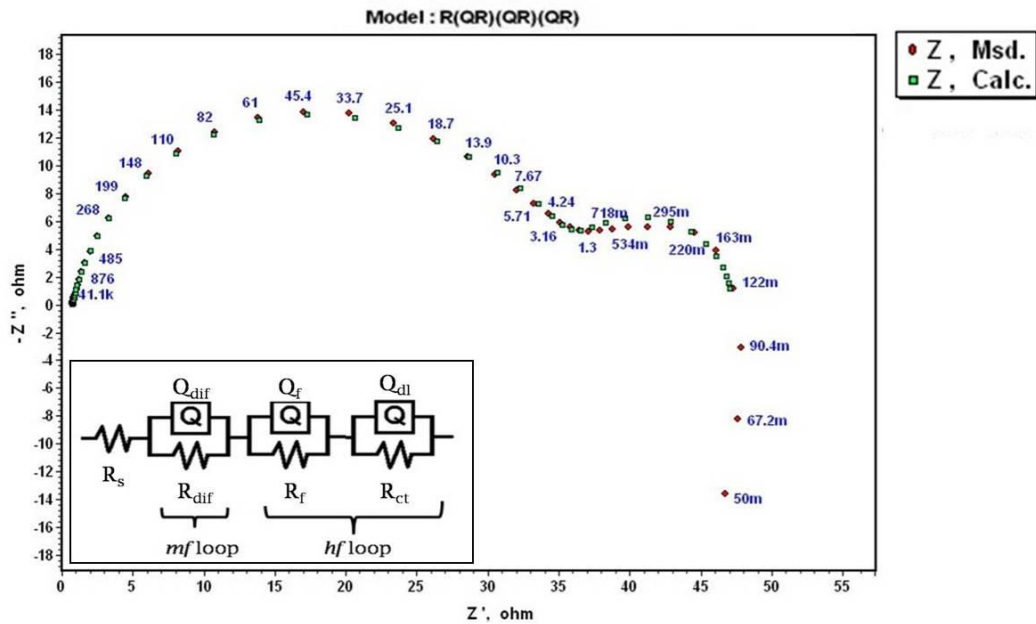
Fig. 3.3 The simulation of experimental impedance data points with theoretical model for the corrosion of ZE41 alloy specimen in the combined medium containing

0.6 M Na₂SO₄ and 1.0 M NaCl at 30 °C (inset: equivalent electrical circuit used for the simulation of the experimental impedance data points).

The impedance parameters are deduced from simulation analyses. The impedance data points excluding the *lf* inductive loop can be analyzed using an equivalent electrical circuit (EEC) most suited for the system under study, as depicted in the inset of Fig. 3.3. A representative simulation plot is shown in Fig. 3.3. In simulation analyses carried out throughout this entire study, the measurement errors in impedance data were well below 5%. The *hf* response which is the resultant of charge transfer and surface film effects is simulated using two parallel combinations of resistance and constant phase element, in series with each other; that is, the charge transfer resistance (R_{ct}) parallel to CPE (Q_{dl}) of the double layer and resistance of surface film (R_f) parallel to CPE of the surface film (Q_f). The *mf* response is fitted with a parallel network of resistance (R_{dif}) and CPE (Q_{dif}) associated with the process of electrolyte diffusion (Zucchi et al. 2006, Frignani et al. 2012).

In simulation analyses in order to achieve a more accurate fit to the depressed semicircles, the capacitive behavior is represented using the constant phase element (Q) instead of the ideal capacitive element. The surface heterogeneities such as porosity and roughness engender frequency dispersion during the impedance analysis and the consequence of which is reflected in the depressed nature of Nyquist semicircles (Jüttner 1990). The impedance of a constant phase element is given by the expression shown below (Eq.3.1) (Mansfeld et al. 1992).

$$Z_Q = Y_0^{-1}(j\omega)^{-n} \tag{3.1}$$

where Y_0 is the CPE constant, ω is the angular frequency (in rad s⁻¹), $j^2 = -1$ is the imaginary unit and n is a CPE exponent which reflects the degree of the surface heterogeneity. The value of n falls in the range from -1 to +1. CPE simulates an ideal capacitor when $n = 1$, an ideal inductor for $n = -1$, and an ideal resistor for $n = 0$. The

actual capacitance after taking into consideration the frequency dispersion is calculated using the following expression (Eq. 3.2) (Mansfeld et al. 1992).

$$C = Y_0(\omega_{max})^{n-1}$$

(3.2)

where ω_{max} is the frequency at which the imaginary part of the impedance (Z'') has a maximum.

The impedance parameters such as R_{hf} (overall resistance associated with higher frequency capacitive loop of the Nyquist plots), C_{dl} (capacitance of electrical double layer), R_f (film resistance) and C_f (capacitance of surface film) are deduced from the impedance measurements. Table 3.2 (a), Table 3.2 (b) and Table 3.2 (c), respectively, shows the evaluated electrochemical impedance parameters for the corrosion of ZE41 alloy, in sodium sulfate media of different ionic concentrations at different temperatures, in combined media of different ionic concentrations at different temperatures and in sodium sulfate solutions with gradually varying pH and sulfate ion concentrations at 30 °C.

For pure magnesium and its alloys R_{hf} has been found to inversely vary with the corrosion rate (Zucchi. et al. 2006) and hence any factor which brings about a decrease in R_{hf} actually enhances the alloy corrosion. The collective observations pertaining to the variations in R_{hf} at any particular temperature as seen from the Table 3.2 (a) and Table 3.2 (b) suggest an increase in corrosion rate with the increase in ionic concentrations of both the sodium sulfate and combined media. A trend of higher corrosion rate corresponding to a higher sulfate ion concentration at each pH and with a lower pH at each sulfate ion concentration is noticed from Table 3.2 (c). Another noteworthy observation that follows from Table 3.2 is the pattern of a higher R_{hf} invariably associated with a higher R_f and lower C_{dl} and C_f. R_f symbolizes the extent of protection offered by the surface film. On the other hand a lower C_{dl} and C_f can result as the consequence of the reduction in local dielectric constant and/or increase in thickness of electrical double

layer and surface film, respectively, as postulated by the Helmholtz model (Eq. 3.3) (Srinivasan 2006).

$$C = \frac{\varepsilon}{4\pi d}$$

(3.3)

where C is the capacitance, ε is the local dielectric constant and d is the thickness of the electrical double layer or that of the surface film. The variations in R_f and C_f together suggest that at lower ionic concentrations and alkaline pH, a more protective and thick film exists on the alloy surface which subsequently protects the underlying alloy by reducing the corrosive attack. This justifies the lower corrosion rates observed at lower ionic concentrations and in alkaline media.

3.1.3 Effect of temperature

The metallic corrosion basically is a redox chemical reaction, the kinetics of which is bound to be influenced to a large extent by the changes in temperature. The temperature effects were examined through electrochemical monitoring of ZE41 corrosion in both sodium sulfate and the combined medium. Fig. 3.4 (a) and Fig. 3.4 (b), respectively, shows the potentiodynamic polarization curves for the corrosion of ZE41 alloy at different solution temperatures, in 0.2 M Na_2SO_4 and in the combined medium containing 0.2 M Na_2SO_4 and 1.0 M NaCl. The Nyquist plots for the same in 0.2 M Na_2SO_4 and in combined medium containing 0.6 M Na_2SO_4 and 0.1 M NaCl are presented in Fig. 3.5 (a) and Fig. 3.5 (b), respectively.

It can be markedly observed from the Fig. 3.4 and Fig. 3.5 that the increase in medium temperature makes the polarization curves to shift towards higher current density region and capacitive semicircles in the Nyquist plots to shrink in diameter, both of which signify an increase in the rate of corrosion. The influence of temperature is rather apparent from the variation in the electrochemical parameters enlisted in Table 3.1 (a), Table 3.1 (b) Table 3.2 (a) and Table 3.2 (b), where in both sodium sulfate and the combined media, at any particular medium concentration the rate of ZE41 corrosion

increases with the increase in the temperature. Furthermore, at any specific medium concentration, the thickness and the protective performance of the surface film are optimal at lower temperatures, as precisely reflected by the combination of values; smaller C_f and larger R_f, which is observed only at lower temperatures.
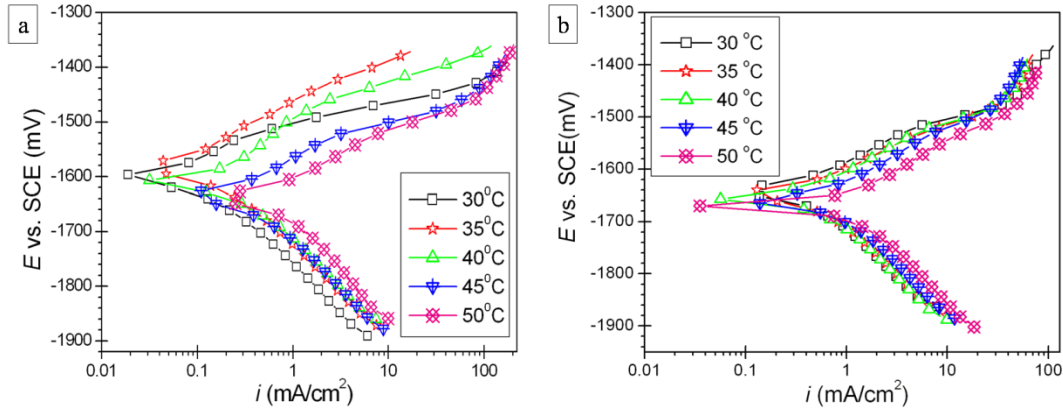
Fig. 3.4 Potentiodynamic polarization curves for the corrosion of ZE41 alloy at different solution temperatures in (a) 0.2 M Na₂SO₄ and (b) the combined medium containing 0.2 M Na₂SO₄ and 1.0 M NaCl.
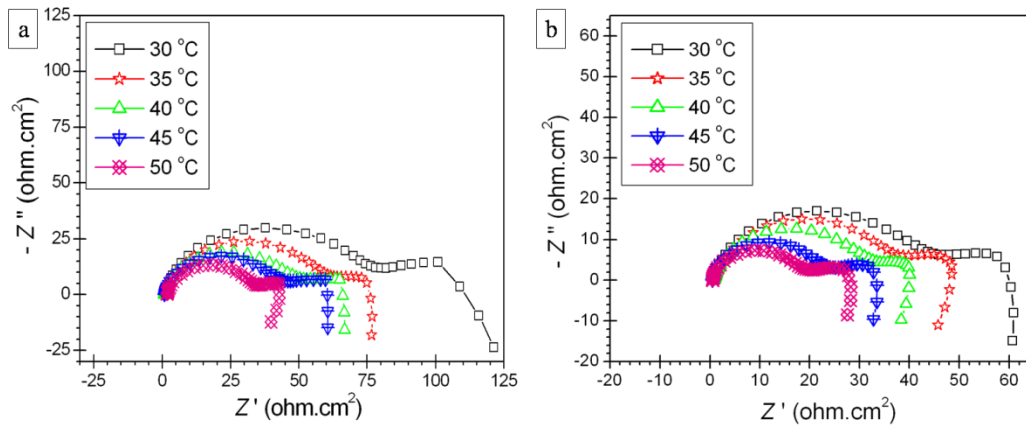
Fig. 3.5 Nyquist plots for the corrosion of ZE41 alloy at different solution temperatures in (a) 0.2 M Na₂SO₄ and (b) the combined medium containing 0.6 M Na₂SO₄ and 0.1 M NaCl.
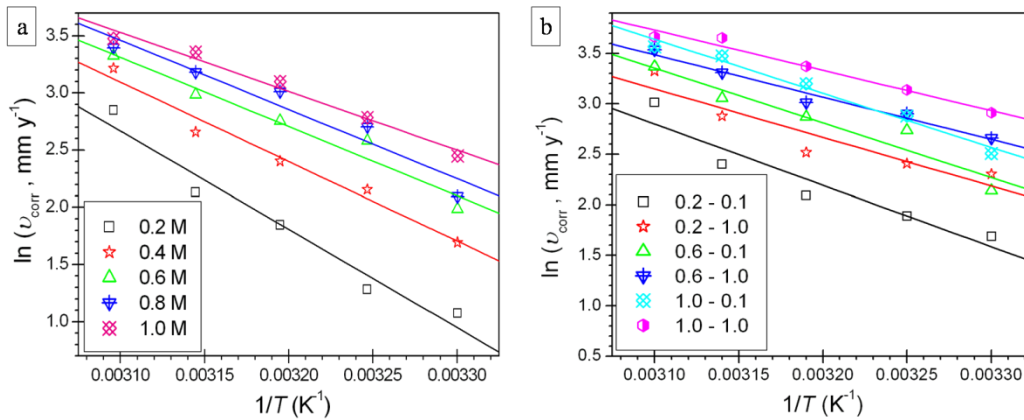
Fig. 3.6 Arrhenius plots for the corrosion of ZE41 alloy specimen at different ionic concentrations of (a) sodium sulfate media and (b) the combined media (Na$_2$SO$_4$ – NaCl in M).
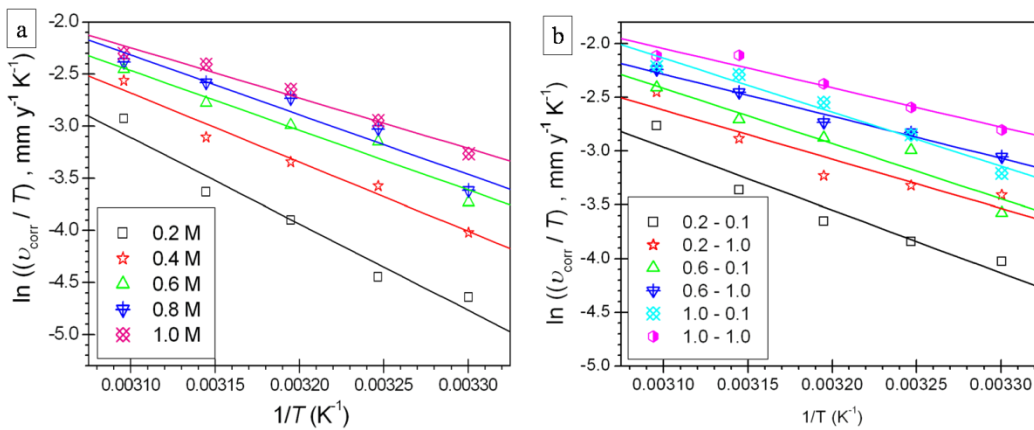
Fig. 3.7 ln (v_{corr}/T) vs. (1/T) plots for the corrosion of ZE41 alloy specimen at different ionic concentrations of (a) sodium sulfate media and (b) the combined media (Na$_2$SO$_4$ – NaCl in M).

The study of corrosion in a range of temperature is fruitful in ways more than one; in terms that, it not only establishes the impact of temperature on the corrosion rate but also facilitates the evaluation of activation parameters pertaining to the alloy dissolution. Arrhenius law equation (Eq.2.7) and transition state equation (Eq.2.8) as stated in the previous chapter, were utilized for the determination of apparent activation energy (E_a), apparent enthalpy of activation ($\Delta H^{\#}$) and apparent entropy ($\Delta S^{\#}$) of activation. Arrhenius

plots for the corrosion of ZE41 alloy specimen in sodium sulfate and the combined media are represented in Fig. 3.6 (a) and Fig. 3.6 (b), respectively. The ln (v_{corr} /T) versus (1/T) plots for the same are shown in Fig. 3.7 (a) and Fig. 3.7 (b), respectively. The calculated activation parameters corresponding to the dissolution of ZE41 alloy in sodium sulfate and the combined media are tabulated in Table 3.3 (a) and Table 3.3 (b), respectively.

The E_a is synonymous with the energy barrier for the occurrence of corrosion. The progressive diminution in E_a with the increased ionic concentration of the media as seen from Table 3.3 (a) and Table 3.3 (b), point out that the corrosion of ZE41 is energetically more feasible in concentrated media (Ashassi-Sorkhabi et al. 2005). The pattern of variation of $\Delta H^{\#}$ values is identical to that of E_a. The negative values of $\Delta S^{\#}$ suggest a decrease in randomness of the system which could be the consequence of association of the reactants during the formation of the activated complex in the rate-determining step of corrosion (Bentiss et al. 2005).

3.1.4 Mechanism of ZE41 alloy corrosion

3.1.4.1 Anodic dissolution of magnesium and negative difference effect [NDE]

The particularities of electrochemical dissolution of pure magnesium holds good even for its alloys. The electrochemical behavior of magnesium anode has been documented extensively and understanding this behavior is a prerequisite to comprehend the corrosion of magnesium alloys. In literature the electrochemical anodic dissolution behavior of pure magnesium and its alloys has been described as an anomalous phenomenon termed as negative difference effect, which is evidenced from a practical perspective on application of anodic overvoltage (Song et al. 1997b). For pure magnesium and its alloys, the application of anodic overvoltage (potential more positive than E_{corr}), is expected to lessen the rate of hydrogen evolution, instead the rate is found to increase and the rate of anodic dissolution of magnesium has been shown to increase to an extent beyond the expected range.

To complete the discussion on negative difference effect, the electrochemical reactions occurring during magnesium corrosion have to be considered. Greenblatt (1956) proposed an overall reaction for magnesium corrosion in aqueous solutions as represented by Equation 3.4 , where magnesium corrodes on reaction with water to form the principal corrosion product magnesium hydroxide ($Mg(OH)_2$), along with the simultaneous evolution of hydrogen.

$$Mg + 2H_2O \rightarrow Mg(OH)_2 + H_2 \tag{3.4}$$

The medium chosen for the present study is a near-neutral aqueous salt solution, in which the predominant cathodic reaction of corrosion will be the hydrogen evolution through electrochemical reduction of water as shown below.

$$2H_2O + 2e^- \rightarrow H_2 + 2OH^- \tag{3.5}$$

The anodic oxidation of magnesium dissolution however has been reported to be a complex multi-step process. At active potentials around - 2.78 V (vs SCE) magnesium oxidizes to form monovalent magnesium ions (Mg^+) and at slightly higher potentials around - 1.56 V (vs SCE) oxidation to divalent magnesium ions (Mg^{2+}) occurs in parallel with the former oxidation step as given below (Lopez and Natta 2001). The involvement of intermediates like monovalent magnesium ions during ZE41 corrosion is substantiated by the appearance of the inductive loops at the lower frequency region in the Nyquist plots.

$$Mg \rightarrow Mg^+ + e^- \tag{3.6}$$

$$Mg \rightarrow Mg^{2+} + 2e^- \tag{3.7}$$

The instability of monovalent magnesium ion is well known (Atrens and Dietzel 2007) and it rapidly undergoes oxidation to form divalent magnesium ion and its compounds through a series of secondary oxidation reactions involving less stable magnesium hydride intermediate. The secondary oxidation eventually produces hydrogen (evolved

through chemical oxidation) and magnesium hydroxide as represented in the following (Baghni et al. 2004).

$$2Mg^+ + 2H_2O \rightarrow Mg^{2+} + Mg(OH)_2 + H_2 \qquad (3.8)$$

$$Mg^+ + 2H^+ + 3e^- \rightarrow MgH_2 \qquad (3.9)$$

$$MgH_2 + 2H_2O \rightarrow Mg(OH)_2 + 2H_2 \qquad (3.10)$$
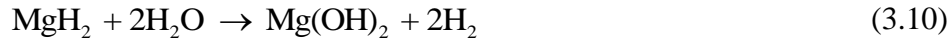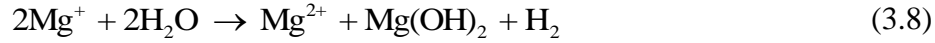
Hence, during magnesium corrosion in aqueous solutions the hydrogen evolution takes place both at cathode and anode, respectively through, electrical reduction and chemical oxidation of Mg^+ to Mg^{2+}. The corrosion product magnesium hydroxide precipitates and deposits over the corroding magnesium surface in the form of a film. The film unfortunately is known to be porous and highly thin with a Pilling-Bedworth ratio nearly equal to 0.81 (Pilling and Bedworth 1923). The efficacy of the surface film to protect the underlying metal is believed to be inadequate and hence the magnesium hydroxide surface film has been termed as partially protective where the corrosion reactions continue unabatedly within the defects of the film (Nordlien et al. 1997).

Four different mechanisms that have been put forward to clarify negative difference effect have already been mentioned in the literature review section of the introductory chapter; to name the same (a) univalent magnesium ion (Mg^+) model, (b) undermining and falling away of cathodic secondary phase particles due to micro-galvanic corrosion, (c) hydride model, (d) partially protective film model. These models independently explain different aspects related to NDE. The first aspect of NDE that is an increased rate of hydrogen evolution instead of the expected decreasing trend at higher anodic overvoltage is the outcome of the chemical evolution of hydrogen at the anode during the secondary oxidation (Eq.3.8 and Eq. 3.10) which over compensates for the reduced rate of cathodic hydrogen evolution. The univalent magnesium ion model and hydride model corroborate the chemical evolution of hydrogen. The second aspect of NDE pertaining to the unexpected and accelerated anodic dissolution results from the

breakdown and dissolution of the surface film at higher anodic overvoltages as predicted by the partially protective film model.

3.1.4.2 Micro-galvanic corrosion of ZE41

The microstructure of as-cast ZE41 alloy and its impact on the alloy corrosion is well known. Three micro-constituent phases make up the microstructure of as-cast ZE41 alloy. The α-Mg matrix constitutes the body of the grain. The secondary phases like β-phase particles are found scattered within the grains and the grain boundary phase is termed as T-phase (Coy et al. 2010). The β-phase particles are known to be rich in zirconium (Zr_4Zn) and the rare earth elements are found to be concentrated along the grain boundary T-phase (Mg_7Zn_3RE) (Neil et al. 2009). The presence of zirconium and rare earths make the secondary phases cathodic to neighboring α-Mg matrix. The alloy ZE41 owing to such a unique microstructure exhibits an extremely high susceptibility to localized micro-galvanic corrosion, where α-Mg matrix corrodes as anode and intermetallic secondary phases remain protected as cathodes.

During ZE41 corrosion, the dissolution of anodic grains causes the accumulation of magnesium ions over the α-Mg matrix. The presence of relatively high concentration of dissolved magnesium ions over the α-phase favors the precipitation of the corrosion product magnesium hydroxide all along the α-Mg matrix. The cathodic intermetallic phases constitute the film-free surfaces which appear as pores and cracks interrupting the continuity of the surface film (Huang et al. 2011). Some electrochemical results of the present work collectively hinted the existence of such a partly protective film over ZE41 surface. For instance, the standard electrode potential of pure magnesium at 25 ℃ is equal to - 2.38 V (De Béthune. and Loud 1965), but the steady state working potential (OCP or E_{corr}) obtained in the present study varied within the range from - 1.5 V to - 1.7 V. Such a drift in the electrode potential suggests the existence of a surface film (Udhayan and Bhatt 1996). Furthermore, the inflection points in the anodic branches of the polarization curves at higher anodic overvoltages eventuated from the deposition and the subsequent dissolution of the surface film. In Nyquist plots the capacitive loops are attained at

intermediate frequency region, this signifies the electrolyte ingress through corrosion product layer which chiefly is the indication of the film porosity (Gao et al. 2010).

Shi et al. (2010) investigated the corrosion of several magnesium alloys including ZE41 in aqueous salt solutions and have highlighted a disparity between the corrosion rates deduced from the Tafel extrapolation (short-term method) and other non-electrochemical methods like hydrogen evolution studies and weight-loss measurements (long-term methods). In Tafel measurements the corrosion rate determination is based upon the rate of electron transfer or the current. The polarization measurements when performed soon after the immersion of the specimen in the electrolyte give instantaneous corrosion rates (Shi et al. 2010). The corrosion rates evaluated through hydrogen evolution studies and weight-loss measurements for long exposure periods correspond to a steady-state. Considering the dynamic nature of the interface of corroding ZE41, the instantaneous and steady-state corrosion rates are bound to differ as the surface topography and the corroding area ceaselessly change with time (Qiao et al. 2012,Cao et al. 2013, King et al. 2014). The potentiodynamic polarization measurements for ZE41, even when performed after the attainment of a steady-state, yield the corrosion rates which, in all likelihood might differ from those evaluated through hydrogen evolution tests and weight-loss techniques, considering the features of negative difference effect. Since magnesium corrosion is only partly electrochemical, hydrogen is evolved both electrically through cathodic reduction and chemically through secondary oxidation; the rate of evolution of hydrogen calculated from the hydrogen evolution studies might overestimate the actual rate of alloy corrosion (Qiao et al. 2012). The disagreement with the results of weight-loss measurements can be justified by considering the after effects of micro-galvanic corrosion, where the cathodic intermetallic particles fall out of the alloy due to accelerated dissolution across the particle boundary. Such undermining and falling away of the cathodic particles results in a weight loss much greater than that arising solely from the electrochemical metal dissolution (Makar and Kruger 1990).

3.1.4.3 The impact of ionic concentration and temperature

The existence of the corrosion product film over ZE41 surface is evident. The response of the alloy ZE41 towards the changes in the environmental factors like ionic concentration or temperature to a great measure is influenced by the surface film properties, especially the film stability. The film dissolution exposes the bare alloy surface to the electrolyte, resulting in an accelerated attack. The protective performance of the surface film is primarily dependent on the electrolyte type. The passivating anions like chromates and fluorides have been reputed to boost the protective ability of the surface film (Williams et al. 2010, Lambertin et al. 2012). On the other hand the anions like chloride and sulfate which act as pitting agents bring about the dissolution of the surface film by transforming magnesium hydroxide film into readily soluble salts of magnesium like magnesium chloride and magnesium sulfate (Wang et al. 2010a). As a consequence of this enhanced surface film dissolution, the rate of ZE41 corrosion increases with increased ionic concentration in both the media. Among the two anions, chloride is known to be more aggressive than sulfate (Zucchi et al. 2006) and this justifies the higher corrosion rates of ZE41 exclusively observed in the combined media.

The rate of ZE41 corrosion as observed from the results of the study increases with the increase in temperature as well. The temperature effects can be attributed to increased surface film dissolution and decreased hydrogen overvoltage. The solubility of magnesium hydroxide increases with the increase in the temperature and hence a higher solution temperature promotes greater dissolution of the surface film. The increase in temperature is also known to increasingly bring down the hydrogen overvoltage which makes the cathodic hydrogen evolution in specific and the alloy corrosion in general, to occur at ease.

3.1.4.4 The influence of medium pH

The effect of pH on the corrosion of pure magnesium can be perceived from the Pourbaix diagram for magnesium-water system, as already shown in Fig. 1.2 (Pourbaix 1974). As per this diagram the magnesium hydroxide as surface film is expected to be

stable only in highly alkaline solutions with a minimum pH of 10.5. On the contrary the electrochemical results from the study point out the existence of a film over ZE41 surface at all the conditions of pH tested; that is even in highly acidic solutions. Such result which appears to be an anomaly can be justified taking into consideration the principal drawback of the Pourbaix diagrams. That is, the Pourbaix diagrams are constructed based on the data which is purely thermodynamic with little consideration to the kinetics of the reactions. Hence from a practical point of view, a corroding magnesium can spontaneously develop magnesium hydroxide surface film even in acidic solutions if the rate of dissolution of magnesium hydroxide is exceeded by the rate of its formation. Furthermore, the pH values mentioned in the study correspond to that of the electrolyte bulk and it is most likely that the local environment at the metal/electrolyte interface is highly alkaline as the cathodic reduction of water generates high concentration of hydroxyl ions at the interface. This alkaline zone developed at the electrode interface might facilitate the precipitation of magnesium hydroxide film, even when the bulk pH is acidic (Zhao et al. 2008).

3.1.5 Surface morphology: SEM and EDX analyses

The surface morphology of ZE41 was examined by means of scanning electron microscopy to further corroborate the impact of the corrosive.
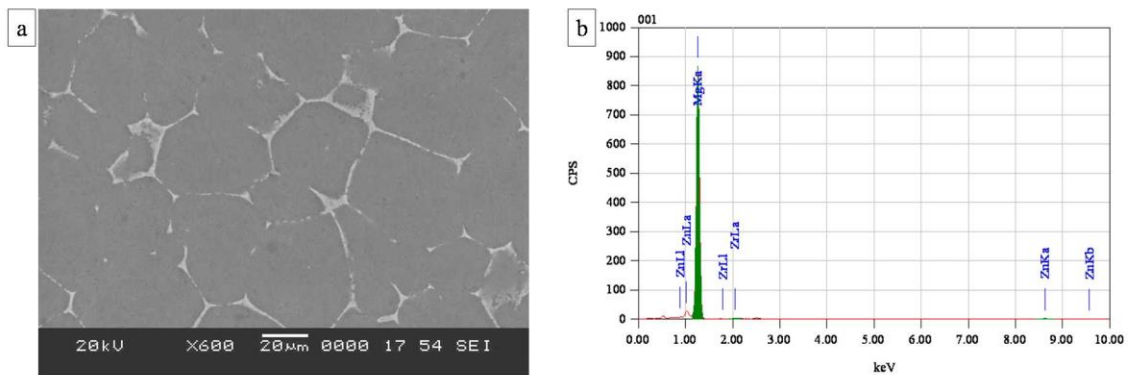
Fig. 3.8 (a) SEM image and (b) EDX spectrum of freshly polished surface of ZE41 alloy.

Fig 3.8 (a) shows the SEM image of a freshly polished surface of ZE41 alloy. The EDX spectrum for the same is represented in Fig. 3.8 (b). The microstructure of the alloy can be markedly seen from the SEM image. The body of the grain seems darker and the grain boundary T-phase, the later appears as a network of white mass. The β-phase particles are scarcely visible at lower magnifications due to their extremely minute size (3-300 nm). In the EDX spectrum a strong peak for magnesium is observed, along with the peaks for other alloying elements to be precise, zinc and zirconium.

The elements constituting the grain area and that of the grain boundary were studied so as to confirm these micro-constituent phases, by precisely recording the EDX spectrum specific to the mentioned regions. Fig. 3.9 (a) and Fig. 3.9 (b), respectively, shows the EDX spectrum recorded for the grain area and the grain boundary along with the respective SEM image highlighting the region under focus.
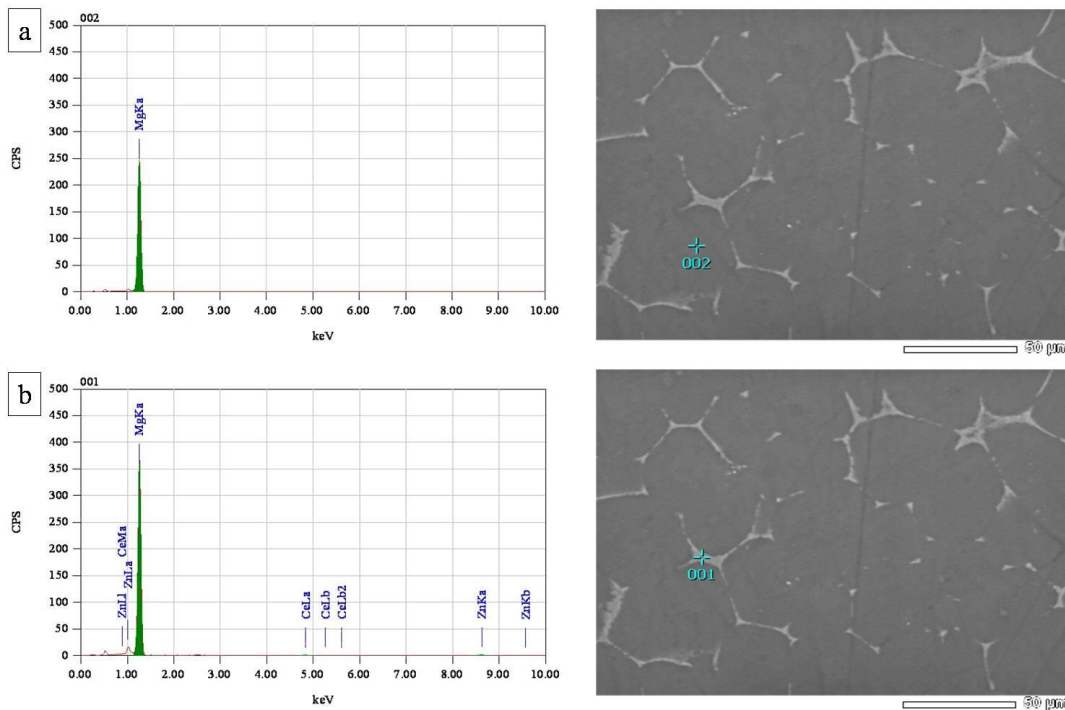
Fig. 3.9 EDX spectra of (a) the grain area and (b) the grain boundary, along with the respective SEM images highlighting the region under focus.

The EDX spectrum for the grain area exhibits a single and strong peak for magnesium, validating that in ZE41 alloy the magnesium matrix constitutes the body of the grain. The EDX spectrum recorded for the grain boundary shows a strong peak corresponding to magnesium and small peaks for zinc and rare earth element cerium. This finding is in close accordance with the reported composition of the grain boundary T-phase (Mg_7Zn_3RE) (Neil et al. 2009).

Fig. 3.10 (a) and Fig. 3.10 (b), are the SEM images of ZE41 specimen surface after one hour immersion in 1.0 M Na_2SO_4 and in combined medium containing 1.0 M Na_2SO_4 and 1.0 M NaCl, respectively. The surface in both the images, after immersion in the salt solutions appears corroded and the microstructure is barely able to be seen, probably the consequence of the corrosion product deposition, over the alloy surface in the form of a film. The surface layer however seems highly uneven with grooves and breaks seen at places.
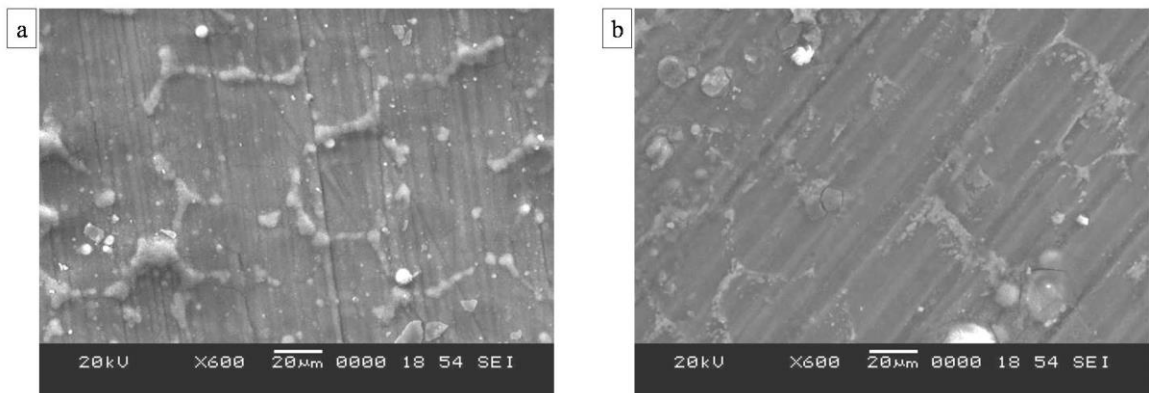
Fig. 3.10 SEM images of the corroded surfaces of ZE41 specimen after one hour immersion in (a) 1.0 M Na_2SO_4 and (b) combined medium containing 1.0 M Na_2SO_4 and 1.0 M NaCl.

The EDX spectra corresponding to SEM images shown in Fig. 3.10 (a) and Fig. 3.10 (b) are shown in Fig. 3.11 (a) and Fig. 3.11 (b), respectively. The peaks for major elements like magnesium, zinc are observed in both the EDX spectra similar to that of the polished surface. However the emergence of an additional strong peak for oxygen in Fig.

3.11 reaffirms the presence of corrosion product film on the surface of the specimen, which most likely is the deposited magnesium hydroxide. The peaks corresponding to sulfur, sodium and chlorine can be attributed to the electrolyte.
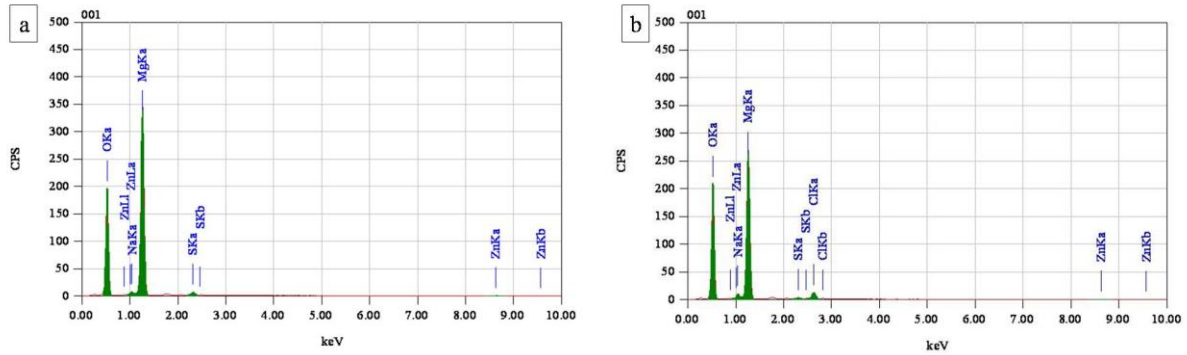
Fig. 3.11 EDX spectra of the corroded surfaces of ZE41 specimen after one hour immersion in (a) 1.0 M Na$_2$SO$_4$ and (b) combined medium containing 1.0 M Na$_2$SO$_4$ and 1.0 M NaCl.

The impact of the medium pH on the surface morphology of the specimen was inspected. Fig. 3.12 (a), Fig. 3.12 (b) and Fig. 3.12 (c) are the SEM images of ZE41 specimen surface after 1 hour immersion in acidic, neutral and alkaline, solutions of 1.0 M Na$_2$SO$_4$with pH 2, 7 and 12, respectively.
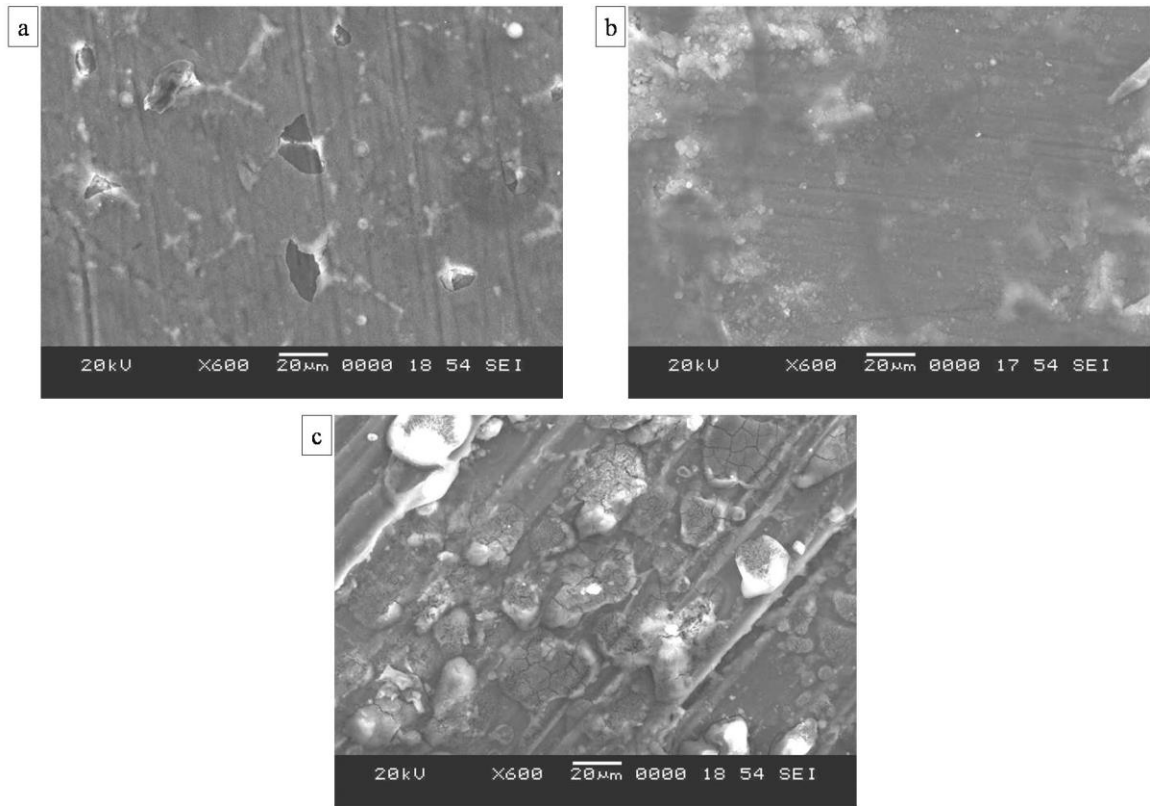
Fig. 3.12 SEM images of ZE41 specimen surface after 1 hour immersion in 1.0 M Na$_2$SO$_4$ solutions with (a) acidic pH of 2, (b) neutral pH of 7 and (c) alkaline pH of 12.

The surface in all the three SEM images appears to be corroded; however, a thickest deposition on the surface is seen for the specimen immersed in alkaline medium. The results agree with the theoretical considerations which expect a higher precipitation of magnesium hydroxide in alkaline conditions.

Table 3.1 (a) Electrochemical polarization parameters for the corrosion of ZE41 alloy in sodium sulfate media of different ionic concentrations at different temperatures.

Na$_2$SO$_4$ concentration [M]	Temp [°C]	E_{corr} vs. SCE [mV]	i_{corr} [µA cm^{-2}]	$-b_c$ [mV dec^{-1}]	v_{corr} [mm y^{-1}]
0.2	30	-1604	131.7	168	2.9
	35	-1608	162.1	177	3.6
	40	-1610	284.9	180	6.3
	45	-1635	378.6	184	8.4
	50	-1638	778.0	189	17.3
0.4	30	-1597	244.4	180	5.4
	35	-1607	387.6	201	8.6
	40	-1627	496.5	196	11.1
	45	-1645	640.1	197	14.3
	50	-1655	1120.3	199	24.9
0.6	30	-1626	327.1	192	7.3
	35	-1628	594.7	199	13.2
	40	-1634	708.0	204	15.8
	45	-1636	886.7	211	19.8
	50	-1639	1250.1	214	27.8
0.8	30	-1645	365.1	187	8.1
	35	-1646	669.8	183	14.9
	40	-1656	912.7	213	20.3
	45	-1665	1080.8	198	24.1
	50	-1673	1338.8	226	29.8
1.0	30	-1648	520.8	190	11.6
	35	-1650	726.7	211	16.2
	40	-1657	996.1	228	22.2
	45	-1681	1287.7	261	28.7
	50	-1686	1451.2	308	32.3

Table 3.1 (b) Electrochemical polarization parameters for the corrosion of ZE41 alloy in combined media of different ionic concentrations at different temperatures.

Na$_2$SO$_4$ concentration [M]	NaCl concentration [M]	Temp [°C]	E_{corr} vs. SCE [mV]	i_{corr} [μA cm^{-2}]	$-b_c$ [mV dec^{-1}]	v_{corr} [mm y^{-1}]
0.2	0.1	30	-1607	242.9	176	5.4
		35	-1628	297.3	195	6.6
		40	-1644	364.9	196	8.1
		45	-1649	495.2	192	11.0
		50	-1655	914.1	213	20.4
0.2	1.0	30	-1642	449.9	195	10.0
		35	-1648	499.0	199	11.1
		40	-1654	556.9	202	12.4
		45	-1658	797.7	204	17.8
		50	-1667	1248.8	210	27.8
0.6	0.1	30	-1635	381.2	186	8.5
		35	-1635	693.0	203	15.4
		40	-1631	792.7	210	17.7
		45	-1657	955.0	190	21.3
		50	-1653	1302.6	226	29.0
0.6	1.0	30	-1644	641.3	198	14.3
		35	-1648	817.2	209	18.2
		40	-1657	913.0	213	20.3
		45	-1668	1229.2	217	27.4
		50	-1667	1541.2	218	34.3
1.0	0.1	30	-1654	554.7	202	12.3
		35	-1659	800.0	199	17.8
		40	-1663	1101.0	198	24.5
		45	-1696	1451.3	228	32.3
		50	-1697	1540.4	219	35.4
1.0	1.0	30	-1669	825.0	204	18.4
		35	-1681	1034.7	214	23.0
		40	-1665	1310.2	221	29.2
		45	-1716	1733.5	317	38.6
		50	-1726	1752.8	224	39.0

Table 3.1 (c) Electrochemical polarization parameters for the corrosion of ZE41 alloy in sodium sulfate solutions with gradually varying pH and sulfate ion concentrations at 30 ºC.

Na$_2$SO$_4$ concentration [M]	pH	E_{corr} vs. SCE [mV]	i_{corr} [µA cm^{-2}]	$-b_c$ [mV dec^{-1}]	v_{corr} [mm yr^{-1}]
	2	-1670	533.6	209	11.9
	5	-1664	241.9	205	5.4
0.2	7	-1662	123.7	207	2.8
	9	-1643	88.6	204	2.0
	12	-1638	58.7	180	1.3
	2	-1673	658.1	208	14.7
	5	-1675	419.7	197	9.3
0.6	7	-1663	276.3	182	6.2
	9	-1655	211.9	182	4.7
	12	-1651	175.7	179	3.9
	2	-1689	902.7	216	20.1
	5	-1681	637.3	209	14.2
1.0	7	-1681	499.5	237	11.1
	9	-1668	364.0	200	8.1
	12	-1665	316.9	198	7.1

Table 3.2 (a) Impedance parameters for the corrosion of ZE41 alloy in sodium sulfate media of different ionic concentrations at different temperatures.

Na_2SO_4 concentration [M]	Temp [°C]	R_{hf} [Ω cm^2]	R_f [Ω cm^2]	C_{dl} [μF cm^{-2}]	C_f [μF cm^{-2}]
0.2	30	83.3	73.1	24.0	101.2
	35	63.7	55.5	32.1	102.7
	40	53.9	40.7	35.3	104.1
	45	47.2	42.7	36.8	104.9
	50	34.2	31.2	39.4	108.1
0.4	30	71.5	68.2	24.8	101.2
	35	62.5	50.0	32.8	102.9
	40	55.0	38.9	36.0	103.9
	45	40.3	36.7	37.6	105.2
	50	25.0	20.7	41.5	108.3
0.6	30	61.1	51.7	26.9	101.2
	35	40.2	31.2	35.0	104.1
	40	36.6	27.8	37.6	104.3
	45	27.6	19.9	41.9	106.7
	50	19.4	17.6	43.4	109.3
0.8	30	48.7	46.5	28.5	103.7
	35	43.6	38.3	37.0	106.3
	40	34.6	30.0	39.5	107.3
	45	28.3	19.1	42.4	109.5
	50	23.0	17.0	43.9	112.7
1.0	30	46.0	42.0	33.9	108.5
	35	39.7	36.2	40.1	108.9
	40	25.0	20.6	42.6	110.2
	45	23.4	18.5	43.2	111.2
	50	22.8	17.4	44.6	115.3

Table 3.2 (b) Impedance parameters for the corrosion of ZE41 alloy in different concentrations of combined media at different temperatures.

Na$_2$SO$_4$ concentration [M]	NaCl concentration [M]	Temp [°C]	R_{hf} [Ω cm^2]	R_f [Ω cm^2]	C_{dl} [μF cm^{-2}]	C_f [μF cm^{-2}]
0.2	0.1	30	74.9	69.7	27.1	101.8
		35	54.6	49.0	36.4	103.6
		40	49.2	34.2	39.0	106.1
		45	43.2	31.8	43.1	107.7
		50	28.8	25.7	45.6	110.6
0.2	1.0	30	52.6	38.6	38.2	108.6
		35	46.1	26.9	48.3	109.6
		40	42.9	21.7	52.2	110.9
		45	34.6	20.1	56.4	112.1
		50	19.3	19.9	61.8	116.9
0.6	0.1	30	47.2	46.0	29.1	102.4
		35	38.1	30.1	37.0	104.9
		40	33.4	24.9	39.8	106.9
		45	25.9	17.9	44.2	109.3
		50	18.8	16.2	47.1	111.4
0.6	1.0	30	38.0	32.5	39.4	108.9
		35	26.3	26.0	48.9	110.1
		40	26.0	20.3	53.3	111.1
		45	20.2	15.8	57.1	112.9
		50	17.7	13.6	62.4	117.0
1.0	0.1	30	42.8	39.7	34.6	109.0
		35	36.8	29.5	42.8	109.2
		40	23.7	19.8	45.6	112.0
		45	17.4	17.1	47.2	112.6
		50	18.3	15.9	48.0	116.7
1.0	1.0	30	34.6	31.4	40.3	112.4
		35	29.3	23.8	49.3	113.4
		40	20.1	16.2	54.3	114.7
		45	15.8	14.9	58.0	114.6
		50	14.9	13.1	63.6	120.1

Table 3.2 (c) Impedance parameters for the corrosion of ZE41 alloy in sodium sulfate solutions with gradually varying pH and sulfate ion concentration at 30 °C.

Na$_2$SO$_4$ concentration [M]	pH	R_{hf} [Ω cm^2]	R_f [Ω cm^2]	C_{dl} [μF cm^{-2}]	C_f [μF cm^{-2}]
	2	56.6	49.8	32.1	110.6
	5	126.4	91.4	27.7	105.8
0.2	7	226.2	178.3	22.9	98.1
	9	316.0	267.2	19.0	92.2
	12	378.2	346.1	16.8	88.5
	2	41.4	34.7	36.7	112.0
	5	56.6	49.8	29.2	107.0
0.6	7	89.7	70.0	24.6	99.0
	9	123.8	104.2	22.0	94.9
	12	182.2	162.9	18.9	91.0
	2	27.8	20.5	41.9	114.0
	5	41.6	33.7	33.7	110.4
1.0	7	51.6	41.4	28.5	107.4
	9	65.0	58.7	25.0	99.6
	12	78.5	65.3	21.2	93.5

Table 3.3 (a) Activation parameters for the corrosion of ZE41 alloy at different ionic concentrations in sodium sulfate media.

Concentration of Na$_2$SO$_4$ [M]	E_a [kJ mol^{-1}]	$\Delta H^{\#}$ [kJ mol^{-1}]	$\Delta S^{\#}$ [J mol^{-1} K^{-1}]
0.2	71.4	68.8	-93.2
0.4	57.7	55.1	-132.3
0.6	50.3	47.7	-153.3
0.8	50.3	47.7	-153.7
1.0	42.8	40.2	-174.9

Table 3.3 (b) Activation parameters for the corrosion of ZE41 alloy at different ionic concentrations in the combined media.

Concentration of Na$_2$SO$_4$ [M]	Concentration of NaCl [M]	E_a [kJ mol^{-1}]	$\Delta H^{\#}$ [kJ mol^{-1}]	$\Delta S^{\#}$ [J mol^{-1} K^{-1}]
0.2	0.1	51.2	48.6	-154.8
0.2	1.0	40.6	38.0	-184.7
0.6	0.1	45.3	42.7	-168.3
0.6	1.0	35.1	32.5	-198.8
1.0	0.1	44.4	41.8	-169.0
1.0	1.0	33.0	30.4	-203.4

3.2 STEARATE AS CORROSION INHIBITOR FOR ZE41 IN AQUEOUS SALT SOLUTIONS

3.2.1 Potentiodynamic polarization measurements

The potentiodynamic polarization curves for the corrosion of ZE41 in 1.0 M Na_2SO_4 at 45 ºC and in the combined medium of 0.2 M Na_2SO_4 – 0.1 M NaCl at 40 ºC, both containing different concentrations of stearate are shown in Fig. 3.13 (a) and Fig. 3.13 (b), respectively.
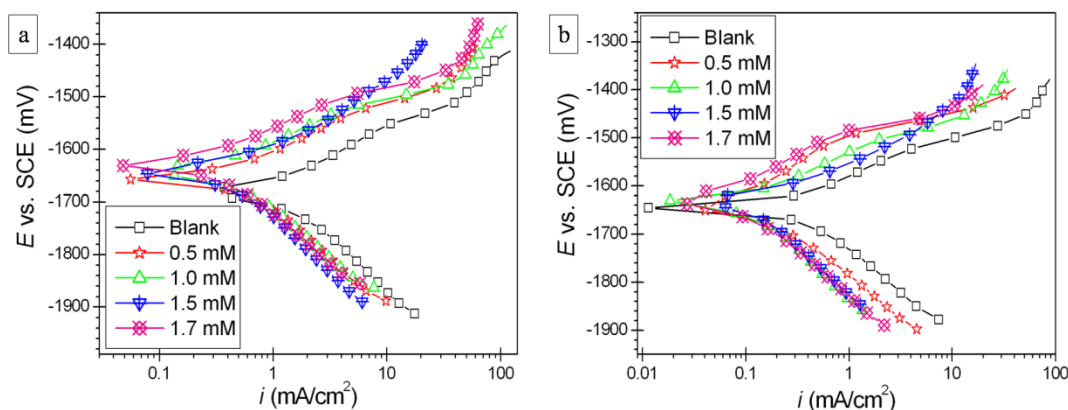
Fig. 3.13 Potentiodynamic polarization curves for the corrosion of ZE41 alloy in the presence of different concentrations stearate in (a) 1.0 M Na_2SO_4 at 45 °C, (b) a medium of 0.2 M Na_2SO_4 - 0.1 M NaCl at 40 °C.

In comparison with the blank the polarization plots for the stearate containing solutions consistently appeared at lower current density regions symbolizing the reduction in the rate of ZE41 alloy dissolution. The basic shape of the Tafel curves unfolds as the consequence of various electrochemical reactions occurring at the surface of the working electrode (Song et al. 2004). The introduction of stearate doesn't seem to affect the shape of the polarization curves, which implies that the added stearate neither alters the mechanism of corrosion nor participates in any of the electrode reactions, but only lessen the rate of corrosion by most likely by blocking the active electrode sites of reaction on the alloy surface through adsorption. The surface film, even in the presence of

stearate, is susceptible to breakdown at higher applied anodic overvoltages, as indicated by the inflection points in the anodic branches. Owing to the non-linear nature of the anodic branches, the corrosion current density values were determined from the cathodic Tafel extrapolation. The inhibition efficiency (η) values were computed as per the previously stated equations; Equation 2.4 and Equation 2.5.

The polarization parameters calculated from the study for the corrosion of ZE41 alloy in the presence of different concentrations of stearate in sodium sulfate and the combined media are, respectively, tabulated in Table 3.4 (a), Table 3.4 (b), Table 3.4 (c) and Table 3.5 (a), Table 3.5 (b). These tables show the results of extensive study at various medium concentrations and temperatures. Some clear-cut trends in the variation of polarization parameters follow from the close observation of the results presented in Tables 3.4 and Tables 3.5. In all the five different media, the presence of stearate lead to an anodic shift in corrosion potential with respect to OCP of the blank solution. Any compound to be classified exclusively as a cathodic or anodic type corrosion inhibitor, a minimum shift in corrosion potential should be of the magnitude of 85 mV (Fekry and Ameer 2010). However the highest anodic shift in corrosion potential observed in the presence of stearate is + 54 mV. Along with an anodic shift in corrosion potential, the introduction of stearate brings about noticeable changes in cathodic slopes, hinting that the kinetics of cathodic reaction are also influenced in the presence of stearate. The anodic drift of corrosion potential is the consequence of greater reduction in the anodic current densities compared to the cathodic ones. Hence the added stearate possibly functions as a mixed-type corrosion inhibitor which predominantly hinders the anodic reaction of metal oxidation. Furthermore, an optimum concentration of 1.7 mM of stearate is evident. Up to this optimum concentration in all the media, the inhibition efficiency substantially increases with the increase in the concentration of stearate and above this concentration the inhibition efficiency increases negligibly. Thus 1.7 mM stands for the most economic concentration (C_{max}) of stearate for the inhibition of ZE41 alloy corrosion, at conditions under consideration. At this optimum concentration, in sodium sulfate media, the maximum inhibition efficiency of 90.8 % is obtained at 30 ºC

in 1.0 M Na$_2$SO$_4$ and in combined media, the maximum inhibition efficiency is 93.7 % is observed at 30 ℃ in the medium of 1.0 M Na$_2$SO$_4$ - 1.0 M NaCl. Additionally at any particular temperature and stearate concentrations the inhibition efficiency values are greater in chloride containing combined media compared to sodium sulfate media and in both the media the inhibition efficiencies increases with the increase in ionic concentration of the media. This feature of stearate exhibiting better efficiency in stronger corrosives is advantageous.

3.2.2 Electrochemical impedance spectroscopy studies

The Nyquist plots obtained from the impedance examinations performed for the corrosion of ZE41 alloy in 1.0 M Na$_2$SO$_4$ at 45 ℃ and in the combined medium of 0.2 M Na$_2$SO$_4$ – 0.1 M NaCl at 40 ℃, both containing different concentrations of stearate are presented in Fig. 3.14 (a) and Fig. 3.14 (b), respectively.
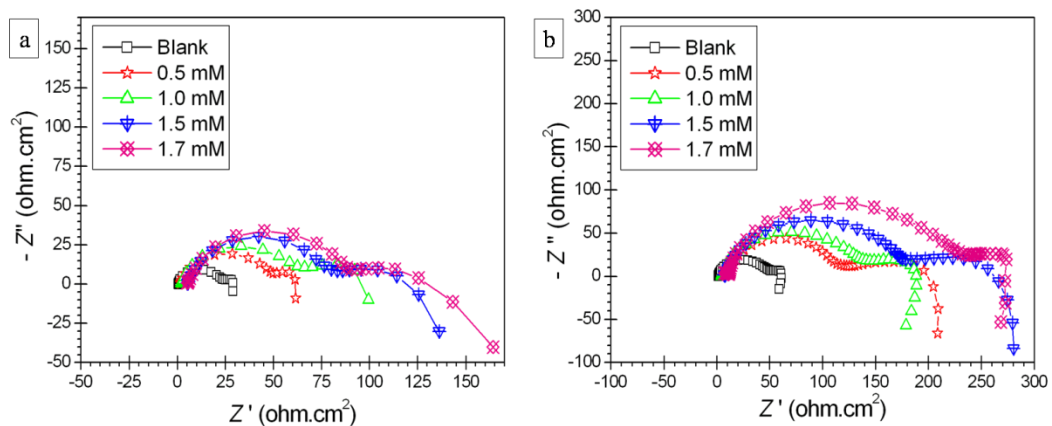
Fig. 3.14 Nyquist plots for the corrosion of ZE41 alloy in the presence of different concentrations stearate in (a) 1.0 M Na$_2$SO$_4$ at 45 °C, (b) a medium of 0.2 M Na$_2$SO$_4$ - 0.1 M NaCl at 40 °C.

As seen from the Nyquist plots in Fig. 3.14, even after the introduction of stearate the primary shape of the Nyquist plots remain unaffected and the capacitive loops successively enlarged in diameter with the increase in the concentration of stearate added. This implies a diminished rate of dissolution of ZE41 achieved without perturbing the

mechanism of corrosion (Huang et al. 2011). The impedance data points were simulated using the same equivalent electrical circuit as shown in Fig. 3.3. Table 3.6 (a), Table 3.6 (b) , Table 3.6 (c) and Table 3.7 (a), Table 3.7 (b), respectively, enlist the evaluated impedance parameters like R_{hf}, C_{dl}, R_f and C_f for the corrosion of ZE41 alloy in the presence of different concentrations of stearate in sodium sulfate and combined media at different medium concentrations and temperatures. Since the overall resistance associated with the higher frequency capacitive loop of the Nyquist plots (R_{hf}) is inversely related to the corrosion rate, the same has been utilized for computation of inhibition efficiency, using both expressions; as given by the Equation 2.4 and the Equation 2.6 (Gao et al. 2011).

The Tables 3.6 and 3.7, collectively display the same trend as observed from the polarization parameters, which is the inhibition efficiency increases with increase in stearate concentration, 1.7 mM is once again obtained as the most economic concentration of stearate for the inhibition of ZE41 corrosion and finally, a superior efficiency is attained in stronger media. The variations in the film characteristics in terms of the film resistance (R_f) and film capacitance (C_f) are interesting. In all the media the increased concentration of stearate brings about an increase in film resistance along with a decrease in film capacitance. Taking into consideration of the implications of higher R_f and lower C_f values, as briefed earlier, it is evident that stearate when present in higher concentrations, boosts the formation of a more protective and thick film over ZE41 surface. The increase in inhibition efficiency with the increase in stearate concentrations thus can be attributed to the formation of a protective and thick surface film which ably shields the underlying alloy from the corrosive attack.

The Bode plots are highly recommended for consideration when the electrochemical systems like the present one, display two relaxation time constants during impedance investigations (Badawy et al. 2010). Fig. 3.15 (a) and Fig. 3.15 (b), respectively, represent Bode magnitude plots for the corrosion of ZE41 alloy immersed in 1.0 M Na_2SO_4 at 45 °C and in the combined medium of 0.2 M Na_2SO_4 - 0.1 M NaCl at

40 °C containing different concentrations of stearate. The phase angle plots for the same are shown in Fig. 3.16 (a) and Fig. 3.16 (b), respectively.
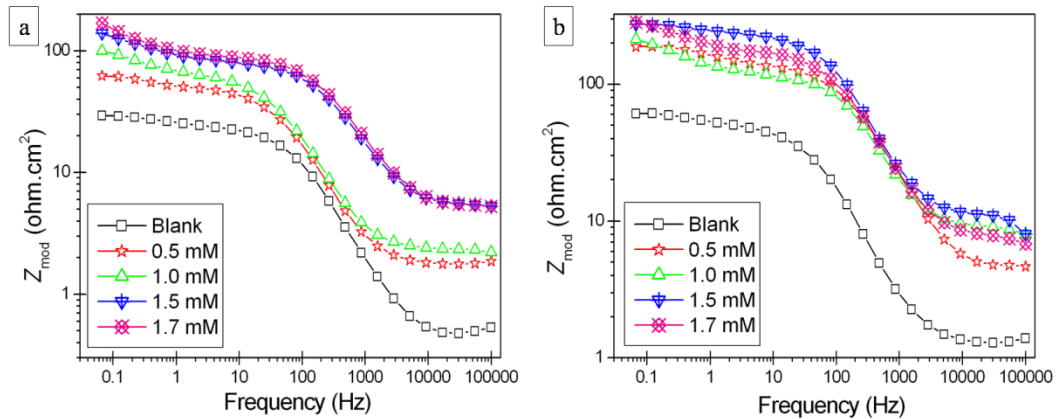
Fig. 3.15 Bode magnitude plots for the corrosion of ZE41 alloy in the presence of different concentrations of stearate in (a) 1.0 M Na$_2$SO$_4$ at 45 °C, (b) a medium of 0.2 M Na$_2$SO$_4$ - 0.1 M NaCl at 40 °C.
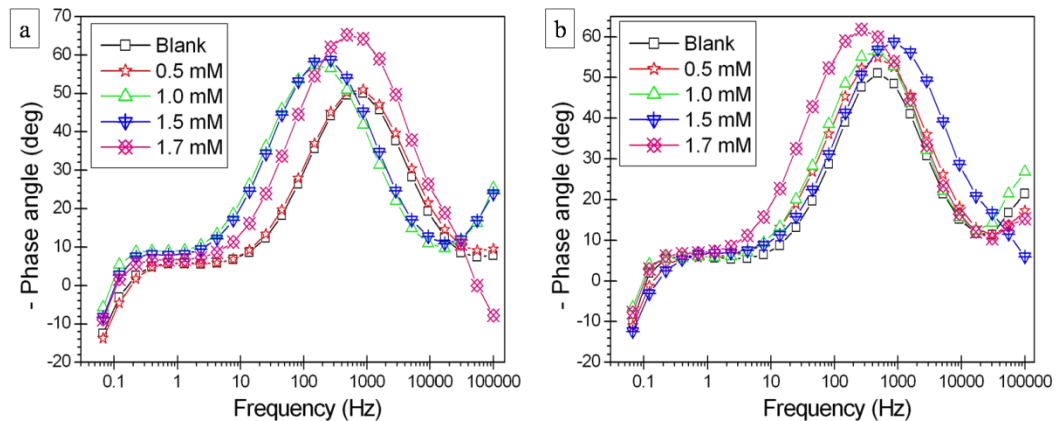
Fig. 3.16 Bode phase angle plots for the corrosion of ZE41 alloy in the presence of different concentrations of stearate in (a) 1.0 M Na$_2$SO$_4$ at 45 °C, (b) a medium of 0.2 M Na$_2$SO$_4$ - 0.1 M NaCl at 40 °C.

The parameters which convey relevant information in Bode magnitude and phase angle plots are low frequency impedance modulus (Z_{mod}) and phase maximum (θ_{max}) at intermediate frequency, respectively (Gao et al. 2011). A larger Z_{mod} at low frequencies showcases a superior corrosion protection performance. Since the intermediate frequency

impedance response is the outcome of electrolyte diffusion through the imperfections of the surface film, a higher θ_{max} at medium frequencies implies greater barrier effect against the electrolyte ingress (Gao et al. 2010). The Bode plots in the Fig. 3.15 and Fig. 3.16, exhibit a monotonic increase in low frequency Z_{mod} and intermediate frequency θ_{max} with the increase in stearate concentration which, respectively, signify the existence of a surface film, offering supreme protection and higher resistance against the corrosive infiltration.

3.2.3 Effect of temperature

The temperature of the medium notably influences the efficiency of the corrosion inhibitors. More often than not the increase in temperature eventuates in to unfavorable decrease in efficiency either due to the thermal decomposition of the organic inhibitors or owing to the desorption of the physisorbed inhibitors. For cases where the interfacial inhibition involves chemisorption, the increased temperature up to an optimum level brings about an enhancement in efficiency due to the activated adsorption of the inhibitors. The comprehensive data tabulated in Table 3.4, Table 3.5, Table 3.6 and Table 3.7, indicate a constant diminution in inhibition efficiency with the rise in temperature, which is a characteristic attribute of physisorbed inhibitors. Moreover, in all the studied media at any particular stearate concentration a smaller value of film capacitance (C_f) in combination with larger film resistance (R_f) is observed at lower temperatures which indicate, respectively, that the thickness and protective performance of the surface film, even in inhibitor containing solutions, are best at lower temperatures. Irrespective of the outcome, the corrosion inhibition studies were performed in a range of temperature so as to evaluate the activation parameters.

Following Arrhenius law equation (Eq.2.7) and transition state equation (Eq.2.8), ln (v_{corr}) versus ($1/T$) and ln (v_{corr}/T) versus ($1/T$) plots were, respectively, constructed and the activation parameters like activation energy (E_a), apparent enthalpy of activation ($\Delta H^{\#}$) and apparent entropy of activation ($\Delta S^{\#}$) for the ZE41 alloy dissolution were evaluated. Fig. 3.17 (a) and Fig. 3.17 (b), respectively, represent the Arrhenius plots for

the corrosion of ZE41 alloy specimen in 1.0 M Na_2SO_4 and in the combined medium of 0.2 M Na_2SO_4 – 0.1 M NaCl containing different concentrations of stearate and the plots of $\ln(v_{corr}/T)$ versus $(1/T)$ for the same are shown in Fig. 3.18 (a) and Fig. 3.18 (b), respectively.
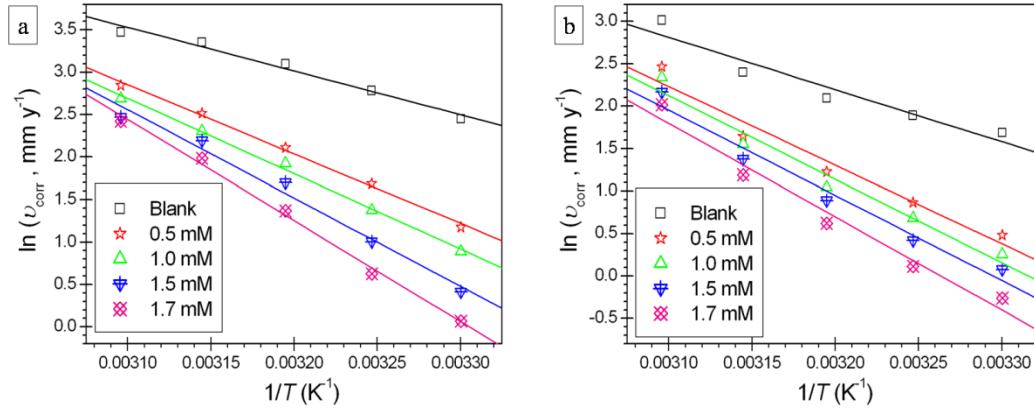
Fig. 3.17 Arrhenius plots for the corrosion of ZE41 alloy in the presence of different concentrations of stearate in (a) 1.0 M Na_2SO_4 (b) a medium of 0.2 M Na_2SO_4 - 0.1 M NaCl.
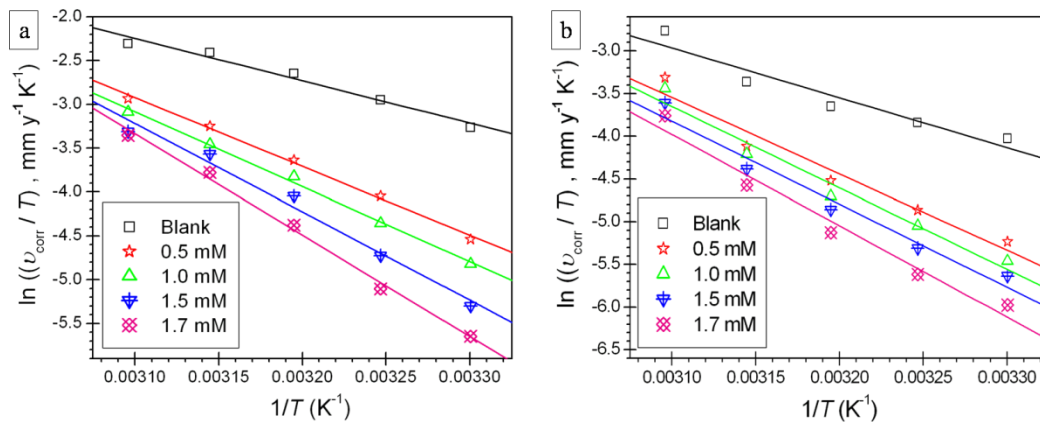
Fig. 3.18 ln (v_{corr}/T) vs. ($1/T$) plots for the corrosion of ZE41 alloy in the presence of different concentrations of stearate in (a) 1.0 M Na_2SO_4 (b) a medium of 0.2 M Na_2SO_4 - 0.1 M NaCl.

The computed activation parameters for the dissolution of ZE41 alloy in the presence of different concentrations of stearate in sodium sulfate and the combined media

are enlisted in Table 3.8 (a) and Table 3.8 (b), respectively. The increased inhibition of ZE41 corrosion brought about by the increased addition of stearate is obvious from the pattern of variation shown by the activation energy values. In comparison with the blank electrolyte, the values of activation energy for the corrosion of the alloy in the solutions containing stearate are much higher and activation energy steadily increases with the increase in the stearate concentration. This trend reflects that the presence of stearate energetically impedes the corrosion of ZE41 and the magnitude of such hindrance enhances with the increase in the amount of stearate added. The variation in $\Delta H^{\#}$ values is similar to that of E_a. The negative values of $\Delta S^{\#}$ are obtained both for blank and stearate containing solutions, which signifies that in the rate-determining step of the alloy dissolution, the activated complex, irrespective of the presence or the absence of the stearate, forms from the association of the reactants. This further corroborates that the added stearate doesn't interfere with the sequence of reactions which constitute the mechanism of ZE41 corrosion.

3.2.4 Adsorption behavior

The metal/electrolyte interface is the region of great interest in any electrochemical investigation and the corrosion inhibition studies are no exception. The inhibition by majority of the interfacial inhibitors like surfactants is achieved principally through adsorption at metal/electrolyte interface. During interfacial adsorption the inhibitor molecules in the electrolyte bulk ($Inh_{(sol)}$) replace the previously adsorbed water molecules at the interface ($H_2O_{(ads)}$), through a quasi-substitution process as shown below (Damaskin et al. 1972):

$$Inh_{(sol)} + \chi H_2O_{(ads)} \rightleftharpoons Inh_{(ads)} + \chi H_2O_{(sol)} \qquad (3.11)$$
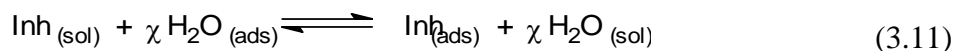
where χ is the size ratio which symbolizes the number of water molecules replaced upon adsorption of one inhibitor molecule. χ is mostly dependent on the type of the inhibitor and is least influenced by the surface charge on the metal. The nature of the interactions

between inhibitor and metal surface and among the adsorbed inhibitor molecules is best understood by taking onto consideration the adsorption behavior.

The values for surface coverage (θ) at different stearate concentrations (C_{inh}) were evaluated from the results of polarization studies using previously mentioned Equation 2.4. It was attempted to graphically fit the values of θ and C_{inh} to various adsorption isotherms, like Langmuir, Temkin, Frumkin and Flory-Huggins isotherms, so as to obtain liner plots. The average values of linear regression coefficient (R^2) were computed and compared for various isotherms. The best linear fitment was accomplished with the Langmuir adsorption isotherm and the Equation 3.12 mentioned in the following describes the mathematical expression for Langmuir adsorption isotherm.

$$\frac{C_{inh}}{\theta} = C_{inh} + \left(\frac{1}{K}\right)$$

(3.12)

where K is the equilibrium constant for the adsorption-desorption process. It is obvious that for a system demonstrating an ideal Langmuir adsorption, the plot of (C_{inh}/θ) versus C_{inh}, will be a straight line with the intercept equal to ($1/K$) and slope equal to unity. The Langmuir adsorption isotherms for adsorption of stearate on ZE41 alloy surface at different temperatures in 1.0 M Na_2SO_4 and in the combined medium of 0.2 M Na_2SO_4 - 1.0 M NaCl are presented in Fig. 3.19 (a) and Fig. 3.19 (b), respectively.

The thermodynamic parameters like standard free energy of adsorption ($\Delta G°_{ads}$), standard enthalpy of adsorption ($\Delta H°_{ads}$) and standard entropy of adsorption ($\Delta S°_{ads}$) were evaluated utilizing the reaction isotherm equation (Eq.2.9) and Gibbs-Helmholtz equation (Eq.2.10). The calculated thermodynamic parameters at different temperatures for the adsorption of stearate on ZE41 alloy surface in sodium sulfate and the combined media are enlisted in Table 3.9 (a) and Table 3.9 (b), respectively.
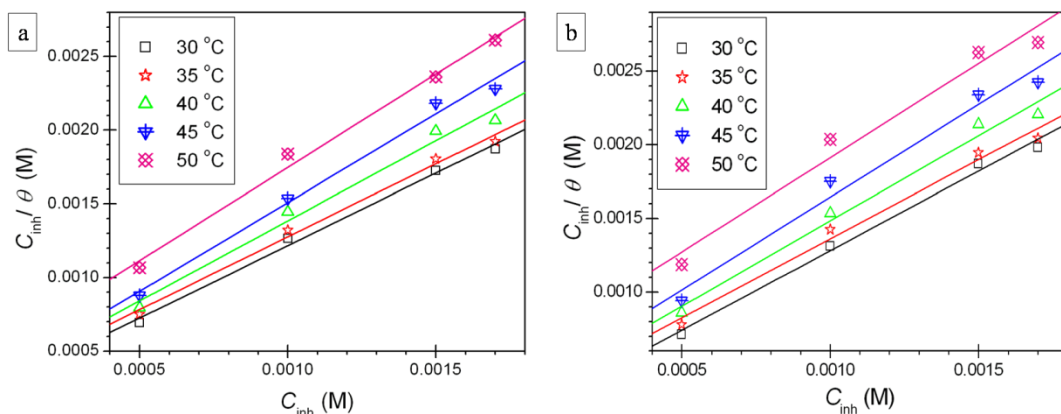
Fig. 3.19 Langmuir adsorption isotherms for the adsorption of stearate on ZE41 alloy surface at different temperatures in (a) 1.0 M Na$_2$SO$_4$ (b) a medium of 0.2 M Na$_2$SO$_4$ - 0.1 M NaCl.

A handful of valuable information can be accessed from the parameters tabulated in Table 3.9. The appreciable linearity of the plots is evident from the average linear regression coefficient (R^2) of 0.99. A deviation from the ideal Langmuir behavior is observed from the values of slope which are close but not exactly equal to unity. Such deviation suggests the existence of some mutual intermolecular interactions among the adsorbed stearate molecules on the alloy surface. The interactions among the adsorbate are forbidden as per the assumptions considered for the statistical derivation of the Langmuir equation (Masel 1996). Furthermore the ΔG°_{ads} values are negative and fall within the narrow range of -30 to -32 kJ mol^{-1}. The negative values of ΔG°_{ads} signify a decrease in standard free energy of the system (El Bribri et al. 2013). The spontaneous processes are accompanied by decrease in free energy and lead the system towards a stable state. Hence it can be inferred that stearate adsorbs spontaneously over ZE41 surface to form a fairly stable layer. The free energy threshold for physisorption and chemisorption, respectively is - 20 kJ mol^{-1} and - 40 kJ mol^{-1} (Bentiss et al. 2005). The experimentally deduced ΔG°_{ads} values are intermediate which imply that both electrostatic forces and coordinate covalent bonding originate during the interaction of stearate molecules with the alloy surface and respectively, lead to physical and chemical

adsorption. The exothermic nature of stearate adsorption is apparent from the negative values of ΔH°_{ads}. The exothermic nature of adsorption is not characteristic unlike the endothermic adsorption which solely corresponds to chemisorption. Hence the differentiation is achieved by taking into account the magnitude of ΔH°_{ads} values, which varied in the range 21 to 47 kJ mol^{-1}. The magnitude of enthalpy of adsorption signifies the strength of the bond formed and hence the physisorption involving weak forces is associated with smaller adsorption enthalpies close to 40 kJ mol^{-1}, whereas that for strong covalent bonds formed during chemisorption is almost 100 kJ mol^{-1} (Martinez and Stern 2002). The physisorption is learnt to be more predominant from the close proximity of the derived ΔH°_{ads} values to the enthalpy threshold for physisorption. The inhibitor molecules, during adsorption, as already explained using the expression 3.11, displace the water molecules which are previously adsorbed at the interface. The inhibitors existing in a state of random motion in the electrolyte bulk, upon adsorption, form orderly arranged monolayer or multilayers at the alloy surface and hence, cause the entropy of the system to decrease. On the other hand, an increase in the entropy (solvent entropy) is brought about by the displacement of the previously adsorbed water molecules, which consequently, go into a freely moving state in the electrolyte bulk. Hence from an entropy point of view, two opposing actions occur simultaneously and the overall entropy change depends on the process which is predominant. In the present study, the decrease in system's entropy brought about by the adsorption of stearate might overcompensate for the increased solvent entropy; hence, the calculated values for ΔS°_{ads} are negative, which indicate an overall decrease in randomness of the system.

Table 3.4 (a) Electrochemical polarization parameters for the corrosion of ZE41 alloy in 0.2 M Na$_2$SO$_4$ containing different concentrations of stearate at different temperatures.

Temp [°C]	Stearate concentration [mM]	E_{corr} vs. SCE [mV]	i_{corr} [μA cm^{-2}]	$-b_c$ [mV dec^{-1}]	η [%]
	Blank	-1604	131.7	168	-
	0.5	-1602	42.4	153	67.8
	1.0	-1598	33.8	147	74.3
30	1.5	-1591	27.9	129	78.8
	1.7	-1589	24.0	114	81.8
	1.8	-1588	22.9	107	82.6
	3.0	-1584	20.0	108	84.8
	Blank	-1608	162.1	177	-
	0.5	-1594	64.9	159	60.0
35	1.0	-1591	52.9	152	67.4
	1.5	-1587	41.7	138	74.3
	1.7	-1585	30.1	122	81.5
	Blank	-1610	284.9	180	-
	0.5	-1607	123.5	165	56.7
40	1.0	-1601	107.7	155	62.2
	1.5	-1596	92.2	139	67.7
	1.7	-1585	72.9	123	74.4
	Blank	-1635	378.6	184	-
	0.5	-1629	185.2	176	51.1
45	1.0	-1626	173.5	157	54.2
	1.5	-1618	143.7	149	62.1
	1.7	-1607	119.6	123	68.4
	Blank	-1638	778.0	189	-
	0.5	-1633	467.4	178	39.9
50	1.0	-1628	405.0	163	48.0
	1.5	-1624	326.0	151	58.1
	1.7	-1616	294.6	138	62.1

Table 3.4 (b) Electrochemical polarization parameters for the corrosion of ZE41 alloy in 0.6 M Na₂SO₄ containing different concentrations of stearate at different temperatures.

Temp [°C]	Stearate concentration [mM]	E_{corr} vs. SCE [mV]	i_{corr} [μA cm^{-2}]	$-b_c$ [mV dec^{-1}]	η [%]
30	Blank	-1626	327.1	192	-
	0.5	-1622	98.9	178	69.8
	1.0	-1615	75.8	176	76.8
	1.5	-1610	53.5	152	83.6
	1.7	-1604	41.5	147	87.3
	1.8	-1602	40.0	142	87.8
	3.0	-1598	37.1	135	88.7
35	Blank	-1628	594.7	199	-
	0.5	-1623	204.5	184	65.6
	1.0	-1621	176.6	163	70.3
	1.5	-1614	114.2	152	80.8
	1.7	-1608	90.1	149	84.9
40	Blank	-1634	708.0	204	-
	0.5	-1627	291.5	192	58.8
	1.0	-1624	231.5	198	67.3
	1.5	-1619	176.4	180	75.1
	1.7	-1611	152.8	169	78.4
45	Blank	-1636	886.7	211	-
	0.5	-1634	419.7	198	52.7
	1.0	-1627	377.6	200	57.4
	1.5	-1620	296.2	187	66.6
	1.7	-1613	245.6	173	72.3
50	Blank	-1639	1250.1	214	-
	0.5	-1637	670.5	207	46.4
	1.0	-1632	579.1	203	53.7
	1.5	-1625	526.9	189	57.9
	1.7	-1617	447.5	192	64.2

Table 3.4 (c) Electrochemical polarization parameters for the corrosion of ZE41 alloy in 1.0 M Na$_2$SO$_4$ containing different concentrations of stearate at different temperatures.

Temp [°C]	Stearate concentration [mM]	E_{corr} vs. SCE [mV]	i_{corr} [μA cm^{-2}]	$-b_c$ [mV dec^{-1}]	η [%]
30	Blank	-1648	520.8	190	-
	0.5	-1644	145.5	186	72.1
	1.0	-1639	109.5	178	79.0
	1.5	-1637	67.9	155	87.0
	1.7	-1632	47.9	152	90.8
	1.8	-1626	46.4	149	91.1
	3.0	-1613	40.0	146	92.3
35	Blank	-1650	726.7	211	-
	0.5	-1642	242.7	192	66.6
	1.0	-1639	177.4	184	75.6
	1.5	-1622	122.8	168	83.1
	1.7	-1628	84.1	157	88.4
40	Blank	-1657	996.1	228	-
	0.5	-1643	370.5	193	62.8
	1.0	-1638	307.8	188	69.1
	1.5	-1632	246.3	179	75.3
	1.7	-1627	176.6	163	82.3
45	Blank	-1681	1287.7	261	-
	0.5	-1653	555.2	232	56.9
	1.0	-1642	449.9	196	65.1
	1.5	-1640	402.6	190	68.7
	1.7	-1627	327.1	192	74.6
50	Blank	-1686	1451.2	308	-
	0.5	-1669	771.2	269	46.9
	1.0	-1655	661.1	205	54.5
	1.5	-1654	529.7	201	63.5
	1.7	-1649	506.5	193	65.1

Table 3.5 (a) Electrochemical polarization parameters for the corrosion of ZE41 alloy in the combined medium of 0.2 M Na₂SO₄ - 0.1M NaCl containing different concentrations of stearate at different temperatures.

Temp [°C]	Stearate concentration [mM]	E_{corr} vs. SCE [mV]	i_{corr} [μA cm^{-2}]	$-b_c$ [mV dec^{-1}]	η [%]
30	Blank	-1607	242.9	176	-
	0.5	-1605	72.6	164	70.1
	1.0	-1601	58.0	166	76.1
	1.5	-1597	48.3	158	80.1
	1.7	-1599	34.5	144	85.8
	1.8	-1594	33.9	142	86.0
	3.0	-1595	29.1	142	88.0
35	Blank	-1628	297.3	195	-
	0.5	-1623	106.7	189	64.1
	1.0	-1619	88.9	187	70.1
	1.5	-1618	68.1	188	77.1
	1.7	-1612	50.2	178	83.1
40	Blank	-1644	364.9	196	-
	0.5	-1639	152.9	197	58.1
	1.0	1634	127.3	194	65.1
	1.5	-1630	109.1	185	70.1
	1.7	-1628	83.6	173	77.1
45	Blank	-1649	495.2	192	-
	0.5	-1647	232.2	184	53.1
	1.0	-1640	212.4	185	57.1
	1.5	1641	177.8	179	64.1
	1.7	-1634	148.1	170	70.1
50	Blank	-1655	914.1	213	-
	0.5	-1653	529.3	198	42.1
	1.0	-1649	465.3	194	49.1
	1.5	-1642	392.2	183	57.1
	1.7	-1638	337.3	180	63.1

Table 3.5 (b) Electrochemical polarization parameters for the corrosion of ZE41 alloy in the combined medium of 1.0 M Na₂SO₄ - 1.0 M NaCl containing different concentrations of stearate at different temperatures.

Temp [°C]	Stearate concentration [mM]	E_{corr} vs. SCE [mV]	i_{corr} [$\mu A\ cm^{-2}$]	$-b_c$ [$mV\ dec^{-1}$]	η [%]
30	Blank	-1669	825.0	204	-
	0.5	-1657	204.0	205	75.3
	1.0	-1645	143.7	193	82.6
	1.5	-1640	88.5	198	89.3
	1.7	-1634	51.8	185	93.7
	1.8	-1632	46.2	187	94.4
	3.0	-1633	40.4	184	95.1
35	Blank	-1681	1034.7	214	-
	0.5	-1679	305.2	193	70.5
	1.0	-1664	222.5	187	78.5
	1.5	-1660	150.0	182	85.5
	1.7	-1652	88.0	169	91.5
40	Blank	-1665	1310.2	221	-
	0.5	-1659	465.1	213	64.5
	1.0	-1656	347.2	196	73.5
	1.5	-1648	281.7	178	78.5
	1.7	-1641	203.1	183	84.5
45	Blank	-1716	1733.5	317	-
	0.5	-1687	719.4	201	58.5
	1.0	-1675	563.4	187	67.5
	1.5	-1670	494.1	189	71.5
	1.7	-1668	390.0	191	77.5
50	Blank	-1726	1752.8	224	-
	0.5	-1704	832.6	203	52.5
	1.0	-1685	727.4	192	58.5
	1.5	-1684	639.8	196	63.5
	1.7	-1679	534.6	185	69.5

Table 3.6 (a) Impedance parameters for the corrosion of ZE41 alloy in 0.2 M Na₂SO₄ containing different concentrations of stearate at different temperatures.

Temp [°C]	Stearate concentration [mM]	R_{hf} [Ω cm^2]	R_f [Ω cm^2]	C_{dl} [μF cm^{-2}]	C_f [μFcm^{-2}]	η [%]
30	Blank	83.3	73.1	24.0	101.2	-
	0.5	267.1	112.7	23.8	99.2	68.8
	1.0	329.5	143.8	21.9	92.3	74.7
	1.5	379.1	187.4	19.7	88.5	78.0
	1.7	473.5	212.6	17.4	80.1	82.4
	1.8	506.2	298.3	12.6	68.4	83.5
	3.0	524.2	474.6	9.3	28.9	84.1
35	Blank	63.7	55.5	32.1	102.7	-
	0.5	174.5	73.4	31.0	101.1	63.5
	1.0	207.8	120.2	30.2	97.5	69.4
	1.5	275.2	156.1	27.6	90.1	76.9
	1.7	334.5	209.5	23.9	82.9	81.0
40	Blank	53.9	40.7	35.3	104.1	-
	0.5	126.1	52.6	33.8	104.0	57.3
	1.0	142.3	66.4	30.2	99.1	62.1
	1.5	175.9	87.1	28.7	93.9	69.4
	1.7	222.3	98.2	25.5	89.2	75.8
45	Blank	47.2	42.7	36.8	104.9	-
	0.5	99.7	43.8	35.5	103.0	52.7
	1.0	108.2	46.5	33.7	101.6	56.4
	1.5	131.8	63.8	29.7	98.3	64.2
	1.7	156.3	80.4	24.3	91.6	69.8
50	Blank	34.2	31.2	39.4	108.1	-
	0.5	55.4	31.9	38.6	107.1	38.3
	1.0	66.8	33.4	36.9	106.0	48.8
	1.5	75.9	38.7	34.7	99.8	55.0
	1.7	87.5	46.1	33.0	93.0	61.0

Table 3.6 (b) Impedance parameters for the corrosion of ZE41 alloy in 0.6 M Na$_2$SO$_4$ containing different concentrations of stearate at different temperatures.

Temp [°C]	Stearate concentration [mM]	R_{hf} [Ω cm^2]	R_f [Ω cm^2]	C_{dl} [μF cm^{-2}]	C_f [μFcm^{-2}]	η [%]
	Blank	61.1	51.7	26.9	101.2	-
	0.5	205.2	126.4	23.7	97.6	70.2
	1.0	243.8	153.7	21.5	89.6	74.9
30	1.5	349.3	198.6	18.2	83.7	82.5
	1.7	482.1	246.4	13.7	75.6	87.3
	1.8	498.7	301.3	9.8	61.3	87.8
	3.0	524.1	488.5	8.9	17.7	88.3
	Blank	40.2	31.2	35.0	104.1	-
	0.5	116.7	89.7	30.9	100.8	65.6
35	1.0	142.6	123.6	29.1	93.3	71.8
	1.5	204.7	168.5	24.4	88.6	80.4
	1.7	260.7	213.8	21.7	80.3	84.6
	Blank	36.6	27.8	37.6	104.3	-
	0.5	90.4	56.4	31.3	103.6	59.5
40	1.0	110.1	71.5	28.9	96.2	66.8
	1.5	141.6	98.6	26.2	91.3	74.2
	1.7	182.2	101.7	22.8	85.6	79.9
	Blank	27.6	19.9	41.9	106.7	-
	0.5	55.7	38.6	35.1	102.2	50.5
45	1.0	66.7	51.8	30.2	100.1	58.7
	1.5	80.4	69.3	26.6	95.4	65.7
	1.7	97.5	81.2	23.7	88.6	71.7
	Blank	19.4	17.6	43.4	109.3	-
	0.5	35.7	24.5	38.0	105.6	45.7
50	1.0	41.1	33.7	36.8	102.3	52.9
	1.5	45.2	39.1	33.1	97.2	57.2
	1.7	54.1	46.9	31.8	90.7	64.1

Table 3.6 (c) Impedance parameters for the corrosion of ZE41 alloy in 1.0 M Na$_2$SO$_4$ containing different concentrations of stearate at different temperatures.

Temp [°C]	Stearate concentration [mM]	R_{hf} [Ω cm^2]	R_f [Ω cm^2]	C_{dl} [μF cm^{-2}]	C_f [μFcm^{-2}]	η [%]
30	Blank	46.0	42.0	33.9	108.5	-
	0.5	182.8	128.9	21.1	96.3	74.8
	1.0	204.3	169.5	18.0	85.0	77.5
	1.5	291.1	186.2	14.8	80.8	84.2
	1.7	497.7	197.8	10.7	71.2	90.8
	1.8	530.6	296.0	9.5	58.3	91.3
	3.0	583.0	556.3	8.1	10.0	92.1
35	Blank	39.7	36.2	40.1	108.9	-
	0.5	123.9	120.7	30.2	99.4	68.0
	1.0	160.3	156.4	27.5	92.0	75.2
	1.5	239.8	174.9	23.1	85.8	83.5
	1.7	324.9	218.1	19.1	74.5	87.8
40	Blank	25.0	20.6	42.6	110.2	-
	0.5	64.3	58.5	30.4	105.0	61.1
	1.0	81.2	72.1	28.5	94.0	69.2
	1.5	106.2	97.9	24.3	87.4	76.6
	1.7	146.1	102.0	22.1	79.6	82.9
45	Blank	23.4	18.5	43.2	111.2	-
	0.5	50.7	46.7	34.2	101.9	53.9
	1.0	66.3	61.2	29.1	99.8	64.8
	1.5	77.8	74.1	26.9	94.9	70.0
	1.7	88.9	81.5	23.6	85.8	73.7
50	Blank	22.8	17.4	44.6	115.3	-
	0.5	43.4	40.6	37.9	104.5	47.4
	1.0	52.9	48.7	33.1	100.5	56.9
	1.5	61.9	57.4	32.7	95.1	63.2
	1.7	67.5	59.6	29.5	87.7	66.2

Table 3.7 (a) Impedance parameters for the corrosion of ZE41 alloy in the combined medium of 0.2 M Na$_2$SO$_4$ - 0.1 M NaCl containing different concentrations of stearate at different temperatures.

Temp [°C]	Stearate concentration [mM]	R_{hf} [Ω cm^2]	R_f [Ω cm^2]	C_{dl} [μF cm^{-2}]	C_f [μFcm^{-2}]	η [%]
30	Blank	74.9	69.7	27.1	101.8	-
	0.5	229.0	142.4	18.9	94.6	67.3
	1.0	286.3	173.7	16.4	82.4	73.8
	1.5	342.1	185.9	14.9	77.0	78.1
	1.7	482.7	210.6	12.4	72.5	84.5
	1.8	536.6	301.2	9.8	57.3	86.0
	3.0	572.3	492.4	7.9	19.3	86.9
35	Blank	54.6	49.0	36.4	103.6	-
	0.5	139.3	132.4	30.0	100.8	60.8
	1.0	168.2	172.3	27.4	95.8	67.6
	1.5	218.4	177.8	23.5	84.4	75.0
	1.7	294.9	192.4	19.8	75.5	81.5
40	Blank	49.2	34.2	39.0	106.1	-
	0.5	107.4	126.6	34.3	103.3	54.3
	1.0	128.0	164.5	27.5	100.3	61.6
	1.5	175.3	179.4	23.5	95.4	72.0
	1.7	211.6	185.3	20.2	83.3	76.8
45	Blank	43.2	31.8	43.1	107.7	-
	0.5	84.3	116.7	36.5	105.4	48.8
	1.0	93.2	136.8	27.4	100.3	53.7
	1.5	110.2	167.9	24.6	96.4	60.8
	1.7	131.3	182.9	21.3	88.9	67.1
50	Blank	28.8	25.7	45.6	110.6	-
	0.5	48.7	98.9	37.2	107.3	40.8
	1.0	51.6	131.9	30.0	101.9	44.2
	1.5	62.3	146.8	28.9	96.3	53.7
	1.7	74.4	167.3	25.0	79.3	61.3

Table 3.7 (b) Impedance parameters for the corrosion of ZE41 alloy in the combined medium of 1.0 M Na₂SO₄ – 1.0 M NaCl containing different concentrations of stearate at different temperatures.

Temp [°C]	Stearate concentration [mM]	R_{hf} [Ω cm^2]	R_f [Ω cm^2]	C_{dl} [μF cm^{-2}]	C_f [μFcm^{-2}]	η [%]
30	Blank	34.6	31.4	40.3	112.4	-
	0.5	128.5	132.7	23.5	98.0	73.1
	1.0	181.3	171.8	18.9	87.5	80.9
	1.5	303.2	188.3	15.9	81.0	88.6
	1.7	503.8	202.4	13.5	75.6	93.1
	1.8	566.7	298.3	10.0	61.3	93.9
	3.0	647.7	487.4	8.9	15.8	94.7
35	Blank	29.3	23.8	49.3	113.4	-
	0.5	91.0	129.4	32.6	101.5	67.8
	1.0	125.8	163.7	29.6	97.8	76.7
	1.5	185.1	176.1	24.7	89.8	84.2
	1.7	316.9	189.8	20.0	78.4	90.8
40	Blank	20.1	16.2	54.3	114.7	-
	0.5	53.0	123.4	38.9	107.8	62.0
	1.0	69.7	158.9	30.0	103.2	71.1
	1.5	85.9	167.4	27.7	98.0	76.5
	1.7	120.2	170.1	23.1	81.4	83.2
45	Blank	15.8	14.9	58.0	114.6	-
	0.5	34.8	114.5	39.8	108.8	54.6
	1.0	44.5	145.3	30.0	104.9	64.5
	1.5	50.7	149.8	28.3	100.0	68.9
	1.7	63.3	157.4	24.6	86.9	75.4
50	Blank	14.9	13.1	63.6	120.1	-
	0.5	28.8	98.5	40.0	110.5	48.0
	1.0	32.0	132.4	34.8	104.4	53.2
	1.5	37.5	134.5	33.0	98.5	60.1
	1.7	43.9	141.6	30.0	89.0	65.9

Table 3.8 (a) Activation parameters for the corrosion of ZE41 alloy in different concentrations of Na$_2$SO$_4$ in the presence of different concentrations of stearate.

Concentration of Na$_2$SO$_4$ [M]	Concentration of stearate [mM]	E_a [kJ mol^{-1}]	$\Delta H^{\#}$ [kJ mol^{-1}]	$\Delta S^{\#}$ [J mol^{-1} K^{-1}]
	Blank	71.4	68.8	-93.2
	0.5	95.2	92.6	-24.2
0.2	1.0	100.2	97.6	-9.3
	1.5	100.3	97.7	-8.3
	1.7	104.1	101.5	-5.3
	Blank	50.3	47.7	-153.5
	0.5	74.0	71.4	-85.1
0.6	1.0	78.7	76.1	-71.7
	1.5	90.1	87.5	-37.6
	1.7	93.9	91.3	-26.9
	Blank	42.8	40.2	-174.9
	0.5	67.8	65.2	-102.8
1.0	1.0	73.7	71.1	-85.8
	1.5	86.4	83.8	-47.6
	1.7	98.9	96.3	-10.0

Table 3.8 (b) Activation parameters for the corrosion of ZE41 alloy in different concentrations of the combined media in the presence of different concentrations stearate.

Concentration of medium [M]	Concentration of stearate [mM]	E_a [kJ mol^{-1}]	$\Delta H^{\#}$ [kJ mol^{-1}]	$\Delta S^{\#}$ [J mol^{-1} K^{-1}]
	Blank	51.2	48.6	-154.8
	0.5	77.0	74.4	-79.7
0.2 M Na$_2$SO$_4$ & 0.1M NaCl	1.0	81.7	79.1	-65.7
	1.5	83.4	80.8	-62.2
	1.7	91.4	88.8	-38.5
	Blank	33.0	30.4	-203.4
1.0 M Na$_2$SO$_4$ & 1.0M NaCl	0.5	59.9	57.3	-126.3
	1.0	68.1	65.5	-102.4
	1.5	83.9	81.3	-53.9
	1.7	100.4	97.8	-4.2

Table 3.9 (a) Thermodynamic parameters for the adsorption of stearate on ZE41 alloy surface in sodium sulfate media.

Concentration of Na_2SO_4 [M]	Temp [°C]	ΔG^o_{ads} [kJ mol^{-1}]	ΔH^o_{ads} [kJ mol^{-1}]	ΔS^o_{ads} [J K^{-1} mol^{-1}]	R^2	Slope
0.2	30	-31.7			0.997	1.13
	35	-30.7			0.982	1.07
	40	-31.3	-46.6	-49.8	0.982	1.20
	45	-31.1			0.968	1.28
	50	-30.2			0.976	1.23
0.6	30	-31.2			0.995	1.03
	35	-31.0			0.985	1.03
	40	-31.3	-27.9	-10.6	0.995	1.09
	45	-31.0			0.973	1.18
	50	-31.5			0.982	1.36
1.0	30	-31.2			0.994	0.98
	35	-31.2			0.992	0.99
	40	-31.6	-24.8	-21.2	0.984	1.09
	45	-32.0			0.991	1.20
	50	-31.3			0.992	1.26

Table 3.9 (b) Thermodynamic parameters for the adsorption of stearate on ZE41 alloy surface in combined media.

Concentration of medium [M]	Temp [°C]	ΔG^o_{ads} [kJ mol^{-1}]	ΔH^o_{ads} [kJ mol^{-1}]	ΔS^o_{ads} [J K^{-1} mol^{-1}]	R^2	Slope
0.2 M Na_2SO_4 & 0.1M NaCl	30	-31.6			0.992	1.08
	35	-31.1			0.987	1.07
	40	-31.3	-42.2	-35.0	0.984	1.16
	45	-31.4			0.978	1.26
	50	-30.6			0.972	1.28
1.0 M Na_2SO_4 & 1.0M NaCl	30	-31.5			0.995	0.97
	35	-31.5			0.991	0.97
	40	-31.8	-21.3	-33.3	0.992	1.06
	45	-32.0			0.991	1.15
	50	-32.1			0.984	1.28

3.3 PALMITATE AS INHIBITOR OF ZE41 CORROSION IN AQUEOUS SALT SOLUTIONS

3.3.1 Potentiodynamic polarization measurements

Fig. 3.20 (a) and Fig. 3.20 (b), respectively, show the potentiodynamic polarization plots for the corrosion of ZE41 in 1.0 M Na$_2$SO$_4$ at 45 ℃ and in the combined medium of 0.2 M Na$_2$SO$_4$ – 0.1 M NaCl at 30 ℃, both containing different concentrations of palmitate.
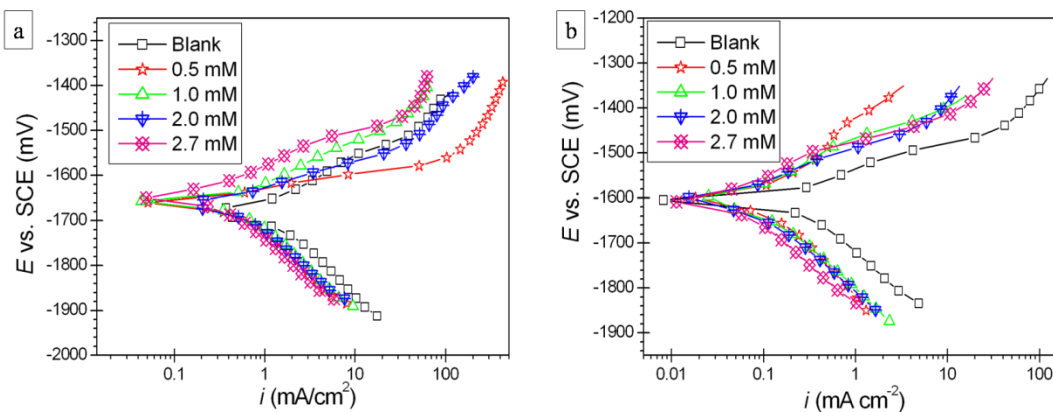
Fig. 3.20 Potentiodynamic polarization curves for the corrosion of ZE41 alloy in the presence of different concentrations palmitate in (a) 1.0 M Na$_2$SO$_4$ at 45 °C, (b) a medium of 0.2 M Na$_2$SO$_4$ - 0.1 M NaCl at 30 °C.

The polarization curves in Fig. 3.20, appear to have been drifted towards the lower current density region on the introduction of palmitate into the blank solution. Such a shift along with no evident alteration in shape of the Tafel curves symbolizes that palmitate inhibits alloy dissolution without meddling with the mechanism of corrosion. The anodic branches of the polarization curves inflected at higher applied anodic overvoltages and hence cathodic Tafel extrapolation is employed for the deduction of corrosion current density values.

Table 3.10 (a), Table 3.10 (b), Table 3.10 (c) and Table 3.11 (a), Table 3.11 (b), respectively, display the experimentally evaluated polarization parameters for the

corrosion of ZE41 alloy in the presence of different concentrations of palmitate in sodium sulfate and the combined media. The ability of palmitate to predominantly control the anodic dissolution while being a mixed-type corrosion inhibitor is perceived from the marginal alterations in cathodic slopes, along with the anodic drift of corrosion potential (not more than 60 mV vs. SCE) with reference to OCP of the blank solution. As seen from the Table 3.10 and Table 3.11, in all the media the optimum or the most economic concentration (C_{max}) of palmitate for the inhibition of ZE41 alloy corrosion is equal to 2.7 mM. At the optimum concentration, the maximum inhibition efficiencies are 89.5 % and 91.1%, observed at 30 ℃ in the medium of 1.0 M Na_2SO_4 and in combined medium of 1.0 M Na_2SO_4 - 1.0 M NaCl, respectively. In both sodium sulfate and combined media the efficiency of palmitate to inhibit ZE41 corrosion evidently increases with the increase in ionic concentration of the media.

3.3.2 Electrochemical impedance spectroscopy studies

Fig. 3.21 (a) and Fig. 3.21 (b), respectively, show the Nyquist plots for the corrosion of ZE41 in 1.0 M Na_2SO_4 at 45 ℃ and in the combined medium of 0.2 M Na_2SO_4 – 0.1 M NaCl at 30 ℃, both containing different concentrations of palmitate.
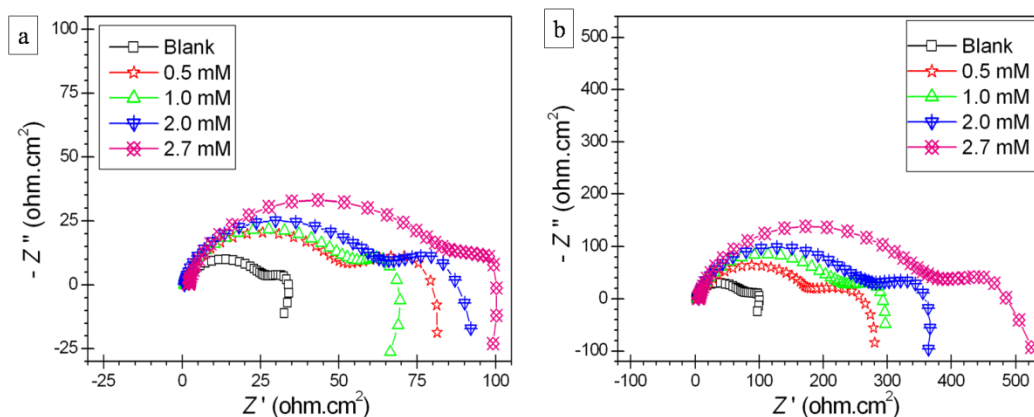
Fig. 3.21 Nyquist plots for the corrosion of ZE41 alloy in the presence of different concentrations palmitate in (a) 1.0 M Na_2SO_4 at 45 °C, (b) a medium of 0.2 M Na_2SO_4 - 0.1 M NaCl at 30 °C.

The capacitive loops of the Nyquist plots enlarge in succession with the increase in the concentration of palmitate, while the nature continues to be the same, suggesting an inhibition accomplished without participation in the electrode reactions. The impedance plots on simulation with equivalent electrical circuit as represented in Fig. 3.3, yielded impedance parameters like R_{hf}, C_{dl}, R_f and C_f for the corrosion of ZE41 alloy in the presence of different concentrations of palmitate in sodium sulfate and combined media, which are, respectively, enlisted in Table 3.12 (a), Table 3.12 (b), Table 3.12 (c) and Table 3.13 (a), Table 3.13 (b).

The efficiency values for palmitate calculated from the impedance analyses are close to those attained from the polarization measurements and moreover the most economic concentration of 2.7 mM and higher efficiency in stronger media are also in accordance with that of polarization results. Palmitate at higher concentrations seems to favor the formation of a thick and highly protective surface film as reflected by the lower film capacitance and higher film resistance values, which are observed exclusively at higher palmitate concentrations at any particular temperature. The formation of such an effective surface film justifies the increase in efficiency with the increase in palmitate concentration.

The Bode plots were examined for a complete understanding of the impedance behavior. Fig. 3.22(a) and Fig. 3.22 (b), respectively, represent Bode magnitude plots for the corrosion of ZE41 alloy immersed in 1.0 M Na_2SO_4 at 45 °C and in the combined medium of 0.2 M Na_2SO_4 - 0.1 M NaCl at 30 °C with varying amounts of palmitate. The phase angle plots for the same are shown in Fig. 3.23 (a) and Fig. 3.23 (b), respectively. As seen from the Bode plots, both the impedance modulus (Z_{mod}) at low frequency and the phase maximum (θ_{max}) at intermediate frequency increase with the increase in palmitate concentration, which collectively point out the presence of highly protective surface film, able enough to oppose corrosive ingress.
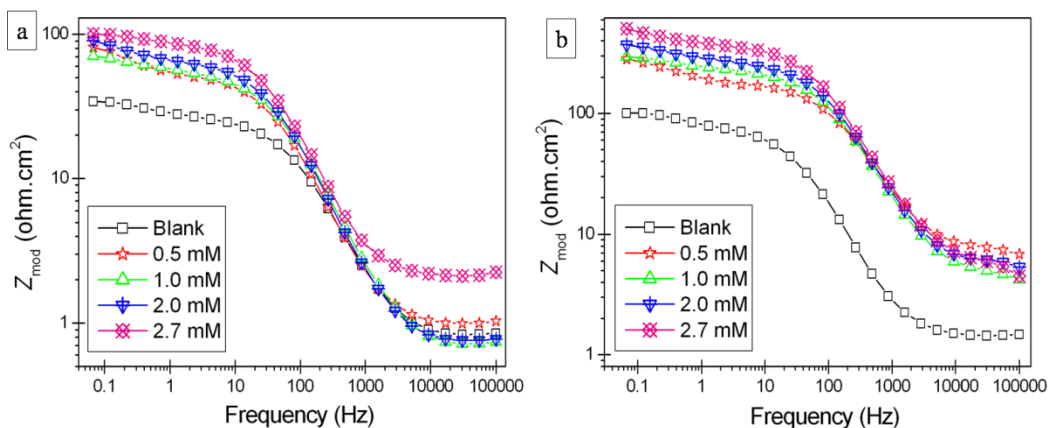
Fig. 3.22 Bode magnitude plots for the corrosion of ZE41 alloy in the presence of different concentrations of palmitate in (a) 1.0 M Na$_2$SO$_4$ at 45 °C, (b) a medium of 0.2 M Na$_2$SO$_4$ - 0.1 M NaCl at 30 °C.
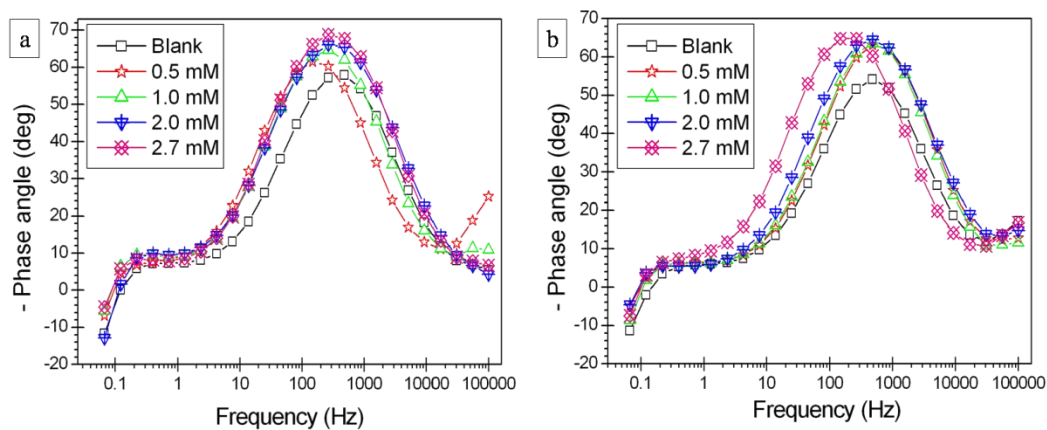
Fig. 3.23 Bode phase angle plots for the corrosion of ZE41 alloy in the presence of different concentrations of palmitate in (a) 1.0 M Na$_2$SO$_4$ at 45 °C, (b) a medium of 0.2 M Na$_2$SO$_4$ - 0.1 M NaCl at 30 °C.

3.3.3 Effect of temperature

The increase in solution temperature eventuates to be unfavorable for inhibition by palmitate, as indicated by the efficiency values tabulated in Table 3.10, Table 3.11, Table 3.12 and Table 3.13, which decrease with the increase in temperature. The

combination of greater film capacitance and lesser film resistance values seen at higher temperatures in all the media further substantiate such an adverse effect.
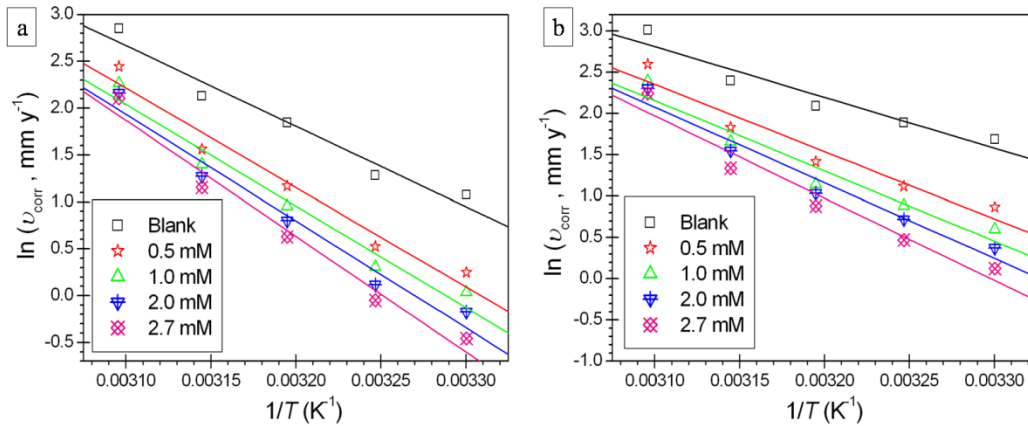
Fig. 3.24 Arrhenius plots for the corrosion of ZE41 alloy in the presence of different concentrations of palmitate in (a) 0.2 M Na₂SO₄ (b) a medium of 0.2 M Na₂SO₄ - 0.1 M NaCl.
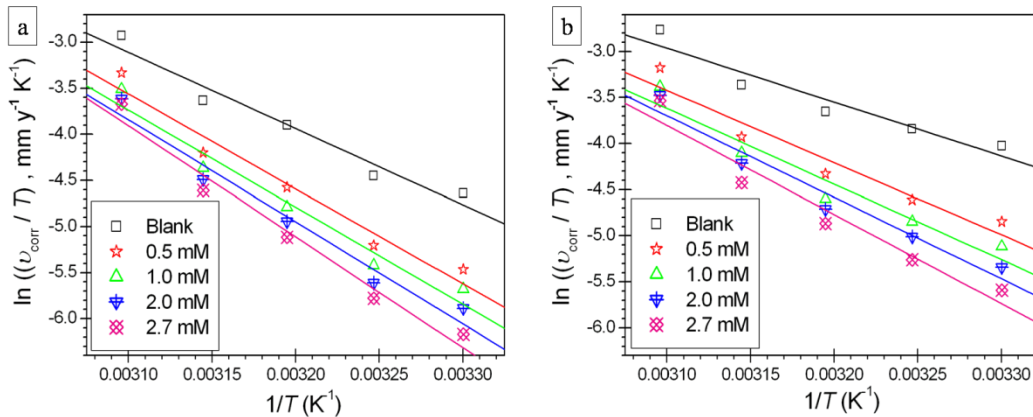
Fig. 3.25 ln (v_{corr}/T) vs. (1/T) plots for the corrosion of ZE41 alloy in the presence of different concentrations of palmitate in (a) 0.2 M Na₂SO₄ (b) a medium of 0.2 M Na₂SO₄ - 0.1 M NaCl.

Fig. 3.24 (a) and Fig. 3.24 (b), respectively, represent the Arrhenius plots for the corrosion of ZE41 alloy specimen in 0.2 M Na₂SO₄ and in the combined medium of 0.2 M Na₂SO₄ – 0.1 M NaCl both containing different concentrations of palmitate. The plots of ln (v_{corr} /T) versus (1/T) for the same are shown in Fig. 3.25 (a) and Fig. 3.25 (b),

respectively. The evaluated activation parameters for the corrosion of ZE41 alloy in sodium sulfate and in the combined media, having different concentrations of palmitate are listed in Table 3.14 (a) and Table 3.14 (b), respectively.

In both the media, the increased addition of palmitate increasingly obstructs the occurrence of ZE41 corrosion, as denoted by the monotonic increase in activation energy values. The pattern of change in $\Delta H^{\#}$ values is identical to that of E_a. The values of $\Delta S^{\#}$ are negative for both blank and electrolyte containing palmitate which suggests the non-involvement of added palmitate in electrode reactions, to be precise, even in the presence of palmitate the activated complex in the rate-determining step of ZE41 corrosion continue to be formed from the association of the reactants resulting in decreased entropy during activation.

3.3.4 Adsorption behavior

By graphical trial and error attempts of substituting the surface coverage (θ) and palmitate concentration (C_{inh}) values into the mathematical relations describing Langmuir, Temkin, Frumkin and Flory-Huggins isotherms, it was recognized that the interfacial adsorption of palmitate can be best expressed using Langmuir adsorption isotherm. The Langmuir adsorption isotherms for adsorption of palmitate on ZE41 alloy surface at different temperatures in 0.2 M Na_2SO_4 and in the combined medium of 0.2 M Na_2SO_4 - 1.0 M NaCl are presented in Fig. 3.26 (a) and Fig. 3.26 (b), respectively.

The evaluated thermodynamic parameters at different temperatures for the adsorption of palmitate on ZE41 alloy surface in sodium sulfate and in the combined media are tabulated in Table 3.15 (a) and Table 3.15 (b), respectively. Although the results comply well with the Langmuir adsorption isotherm (average linear regression coefficient equal to 0.99) and divergence from an ideal Langmuir behavior is evident from the values of slope, which convey that the palmitate molecules after adsorption over the alloy surface interact mutually. The spontaneity of palmitate adsorption is ascertained from the negative values of ΔG°_{ads}. The comparison between the magnitude of the

evaluated $\Delta G°_{ads}$ and $\Delta H°_{ads}$ values, respectively, with the free energy and enthalpy thresholds for physisorption and chemisorption, hints the predominance of physisorption. The decrease in entropy caused by the orderly arrangement of palmitate molecules at the alloy surface, which might more than compensate for the increased solvent entropy, is apparent from the negative values of $\Delta S°_{ads}$.
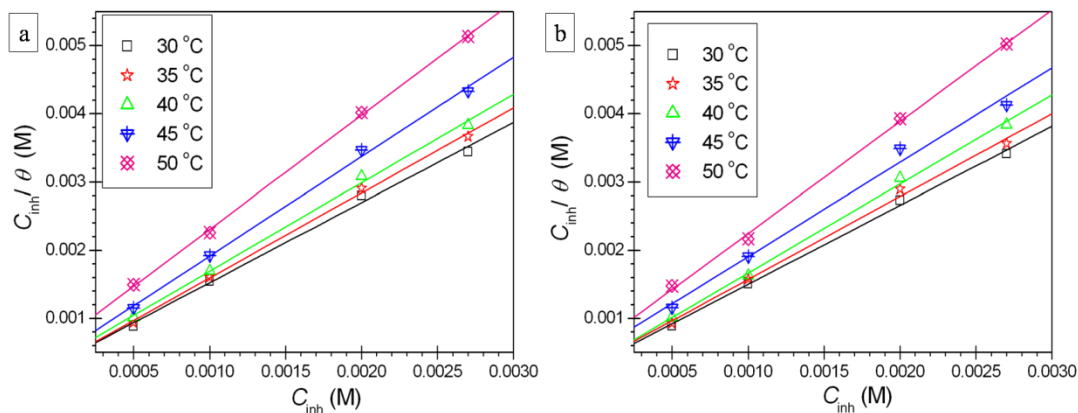
Fig. 3.26: Langmuir adsorption isotherms for the adsorption of palmitate on ZE41 alloy surface at different temperatures in (a) 0.2 M Na₂SO₄ (b) a medium of 0.2 M Na₂SO₄ - 0.1 M NaCl.

Table 3.10 (a) Electrochemical polarization parameters for the corrosion of ZE41 alloy in 0.2 M Na₂SO₄ containing different concentrations of palmitate at different temperatures.

Temp [°C]	Palmitate concentration [mM]	E_{corr} vs. SCE [mV]	i_{corr} [$\mu A\ cm^{-2}$]	$-b_c$ [$mV\ dec^{-1}$]	η [%]
	Blank	-1604	131.7	168	-
	0.5	-1602	55.6	162	56.2
	1.0	-1603	46.5	157	64.7
30	2.0	-1604	37.7	160	71.4
	2.7	-1600	27.5	169	78.4
	2.8	-1597	26.2	173	78.6
	4.0	-1598	24.5	171	79.9
	Blank	-1608	162.1	177	-
	0.5	-1607	73.0	172	53.2
35	1.0	-1604	61.3	156	62.2
	2.0	-1601	50.5	162	68.8
	2.7	-1607	42.8	145	73.6
	Blank	-1610	284.9	180	-
	0.5	-1609	141.7	174	49.2
40	1.0	-1602	116.9	181	59.0
	2.0	-1607	100.0	163	64.9
	2.7	-1604	81.3	158	70.4
	Blank	-1635	378.6	184	-
	0.5	-1629	214.4	173	43.4
45	1.0	-1624	181.7	185	52.0
	2.0	-1627	160.3	179	57.7
	2.7	-1618	142.6	160	62.4
	Blank	-1638	778.0	189	-
	0.5	-1635	511.3	191	33.4
50	1.0	-1637	413.6	182	44.3
	2.0	-1628	380.6	185	49.8
	2.7	-1630	358.9	165	52.6

Table 3.10 (b) Electrochemical polarization parameters for the corrosion of ZE41 alloy in 0.6 M Na₂SO₄ containing different concentrations of palmitate at different temperatures.

Temp [°C]	Palmitate concentration [mM]	E_{corr} vs. SCE [mV]	i_{corr} [$\mu A\ cm^{-2}$]	$-b_c$ [$mV\ dec^{-1}$]	η [%]
	Blank	-1626	327.1	192	-
	0.5	-1622	123.8	168	62.1
	1.0	-1618	85.0	182	74.0
30	2.0	-1617	64.9	173	80.2
	2.7	-1620	51.0	170	84.4
	2.8	-1613	49.4	189	84.9
	4.0	-1610	46.8	191	85.7
	Blank	-1628	594.7	199	-
	0.5	-1621	230.1	183	61.3
35	1.0	-1618	179.0	192	69.9
	2.0	-1612	160.6	195	73.0
	2.7	-1609	119.4	178	79.9
	Blank	-1634	708.0	204	-
	0.5	-1629	304.4	198	57.0
40	1.0	-1625	248.2	193	65.0
	2.0	-1630	212.5	200	70.0
	2.7	-1633	156.3	201	77.9
	Blank	-1636	886.7	211	-
	0.5	-1632	426.8	204	51.9
45	1.0	-1619	392.2	210	55.8
	2.0	-1628	320.0	197	63.9
	2.7	-1621	250.2	185	71.8
	Blank	-1639	1250.1	214	-
	0.5	-1637	724.7	206	42.0
50	1.0	-1629	626.8	210	49.9
	2.0	-1630	564.0	215	54.9
	2.7	-1617	513.7	208	58.9

Table 3.10 (c) Electrochemical polarization parameters for the corrosion of ZE41 alloy in 1.0 M Na$_2$SO$_4$ containing different concentrations of palmitate at different temperatures.

Temp [°C]	Palmitate concentration [mM]	E_{corr} vs. SCE [mV]	i_{corr} [μA cm^{-2}]	$-b_c$ [mV dec^{-1}]	η [%]
30	Blank	-1648	520.8	190	-
	0.5	-1639	176.7	187	66.1
	1.0	-1640	115.2	191	77.9
	2.0	-1643	88.5	190	83.0
	2.7	-1628	54.7	173	89.5
	2.8	-1634	51.6	178	90.1
	4.0	-1632	45.2	181	91.3
35	Blank	-1650	726.7	211	-
	0.5	-1639	262.5	206	63.9
	1.0	-1646	181.7	210	75.0
	2.0	-1632	146.7	215	79.8
	2.7	-1638	87.4	198	88.0
40	Blank	-1657	996.1	228	-
	0.5	-1651	390.0	214	60.8
	1.0	-1654	339.1	217	66.0
	2.0	-1637	276.8	220	72.2
	2.7	-1648	178.2	202	82.1
45	Blank	-1681	1287.7	261	-
	0.5	-1663	607.8	256	52.8
	1.0	-1660	542.5	247	57.9
	2.0	-1663	478.9	251	62.8
	2.7	-1645	331.3	234	74.3
50	Blank	-1686	1451.2	308	-
	0.5	-1672	810.0	289	44.2
	1.0	-1665	716.7	302	50.6
	2.0	-1668	638.6	276	56.0
	2.7	-1649	550.1	245	62.1

Table 3.11 (a) Electrochemical polarization parameters for the corrosion of ZE41 alloy in the combined medium of 0.2 M Na₂SO₄ - 0.1 M NaCl containing different concentrations of palmitate at different temperatures.

Temp [°C]	Palmitate concentration [mM]	E_{corr} vs. SCE [mV]	i_{corr} [$\mu A\ cm^{-2}$]	$-b_c$ [$mV\ dec^{-1}$]	η [%]
	Blank	-1607	242.9	176	-
	0.5	-1606	106.8	174	56.0
	1.0	-1606	81.8	163	66.3
30	2.0	-1605	65.3	170	73.1
	2.7	-1602	50.8	145	79.1
	2.8	-1604	49.5	141	79.6
	4.0	-1605	47.3	148	80.5
	Blank	-1628	297.3	195	-
	0.5	-1623	137.6	189	53.7
35	1.0	-1626	108.8	158	63.4
	2.0	-1619	92.1	165	69.0
	2.7	-1621	71.9	183	75.8
	Blank	-1644	364.9	196	-
	0.5	-1639	185.3	201	49.2
40	1.0	-1631	141.1	194	61.3
	2.0	-1642	126.3	187	65.4
	2.7	-1628	108.1	190	70.4
	Blank	-1649	495.2	192	-
	0.5	-1642	280.9	199	43.3
45	1.0	-1645	235.6	203	52.4
	2.0	-1637	211.2	185	57.4
	2.7	-1642	171.3	186	65.4
	Blank	-1655	914.1	213	-
	0.5	-1654	604.5	186	33.9
50	1.0	-1639	492.3	211	46.1
	2.0	-1643	448.7	195	50.9
	2.7	-1641	423.0	189	53.7

Table 3.11 (b) Electrochemical polarization parameters for the corrosion of ZE41 alloy in the combined medium of 1.0 M Na₂SO₄ - 1.0 M NaCl containing different concentrations of palmitate at different temperatures.

Temp [°C]	Palmitate concentration [mM]	E_{corr} vs. SCE [mV]	i_{corr} [$\mu A\ cm^{-2}$]	$-b_c$ [$mV\ dec^{-1}$]	η [%]
	Blank	-1669	825.0	204	-
	0.5	-1658	265.9	198	67.8
	1.0	-1647	168.3	201	79.6
30	2.0	-1650	126.0	191	84.7
	2.7	-1662	73.3	187	91.1
	2.8	-1667	67.7	182	91.8
	4.0	-1648	57.5	186	93.0
	Blank	-1681	1034.7	214	-
	0.5	-1667	356.4	205	65.6
35	1.0	-1674	241.3	197	76.7
	2.0	-1670	190.7	189	81.6
	2.7	-1663	106.3	191	89.7
	Blank	-1665	1310.2	221	-
	0.5	-1662	490.5	213	62.6
40	1.0	-1656	421.0	206	67.9
	2.0	-1650	342.3	210	73.9
	2.7	-1661	213.8	219	83.7
	Blank	-1716	1733.5	317	-
	0.5	-1692	790.0	289	54.4
45	1.0	-1687	698.4	302	59.7
	2.0	-1688	615.3	313	64.5
	2.7	-1656	416.4	304	76.0
	Blank	-1726	1752.8	224	-
	0.5	-1700	948.3	229	45.9
50	1.0	-1687	836.5	256	52.3
	2.0	-1691	743.3	214	57.6
	2.7	-1684	636.7	238	63.7

Table 3.12 (a) Impedance parameters for the corrosion of ZE41 alloy in 0.2 M Na₂SO₄ containing different concentrations of palmitate at different temperatures.

Temp [°C]	Palmitate concentration [mM]	R_{hf} [Ω cm^2]	R_f [Ω cm^2]	C_{dl} [μF cm^{-2}]	C_f [μFcm^{-2}]	η [%]
	Blank	83.3	73.1	24.0	101.2	-
	0.5	194.8	108.3	23.9	100.1	57.2
	1.0	238.7	140.8	22.0	94.6	65.1
30	2.0	302.2	173.7	19.9	89.2	72.4
	2.7	397.6	190.1	18.1	81.3	79.1
	2.8	421.5	273.9	15.6	72.3	80.2
	4.0	442.6	397.3	12.5	34.7	81.2
	Blank	63.7	55.5	32.1	102.7	-
	0.5	141.3	73.0	31.3	101.4	55.0
35	1.0	170.3	116.8	30.7	98.5	62.6
	2.0	208.7	151.4	28.6	92.5	69.5
	2.7	229.8	198.3	24.8	85.3	72.3
	Blank	53.9	40.7	35.3	104.1	-
	0.5	108.5	50.1	33.9	103.7	50.3
40	1.0	134.2	63.3	31.7	100.3	59.9
	2.0	158.3	82.1	28.9	95.8	66.0
	2.7	191.7	96.8	25.8	91.4	71.9
	Blank	47.2	42.7	36.8	104.9	-
	0.5	80.2	43.0	35.7	103.5	41.2
45	1.0	96.8	47.8	34.1	101.9	51.3
	2.0	114.2	64.8	30.7	99.0	58.7
	2.7	128.9	74.2	26.6	94.4	63.4
	Blank	34.2	31.2	39.4	108.1	-
	0.5	51.9	31.7	38.8	107.8	34.2
50	1.0	62.7	32.8	37.0	106.8	45.5
	2.0	70.3	37.1	35.1	103.4	51.4
	2.7	75.7	43.9	33.5	94.8	54.9

Table 3.12 (b) Impedance parameters for the corrosion of ZE41 alloy in 0.6 M Na₂SO₄ containing different concentrations of palmitate at different temperatures.

Temp [°C]	Palmitate concentration [mM]	R_{hf} [Ω cm²]	R_f [Ω cm²]	C_{dl} [μF cm⁻²]	C_f [μFcm⁻²]	η [%]
30	Blank	61.1	51.7	26.9	101.2	-
	0.5	157.9	120.5	23.8	98.4	61.3
	1.0	236.8	152.8	21.8	90.6	74.2
	2.0	302.2	176.9	19.0	86.7	79.8
	2.7	393.6	192.8	17.5	77.0	84.5
	2.8	408.5	281.9	14.6	64.8	85.0
	4.0	439.7	408.6	11.7	26.6	86.1
35	Blank	40.2	31.2	35.0	104.1	-
	0.5	107.2	88.9	31.0	102.6	62.5
	1.0	134.5	120.8	29.6	95.8	70.1
	2.0	156.7	165.9	25.7	89.6	74.4
	2.7	204.6	197.4	22.5	82.4	80.4
40	Blank	36.6	27.8	37.6	104.3	-
	0.5	88.3	51.9	32.7	103.5	58.6
	1.0	104.8	67.7	29.0	98.6	65.1
	2.0	123.7	88.3	26.8	93.8	70.4
	2.7	170.1	95.8	23.3	86.4	78.5
45	Blank	27.6	19.9	41.9	106.7	-
	0.5	59.4	36.8	35.6	105.6	53.5
	1.0	63.8	50.0	30.8	100.8	56.7
	2.0	76.9	65.7	28.0	98.3	64.1
	2.7	101.2	76.5	24.7	91.5	72.7
50	Blank	19.4	17.6	43.4	109.3	-
	0.5	32.4	23.8	38.4	107.9	40.1
	1.0	37.1	33.0	35.6	105.2	47.7
	2.0	44.8	38.3	34.5	101.3	56.7
	2.7	48.9	45.3	31.8	93.6	60.3

Table 3.12 (c) Impedance parameters for the corrosion of ZE41 alloy in 1.0 M Na₂SO₄ containing different concentrations of palmitate at different temperatures.

Temp [°C]	Palmitate concentration [mM]	R_{hf} [Ω cm^2]	R_f [Ω cm^2]	C_{dl} [μF cm^{-2}]	C_f [μFcm^{-2}]	η [%]
30	Blank	46.0	42.0	33.9	108.5	-
	0.5	133.7	123.7	22.8	97.1	65.6
	1.0	211.4	162.8	20.1	86.8	78.2
	2.0	274.8	180.9	17.6	80.9	83.3
	2.7	412.6	196.3	14.5	71.7	88.8
	2.8	424.8	284.7	12.8	60.6	89.2
	4.0	489.7	412.6	10.1	14.7	90.6
35	Blank	39.7	36.2	40.1	108.9	-
	0.5	102.2	114.8	30.7	100.3	61.1
	1.0	165.9	142.7	28.5	93.3	76.1
	2.0	182.7	171.5	23.6	87.6	78.3
	2.7	351.3	201.5	20.5	80.8	88.7
40	Blank	25.0	20.6	42.6	110.2	-
	0.5	59.0	52.9	32.0	105.8	57.6
	1.0	76.8	69.2	28.8	96.2	67.4
	2.0	95.9	90.0	25.7	88.3	73.9
	2.7	145.7	98.8	22.2	81.0	82.8
45	Blank	23.4	18.5	43.2	111.2	-
	0.5	53.3	43.9	35.2	106.6	56.1
	1.0	59.8	60.2	30.3	99.8	60.9
	2.0	64.1	69.3	27.8	97.2	63.5
	2.7	89.8	77.3	24.1	89.9	73.9
50	Blank	22.8	17.4	44.6	115.3	-
	0.5	38.9	37.8	38.2	107.2	41.4
	1.0	43.3	46.3	35.2	101.5	47.3
	2.0	52.4	52.2	33.7	98.3	56.5
	2.7	62.2	58.7	30.2	90.0	63.3

Table 3.13 (a) Impedance parameters for the corrosion of ZE41 alloy in the combined medium of 0.2 M Na$_2$SO$_4$ - 0.1 M NaCl containing different concentrations of palmitate at different temperatures.

Temp [°C]	Palmitate concentration [mM]	R_{hf} [Ω cm^2]	R_f [Ω cm^2]	C_{dl} [μF cm^{-2}]	C_f [μFcm^{-2}]	η [%]
	Blank	74.9	69.7	27.1	101.8	-
	0.5	176.1	138.6	19.4	94.9	57.4
	1.0	222.7	173.1	18.0	85.0	66.4
30	2.0	266.3	182.4	15.6	79.0	71.9
	2.7	360.1	200.4	13.8	74.7	79.2
	2.8	369.3	305.6	11.3	61.5	79.7
	4.0	378.7	368.8	8.9	34.6	80.2
	Blank	54.6	49.0	36.4	103.6	-
	0.5	120.8	112.4	32.1	101.2	54.8
35	1.0	141.9	138.3	29.6	97.8	61.5
	2.0	167.2	149.5	26.7	87.3	67.4
	2.7	200.1	174.7	22.1	76.4	72.7
	Blank	49.2	34.2	39.0	106.1	-
	0.5	97.9	76.5	35.7	104.3	49.8
40	1.0	120.1	109.2	29.0	100.8	61.0
	2.0	140.1	118.2	24.7	97.3	66.8
	2.7	164.9	145.7	21.2	88.9	73.6
	Blank	43.2	31.8	43.1	107.7	-
	0.5	75.0	63.3	38.5	105.8	42.4
45	1.0	91.1	82.4	29.3	102.2	52.6
	2.0	103.7	94.9	25.4	98.3	58.4
	2.7	114.8	102.5	21.9	91.0	62.4
	Blank	28.8	25.7	45.6	110.6	-
	0.5	40.0	34.6	38.3	108.9	28.1
50	1.0	55.7	48.4	33.2	104.2	48.3
	2.0	58.9	52.7	30.1	100.3	51.1
	2.7	63.0	60.0	27.7	83.3	54.3

Table 3.13 (b) Impedance parameters for the corrosion of ZE41 alloy in the combined medium of 1.0 M Na_2SO_4 - 1.0 M NaCl containing different concentrations of palmitate at different temperatures.

Temp [°C]	Palmitate concentration [mM]	R_{hf} [Ω cm^2]	R_f [Ω cm^2]	C_{dl} [μF cm^{-2}]	C_f [μFcm^{-2}]	η [%]
	Blank	34.6	31.4	40.3	112.4	-
	0.5	102.4	100.4	19.0	94.2	66.2
	1.0	173.8	168.2	16.1	82.1	80.1
30	2.0	228.4	182.4	14.8	75.7	84.8
	2.7	382.5	197.6	12.4	70.7	91.0
	2.8	417.4	293.7	10.3	60.7	91.7
	4.0	486.2	436.3	8.7	21.4	92.9
	Blank	29.3	23.8	49.3	113.4	-
	0.5	82.1	80.2	31.3	97.8	64.3
35	1.0	130.8	112.7	28.1	92.4	77.6
	2.0	167.3	153.7	24.7	87.8	82.5
	2.7	298.7	181.5	20.2	73.3	90.2
	Blank	20.1	16.2	54.3	114.7	-
	0.5	51.3	41.3	33.3	105.2	60.8
40	1.0	68.9	53.8	28.2	94.3	70.8
	2.0	76.8	64.9	24.1	86.5	73.8
	2.7	116.2	105.6	20.2	82.4	82.7
	Blank	15.8	14.9	58.0	114.6	-
	0.5	35.2	25.8	34.2	100.2	55.2
45	1.0	40.3	32.7	28.2	96.2	60.8
	2.0	45.6	42.7	23.2	92.7	65.4
	2.7	61.3	55.3	20.9	84.2	74.2
	Blank	15.0	13.1	63.6	120.1	-
	0.5	26.2	23.9	41.6	112.5	42.8
50	1.0	32.4	29.0	31.2	100.1	53.8
	2.0	38.3	34.0	29.2	94.8	60.9
	2.7	42.2	39.7	24.8	79.0	64.5

Table 3.14 (a) Activation parameters for the corrosion of ZE41 alloy in different concentrations of sodium sulfate in the presence of different concentrations of palmitate.

Concentration of Na$_2$SO$_4$ [M]	Concentration of palmitate [mM]	E_a [kJ mol^{-1}]	$\Delta H^{\#}$ [kJ mol^{-1}]	$\Delta S^{\#}$ [J mol^{-1} K^{-1}]
	Blank	71.4	68.8	-93.2
	0.5	88.1	85.5	-45.3
0.2	1.0	90.1	87.5	-40.6
	2.0	94.6	92.0	-27.4
	2.7	102.7	100.1	-2.7
	Blank	50.3	47.7	-153.5
	0.5	67.6	65.0	-104.8
0.6	1.0	77.9	75.3	-73.7
	2.0	81.8	79.2	-62.7
	2.7	87.2	84.6	-47.2
	Blank	42.8	40.2	-174.9
	0.5	63.3	60.7	-116.7
1.0	1.0	77.4	74.8	-73.3
	2.0	83.7	81.1	-54.8
	2.7	96.8	94.2	-16.1

Table 3.14 (b) Activation parameters for the corrosion of ZE41 alloy in different concentrations of combined medium in the presence of different concentrations of palmitate.

Concentration of medium [M]	Concentration of palmitate [mM]	E_a [kJ mol^{-1}]	$\Delta H^{\#}$ [kJ mol^{-1}]	$\Delta S^{\#}$ [J mol^{-1} K^{-1}]
	Blank	51.2	48.6	-154.8
	0.5	67.7	65.1	-107.3
0.2 M Na$_2$SO$_4$ & 0.1M NaCl	1.0	70.7	68.1	-99.6
	2.0	76.1	73.5	-83.8
	2.7	82.8	80.2	-63.6
	Blank	33.0	30.4	-203.4
1.0 M Na$_2$SO$_4$ & 1.0M NaCl	0.5	54.3	51.7	-142.9
	1.0	69.6	67.0	-96.3
	2.0	76.9	74.3	-74.4
	2.7	92.6	90.0	-28.0

Table 3.15 (a) Thermodynamic parameters for the adsorption of palmitate on ZE41 alloy surface in sodium sulfate media.

Concentration of Na_2SO_4 [M]	Temp [°C]	$\Delta G°_{ads}$ [kJ mol^{-1}]	$\Delta H°_{ads}$ [kJ mol^{-1}]	$\Delta S°_{ads}$ [J K^{-1}mol^{-1}]	R^2	Slope
0.2	30	-30.2			0.995	1.17
	35	-30.7			0.998	1.25
	40	-30.8	-24.0	-21.4	0.997	1.30
	45	-30.9			0.998	1.46
	50	-30.6			0.999	1.67
0.6	30	-30.9			0.999	1.10
	35	-31.5			0.995	1.19
	40	-31.3	-26.0	-16.7	0.993	1.20
	45	-31.1			0.989	1.27
	50	-31.5			0.998	1.56
1.0	30	-31.0			0.997	1.04
	35	-31.2			0.995	1.06
	40	-31.3	-26.9	-13.6	0.987	1.14
	45	-31.1			0.977	1.25
	50	-31.4			0.994	1.48

Table 3.15 (b) Thermodynamic parameters for the adsorption of palmitate on ZE41 alloy surface in combined media.

Concentration of medium [M]	Temp [°C]	$\Delta G°_{ads}$ [kJ mol^{-1}]	$\Delta H°_{ads}$ [kJ mol^{-1}]	$\Delta S°_{ads}$ [J K^{-1}mol^{-1}]	R^2	Slope
0.2 M Na_2SO_4 & 0.1M NaCl	30	-30.2			0.998	1.16
	35	-30.6			0.996	1.21
	40	-31.1	-24.8	-18.6	0.998	1.31
	45	-30.6			0.989	1.38
	50	-30.7			0.999	1.64
1.0 M Na_2SO_4 & 1.0M NaCl	30	-31.1			0.998	1.03
	35	-31.3			0.995	1.04
	40	-31.4	-26.0	-17.1	0.988	1.12
	45	-31.2			0.979	1.23
	50	-31.6			0.994	1.45

3.4 MYRISTATE AS CORROSION INHIBITOR FOR ZE41 IN AQUEOUS SALT SOLUTIONS

3.4.1 Potentiodynamic polarization measurements

The potentiodynamic polarization plots for the corrosion of ZE41 in 1.0 M Na_2SO_4 at 45 ºC and in the combined medium of 0.2 M Na_2SO_4 – 0.1 M NaCl at 40 ºC, both containing different concentrations of myristate are represented Fig. 3.27 (a) and Fig. 3.27 (b), respectively.
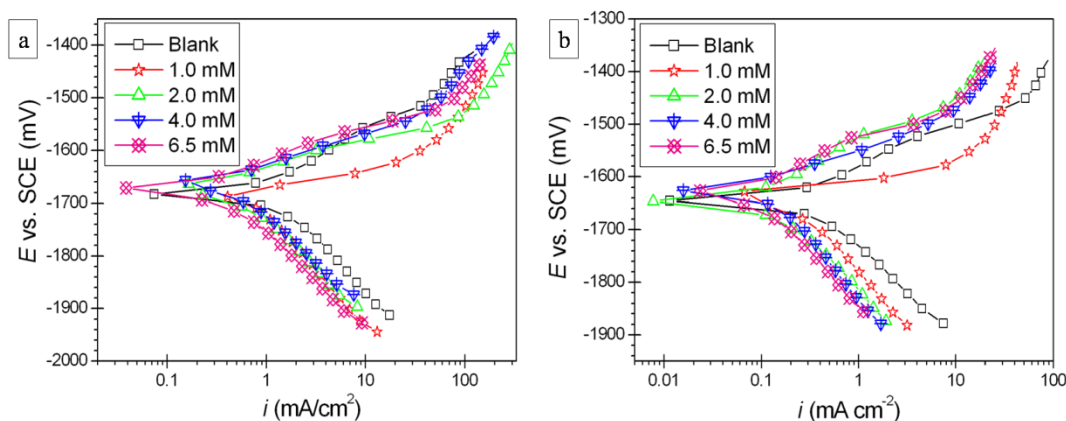
Fig. 3.27 Potentiodynamic polarization curves for the corrosion of ZE41 alloy in the presence of different concentrations of myristate in (a) 1.0 M Na_2SO_4 at 45 °C, (b) a medium of 0.2 M Na_2SO_4 - 0.1 M NaCl at 40 °C.

The prominent observations from Fig. 3.27 are the successive shift of polarization curves towards lower current density region on increase in myristate concentration, with no apparent change in overall shape, the implication of this result is same as that explained for stearate and palmitate. Once again the linear Tafel behavior is exclusive to cathodic branches and hence corrosion current density (i_{corr}) is deduced from cathodic extrapolation of Tafel plots at corrosion potential. Table 3.16 (a), Table 3.16 (b), Table 3.16 (c) and Table 3.17 (a), Table 3.17 (b), respectively, show the calculated potentiodynamic polarization parameters associated with the polarization measurements

performed in the presence of different concentrations of myristate in sodium sulfate and in the combined media at different medium concentrations and temperatures.

It follows from Table 3.16 and Table 3.17 that myristate too functions as mixed-type inhibitor which for the most part limits the anodic reaction because the addition of myristate produces a successive anodic shift in corrosion potential (not more than 30 mV vs. SCE), along with slight variations in cathodic slopes. Furthermore, the increase in addition of myristate enhances the inhibition efficiency, the optimum or the most economic concentration (C_{max}) of myristate is 6.5 mM at which a maximum inhibition efficiencies in sodium sulfate and in combined media, respectively, are 81.1 % and 86.6 %, observed at 30 ºC in the medium of 1.0 M Na_2SO_4 and in combined medium of 1.0 M Na_2SO_4 - 1.0 M NaCl, respectively. Furthermore, myristate exhibits higher efficiency in the concentrated media.

3.4.2 Electrochemical impedance spectroscopy studies

The Nyquist plots for the corrosion of ZE41 in 1.0 M Na_2SO_4 at 45 ºC and in the combined medium of 0.2 M Na_2SO_4 – 0.1 M NaCl at 40 ºC, both having different concentrations of myristate, are illustrated in Fig. 3.28 (a) and Fig. 3.28 (b), respectively.
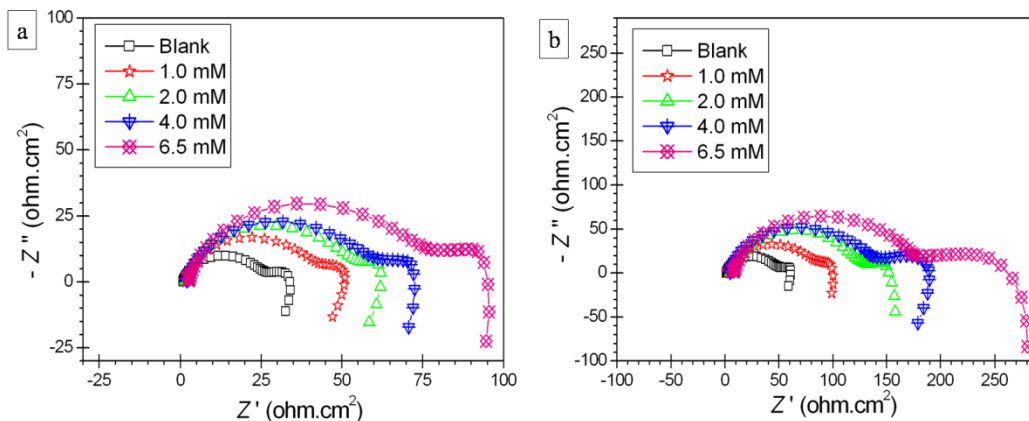
Fig. 3.28 Nyquist plots for the corrosion of ZE41 alloy in the presence of different concentrations of myristate in (a) 1.0 M Na_2SO_4 at 45 °C, (b) a medium of 0.2 M Na_2SO_4 - 0.1 M NaCl at 40 °C.

The Nyquist plots exhibited characteristic shape, comprising of two capacitive loops at higher and medium frequencies, followed by the beginning of an inductive loop at lower frequency region. With the gradual rise in myristate concentration in both the media, a successive enlargement of capacitive loops resulted, with no significant change in shape, which implies that the added myristate reduces corrosion rate without interfering with the mechanism or the reactions of corrosion.

The impedance parameters such as R_{hf}, C_{dl}, R_f and C_f were deduced from simulation studies and the same for varying amounts of myristate in sodium sulfate and combined media at different medium concentrations and temperatures are enlisted in Table 3.18 (a), Table 3.18 (b) , Table 3.18 (c) and Table 3.19 (a), Table 3.19 (b), respectively. An appreciable accordance is obtained between the results of polarization and impedance measurements, in terms that, the inhibition efficiency increases significantly with the increase in myristate concentration up to the optimum concentration of 6.5 mM, greater values of efficiency are observed in more concentrated media. The film resistance successively increases whereas film capacitance decreases on increased introduction of myristate, which respectively reflects the enhancement in defensive ability and thickness of the surface film.

The inhibition brought about by myristate is further verified by constructing Bode plots. The Bode magnitude plots for the corrosion of ZE41 alloy immersed in 1.0 M Na_2SO_4 at 45 °C and in the combined medium of 0.2 M Na_2SO_4 - 0.1 M NaCl at 40 °C with varying amounts of myristate are shown in Fig. 3.29 (a) and Fig. 3.29 (b), respectively. The phase angle plots for the same are depicted in Fig. 3.30 (a) and Fig. 3.30 (b), respectively.

As evidently seen from Fig. 3.29 and Fig. 3.30 a progressive increase in impedance modulus at low frequency and phase maximum at medium frequency is consistent with the increase in the concentration of myristate, which together indicates a better corrosion protection performance.
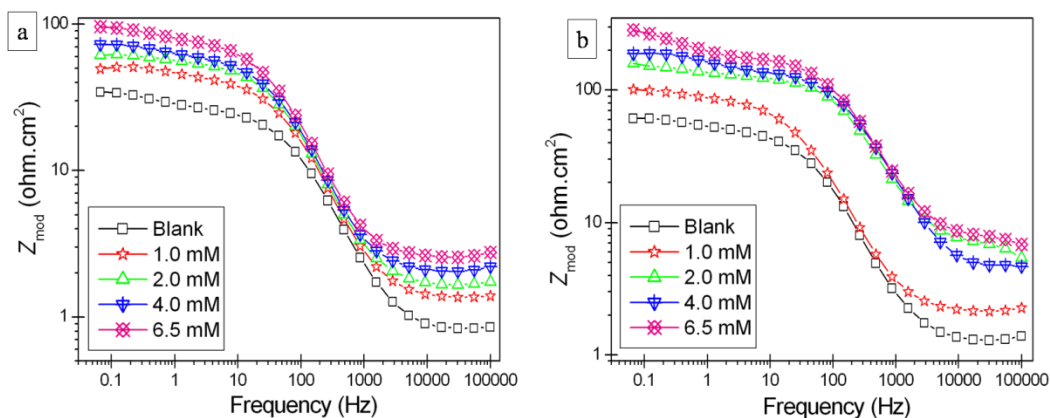
Fig. 3.29 Bode magnitude plots for the corrosion of ZE41 alloy in the presence of different concentrations of myristate in (a) 1.0 M Na$_2$SO$_4$ at 45 °C, (b) medium 0.2 M Na$_2$SO$_4$ - 0.1 M NaCl at 40 °C.
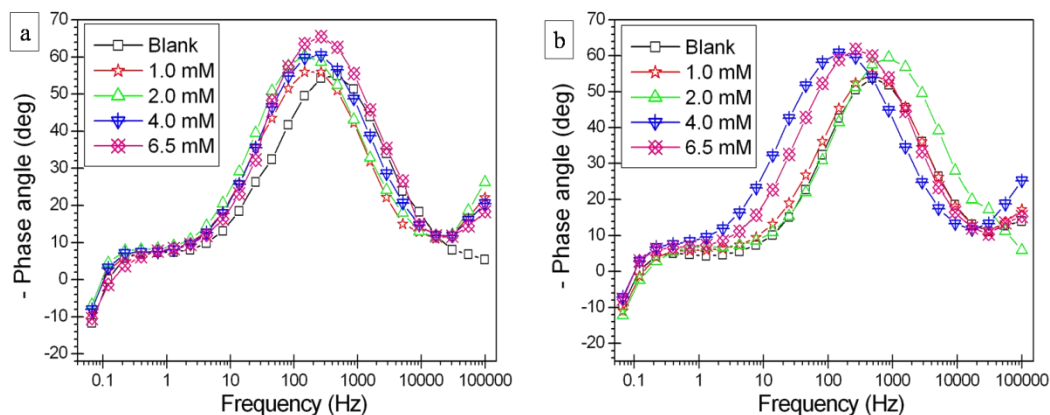
Fig. 3.30: Bode phase angle plots for the corrosion of ZE41 alloy in the presence of different concentrations of myristate in (a) 1.0 M Na$_2$SO$_4$ at 45 °C, (b) medium 0.2 M Na$_2$SO$_4$ - 0.1 M NaCl at 40 °C.

3.4.3 Effect of temperature

An increase in temperature in both the media diminishes the efficiency of myristate to inhibit ZE41 corrosion which is apparent from the parameters shown in Table 3.16, Table 3.17, Table 3.18 and Table 3.19. A lower efficiency at higher temperatures is invariably accompanied by higher film capacitance and lower film

resistance values which point out to the presence of a thin surface film with poor protective ability. The Arrhenius plots for the corrosion of ZE41 alloy specimen in 0.2 M Na$_2$SO$_4$ and in the combined medium of 0.2 M Na$_2$SO$_4$ -1.0 M NaCl containing different concentrations of myristate are presented in Fig. 3.31 (a) and Fig. 3.31 (b), respectively. The ln (v_{corr} /T) versus (1/T) plots for the same are shown in Fig. 3.32 (a) and Fig. 3.32 (b), respectively.
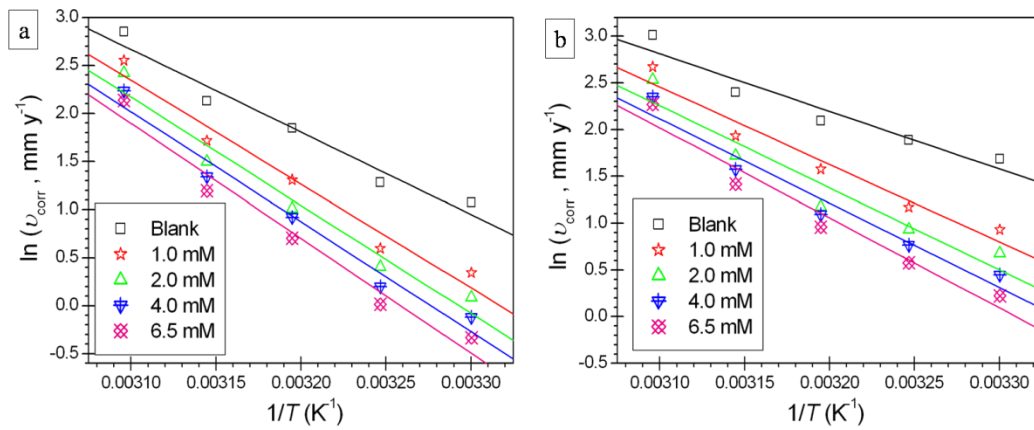
Fig. 3.31 Arrhenius plots for the corrosion of ZE41 alloy in the presence of different concentrations of myristate in (a) 0.2 M Na$_2$SO$_4$ (b) a medium of 0.2 M Na$_2$SO$_4$ - 0.1 M NaCl.
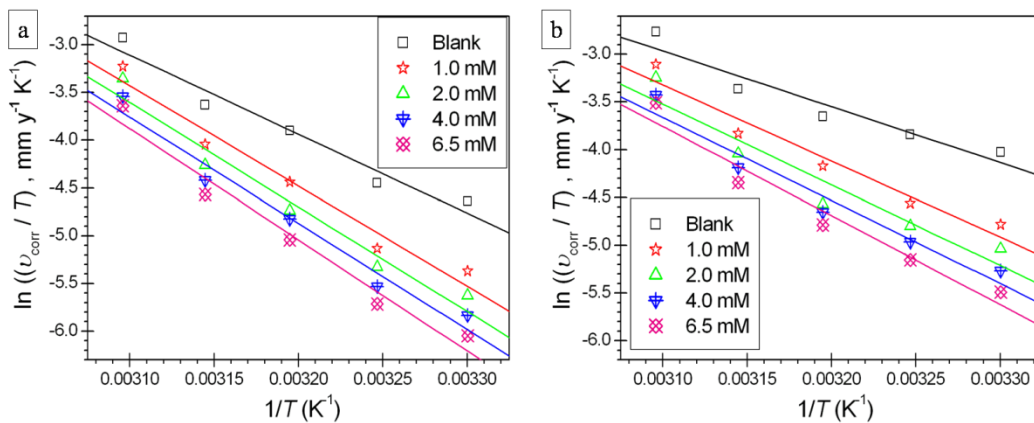
Fig. 3.32 ln (v_{corr}/T) vs. (1/T) plots for the corrosion of ZE41 alloy in the presence of different concentrations of myristate in (a) 0.2 M Na$_2$SO$_4$ (b) a medium of 0.2 M Na$_2$SO$_4$ - 0.1 M NaCl.

Table 3.20 (a) and Table 3.20 (b), respectively, show the calculated activation parameters for the alloy dissolution in sodium sulfate and combined media in the presence of different concentrations of myristate. The data presented in Table 3.20 evidently indicate that in both the media the increased addition of myristate leads to a gradual increase in activation energy suggesting an enhanced opposition to oxidation of ZE41. The entropy of activation ($\Delta S^{\#}$) continues to decrease owing to the association of reactants, even after the introduction of myristate into the blank, hinting that the mechanistic aspects pertaining to the formation of the activated complex remain unaltered even in the presence of myristate.

3.4.4 Adsorption behavior

The system with myristate as the inhibitor showed best agreement with Langmuir adsorption isotherm. The (C_{inh}/θ) versus C_{inh} plots used for the verification of suitability of Langmuir isotherm to explain the adsorption of myristate on ZE41 alloy surface at different temperatures in 0.2 M Na_2SO_4 and in combined medium 0.2 M Na_2SO_4 -1.0 M NaCl are presented in Fig. 3.33 (a) and Fig. 3.33 (b), respectively.
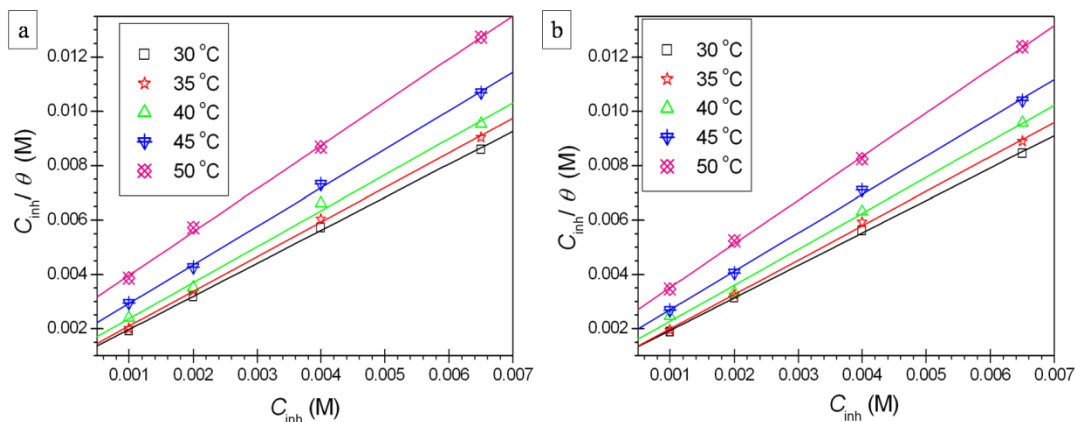
Fig. 3.33 Langmuir adsorption isotherms for the adsorption of myristate on ZE41 alloy surface at different temperatures in (a) 0.2 M Na_2SO_4 (b) a medium of 0.2 M Na_2SO_4 - 0.1 M NaCl.

The reaction isotherm equation (Eq.2.9) and Gibbs-Helmholtz equation (Eq.2.10) were made use of for the deduction of the thermodynamic parameters like ΔG°_{ads}, ΔH°_{ads} and ΔS°_{ads}. The evaluated thermodynamic parameters along with slope and linear regression coefficient (R^2) of the constructed isotherms, at different temperatures for the adsorption of myristate on ZE41 alloy surface in sodium sulfate and the combined media are tabulated in Table 3.21 (a) and Table 3.21 (b), respectively. The linear plots (average $R^2 = 0.99$) show deviation from ideal Langmuir behavior in terms that the slopes are not equal to unity. This deviation hints at the intermolecular interactions operating between the adsorbed myristate molecules. The ΔG°_{ads} values for myristate adsorption are negative and intermediate of the free energy thresholds for physisorption and chemisorption, which respectively, imply that myristate adsorbs spontaneously and both physisorption and chemisorption come into existence when myristate molecules interact with ZE41 surface. However the physisorption appears to be more predominant as the obtained values of ΔH°_{ads} are close to adsorption enthalpy threshold for physisorption. The adsorption of myristate leading to the formation of orderly arranged layers at the alloy surface is evident from the decrease in entropy of the system as signified by the negative ΔS°_{ads} values.

Table 3.16 (a) Electrochemical polarization parameters for the corrosion of ZE41 alloy in 0.2 M Na₂SO₄ containing different concentrations of myristate at different temperatures.

Temp [°C]	Myristate concentration [mM]	E_{corr} vs. SCE [mV]	i_{corr} [$\mu A\ cm^{-2}$]	$-b_c$ [$mV\ dec^{-1}$]	η [%]
30	Blank	-1604	131.7	168	-
	1.0	-1600	63.4	160	51.9
	2.0	-1602	49.0	152	62.8
	4.0	-1603	39.8	164	69.8
	6.5	-1600	32.2	147	75.6
	6.6	-1594	31.4	139	76.2
	8.0	-1599	29.5	152	77.6
35	Blank	-1608	162.1	177	-
	1.0	-1603	81.6	172	49.7
	2.0	-1607	67.3	168	58.5
	4.0	-1606	54.7	159	66.3
	6.5	-1601	45.6	137	71.9
40	Blank	-1610	284.9	180	-
	1.0	-1607	166.0	149	41.7
	2.0	-1604	123.2	157	56.8
	4.0	-1603	112.6	172	60.5
	6.5	-1600	90.9	170	68.1
45	Blank	-1635	378.6	184	-
	1.0	-1627	250.2	167	33.9
	2.0	-1615	201.1	173	46.9
	4.0	-1620	171.7	156	54.6
	6.5	-1614	148.3	162	60.8
50	Blank	-1638	778.0	189	-
	1.0	-1632	576.7	172	25.9
	2.0	-1629	506.2	180	34.9
	4.0	-1620	419.7	177	46.1
	6.5	-1635	380.9	164	51.0

Table 3.16 (b) Electrochemical polarization parameters for the corrosion of ZE41 alloy in 0.6 M Na₂SO₄ containing different concentrations of myristate at different temperatures.

Temp [°C]	Myristate concentration [mM]	E_{corr} vs. SCE [mV]	i_{corr} [$\mu A\ cm^{-2}$]	$-b_c$ [$mV\ dec^{-1}$]	η [%]
30	Blank	-1626	327.1	192	-
	1.0	-1619	146.9	173	55.1
	2.0	-1624	117.4	166	64.1
	4.0	-1622	85.9	181	73.7
	6.5	-1616	72.0	189	78.0
	6.6	-1614	70.2	190	78.6
	8.0	-1610	66.8	186	79.6
35	Blank	-1628	594.7	199	-
	1.0	-1625	275.8	190	53.6
	2.0	-1626	220.7	193	62.9
	4.0	-1620	170.1	187	71.4
	6.5	-1621	139.0	180	76.6
40	Blank	-1634	708.0	204	-
	1.0	-1630	372.8	201	47.4
	2.0	-1632	295.3	193	58.3
	4.0	-1627	237.8	197	66.4
	6.5	-1629	184.1	202	74.0
45	Blank	-1636	886.7	211	-
	1.0	-1631	515.0	213	41.9
	2.0	-1624	445.3	204	49.8
	4.0	-1628	387.2	210	56.3
	6.5	-1619	310.6	197	65.0
50	Blank	-1639	1250.1	214	-
	1.0	-1627	790.0	206	36.8
	2.0	-1632	743.3	192	40.5
	4.0	-1630	658.1	210	47.4
	6.5	-1621	579.0	211	53.7

Table 3.16 (c) Electrochemical polarization parameters for the corrosion of ZE41 alloy in 1.0 M Na₂SO₄ containing different concentrations of myristate at different temperatures.

Temp [°C]	Myristate concentration [mM]	E_{corr} vs. SCE [mV]	i_{corr} [μA cm^{-2}]	$-b_c$ [mV dec^{-1}]	η [%]
	Blank	-1648	520.8	190	-
	1.0	-1641	220.0	183	57.8
	2.0	-1644	179.4	192	65.6
30	4.0	-1640	136.3	187	73.8
	6.5	-1636	98.3	173	81.1
	6.6	-1635	90.4	175	82.7
	8.0	-1638	84.0	180	83.9
	Blank	-1650	726.7	211	-
	1.0	-1642	335.6	203	53.8
35	2.0	-1648	270.0	210	62.8
	4.0	-1646	197.3	197	72.9
	6.5	-1637	158.4	205	78.2
	Blank	-1657	996.1	228	-
	1.0	-1650	482.3	221	51.6
40	2.0	-1651	380.6	218	61.8
	4.0	-1642	324.5	205	67.4
	6.5	-1646	231.2	210	76.8
	Blank	-1681	1287.7	261	-
	1.0	-1678	672.6	246	47.8
45	2.0	-1672	580.0	257	55.0
	4.0	-1662	493.8	260	61.7
	6.5	-1675	406.2	258	68.5
	Blank	-1686	1451.2	308	-
	1.0	-1681	906.2	302	37.6
50	2.0	-1683	789.5	289	45.6
	4.0	-1676	738.8	304	49.1
	6.5	-1672	640.1	294	55.9

Table 3.17 (a) Electrochemical polarization parameters for the corrosion of ZE41 alloy in a medium of 0.2 M Na$_2$SO$_4$ - 0.1M NaCl containing different concentrations of myristate at different temperatures.

Temp [°C]	Myristate concentration [mM]	E_{corr} vs. SCE [mV]	i_{corr} [μA cm^{-2}]	$-b_c$ [mV dec^{-1}]	η [%]
30	Blank	-1607	242.9	176	-
	1.0	-1600	114.3	170	53.0
	2.0	-1592	88.3	162	63.6
	4.0	-1602	70.0	163	71.2
	6.5	-1601	56.2	149	76.9
	6.6	-1597	55.8	147	77.0
	8.0	-1595	49.6	140	79.6
35	Blank	-1628	297.3	195	-
	1.0	-1625	144.8	184	51.3
	2.0	-1617	114.0	188	61.6
	4.0	-1620	96.7	191	67.5
	6.5	-1619	80.0	178	73.1
40	Blank	-1644	364.9	196	-
	1.0	-1637	216.9	192	40.6
	2.0	-1643	145.5	195	60.1
	4.0	-1622	133.8	188	63.3
	6.5	-1635	117.2	182	67.9
45	Blank	-1649	495.2	192	-
	1.0	-1642	310.0	173	37.4
	2.0	-1647	250.9	182	49.3
	4.0	-1629	216.3	188	56.3
	6.5	-1631	185.6	191	62.5
50	Blank	-1655	914.1	213	-
	1.0	-1642	650.0	201	28.9
	2.0	-1649	565.3	209	38.2
	4.0	-1650	471.2	195	48.5
	6.5	-1646	434.2	198	52.5

Table 3.17 (b) Electrochemical polarization parameters for the corrosion of ZE41 alloy in a medium of 1.0 M Na$_2$SO$_4$ - 1.0 M NaCl containing different concentrations of myristate at different temperatures.

Temp [°C]	Myristate concentration [mM]	E_{corr} vs. SCE [mV]	i_{corr} [μA cm^{-2}]	$-b_c$ [mV dec^{-1}]	η [%]
	Blank	-1669	825.0	204	-
	1.0	-1661	312.6	195	62.1
	2.0	-1657	242.3	201	70.6
30	4.0	-1652	166.1	198	79.9
	6.5	-1663	110.5	191	86.6
	6.6	-1660	103.7	188	87.4
	8.0	-1651	98.7	190	88.0
	Blank	-1681	1034.7	214	-
	1.0	-1672	415.2	205	59.9
35	2.0	-1676	332.1	201	67.9
	4.0	-1680	240.3	210	76.8
	6.5	-1675	157.6	196	84.8
	Blank	-1665	1310.2	221	-
	1.0	-1659	566.1	206	56.8
40	2.0	-1664	431.3	218	67.1
	4.0	-1661	358.7	211	72.6
	6.5	-1653	240.1	204	81.7
	Blank	-1716	1733.5	317	-
	1.0	-1694	819.3	312	52.7
45	2.0	-1703	700.2	306	59.6
	4.0	-1710	587.3	301	66.1
	6.5	-1712	449.8	295	74.1
	Blank	-1726	1752.8	224	-
	1.0	-1718	998.7	219	43.0
50	2.0	-1702	859.2	212	51.0
	4.0	-1696	810.7	203	53.8
	6.5	-1707	685.3	210	60.9

Table 3.18 (a) Impedance parameters for the corrosion of ZE41 alloy in 0.2 M Na₂SO₄ containing different concentrations of myristate at different temperatures.

Temp [°C]	Myristate concentration [mM]	R_{hf} [Ω cm^2]	R_f [Ω cm^2]	C_{dl} [μF cm^{-2}]	C_f [μF cm^{-2}]	η [%]
30	Blank	83.3	73.1	24.0	101.2	-
	1.0	173.7	97.3	23.7	100.2	52.0
	2.0	225.9	120.5	22.8	97.3	63.1
	4.0	279.2	136.8	20.8	93.3	70.2
	6.5	358.7	169.2	19.4	91.9	76.8
	6.6	364.1	186.3	17.3	84.3	77.1
	8.0	387.3	290.7	14.3	39.8	78.5
35	Blank	63.7	55.5	32.1	102.7	-
	1.0	128.2	80.3	30.2	100.5	50.3
	2.0	167.5	91.5	29.2	99.2	62.0
	4.0	171.8	126.8	28.9	95.5	63.0
	6.5	229.4	162.7	25.8	90.2	72.3
40	Blank	53.9	40.7	35.3	104.1	-
	1.0	93.8	44.1	34.0	103.8	42.6
	2.0	136.2	70.0	32.8	102.3	60.4
	4.0	144.2	81.3	29.8	97.3	62.6
	6.5	178.5	96.2	26.8	94.4	69.8
45	Blank	47.2	42.7	36.8	104.9	-
	1.0	74.4	37.8	37.9	103.6	36.6
	2.0	90.3	46.5	34.8	102.3	47.8
	4.0	108.2	50.0	32.3	100.8	56.4
	6.5	118.3	64.9	29.8	97.4	60.1
50	Blank	34.2	31.2	39.4	108.1	-
	1.0	44.7	20.0	38.7	107.8	23.6
	2.0	54.3	31.8	37.1	107.1	37.0
	4.0	64.8	36.2	36.0	105.8	47.3
	6.5	72.2	42.3	34.3	96.5	52.7

Table 3.18 (b) Impedance parameters for the corrosion of ZE41 alloy in 0.6 M Na₂SO₄ containing different concentrations of myristate at different temperatures.

Temp [°C]	Myristate concentration [mM]	R_{hf} [Ω cm^2]	R_f [Ω cm^2]	C_{dl} [μF cm^{-2}]	C_f [μF cm^{-2}]	η [%]
30	Blank	61.1	51.7	26.9	101.2	-
	1.0	141.3	100.4	24.2	99.0	56.8
	2.0	182.7	128.9	23.6	94.1	66.6
	4.0	226.2	147.9	20.0	89.2	73.0
	6.5	278.9	168.4	18.8	80.3	78.1
	6.6	287.1	190.2	15.8	71.5	78.7
	8.0	305.9	267.9	12.3	30.0	80.0
35	Blank	40.2	31.2	35.0	104.1	-
	1.0	87.9	79.3	31.9	102.8	54.3
	2.0	110.3	93.6	30.6	98.3	63.6
	4.0	135.9	121.5	27.7	92.8	70.4
	6.5	178.4	160.3	25.7	86.3	77.5
40	Blank	36.6	27.8	37.6	104.3	-
	1.0	73.8	45.7	34.8	103.7	50.4
	2.0	91.3	67.4	30.7	100.6	59.9
	4.0	116.1	79.3	28.4	96.7	68.5
	6.5	136.8	94.4	25.8	91.3	73.3
45	Blank	27.6	19.9	41.9	106.7	-
	1.0	49.8	35.7	39.8	105.8	44.5
	2.0	53.3	44.8	34.6	102.4	48.1
	4.0	66.9	51.0	30.0	99.3	58.7
	6.5	79.6	67.2	26.4	96.3	65.3
50	Blank	19.4	17.6	43.4	109.3	-
	1.0	32.3	22.0	40.8	107.9	40.0
	2.0	35.8	30.3	38.3	105.8	45.8
	4.0	38.0	36.0	35.7	103.2	49.0
	6.5	43.8	40.7	32.2	96.6	55.7

Table 3.18 (c) Impedance parameters for the corrosion of ZE41 alloy in 1.0 M Na$_2$SO$_4$ containing different concentrations of myristate at different temperatures.

Temp [°C]	Myristate concentration [mM]	R_{hf} [Ω cm^2]	R_f [Ω cm^2]	C_{dl} [μF cm^{-2}]	C_f [μF cm^{-2}]	η [%]
30	Blank	46.0	42.0	33.9	108.5	-
	1.0	104.2	102.5	25.9	98.0	55.8
	2.0	138.9	130.4	21.5	91.2	66.9
	4.0	184.5	145.2	17.9	85.6	75.1
	6.5	261.7	174.8	15.2	74.3	82.4
	6.6	271.4	199.1	11.8	68.3	83.0
	8.0	292.4	285.2	10.8	21.4	84.3
35	Blank	39.7	36.2	40.1	108.9	-
	1.0	84.5	80.2	36.6	102.3	53.0
	2.0	107.2	101.4	30.0	94.4	63.0
	4.0	141.5	132.6	25.6	89.3	71.9
	6.5	184.7	167.8	20.9	81.3	78.5
40	Blank	25.0	20.6	42.6	110.2	-
	1.0	54.8	47.8	39.0	105.9	54.4
	2.0	65.9	58.0	30.2	97.2	62.1
	4.0	80.3	78.2	27.3	91.4	68.9
	6.5	115.7	103.2	22.9	83.5	78.4
45	Blank	23.4	18.5	43.2	111.2	-
	1.0	46.9	40.4	38.7	109.2	50.1
	2.0	53.2	49.0	32.3	102.5	56.0
	4.0	59.2	55.7	29.2	98.3	60.4
	6.5	76.0	71.1	26.0	92.0	69.2
50	Blank	22.8	17.4	44.6	115.3	-
	1.0	37.9	33.9	40.4	110.4	39.9
	2.0	42.9	40.7	35.9	98.3	46.8
	4.0	47.0	45.7	33.9	100.2	51.5
	6.5	54.1	50.9	30.8	91.2	57.8

Table 3.19 (a) Impedance parameters for the corrosion of ZE41 alloy in the combined medium of 0.2 M Na₂SO₄ - 0.1 M NaCl containing different concentrations of myristate at different temperatures.

Temp [°C]	Myristate concentration [mM]	R_{hf} [Ω cm^2]	R_f [Ω cm^2]	C_{dl} [μF cm^{-2}]	C_f [μF cm^{-2}]	η [%]
30	Blank	74.9	69.7	27.1	101.8	-
	1.0	164.2	127.2	20.0	95.5	54.4
	2.0	223.1	168.4	18.9	88.2	66.0
	4.0	280.1	180.2	15.4	78.3	70.2
	6.5	354.2	190.3	16.3	73.9	78.7
	6.6	364.7	298.2	12.3	63.9	79.5
	8.0	380.7	357.3	10.5	36.3	79.9
35	Blank	54.6	49.0	36.4	103.6	-
	1.0	118.3	110.2	32.9	102.4	53.9
	2.0	145.9	129.1	30.0	103.2	61.0
	4.0	190.1	147.8	28.2	91.3	65.9
	6.5	231.6	170.2	25.5	83.3	72.0
40	Blank	49.2	34.2	39.0	106.1	-
	1.0	90.2	75.6	36.5	107.2	45.5
	2.0	124.6	105.7	32.1	102.1	60.6
	4.0	139.3	117.2	29.2	99.3	64.7
	6.5	178.1	143.2	30.0	92.4	72.4
45	Blank	43.2	31.8	43.1	107.7	-
	1.0	70.0	60.1	40.0	106.5	38.3
	2.0	88.3	79.9	35.9	107.1	51.1
	4.0	100.4	93.3	31.4	100.7	57.0
	6.5	126.5	100.2	27.4	94.4	60.2
50	Blank	28.8	25.7	45.6	110.6	-
	1.0	34.3	31.3	41.3	109.2	16.0
	2.0	45.6	43.7	40.2	107.2	36.9
	4.0	59.0	51.0	36.0	108.8	48.6
	6.5	65.2	59.3	31.8	93.2	55.8

Table 3.19 (b) Impedance parameters for the corrosion of ZE41 alloy in the combined medium of 1.0 M Na$_2$SO$_4$ - 1.0 M NaCl containing different concentrations of myristate at different temperatures.

Temp [°C]	Myristate concentration [mM]	R_{hf} [Ω cm^2]	R_f [Ω cm^2]	C_{dl} [μF cm^{-2}]	C_f [μF cm^{-2}]	η [%]
	Blank	34.6	31.4	40.3	112.4	-
	1.0	86.3	80.2	23.5	95.7	59.9
	2.0	123.5	112.4	20.0	85.4	72.0
30	4.0	180.7	157.3	15.7	81.3	80.8
	6.5	245.3	187.3	12.9	73.6	85.9
	6.6	258.7	213.4	10.7	62.2	86.6
	8.0	320.6	297.3	8.9	21.3	89.2
	Blank	29.3	23.8	49.3	113.4	-
	1.0	78.3	74.4	32.6	98.1	62.6
35	2.0	94.2	90.0	28.9	93.7	68.9
	4.0	135.7	133.5	25.0	88.0	78.4
	6.5	192.6	179.5	18.9	77.6	84.8
	Blank	20.2	16.2	54.3	114.7	-
	1.0	48.7	40.2	34.6	103.2	58.6
40	2.0	57.3	52.2	28.8	96.7	64.8
	4.0	78.4	64.0	25.0	88.1	74.3
	6.5	115.7	104.3	20.8	81.3	82.6
	Blank	15.8	14.9	58.0	114.6	-
	1.0	31.7	23.7	34.8	103.7	50.1
45	2.0	41.4	31.3	31.3	97.7	61.8
	4.0	46.8	40.7	24.1	98.0	66.3
	6.5	58.4	52.6	21.2	88.7	73.0
	Blank	15.0	13.1	63.6	120.1	-
	1.0	28.0	22.6	44.3	114.3	46.6
50	2.0	31.4	27.9	32.2	94.4	52.3
	4.0	35.6	32.7	30.0	95.6	58.0
	6.5	39.9	36.1	25.2	82.4	62.5

Table 3.20 (a) Activation parameters for the corrosion of ZE41 alloy in different concentrations of Na$_2$SO$_4$ in the presence of different concentrations of myristate.

Concentration of Na$_2$SO$_4$ [M]	Concentration of myristate [mM]	E_a [kJ mol^{-1}]	$\Delta H^{\#}$ [kJ mol^{-1}]	$\Delta S^{\#}$ [J mol^{-1} K^{-1}]
	Blank	71.4	68.8	-93.2
	1.0	89.8	87.2	-38.8
0.2	2.0	93.5	90.9	-28.9
	4.0	95.0	92.4	-25.4
	6.5	99.4	96.8	-13.0
	Blank	50.3	47.7	-153.5
	1.0	65.0	62.4	-111.7
0.6	2.0	71.5	68.9	-92.3
	4.0	79.7	77.1	-68.0
	6.5	80.9	78.3	-65.8
	Blank	42.8	40.2	-174.8
	1.0	57.5	54.9	-133.7
1.0	2.0	60.7	58.1	-124.9
	4.0	69.9	67.3	-97.0
	6.5	76.3	73.7	-78.8

Table 3.20 (b) Activation parameters for the corrosion of ZE41 alloy in different concentrations of the combined media in the presence of different concentrations of myristate.

Concentration of medium [M]	Concentration of myristate [mM]	E_a [kJ mol^{-1}]	$\Delta H^{\#}$ [kJ mol^{-1}]	$\Delta S^{\#}$ [J mol^{-1} K^{-1}]
	Blank	51.2	48.6	-154.8
	1.0	68.8	66.2	-103.1
0.2 M Na$_2$SO$_4$ & 0.1M NaCl	2.0	72.8	70.2	-92.3
	4.0	74.9	72.3	-87.1
	6.5	80.0	77.4	-72.0
	Blank	33.0	30.4	-203.4
1.0 M Na$_2$SO$_4$ & 1.0M NaCl	1.0	48.9	46.3	-159.4
	2.0	53.3	50.7	-147.0
	4.0	66.1	63.5	-107.9
	6.5	76.4	73.8	-78.0

Table 3.21 (a) Thermodynamic parameters for the adsorption of myristate on ZE41 alloy surface in sodium sulfate media.

Concentration of Na_2SO_4 [M]	Temp [°C]	ΔG^o_{ads} [kJ mol^{-1}]	ΔH^o_{ads} [kJ mol^{-1}]	ΔS^o_{ads} [J K^{-1} mol^{-1}]	R^2	Slope
0.2	30	-28.2			0.999	1.22
	35	-28.5			0.999	1.28
	40	-28.3	-47.2	-61.6	0.996	1.32
	45	-27.8			0.999	1.42
	50	-27.0			0.999	1.59
0.6	30	-28.4			1.000	1.18
	35	-28.8			0.999	1.20
	40	-28.5	-29.5	-3.0	0.998	1.21
	45	-28.4			0.994	1.39
	50	-28.5			0.994	1.69
1.0	30	-28.4			0.998	1.14
	35	-28.6			0.999	1.17
	40	-28.8	-18.2	-33.9	0.995	1.19
	45	-29.2			0.997	1.34
	50	-28.9			0.995	1.64

Table 3.21 (b) Thermodynamic parameters for the adsorption of myristate on ZE41 alloy surface in combined media.

Concentration of medium [M]	Temp [°C]	ΔG^o_{ads} [kJ mol^{-1}]	ΔH^o_{ads} [kJ mol^{-1}]	ΔS^o_{ads} [J K^{-1} mol^{-1}]	R^2	Slope
0.2 M Na_2SO_4 & 0.1M NaCl	30	-28.3			0.999	1.20
	35	-28.8			0.999	1.27
	40	-28.6	-40.2	-38.2	0.996	1.33
	45	-28.2			0.999	1.41
	50	-27.6			0.999	1.61
1.0 M Na_2SO_4 & 1.0M NaCl	30	-28.7			0.999	1.07
	35	-28.9			0.997	1.09
	40	-29.2	-14.0	-48.4	0.996	1.13
	45	-29.5			0.996	1.25
	50	-29.6			0.995	1.53

3.5 LAURATE AS CORROSION INHIBITOR FOR ZE41 IN AQUEOUS SALT SOLUTIONS

3.5.1 Potentiodynamic polarization measurements

The potentiodynamic polarization curves for the corrosion of ZE41 at 45 ºC in 1.0 M Na_2SO_4 and in the combined medium of 0.2 M Na_2SO_4 – 0.1 M NaCl, both containing different concentrations of laurate are represented in Fig. 3.34 (a) and Fig. 3.34 (b), respectively.
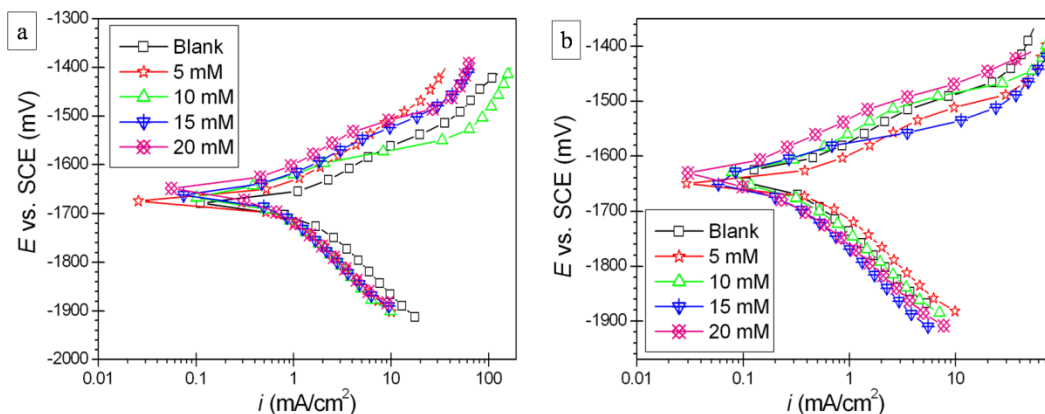
Fig. 3.34 Potentiodynamic polarization curves for the corrosion of ZE41 alloy in the presence of different concentrations of laurate at 45 °C in (a) 1.0 M Na_2SO_4, (b) a medium of 0.2 M Na_2SO_4 - 0.1 M NaCl.

It follows from Fig. 3.34 that after the addition of laurate the Tafel curves develop mostly at lower current density region and the shape of the plots remains unaltered. Only cathodic Tafel branches are linear and hence were extrapolated to evaluate polarization parameters. Table 3.22 (a), Table 3.22 (b), Table 3.22 (c) and Table 3.23 (a), Table 3.23 (b), respectively, enlist the potentiodynamic polarization parameters pertaining to the polarization measurements conducted in the presence of different concentrations of laurate in sodium sulfate and the combined media at different medium concentrations and temperatures.

The maximum inhibition efficiencies shown by laurate at an optimum concentration (C_{max}) of 20 mM, in sodium sulfate and in combined media, respectively, are 79.3 % and 82.4 % in the medium of 1.0 M Na_2SO_4 and in the medium of 1.0 M Na_2SO_4 - 1.0 M NaCl, both at 30 ℃. The trend of the drift in the corrosion potential towards anodic (more positive) side (not greater than 31 mV), the variation of efficiency with inhibitor concentration and an enhanced efficiency in more concentrated media remains same as the trends in polarization results observed for stearate, palmitate and myristate.

3.5.2 Electrochemical impedance spectroscopy studies

Fig. 3.35 (a) and Fig. 3.35 (b), respectively, represents the Nyquist plots for the corrosion of ZE41 at 45 ℃ in 1.0 M Na_2SO_4 and in the combined medium of 0.2 M Na_2SO_4 – 0.1 M NaCl, both containing different concentrations of laurate.
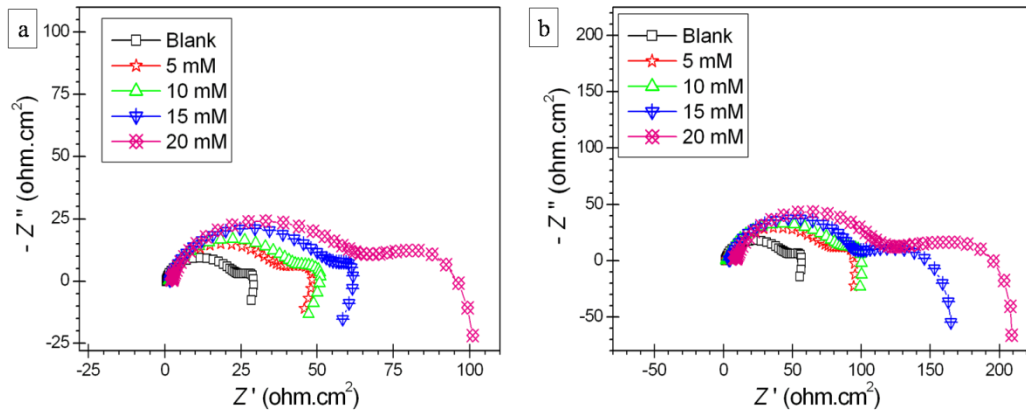
Fig. 3.35 Nyquist plots for the corrosion of ZE41 alloy in the presence of different concentrations of laurate at 45 °C in (a) 1.0 M Na_2SO_4, (b) a medium of 0.2 M Na_2SO_4 - 0.1 M NaCl.

Two capacitive loops and an inductive loop are observed in all the Nyquist plots. The introduction of laurate in increased concentrations boosts up the resistance towards corrosion as reflected by the enlargement of the capacitive loops. The plots were simulated with the proposed equivalent circuit and the impedance parameters such as R_{hf},

C_{dl}, R_f and C_f were deduced. Table 3.24 (a), Table 3.24 (b), Table 3.24 (c) and Table 3.25 (a), Table 3.25 (b), respectively, show the calculated impedance parameters for varying amounts of laurate in sodium sulfate and combined media at different medium concentrations and temperatures. The values of inhibition efficiency and the pattern of their variation with laurate and medium concentrations are in good agreement with that obtained from the results of polarization studies. The efficiency increases negligibly above an optimum concentration of 20 mM of laurate. Most desirable film characteristics in terms of lower film capacitance and higher film resistance are exclusively seen at higher laurate concentrations.

Bode plots were also drawn to further substantiate the ability of laurate to inhibit ZE41 corrosion. The Bode magnitude plots for the corrosion of ZE41 alloy at 45 °C in 1.0 M Na_2SO_4 and in the combined medium of 0.2 M Na_2SO_4 - 0.1 M NaCl with varying amounts of laurate are shown in Fig. 3.36 (a) and Fig. 3.36 (b), respectively. The phase angle plots for the same have been depicted in Fig. 3.37 (a) and Fig. 3.37 (b), respectively.
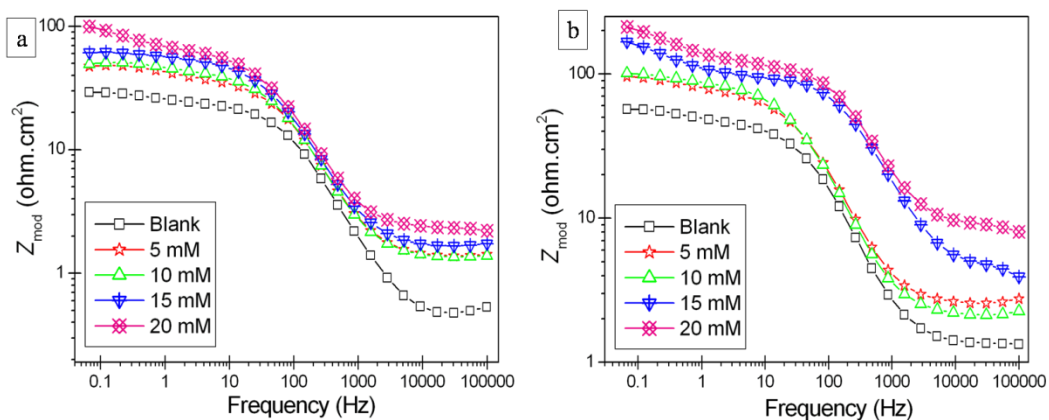
Fig. 3.36 Bode magnitude plots for the corrosion of ZE41 alloy in the presence of different concentrations of laurate at 45 °C in (a) 1.0 M Na_2SO_4, (b) the combined medium of 0.2 M Na_2SO_4 - 0.1 M NaCl.
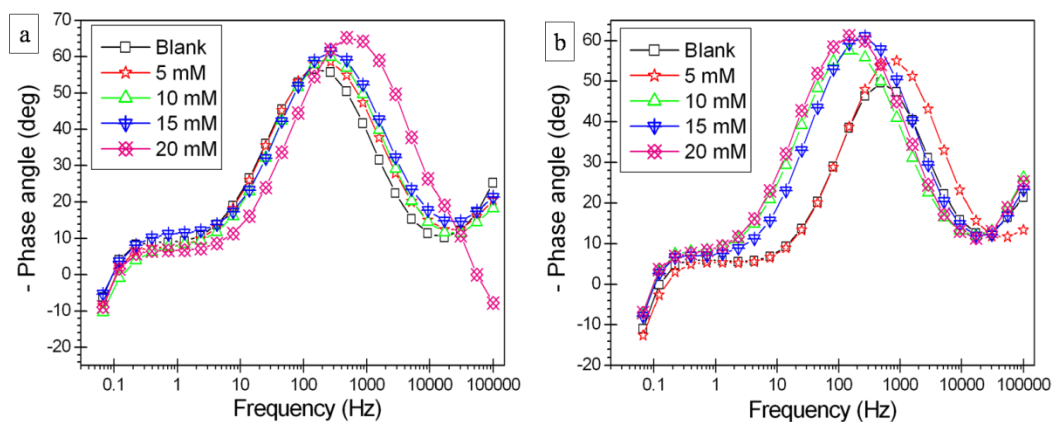
Fig. 3.37 Bode magnitude plots for the corrosion of ZE41 alloy in the presence of different concentrations of laurate at 45 °C in (a) 1.0 M Na$_2$SO$_4$, (b) the combined medium of 0.2 M Na$_2$SO$_4$ - 0.1 M NaCl.

A better efficiency of laurate in inhibiting the alloy corrosion at higher concentrations can be comprehended as the consequence of augmentation of resistance to corrosion and electrolyte inflow, as seen from the increase in low frequency impedance modulus and phase maximum at medium frequencies, in Fig. 3.37 and Fig. 3.38, respectively.

3.5.3 Effect of temperature

The results of electrochemical studies shown in Table 3.22, Table 3.23, Table 3.24 and Table 3.25 indicate the adversity of higher temperature on the inhibition efficiency of laurate, as in any media at higher temperatures a lower efficiency is observed along with higher film capacitance and lower film resistance values, which signifies the existence of a thin film offering inferior protection to the underlying alloy. The Arrhenius plots for the corrosion of ZE41 alloy specimen in 0.2 M Na$_2$SO$_4$ and in the combined medium of 0.2 M Na$_2$SO$_4$ - 1.0 M NaCl containing different concentrations of laurate are presented in Fig. 3.38 (a) and Fig. 3.38 (b), respectively. The ln (v_{corr} /T) versus (1/T) plots for the same are shown in Fig. 3.39 (a) and Fig. 3.39 (b), respectively.
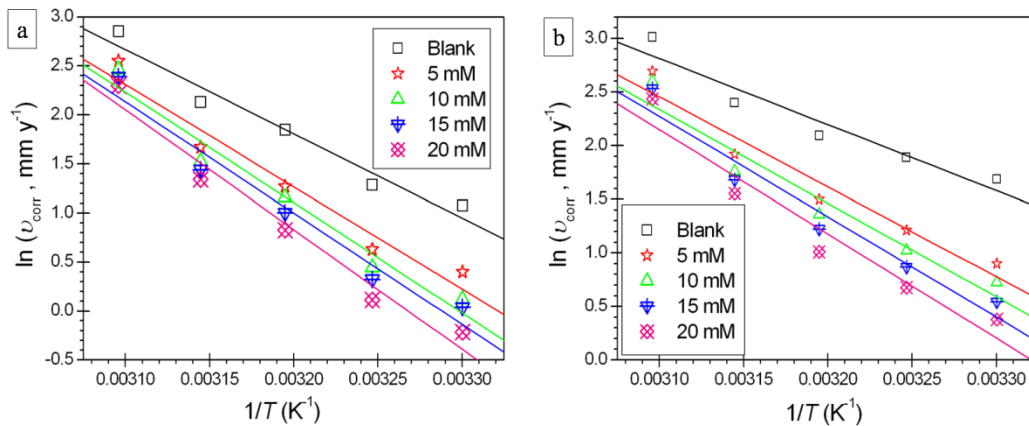
Fig. 3.38 Arrhenius plots for the corrosion of ZE41 alloy in the presence of different concentrations of laurate in (a) 0.2 M Na₂SO₄ (b) the combined medium of 0.2 M Na₂SO₄ - 0.1 M NaCl.
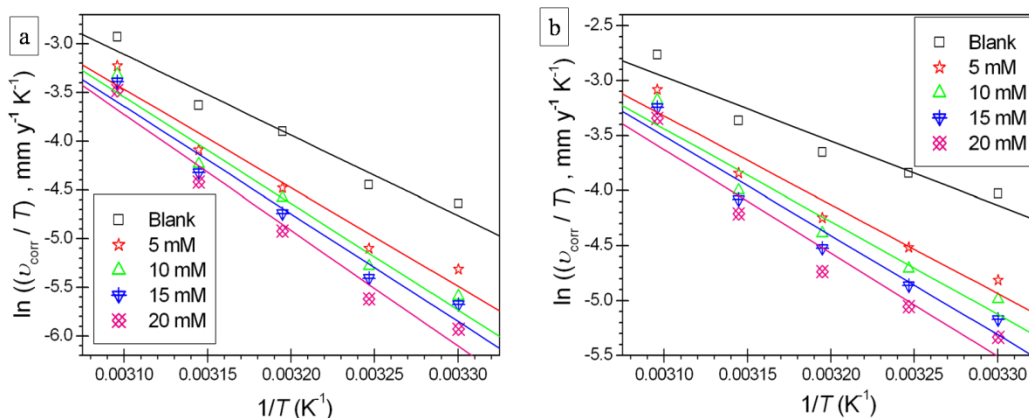
Fig. 3.39 ln (v_{corr}/T) vs. (1/T) plots for the corrosion of ZE41 alloy in the presence of different concentrations of laurate in (a) 0.2 M Na₂SO₄ (b) the combined medium of 0.2 M Na₂SO₄ - 0.1 M NaCl.

The calculated activation parameters for ZE41 dissolution in sodium sulfate and the combined media having different concentrations of laurate are, respectively, listed in Table 3.26 (a) and Table 3.26 (b). The activation parameters listed in Table 3.26 show that in the presence of laurate the corrosion of ZE41 in both the media is energetically less favored, as the energy barrier or activation energy increases with the increased addition of laurate. The $\Delta H^{\#}$ values vary in a way similar to that of E_a. Furthermore the

entropy of the system regardless of the presence or the absence of laurate decreases during the formation of activated complex, on account of association of reactants, as seen from the negative $\Delta S^{\#}$ values.

3.5.4 Adsorption behavior

The adsorption of laurate on ZE41 surface obeys Langmuir adsorption isotherm. The Langmuir isotherms for the adsorption of laurate on ZE41 alloy surface at different temperatures in 0.2 M Na_2SO_4 and in the combined medium of 0.2 M Na_2SO_4 - 1.0 M NaCl are presented in Fig. 3.40 (a) and Fig. 3.40 (b), respectively.
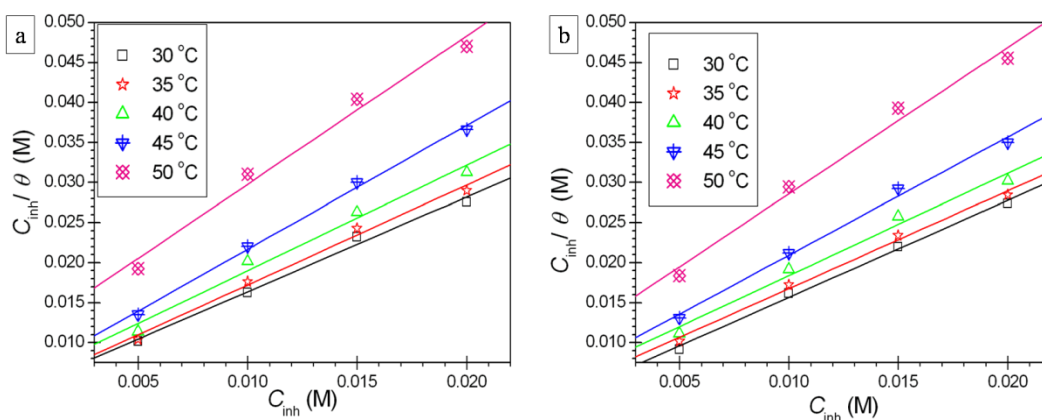
Fig. 3.40 Langmuir adsorption isotherms for the adsorption of laurate on ZE41 alloy surface at different temperatures in (a) 0.2 M Na_2SO_4 (b) the combined medium of 0.2 M Na_2SO_4 - 0.1 M NaCl.

Table 3.27 (a) and Table 3.27 (b), respectively, show the thermodynamic parameters, slope and linear regression coefficient (R^2) determined from the analysis of various Langmuir isotherms developed at different temperatures for adsorption of laurate on ZE41 alloy surface in sodium sulfate and the combined media. As seen from Table 3.27, the extent of agreement with the ideal Langmuir isotherm is imprecise, that is to say, the average linear regression coefficient equal to 0.99 indicated substantial agreement, at the same time marginal deviation is obvious from the slope values. The suitability of the Langmuir isotherm is accepted by attributing the deviation to

intermolecular interactions of laurate molecules after adsorption. The adsorption of laurate from solution onto alloy surface is validated from the large negative values of $\Delta S°_{ads}$ which signify a reduction in disorderliness. The other two thermodynamic parameters $\Delta G°_{ads}$ and $\Delta H°_{ads}$ signify a spontaneous adsorption which predominantly is physical adsorption, where principal interactive forces are weak and electrostatic in nature.

Table 3.22 (a) Electrochemical polarization parameters for the corrosion of ZE41 alloy in 0.2 M Na₂SO₄ containing different concentrations of laurate at different temperatures.

Temp [°C]	Laurate concentration [mM]	E_{corr} vs. SCE [mV]	i_{corr} [$\mu A\ cm^{-2}$]	$-b_c$ [$mV\ dec^{-1}$]	η [%]
	Blank	-1604	131.7	168	-
	5	-1596	67.0	167	49.1
	10	-1601	50.8	159	61.4
30	15	-1600	46.7	152	64.5
	20	-1602	36.2	164	72.5
	21	-1598	35.4	160	73.1
	30	-1596	32.6	161	75.3
	Blank	-1608	162.1	177	-
	5	-1600	84.3	170	48.0
35	10	-1602	70.3	175	56.7
	15	-1592	62.1	182	61.7
	20	-1596	50.3	167	69.0
	Blank	-1610	284.9	180	-
	5	-1603	159.6	181	44.0
40	10	-1601	143.7	173	49.6
	15	-1594	122.5	169	57.0
	20	-1591	102.6	176	64.0
	Blank	-1635	378.6	184	-
	5	-1639	238.5	181	37.0
45	10	-1623	206.8	178	45.4
	15	-1615	189.3	182	50.0
	20	-1630	171.8	186	54.6
	Blank	-1638	778.0	189	-
	5	-1631	575.8	197	26.0
50	10	-1626	527.3	201	32.2
	15	-1628	489.3	184	37.1
	20	-1625	447.0	171	42.5

Table 3.22 (b) Electrochemical polarization parameters for the corrosion of ZE41 alloy in 0.6 M Na$_2$SO$_4$ containing different concentrations of laurate at different temperatures.

Temp [°C]	Laurate concentration [mM]	E_{corr} vs. SCE [mV]	i_{corr} [μA cm^{-2}]	$-b_c$ [mV dec^{-1}]	η [%]
	Blank	-1626	327.1	192	-
	5	-1622	147.2	203	55.0
	10	-1617	119.3	199	63.5
30	15	-1620	99.0	185	69.7
	20	-1615	81.3	182	75.2
	21	-1618	78.5	178	76.0
	30	-1616	74.6	176	77.2
	Blank	-1628	594.7	199	-
	5	-1626	297.8	196	49.9
35	10	-1621	245.7	203	58.7
	15	-1618	211.9	204	64.4
	20	-1620	160.6	192	73.0
	Blank	-1634	708.0	204	-
	5	-1630	375.3	201	47.0
40	10	-1629	324.8	196	54.1
	15	-1625	279.0	192	60.6
	20	-1621	231.5	185	67.3
	Blank	-1636	886.7	211	-
	5	-1633	530.2	204	40.2
45	10	-1630	463.7	200	47.7
	15	-1619	401.0	183	54.8
	20	-1628	359.8	194	59.4
	Blank	-1639	1250.1	214	-
	5	-1634	835.7	210	33.2
50	10	-1625	797.8	207	36.2
	15	-1632	696.2	211	44.3
	20	-1621	663.9	196	46.9

Table 3.22 (c) Electrochemical polarization parameters for the corrosion of ZE41 alloy in 1.0 M Na$_2$SO$_4$ containing different concentrations of laurate at different temperatures.

Temp [°C]	Laurate concentration [mM]	E_{corr} vs. SCE [mV]	i_{corr} [μA cm^{-2}]	$-b_c$ [mV dec^{-1}]	η [%]
	Blank	-1648	520.8	190	-
	5	-1639	228.8	187	56.1
	10	-1627	187.1	172	64.1
30	15	-1641	150.7	185	71.1
	20	-1638	107.8	179	79.3
	21	-1640	105.0	180	79.8
	30	-1636	101.6	163	80.5
	Blank	-1650	726.7	211	-
	5	-1647	340.2	201	53.2
35	10	-1648	272.5	199	62.5
	15	-1634	234.6	209	67.7
	20	-1642	177.5	187	75.6
	Blank	-1657	996.1	228	-
	5	-1652	508.4	231	49.0
40	10	-1647	424.4	217	57.4
	15	-1651	363.3	219	63.5
	20	-1639	291.3	214	70.8
	Blank	-1681	1287.7	261	-
	5	-1673	738.3	247	42.7
45	10	-1662	645.5	235	49.9
	15	-1659	552.5	253	57.1
	20	-1653	508.3	249	60.5
	Blank	-1686	1451.2	308	-
	5	-1657	927.8	304	36.1
50	10	-1663	899.1	289	38.1
	15	-1655	782.3	292	46.1
	20	-1666	738.7	278	49.1

Table 3.23 (a) Electrochemical polarization parameters for the corrosion of ZE41 alloy in a medium of 0.2 M Na₂SO₄ - 0.1 M NaCl containing different concentrations of laurate at different temperatures.

Temp [°C]	Laurate concentration [mM]	E_{corr} vs. SCE [mV]	i_{corr} [$\mu A\ cm^{-2}$]	$-b_c$ [$mV\ dec^{-1}$]	η [%]
30	Blank	-1607	242.9	176	-
	5	-1603	110.4	162	54.6
	10	-1592	92.7	171	61.8
	15	-1596	77.3	178	68.2
	20	-1599	65.7	186	73.0
	21	-1605	64.2	191	73.6
	30	-1601	59.0	179	75.7
35	Blank	-1628	297.3	195	-
	5	-1620	151.0	194	49.2
	10	-1617	124.7	205	58.0
	15	-1625	106.8	186	64.1
	20	-1622	88.3	190	70.3
40	Blank	-1644	364.9	196	-
	5	-1639	200.8	182	45.0
	10	-1643	174.7	179	52.1
	15	-1640	152.5	191	58.2
	20	-1633	123.4	195	66.2
45	Blank	-1649	495.2	192	-
	5	-1638	306.0	174	38.2
	10	-1640	261.5	178	47.2
	15	-1642	241.2	193	51.3
	20	-1637	212.0	202	57.2
50	Blank	-1655	914.1	213	-
	5	-1651	665.5	210	27.2
	10	-1648	603.8	181	34.0
	15	-1639	564.9	179	38.2
	20	-1647	512.8	198	43.9

Table 3.23 (b) Electrochemical polarization parameters for the corrosion of ZE41 alloy in a medium of 1.0 M Na$_2$SO$_4$ - 1.0 M NaCl containing different concentrations of laurate at different temperatures.

Temp [°C]	Laurate concentration [mM]	E_{corr} vs. SCE [mV]	i_{corr} [μA cm^{-2}]	$-b_c$ [mV dec^{-1}]	η [%]
	Blank	-1669	825.0	204	-
	5	-1661	335.0	208	59.4
	10	-1653	270.1	203	67.3
30	15	-1659	213.7	197	74.1
	20	-1660	145.4	182	82.4
	21	-1663	140.3	188	83.0
	30	-1667	139.8	191	83.1
	Blank	-1681	1034.7	214	-
	5	-1670	453.9	204	56.1
35	10	-1664	357.2	211	65.5
	15	-1678	295.9	218	71.4
	20	-1673	213.2	207	79.4
	Blank	-1665	1310.2	221	-
	5	-1661	620.1	228	52.7
40	10	-1660	519.5	235	60.4
	15	-1651	440.3	217	66.4
	20	-1658	348.5	203	73.4
	Blank	-1716	1733.5	317	-
	5	-1703	932.7	275	46.2
45	10	-1697	807.8	284	53.4
	15	-1692	686.5	296	60.4
	20	-1706	620.2	302	64.2
	Blank	-1726	1752.8	224	-
	5	-1708	1063.3	248	39.3
50	10	-1719	1027.8	227	41.4
	15	-1703	904.4	219	48.4
	20	-1695	836.7	203	52.3

Table 3.24 (a) Impedance parameters for the corrosion of ZE41 alloy in 0.2 M Na$_2$SO$_4$ containing different concentrations of laurate at different temperatures.

Temp [°C]	Laurate concentration [mM]	R_{hf} [Ω cm^2]	R_f [Ω cm^2]	C_{dl} [μF cm^{-2}]	C_f [μF cm^{-2}]	η [%]
30	Blank	83.3	73.1	24.0	101.2	-
	5	171.6	90.2	23.6	100.6	51.5
	10	219.4	119.4	20.2	98.3	62.0
	15	248.7	142.7	24.4	95.6	66.5
	20	310.5	170.3	20.0	88.3	73.2
	21	322.6	192.3	18.8	80.3	74.2
	30	347.5	256.7	15.8	41.7	76.0
35	Blank	63.7	55.5	32.1	102.7	-
	5	125.6	77.3	29.4	98.4	49.3
	10	149.9	90.2	27.6	95.4	57.5
	15	172.3	120.4	28.4	93.8	63.1
	20	208.6	157.9	25.8	89.8	69.5
40	Blank	53.9	40.7	35.3	104.1	-
	5	98.9	52.6	33.8	102.4	45.5
	10	109.2	65.4	30.0	99.8	50.7
	15	128.7	75.3	27.6	97.2	58.1
	20	153.1	94.2	24.2	94.5	64.8
45	Blank	47.2	42.7	36.8	104.9	-
	5	75.8	30.0	33.7	101.5	37.8
	10	89.7	43.3	31.5	98.9	47.4
	15	92.9	54.4	29.3	97.6	49.2
	20	107.6	71.2	27.6	94.4	56.2
50	Blank	34.2	31.2	39.4	108.1	-
	5	47.8	20.0	37.1	106.7	28.5
	10	53.0	28.2	36.9	107.2	35.6
	15	55.2	37.8	34.3	103.5	38.1
	20	60.3	48.8	31.3	98.3	43.3

Table 3.24 (b) Impedance parameters for the corrosion of ZE41 alloy in 0.6 M Na$_2$SO$_4$ containing different concentrations of laurate at different temperatures.

Temp [°C]	Laurate concentration [mM]	R_{hf} [Ω cm^2]	R_f [Ω cm^2]	C_{dl} [μF cm^{-2}]	C_f [μF cm^{-2}]	η [%]
30	Blank	61.1	51.7	26.9	101.2	-
	5	130.2	96.2	23.2	99.8	53.1
	10	167.8	120.3	22.9	97.0	63.6
	15	204.5	148.7	20.7	91.2	70.1
	20	254.7	173.7	19.9	82.4	76.0
	21	262.5	187.3	18.2	77.3	76.7
	30	282.4	234.7	14.3	33.5	78.4
35	Blank	40.2	31.2	35.0	104.1	-
	5	80.5	74.2	31.8	101.4	50.0
	10	100.3	89.0	30.8	99.0	59.9
	15	118.1	108.3	27.9	93.5	66.0
	20	156.9	150.2	24.7	87.4	74.4
40	Blank	36.6	27.8	37.6	104.3	-
	5	71.8	57.8	35.1	103.8	49.0
	10	80.0	61.3	32.2	101.5	54.3
	15	95.7	78.1	29.2	97.6	61.7
	20	117.8	90.2	26.5	93.6	68.9
45	Blank	27.6	19.9	41.9	106.7	-
	5	44.6	33.1	38.6	104.2	38.1
	10	53.8	41.7	36.9	101.6	48.7
	15	63.1	50.1	32.6	97.0	56.2
	20	69.1	58.2	27.0	96.9	60.0
50	Blank	19.4	17.6	43.4	109.3	-
	5	29.4	21.5	40.2	107.9	33.9
	10	31.1	29.2	39.2	105.8	37.5
	15	35.8	33.0	34.7	102.9	45.8
	20	37.6	36.1	30.7	96.6	48.4

Table 3.24 (c) Impedance parameters for the corrosion of ZE41 alloy in 1.0 M Na₂SO₄ containing different concentrations of laurate at different temperatures.

Temp [°C]	Laurate concentration [mM]	R_{hf} [Ω cm^2]	R_f [Ω cm^2]	C_{dl} [μF cm^{-2}]	C_f [μF cm^{-2}]	η [%]
30	Blank	46.0	42.0	33.9	108.5	-
	5	104.6	99.6	27.2	102.3	56.0
	10	127.9	124.3	22.4	96.7	64.0
	15	158.7	141.2	19.2	90.0	71.0
	20	219.1	168.9	17.1	83.3	79.0
	21	225.6	175.6	13.3	71.3	79.6
	30	231.3	224.6	11.0	29.4	80.1
35	Blank	39.7	36.2	40.1	108.9	-
	5	84.4	77.0	34.3	101.2	53.0
	10	104.4	98.6	29.8	95.4	62.0
	15	124.8	120.1	26.2	83.3	68.2
	20	165.3	157.8	21.1	75.5	76.0
40	Blank	25.0	20.6	42.6	110.2	-
	5	49.0	44.1	38.6	103.2	49.0
	10	58.2	53.1	31.2	98.1	57.0
	15	67.6	59.2	26.2	95.9	63.1
	20	83.4	75.6	23.3	87.2	70.0
45	Blank	23.4	18.5	43.2	111.2	-
	5	41.0	36.9	40.7	107.2	42.9
	10	46.5	40.2	36.2	103.2	49.6
	15	54.3	48.0	30.1	101.5	56.9
	20	59.8	52.2	26.9	93.8	60.9
50	Blank	22.8	17.4	44.6	115.3	-
	5	35.2	34.3	41.2	112.3	35.2
	10	38.1	35.0	37.8	106.2	40.2
	15	41.0	38.2	32.2	102.7	44.3
	20	45.3	42.3	27.4	94.2	49.6

Table 3.25 (a) Impedance parameters for the corrosion of ZE41 alloy in the combined medium of 0.2 M Na$_2$SO$_4$ - 0.1M NaCl containing different concentrations of laurate at different temperatures.

Temp [°C]	Laurate concentration [mM]	R_{hf} [Ω cm^2]	R_f [Ω cm^2]	C_{dl} [μF cm^{-2}]	C_f [μF cm^{-2}]	η [%]
	Blank	74.9	69.7	27.1	101.8	-
	5	171.3	120.4	21.3	98.0	56.3
	10	198.8	143.7	19.2	95.3	62.3
30	15	242.7	158.3	18.3	86.8	69.1
	20	288.9	180.4	16.7	80.2	74.1
	21	295.7	221.5	14.3	71.2	74.7
	30	327.3	286.4	11.3	38.9	77.1
	Blank	54.6	49.0	36.4	103.6	-
	5	112.6	98.4	33.3	100.4	51.5
35	10	138.7	102.3	28.2	95.6	60.7
	15	166.8	130.4	26.2	92.4	67.3
	20	189.2	162.3	23.5	87.3	71.2
	Blank	49.2	34.2	39.0	106.1	-
	5	86.7	60.3	36.8	104.4	43.3
40	10	107.8	78.8	33.3	98.3	54.4
	15	117.1	93.3	30.2	95.7	58.0
	20	156.4	112.3	22.4	93.7	68.6
	Blank	43.2	31.8	43.1	107.7	-
	5	75.3	37.9	40.9	106.8	42.6
45	10	85.8	57.8	36.2	103.2	49.7
	15	91.0	79.2	32.3	101.3	52.6
	20	112.4	87.7	28.8	96.4	61.6
	Blank	28.8	25.7	45.6	110.6	-
	5	37.7	28.7	42.3	109.7	23.5
50	10	44.6	36.2	40.8	107.7	35.3
	15	46.0	43.3	37.5	98.3	37.4
	20	53.3	51.6	32.5	95.4	45.9

Table 3.25 (b) Impedance parameters for the corrosion of ZE41 alloy in the combined medium of 1.0 M Na₂SO₄ - 1.0 M NaCl containing different concentrations of laurate at different temperatures.

Temp [°C]	Laurate concentration [mM]	R_{hf} [Ω cm^2]	R_f [Ω cm^2]	C_{dl} [μF cm^{-2}]	C_f [μF cm^{-2}]	η [%]
30	Blank	34.6	31.4	40.3	112.4	-
	5	88.5	78.7	26.2	97.4	60.9
	10	98.7	94.6	21.3	90.3	64.9
	15	128.7	120.4	17.2	83.3	73.1
	20	205.8	170.4	13.3	77.4	83.2
	21	215.7	181.5	11.3	68.3	84.0
	30	234.8	228.5	10.2	27.4	85.3
35	Blank	29.3	23.8	49.3	113.4	-
	5	62.7	59.5	32.7	99.3	53.3
	10	80.1	75.0	29.0	94.3	63.4
	15	107.8	102.5	23.5	81.3	72.8
	20	130.3	118.9	20.1	72.2	77.5
40	Blank	20.2	16.2	54.3	114.7	-
	5	40.1	37.8	35.6	103.7	49.7
	10	51.4	48.2	30.2	94.4	60.8
	15	66.7	62.7	26.0	92.2	69.8
	20	78.2	76.3	22.2	85.4	74.2
45	Blank	15.8	14.9	58.0	114.6	-
	5	28.1	22.6	38.2	106.4	43.7
	10	34.5	30.0	33.6	100.9	54.1
	15	43.7	39.7	27.6	99.3	63.9
	20	49.3	45.8	23.6	90.5	67.9
50	Blank	15.0	13.1	63.6	120.1	-
	5	23.1	20.2	39.7	108.4	35.3
	10	26.8	22.5	36.4	96.2	44.2
	15	31.1	28.9	31.2	97.3	51.8
	20	35.6	32.6	26.1	90.4	58.0

Table 3.26 (a) Activation parameters for the corrosion of ZE41 alloy in different concentrations of Na_2SO_4 in the presence of different concentrations of laurate.

Concentration of Na_2SO_4 [M]	Concentration of laurate [mM]	E_a [kJ mol^{-1}]	$\Delta H^{\#}$ [kJ mol^{-1}]	$\Delta S^{\#}$ [J mol^{-1} K^{-1}]
	Blank	71.4	68.8	-93.2
	5	86.6	84.0	-49.0
0.2	10	93.5	90.9	-28.5
	15	94.3	91.7	-26.7
	20	101.5	98.9	-13.4
	Blank	50.3	47.7	-153.5
	5	66.0	63.4	-108.2
0.6	10	72.3	69.7	-89.4
	15	73.9	71.3	-85.3
	20	81.5	78.9	-62.5
	Blank	42.8	40.2	-174.8
	5	58.3	55.7	-130.7
1.0	10	65.1	62.5	-110.2
	15	67.7	65.1	-103.4
	20	79.8	77.2	- 66.1

Table 3.26 (b) Activation parameters for the corrosion of ZE41 alloy in different concentrations of the combined media in the presence of different concentrations of laurate.

Concentration of medium [M]	Concentration of laurate [mM]	E_a [kJ mol^{-1}]	$\Delta H^{\#}$ [kJ mol^{-1}]	$\Delta S^{\#}$ [J mol^{-1} K^{-1}]
	Blank	51.2	48.6	-154.7
	5	69.7	67.1	-100.4
0.2 M Na_2SO_4 & 0.1M NaCl	10	72.7	70.1	-91.9
	15	77.7	75.1	-77.1
	20	80.8	78.2	-68.5
	Blank	33.0	30.4	-203.4
1.0 M Na_2SO_4 & 1.0M NaCl	5	49.4	46.8	-157.1
	10	56.8	54.2	-134.8
	15	60.7	58.1	-123.9
	20	74.4	71.8	-81.9

Table 3.27 (a) Thermodynamic parameters for the adsorption of laurate on ZE41 alloy surface in sodium sulfate media.

Concentration of Na_2SO_4 [M]	Temp [°C]	ΔG^o_{ads} [kJ mol^{-1}]	ΔH^o_{ads} [kJ mol^{-1}]	ΔS^o_{ads} [J K^{-1} mol^{-1}]	R^2	Slope
0.2	30	-23.7			0.992	1.18
	35	-24.0			0.991	1.25
	40	-23.8	-34.3	-34.0	0.983	1.32
	45	-24.0			0.997	1.55
	50	-22.8			0.985	1.85
0.6	30	-24.3			0.996	1.17
	35	-23.9			0.987	1.17
	40	-24.2	-27.6	-11.1	0.990	1.27
	45	-24.1			0.994	1.40
	50	-23.9			0.981	1.78
1.0	30	-24.0			0.989	1.09
	35	-24.3			0.992	1.15
	40	-24.4	-19.3	-15.7	0.991	1.21
	45	-24.5			0.996	1.40
	50	-24.3			0.980	1.74

Table 3.27 (b) Thermodynamic parameters for the adsorption of laurate on ZE41 alloy surface in combined media.

Concentration of medium [M]	Temp [°C]	ΔG^o_{ads} [kJ mol^{-1}]	ΔH^o_{ads} [kJ mol^{-1}]	ΔS^o_{ads} [J K^{-1} mol^{-1}]	R^2	Slope
0.2 M Na_2SO_4 & 0.1M NaCl	30	-24.3			0.996	1.21
	35	-24.1			0.994	1.22
	40	-23.9	-39.9	-51.2	0.984	1.28
	45	-24.1			0.994	1.47
	50	-23.1			0.986	1.83
1.0 M Na_2SO_4 & 1.0M NaCl	30	-24.2			0.990	1.06
	35	-24.5			0.992	1.09
	40	-24.7	-16.4	-26.2	0.992	1.19
	45	-24.8			0.996	1.34
	50	-24.7			0.984	1.67

3.6 CAPRYLATE AS CORROSION INHIBITOR FOR ZE41 IN AQUEOUS SALT SOLUTIONS

3.6.1 Potentiodynamic polarization measurements

The potentiodynamic polarization plots for the corrosion of ZE41 alloy at 45 ºC in 1.0 M Na_2SO_4 and in the combined medium of 0.2 M Na_2SO_4 – 0.1 M NaCl, both containing caprylate in a range of concentrations, are shown in Fig. 3.41 (a) and Fig. 3.41 (b), respectively.
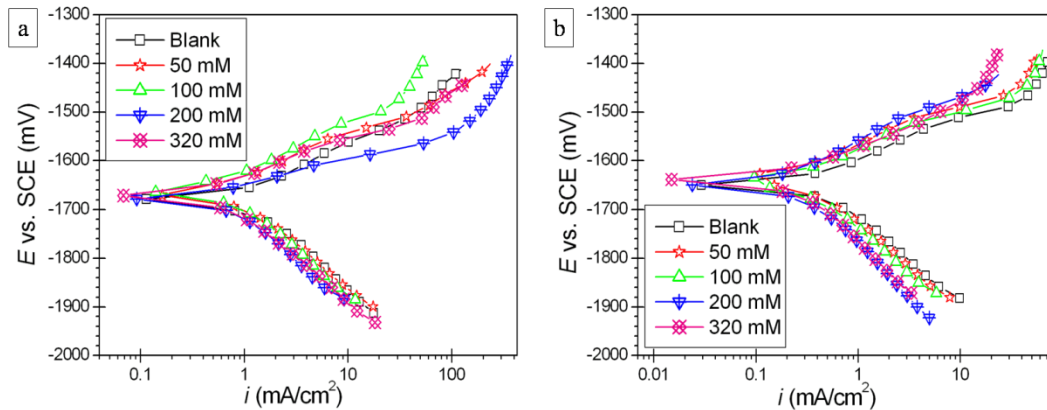
Fig. 3.41 Potentiodynamic polarization curves for the corrosion of ZE41 alloy in the presence of different concentrations of caprylate at 45 °C in (a) 1.0 M Na_2SO_4, (b) a medium of 0.2 M Na_2SO_4 - 0.1 M NaCl.

When compared to the blank, the polarization curves in Fig. 3.41, for the electrolyte containing caprylate, are drifted towards the lower current density region, without any noteworthy change in shape, which demonstrates the reduction in corrosion rate achieved with no interference in the mechanism of corrosion. The corrosion current density values were derived from the cathodic Tafel extrapolation as the linearity of the anodic branches was unsatisfactory. Table 3.28 (a), Table 3.28 (b), Table 3.28 (c) and Table 3.29 (a), Table 3.29 (b), respectively, show the experimentally evaluated polarization parameters for the corrosion of ZE41 alloy in the presence of different concentrations of caprylate in sodium sulfate and the combined media.

The optimum concentration of caprylate for the inhibition of ZE41 alloy corrosion is 320 mM, very high when compared to that of the other four carboxylate inhibitors studied. Apart from this exception the variations in the polarization parameters are pretty much similar to what has been highlighted earlier for rest of the carboxylates. Caprylate reduces the rate of anodic reaction to greater extent as indicated by the anodic drift of corrosion potential (not more than 27 mV vs. SCE) with reference to OCP of the blank solution. The maximum inhibition efficiencies at the optimum concentration of 320 mM of caprylate in sodium sulfate and in combined media, respectively, are 68.5 % and 72.0 %, in the medium of 1.0 M Na_2SO_4 and in the combined medium of 1.0 M Na_2SO_4 - 1.0 M NaCl, both at 30 ℃. The inhibition efficiency of caprylate increases with the increase in the ionic concentration of the media.

3.5.2 Electrochemical impedance spectroscopy studies

The Nyquist plots for the corrosion of ZE41 at 45 ℃ in 1.0 M Na_2SO_4 and in the combined medium of 0.2 M Na_2SO_4 – 0.1 M NaCl, both having different concentrations of caprylate, are illustrated in Fig. 3.42 (a) and Fig. 3.42 (b), respectively.
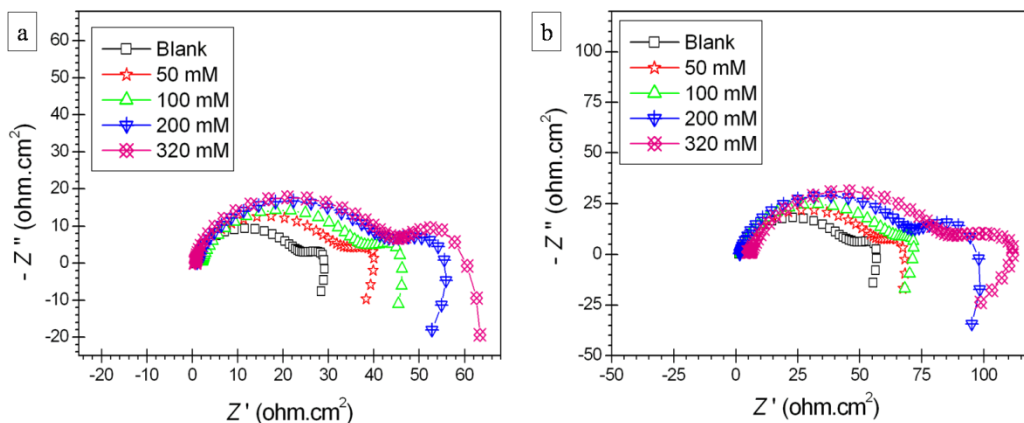
Fig. 3.42 Nyquist plots for the corrosion of ZE41 alloy in the presence of different concentrations of caprylate at 45 °C in (a) 1.0 M Na_2SO_4, (b) a medium of 0.2 M Na_2SO_4 - 0.1 M NaCl.

The successive enlargement of capacitive loops with the increase in caprylate concentration is indicative of the augmentation of corrosion resistance of ZE41. Individual Nyquist plots were simulated with the equivalent electrical circuit shown in Fig. 3.3, so as to evaluate the impedance parameters. The impedance parameters such as R_{hf}, C_{dl}, R_f and C_f, along with the calculated efficiency values for various amounts of caprylate in sodium sulfate and combined media at different medium concentrations and temperatures have been enlisted in Table 3.30 (a), Table 3.30 (b) , Table 3.30 (c) and Table 3.31 (a), Table 3.31 (b), respectively. The impedance results too establish 320 mM as the most economic concentration of caprylate for the inhibition of ZE41 corrosion. The calculated efficiency values are close to those evaluated from the polarization measurements for caprylate and higher efficiencies are exclusive to more concentrated media. The film thickness and resistance are higher at higher caprylate concentrations.

The Bode magnitude plots for the corrosion of ZE41 alloy at 45 °C in 1.0 M Na$_2$SO$_4$ and in the combined medium of 0.2 M Na$_2$SO$_4$ - 0.1 M NaCl in the presence of different concentrations of caprylate are shown in Fig. 3.43 (a) and Fig. 3.43 (b), respectively.
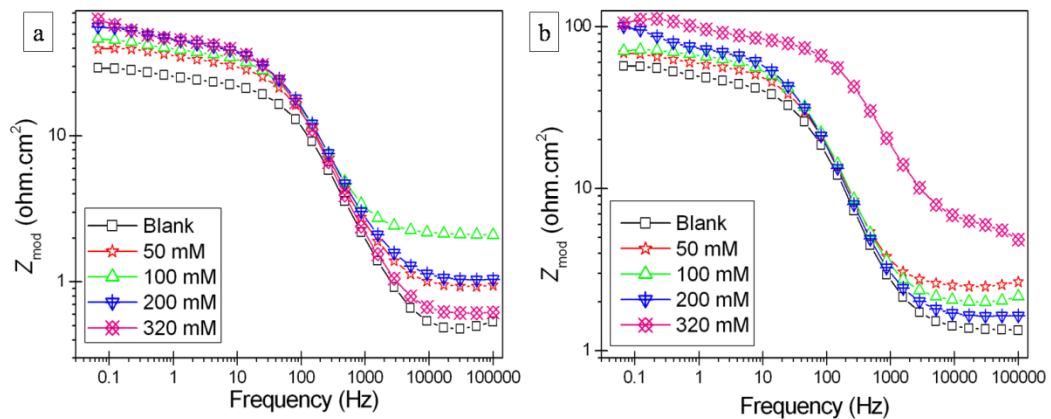
Fig. 3.43 Bode magnitude plots for the corrosion of ZE41 alloy in the presence of different concentrations of caprylate at 45 °C in (a) 1.0 M Na$_2$SO$_4$, (b) the combined medium of 0.2 M Na$_2$SO$_4$ - 0.1 M NaCl.
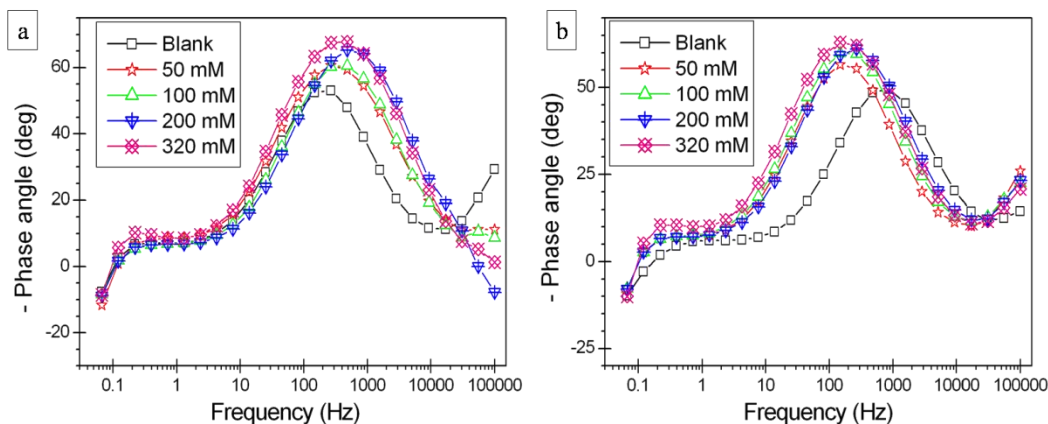
Fig. 3.44 Bode phase angle plots for the corrosion of ZE41 alloy in the presence of different concentrations of caprylate at 45 °C in (a) 1.0 M Na₂SO₄, (b) the combined medium of 0.2 M Na₂SO₄ - 0.1 M NaCl.

The phase angle plots for the same have been depicted in Fig. 3.44 (a) and Fig. 3.44 (b), respectively. It can be inferred from the increase in the impedance modulus (Z_{mod}) at low frequencies and the phase maximum (θ_{max}) at intermediate frequencies that increased concentration of caprylate facilitates the formation of a defensive surface film which effectively functions as a barrier against corrosive ingress.

3.6.3 Effect of temperature

The efficiency of caprylate remarkably diminishes with the increase in solution temperature as indicated by the comprehensive electrochemical data enlisted in Table 3.28, Table 3.29, Table 3.30 and Table 3.31. The increase in temperature causes an increase in film capacitance and a decrease in film resistance signifying the film dissolution and disruption. Fig. 3.45 (a) and Fig. 3.45 (b), respectively, are the Arrhenius plots for the corrosion of ZE41 alloy specimen 0.2 M Na₂SO₄ and in the combined medium of 0.2 M Na₂SO₄ - 1.0 M NaCl containing different concentrations of caprylate. The ln (v_{corr} /T) versus (1/T) plots for the same are shown in Fig. 3.46 (a) and Fig. 3.46 (b), respectively.
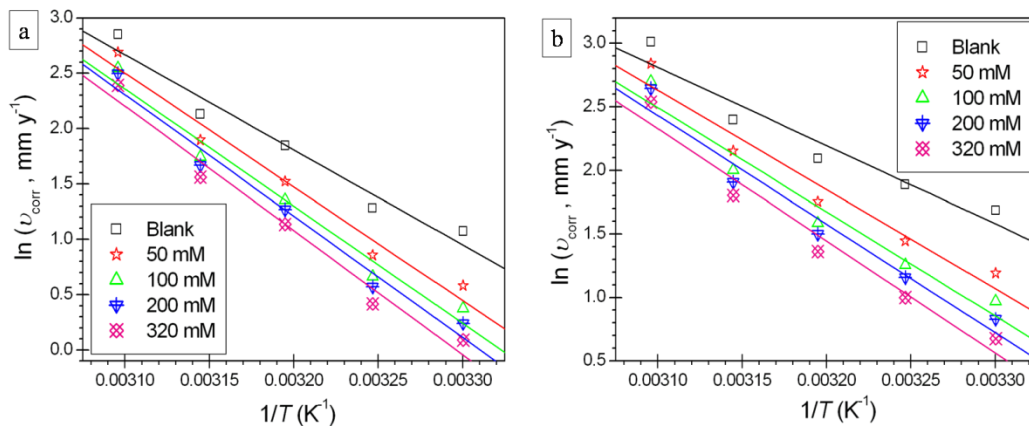
Fig. 3.45 Arrhenius plots for the corrosion of ZE41 alloy in the presence of different concentrations of caprylate in (a) 0.2 M Na$_2$SO$_4$ (b) the combined medium of 0.2 M Na$_2$SO$_4$ - 0.1 M NaCl.
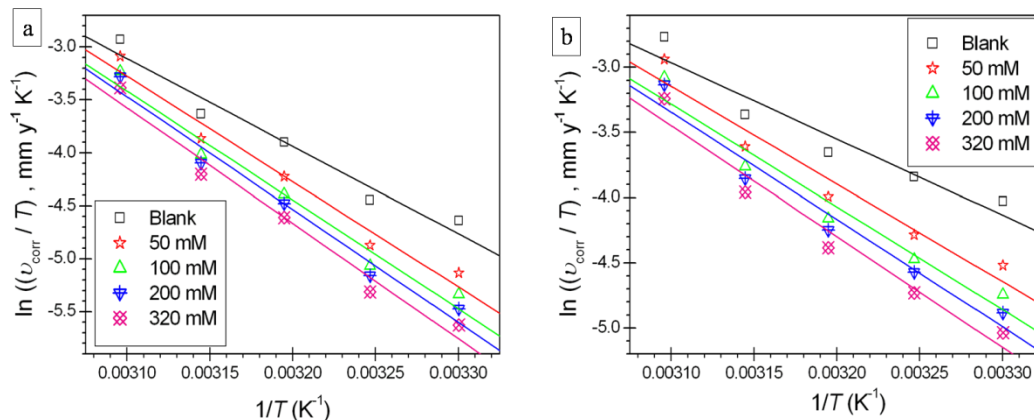
Fig. 3.46 ln (v_{corr}/T) vs. (1/T) plots for the corrosion of ZE41 alloy in the presence of different concentrations of caprylate in (a) 0.2 M Na$_2$SO$_4$ (b) the combined medium of 0.2 M Na$_2$SO$_4$ - 0.1 M NaCl.

The computed activation parameters for the dissolution of ZE41 in sodium sulfate and the combined media, in the presence of different concentrations of caprylate are enlisted in Table 3.32 (a) and Table 3.32 (b), respectively. Even from the reaction energetics point of view, the increase in concentration of caprylate retards ZE41 dissolution, as seen from the increase in activation energy values. During ZE41 oxidation the reactants combine together to form the activated complex, in a reaction which controls the overall rate of

dissolution. Such association of reactants is evident from the decrease in entropy of the system during activation, as observed from the negative $\Delta S^{\#}$ values.

3.6.4 Adsorption behavior

Among the adsorption isotherms considered, Langmuir adsorption isotherm was most appropriate to describe the adsorption mediated inhibition by caprylate. The Langmuir adsorption isotherms for adsorption of caprylate on ZE41 alloy surface at different temperatures in 0.2 M Na_2SO_4 and in the combined medium of 0.2 M Na_2SO_4 - 1.0 M NaCl are presented in Fig. 3.47 (a) and Fig. 3.47 (b), respectively.
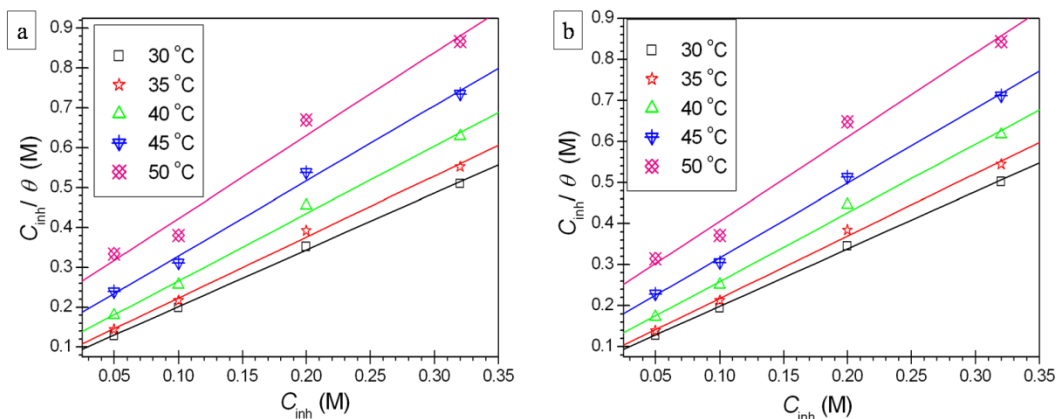
Fig. 3.47 Langmuir adsorption isotherms for the adsorption of caprylate on ZE41 alloy surface at different temperatures in (a) 0.2 M Na_2SO_4 (b) the combined medium of 0.2 M Na_2SO_4 - 0.1 M NaCl.

The calculated thermodynamic parameters like ΔG°_{ads}, ΔH°_{ads} and ΔS°_{ads} along with the slope and linear regression coefficient (R^2) for the adsorption of caprylate at different temperatures in sodium sulfate and the combined media are listed in Table 3.33 (a) and Table 3.33 (b), respectively. The aptness of Langmuir isotherm to elucidate the adsorption of caprylate is evident from the linear regression coefficient values, average of which is close to unity (average $R^2 = 0.99$). The minute deviation from ideal Langmuir behavior as evident from the slope values is the consequence of interactions among the adsorbed caprylate molecules. The thermodynamic parameters collectively suggest a

spontaneous adsorption of caprylate, which is predominantly physisorption and accompanied by decrease in entropy of the system.

Table 3.28 (a) Electrochemical polarization parameters for the corrosion of ZE41 alloy in 0.2 M Na$_2$SO$_4$ containing different concentrations of caprylate at different temperatures.

Temp [°C]	Caprylate concentration [mM]	E_{corr} vs. SCE [mV]	i_{corr} [μA cm^{-2}]	$-b_c$ [mV dec^{-1}]	η [%]
	Blank	-1604	131.7	168	-
	50	-1601	80.4	174	39.0
	100	-1589	65.5	183	50.3
30	200	-1592	57.0	166	56.7
	320	-1598	49.1	162	62.7
	330	-1596	48.6	160	63.1
	400	-1599	44.0	161	66.6
	Blank	-1608	162.1	177	-
	50	-1603	105.9	178	34.7
35	100	-1601	87.3	183	46.2
	200	-1607	79.5	191	51.0
	320	-1600	68.2	167	58.0
	Blank	-1610	284.9	180	-
	50	-1602	205.7	178	27.8
40	100	-1605	173.8	172	39.0
	200	-1597	159.6	167	44.0
	320	-1608	139.8	161	50.9
	Blank	-1635	378.6	184	-
	50	-1615	299.5	182	20.9
45	100	-1621	257.0	188	32.1
	200	-1632	237.8	191	37.2
	320	-1628	213.7	180	43.6
	Blank	-1638	778.0	189	-
	50	-1634	661.6	187	15.0
50	100	-1629	573.7	190	26.3
	200	-1622	545.7	194	29.9
	320	1620	490.9	176	36.9

Table 3.28 (b) Electrochemical polarization parameters for the corrosion of ZE41 alloy in 0.6 M Na₂SO₄ containing different concentrations of caprylate at different temperatures.

Temp [°C]	Caprylate concentration [mM]	E_{corr} vs. SCE [mV]	i_{corr} [$\mu A\ cm^{-2}$]	$-b_c$ [$mV\ dec^{-1}$]	η [%]
	Blank	-1626	327.1	192	-
	50	-1619	196.1	195	40.1
	100	-1622	160.4	190	51.0
30	200	-1624	134.6	184	58.8
	320	-1614	112.2	186	65.7
	330	-1618	110.8	188	66.1
	400	-1616	103.3	192	68.4
	Blank	-1628	594.7	199	-
	50	-1620	376.8	206	36.6
35	100	-1623	313.9	201	47.2
	200	-1618	267.6	195	55.0
	320	-1624	231.9	192	61.0
	Blank	-1634	708.0	204	-
	50	-1627	503.7	201	28.9
40	100	-1621	423.8	198	40.1
	200	-1632	368.9	206	47.9
	320	-1630	325.3	205	54.1
	Blank	-1636	886.7	211	-
	50	-1631	656.3	204	26.0
45	100	-1629	594.4	210	33.0
	200	-1622	532.8	218	39.9
	320	-1630	478.3	215	46.1
	Blank	-1639	1250.1	214	-
	50	-1636	1025.4	217	18.0
50	100	-1635	912.4	203	27.0
	200	-1631	837.9	198	33.0
	320	-1629	775.7	196	38.0

Table 3.28 (c) Electrochemical polarization parameters for the corrosion of ZE41 alloy in 1.0 M Na$_2$SO$_4$ containing different concentrations of caprylate at different temperatures.

Temp [°C]	Caprylate concentration [mM]	E_{corr} vs. SCE [mV]	i_{corr} [µA cm^{-2}]	$-b_c$ [mV dec^{-1}]	η [%]
30	Blank	-1648	520.8	190	-
	50	-1638	284.7	187	45.3
	100	-1641	238.9	191	54.1
	200	-1640	209.8	194	59.7
	320	-1647	164.1	186	68.5
	330	-1644	160.6	183	69.1
	400	-1639	150.5	181	71.1
35	Blank	-1650	726.7	211	-
	50	-1647	429.7	207	40.9
	100	-1649	362.3	205	50.1
	200	-1641	311.7	201	57.1
	320	-1644	254.5	215	65.0
40	Blank	-1657	996.1	228	-
	50	-1648	626.4	207	37.1
	100	-1654	549.4	223	44.8
	200	-1653	488.3	218	51.0
	320	-1650	417.3	214	58.1
45	Blank	-1681	1287.7	261	-
	50	-1663	886.5	276	31.2
	100	-1659	793.6	264	38.4
	200	-1675	743.4	252	42.3
	320	-1669	658.4	257	48.9
50	Blank	-1686	1451.2	308	-
	50	-1668	1099.3	298	24.3
	100	-1681	1013.2	291	30.2
	200	-1672	940.4	284	35.2
	320	-1673	864.1	282	40.5

Table 3.29 (a) Electrochemical polarization parameters for the corrosion of ZE41 alloy in the combined medium of 0.2 M Na$_2$SO$_4$ - 0.1 M NaCl containing different concentrations of caprylate at different temperatures.

Temp [°C]	Caprylate concentration [mM]	E_{corr} vs. SCE [mV]	i_{corr} [µA cm^{-2}]	$-b_c$ [mV dec^{-1}]	η [%]
	Blank	-1607	242.9	176	-
	50	-1602	148.2	189	39.0
	100	-1603	118.4	167	51.3
30	200	-1592	102.5	171	57.8
	320	-1595	88.2	179	63.7
	330	-1600	87.4	167	64.0
	400	-1605	84.0	170	65.4
	Blank	-1628	297.3	195	-
	50	-1621	190.2	186	36.0
35	100	-1624	157.8	191	46.9
	200	-1618	142.6	194	52.0
	320	-1620	122.5	203	58.8
	Blank	-1644	364.9	196	-
	50	-1639	259.3	204	28.9
40	100	-1632	219.7	207	39.8
	200	-1626	201.3	197	44.8
	320	-1640	175.5	198	51.9
	Blank	-1649	495.2	192	-
	50	-1637	386.9	190	21.9
45	100	-1643	332.9	187	32.8
	200	-1648	302.0	184	39.0
	320	-1641	272.3	181	45.0
	Blank	-1655	914.1	213	-
	50	-1650	768.7	208	15.9
50	100	-1643	668.2	210	26.9
	200	-1638	631.6	204	30.9
	320	-1647	567.1	198	38.0

Table 3.29 (b) Electrochemical polarization parameters for the corrosion of ZE41 alloy in the combined medium of 1.0 M Na$_2$SO$_4$ – 1.0 M NaCl containing different concentrations of caprylate at different temperatures.

Temp [°C]	Caprylate concentration [mM]	E_{corr} vs. SCE [mV]	i_{corr} [μA cm^{-2}]	$-b_c$ [mV dec^{-1}]	η [%]
	Blank	-1669	825.0	204	-
	50	-1661	421.8	201	48.9
	100	-1654	348.3	196	57.8
30	200	-1652	301.0	195	63.5
	320	-1666	231.2	192	72.0
	330	-1657	227.0	189	72.5
	400	-1650	220.7	195	73.2
	Blank	-1681	1034.7	214	-
	50	-1673	574.8	204	44.5
35	100	-1675	479.9	207	53.6
	200	-1662	406.6	212	60.7
	320	-1668	325.9	217	68.5
	Blank	-1665	1310.2	221	-
	50	-1663	777.3	220	40.7
40	100	-1660	675.2	232	48.5
	200	-1657	595.7	228	54.5
	320	-1651	501.6	216	61.7
	Blank	-1716	1733.5	317	-
	50	-1702	1130.9	285	34.8
45	100	-1710	1005.6	312	42.0
	200	-1689	937.8	293	45.9
	320	-1697	823.9	303	52.5
	Blank	-1726	1752.8	224	-
	50	-1704	1264.7	218	27.8
50	100	-1715	1160.9	213	33.8
	200	-1708	1072.6	210	38.8
	320	-1721	981.8	202	44.0

Table 3.30 (a) Impedance parameters for the corrosion of ZE41 alloy in 0.2 M Na$_2$SO$_4$ containing different concentrations of caprylate at different temperatures.

Temp [°C]	Caprylate concentration [mM]	R_{hf} [Ω cm^2]	R_f [Ω cm^2]	C_{dl} [μF cm^{-2}]	C_f [μF cm^{-2}]	η [%]
30	Blank	83.3	73.1	24.0	101.2	-
	50	140.4	42.5	21.8	99.3	40.7
	100	165.2	59.4	21.0	98.9	49.6
	200	190.1	72.4	23.8	96.3	56.2
	320	227.5	98.2	21.2	92.8	63.4
	330	231.6	104.7	19.2	87.3	64.0
	400	258.1	167.2	16.2	55.8	67.7
35	Blank	63.7	55.5	32.1	102.7	-
	50	98.6	68.4	30.2	99.7	35.4
	100	124.3	89.5	27.8	94.3	48.8
	200	133.2	117.4	29.8	97.2	52.2
	320	152.8	132.5	26.2	93.7	58.3
40	Blank	53.9	40.7	35.3	104.1	-
	50	76.7	45.3	34.7	102.9	29.8
	100	90.1	50.1	30.7	100.4	40.2
	200	96.7	73.5	27.9	98.9	44.3
	320	110.2	96.5	25.2	96.7	51.1
45	Blank	47.2	42.7	36.8	104.9	-
	50	61.2	43.5	34.5	101.8	22.9
	100	71.8	57.3	31.8	99.3	34.3
	200	76.1	62.7	29.8	98.4	38.0
	320	84.2	78.3	27.7	95.6	44.0
50	Blank	34.2	31.2	39.4	108.1	-
	50	41.4	33.5	38.0	106.8	17.3
	100	47.3	40.9	34.8	103.8	27.7
	200	48.9	37.2	30.8	100.8	30.0
	320	55.2	47.2	26.8	96.7	38.0

Table 3.30 (b) Impedance parameters for the corrosion of ZE41 alloy in 0.6 M Na₂SO₄ containing different concentrations of caprylate at different temperatures.

Temp [°C]	Caprylate concentration [mM]	R_{hf} [Ω cm^2]	R_f [Ω cm^2]	C_{dl} [μF cm^{-2}]	C_f [μF cm^{-2}]	η [%]
	Blank	61.1	51.7	26.9	101.2	-
	50	104.3	58.4	25.0	100.2	41.4
	100	120.1	69.3	24.0	99.3	49.1
30	200	151.5	88.8	21.8	95.5	59.7
	320	180.2	94.9	20.2	90.3	66.1
	330	183.7	106.2	18.8	83.3	66.7
	400	197.9	172.4	15.6	42.8	69.1
	Blank	40.2	31.2	35.0	104.1	-
	50	64.8	54.3	32.2	102.3	37.9
35	100	78.3	68.5	30.9	100.2	48.6
	200	91.1	80.0	29.0	96.8	55.9
	320	109.6	98.3	25.7	92.7	63.3
	Blank	36.6	27.8	37.6	104.3	-
	50	53.8	38.2	35.8	103.9	31.9
40	100	61.9	55.5	34.0	102.3	40.8
	200	72.7	60.2	30.0	98.3	49.6
	320	81.3	80.2	27.7	95.2	55.0
	Blank	27.6	19.9	41.9	106.7	-
	50	38.5	32.2	40.2	104.9	28.2
45	100	42.6	38.4	37.3	101.8	35.1
	200	46.1	42.2	35.5	98.2	40.1
	320	50.7	49.0	30.3	96.8	45.5
	Blank	19.4	17.6	43.4	109.3	-
	50	24.2	20.2	41.2	107.8	19.7
50	100	28.3	24.5	39.2	103.8	31.4
	200	29.8	28.0	35.7	100.4	35.0
	320	33.6	31.8	31.2	98.3	42.3

Table 3.30 (c) Impedance parameters for the corrosion of ZE41 alloy in 1.0 M Na₂SO₄ containing different concentrations of caprylate at different temperatures.

Temp [°C]	Caprylate concentration [mM]	R_{hf} [Ω cm^2]	R_f [Ω cm^2]	C_{dl} [μF cm^{-2}]	C_f [μF cm^{-2}]	η [%]
30	Blank	46.0	42.0	33.9	108.5	-
	50	87.6	51.8	28.2	104.3	47.4
	100	108.4	76.2	23.5	98.3	57.5
	200	116.8	82.3	21.2	92.4	60.6
	320	147.4	97.2	19.0	87.6	68.8
	330	151.3	102.4	15.7	70.0	69.6
	400	166.8	143.2	13.2	35.5	72.4
35	Blank	39.7	36.2	40.1	108.9	-
	50	67.1	59.4	36.7	104.7	40.9
	100	78.3	71.3	30.3	98.0	49.3
	200	90.6	87.6	28.4	92.4	56.2
	320	114.7	105.3	24.5	84.7	65.4
40	Blank	25.0	20.6	42.6	110.2	-
	50	42.3	39.4	39.3	105.4	40.9
	100	46.1	42.3	33.5	100.9	45.7
	200	53.7	50.1	29.4	97.3	53.5
	320	66.3	61.3	25.2	90.3	62.3
45	Blank	23.4	18.5	43.2	111.2	-
	50	35.9	34.6	41.3	109.2	34.7
	100	39.0	38.0	39.2	105.3	39.9
	200	43.6	40.2	34.3	102.4	46.3
	320	47.8	44.9	29.2	95.5	51.1
50	Blank	22.8	17.4	44.6	115.3	-
	50	29.6	24.6	40.3	110.2	22.9
	100	31.6	30.0	38.3	108.3	27.7
	200	35.7	31.3	34.8	104.7	36.1
	320	41.8	38.5	30.2	96.6	45.5

Table 3.31 (a) Impedance parameters for the corrosion of ZE41 alloy in the combined medium of 0.2 M Na$_2$SO$_4$ - 0.1M NaCl containing different concentrations of caprylate at different temperatures.

Temp [°C]	Caprylate concentration [mM]	R_{hf} [Ω cm^2]	R_f [Ω cm^2]	C_{dl} [μF cm^{-2}]	C_f [μF cm^{-2}]	η [%]
30	Blank	74.9	69.7	27.1	101.8	-
	50	128.2	88.7	20.2	97.9	41.5
	100	150.5	112.4	18.2	96.7	50.2
	200	165.2	131.1	20.7	91.7	54.6
	320	202.5	152.3	17.1	86.2	63.0
	330	206.4	165.8	15.6	77.1	63.7
	400	231.5	203.7	12.6	46.6	67.6
35	Blank	54.6	49.0	36.4	103.6	-
	50	83.3	75.8	34.7	101.2	34.5
	100	109.3	97.3	26.6	93.9	50.1
	200	119.6	112.8	27.2	95.4	54.4
	320	136.8	133.2	23.9	90.1	60.1
40	Blank	49.2	34.2	39.0	106.1	-
	50	67.4	52.8	33.3	102.6	27.0
	100	84.3	69.9	28.2	97.3	41.7
	200	92.8	80.0	25.5	96.7	47.1
	320	108.7	102.4	24.0	94.0	54.8
45	Blank	43.2	31.8	43.1	107.7	-
	50	56.9	47.8	37.8	100.7	24.1
	100	67.3	59.2	30.9	97.3	35.9
	200	73.6	68.1	26.2	95.7	41.3
	320	81.8	78.8	22.2	91.3	47.2
50	Blank	28.8	25.7	45.6	110.6	-
	50	34.7	27.2	43.2	105.7	17.0
	100	41.1	24.8	32.7	101.3	29.9
	200	43.8	40.7	28.0	99.2	34.3
	320	48.7	43.3	23.6	95.9	40.9

Table 3.31 (b) Impedance parameters for the corrosion of ZE41 alloy in the combined medium of 1.0 M Na$_2$SO$_4$ – 1.0 M NaCl containing different concentrations of caprylate at different temperatures.

Temp [°C]	Caprylate concentration [mM]	R_{hf} [Ω cm^2]	R_f [Ω cm^2]	C_{dl} [μF cm^{-2}]	C_f [μF cm^{-2}]	η [%]
30	Blank	34.6	31.4	40.3	112.4	-
	50	69.7	56.8	27.8	100.5	50.3
	100	85.1	78.7	22.6	95.7	59.3
	200	98.7	84.3	19.0	86.9	64.9
	320	120.5	100.8	17.2	80.5	71.3
	330	125.3	105.5	14.6	70.2	72.4
	400	139.5	134.7	11.7	30.8	75.2
35	Blank	29.3	23.8	49.3	113.4	-
	50	51.5	48.3	36.2	102.4	43.1
	100	66.8	60.8	32.7	96.5	56.1
	200	76.7	67.0	27.6	88.6	61.8
	320	93.4	90.5	21.1	78.1	68.6
40	Blank	20.2	16.2	54.3	114.7	-
	50	31.7	28.2	36.9	105.1	36.4
	100	40.8	34.6	31.4	97.3	50.5
	200	47.2	40.7	28.0	95.7	57.2
	320	54.9	44.6	24.6	87.9	63.3
45	Blank	15.8	14.9	58.0	114.6	-
	50	23.3	20.8	40.8	108.5	32.1
	100	28.0	26.4	35.8	101.4	43.6
	200	31.5	25.7	32.1	100.7	49.9
	320	35.8	30.9	26.7	94.7	55.9
50	Blank	15.0	13.1	63.6	120.1	-
	50	20.0	18.9	40.2	108.9	25.2
	100	23.2	21.5	38.1	98.7	35.4
	200	24.9	20.1	33.2	97.8	40.0
	320	28.4	25.7	29.0	94.5	47.2

Table 3.32 (a) Activation parameters for the corrosion of ZE41 alloy in different concentrations of Na$_2$SO$_4$ in the presence of different concentrations of caprylate.

Concentration of Na$_2$SO$_4$ [M]	Concentration of caprylate [mM]	E_a [kJ mol^{-1}]	$\Delta H^{\#}$ [kJ mol^{-1}]	$\Delta S^{\#}$ [J mol^{-1} K^{-1}]
	Blank	71.4	68.8	-93.2
	50	85.3	82.7	-51.5
0.2	100	88.0	85.4	-44.4
	200	91.2	88.6	-35.0
	320	93.3	90.7	-29.2
	Blank	50.3	47.7	-153.5
	50	63.0	60.4	-115.8
0.6	100	67.1	64.5	-104.0
	200	70.8	68.2	-93.2
	320	74.8	72.2	-81.4
	Blank	42.8	40.2	-174.8
	50	55.9	53.3	-136.8
1.0	100	59.9	57.3	-125.0
	200	63.1	60.5	-115.7
	320	69.6	67.0	-96.1

Table 3.32 (b) Activation parameters for the corrosion of ZE41 alloy in different concentrations of the combined media in the presence of different concentrations of caprylate.

Concentration of medium [M]	Concentration of caprylate [mM]	E_a [kJ mol^{-1}]	$\Delta H^{\#}$ [kJ mol^{-1}]	$\Delta S^{\#}$ [J mol^{-1} K^{-1}]
	Blank	51.2	48.6	-154.8
	50	64.9	62.3	-113.9
0.2 M Na$_2$SO$_4$ & 0.1M NaCl	100	68.1	65.5	-104.9
	200	71.0	68.4	-96.5
	320	73.4	70.8	-90.0
	Blank	33.0	30.4	-203.4
1.0 M Na$_2$SO$_4$ & 1.0M NaCl	50	46.8	44.2	-163.5
	100	51.3	48.7	-150.4
	200	55.0	52.4	-139.5
	320	62.2	59.6	-117.9

Table 3.33 (a) Thermodynamic parameters for the adsorption of caprylate on ZE41 alloy surface in sodium sulfate media.

Concentration of Na_2SO_4 [M]	Temp [°C]	ΔG^o_{ads} [kJ mol^{-1}]	ΔH^o_{ads} [kJ mol^{-1}]	ΔS^o_{ads} [J K^{-1} mol^{-1}]	R^2	Slope
0.2	30	-17.2			0.999	1.42
	35	-17.1			0.996	1.53
	40	-16.5	-53.4	-118.4	0.995	1.69
	45	-15.8			0.995	1.88
	50	-14.9			0.980	2.09
0.6	30	-17.1			0.998	1.35
	35	-17.2			0.999	1.44
	40	-16.5	-41.1	-78.5	0.999	1.56
	45	-16.4			0.996	1.85
	50	-15.6			0.998	2.12
1.0	30	-17.6			0.994	1.33
	35	-17.5			0.996	1.37
	40	-17.5	-29.1	-37.5	0.995	1.54
	45	-17.4			0.993	1.85
	50	-16.7			0.995	2.17

Table 3.33 (b) Thermodynamic parameters for the adsorption of caprylate on ZE41 alloy surface in combined media.

Concentration of medium [M]	Temp [°C]	ΔG^o_{ads} [kJ mol^{-1}]	ΔH^o_{ads} [kJ mol^{-1}]	ΔS^o_{ads} [J K^{-1} mol^{-1}]	R^2	Slope
0.2 M Na_2SO_4 & 0.1M NaCl	30	-17.3			0.999	1.40
	35	-17.3			0.997	1.52
	40	-16.7	-51.7	-112.7	0.995	1.67
	45	-15.9			0.997	1.82
	50	-15.1			0.985	2.05
1.0 M Na_2SO_4 & 1.0M NaCl	30	-17.9			0.995	1.27
	35	-17.8			0.996	1.32
	40	-17.9	-25.6	-25.0	0.996	1.47
	45	-17.8			0.994	1.74
	50	-17.3			0.996	2.03

3.7 THE MECHANISM OF CORROSION INHIBITION

3.7.1 Surfactant aggregation at alloy/electrolyte interface

The alkyl carboxylates namely, stearate, palmitate, myristate, laurate and caprylate are basically surface active agents. The surfactants exhibit a unique tendency to self-aggregate in solutions and at interfaces, above a definite threshold concentration. The nature of interfaces is crucial in deciding the pattern of aggregation of surfactants. The monomeric surfactants at air-liquid interface self-aggregate above critical micelle concentration (CMC) to form spherical micelles in solutions. A transition of similar nature ensues at solid-liquid interfaces, where the monolayer of surfactants beyond a threshold concentration, referred to as aggregate transition concentration (ATC), self-aggregate to generate bilayers or multilayers. In general, for surfactants ATC and CMC have been reported to be equivalent (Free 2004), and more often than not, of the same orders of magnitude. Any minuscule difference, if at all existing between ATC and CMC, is most likely the consequence of the dissimilarity in the interaction energies of surfactant molecules with solid-liquid and air-liquid interfaces.

3.7.2 Adsorption of carboxylates over ZE41 surface

Conventionally the chemical corrosion inhibitors are accredited to bring about the inhibition through surface adsorption and barrier film formation. However, achieving the inhibition in the present context is challenging as the alloy ZE41, as briefed earlier, undergoes microgalvanic corrosion and possesses a defective and porous film of corrosion products on its surface. Taking into consideration the nature of the primary surface film, the self aggregation of surfactants and the comprehensive results from the electrochemical study, the following plausible mechanism has been proposed to explicate corrosion inhibition of ZE41 by long chain alkyl monocarboxylates.

The examined alkyl carboxylates being anionic surfactants possess both hydrophilic carboxylate head and long alkyl hydrophobic tail. The thermodynamic parameters evaluated in the present study hinted at the possible occurrence of both type

of adsorption; physisorption and chemisorption during the interaction of carboxylates with ZE41 surface. The presence of zirconium and rare earth elements in the cathodic intermetallic phases might facilitate the chemisorption of the carboxylates. At these film-free surfaces the development of strong coordinate covalent bonds can occur through the donor-accepter interactions between the unshared electron pairs of oxygen of the carboxylates and the vacant d-orbitals of zirconium and rare earth metal atoms, eventuating into chemisorption (Huang et al. 2011). The carboxylates chemisorbed along the secondary phases, most likely block the active cathodic reaction sites and hence impede the cathodic hydrogen evolution reaction. The electrostatic interactions are most likely between the anionic head of the carboxylates and magnesium ions (Mg^{2+}) confined within the defects of the surface film developed over α-Mg matrix. The two different carboxylate adsorptions driven by the microstructure of the ZE41 alloy are schematically represented in Fig. 3.48.
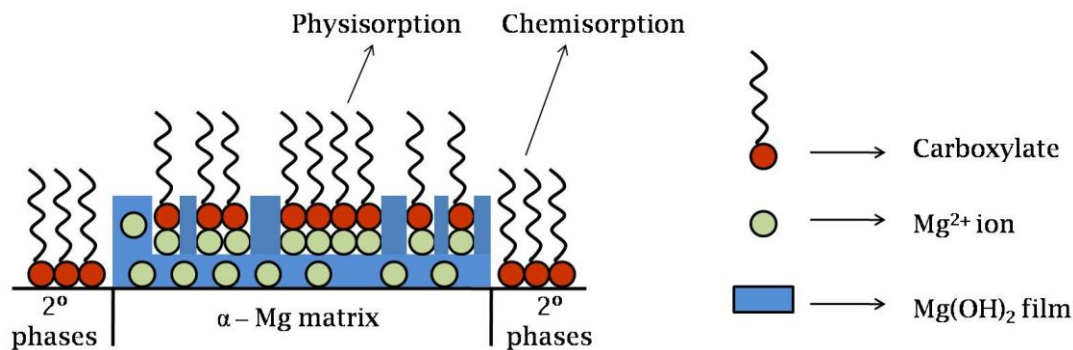
Fig. 3.48 The schematic representation of physisorption and chemisorption of the alkyl carboxylates over ZE41 surface.

The low solubility products of magnesium carboxylates are easily exceeded due to the presence of surplus of dissolved Mg^{2+} ions, and hence the physisorbed carboxylates preferentially precipitate as magnesium salts within defects of the surface film over the α-Mg matrix. The precipitates fill-up the pores and appreciably rectify the defects of the surface film. The modified surface film, owing to the presence of precipitated carboxylates might also acquire hydrophobicity to some extent (Frignani et al. 2012), which is advantageous given the tendency of the hydrophobic film to repel the aqueous

electrolyte. The deviation from ideal Langmuir behavior observed for all the carboxylates hinted at the existence of intermolecular forces which in all likelihood are van der Waals interactions existing between the long alkyl chains of adsorbed carboxylate molecules. Such mutual interactions might further contribute towards the densification the film. To sum up, the carboxylates are instrumental in the formation of a compact modified surface film over α-Mg matrix, which subsequently impedes the anodic reaction of magnesium dissolution through an enhanced barrier effect against electrolyte ingress. This mechanism suggesting the compaction of the surface film on addition of carboxylates is corroborated by some results of the study, like the Bode phase angle plots and the impedance parameters such as film resistance (R_f) and film capacitance (C_f) whose variations collectively pointed out the augmentation of the barrier effect, the resistance and the thickness of the surface film in the presence of the carboxylates.

3.7.3 The predominance of physisorption (influence of temperature)

Even though both type of adsorption are likely to occur, some results from the study indicated the predominance of physisorption over chemisorption; especially at higher temperatures, like the propinquity of calculated standard adsorption enthalpy ($\Delta H°_{ads}$) values to the enthalpy threshold for physisorption and the decline in the inhibition efficiency with the increase in temperature, later of which is an attribute of physisorbed inhibitors which undergo desorption at higher temperatures. This prevalence of physisorption at higher temperatures can be attributed to the increased ionic mobility, as the consequence of which magnesium ions diffuse afar even to cathodic regions which primarily are the sites of chemisorption. The accessibility to magnesium ions at cathodic regions might make a more instantaneous physisorption to occur at ease (Huang et al. 2011). Hence the proportion of carboxylates undergoing chemisorption tends to diminish with the rise in temperature. The physisorbed carboxylates nevertheless are susceptible to desorption at higher temperatures and hence the efficiency decreases. Besides predominance of physisorption, there exist other causative factors which are partly responsible for the reduction in inhibition efficiency at higher temperatures; like the

increased solubility of magnesium carboxylates and reduced hydrogen overvoltage, later of which generate hydrogen effervesces at the interface and hence obstructs the carboxylate adsorption.

3.7.4 Mode of inhibition by monolayer and multilayers (influence of carboxylate concentration)

The aggregate transition concentration (ATC) of carboxylates makes more sense when understood from the inhibition perspective. For investigations involving surfactant inhibitors ATC is graphically deduced from the plot of $(1/i_{corr})$ versus the concentration of inhibitor (C_{inh}), as the inhibitor concentration at which a steep slope abruptly transforms into a gradual slope. Fig. 3.49 (a), Fig. 3.49 (b), Fig. 3.49 (c), Fig. 3.49 (d) and Fig. 3.49 (e), respectively, are the representative $(1/i_{corr})$ vs. C_{inh} plots for stearate, palmitate, myristate, laurate and caprylate at 30 °C.

The graphically determined ATC values; 1.7 mM for stearate, 2.7 mM for palmitate, 6.5 mM for myristate, 20 mM for laurate and 320 mM for caprylate, are identical to optimum concentration or most economic concentration (C_{max}) of the corresponding carboxylates. Hence, up to the optimum concentration or the most economic concentration the carboxylates adsorb over ZE41 surface to form a monolayer. Such monolayer adsorption increasingly blocks the active reaction sites and augments the resistance to the corrosive permeation. On the other hand, when concentration surpasses C_{max} (or ATC) the transition from monolayer to multilayers occurs and alloy surface will no longer be accessible to the carboxylate molecules which settle into multilayers. Hence such carboxylate molecules adsorbed as bilayers or multilayers merely contribute to build-up additional layers. The blocking of the reaction sites being the most effective means of inhibition, the efficiency of carboxylates as seen from the electrochemical results of the study, increases significantly only up to the optimum concentration. The multilayers formed beyond the optimum concentration does increase the efficiency but to a negligible extent.
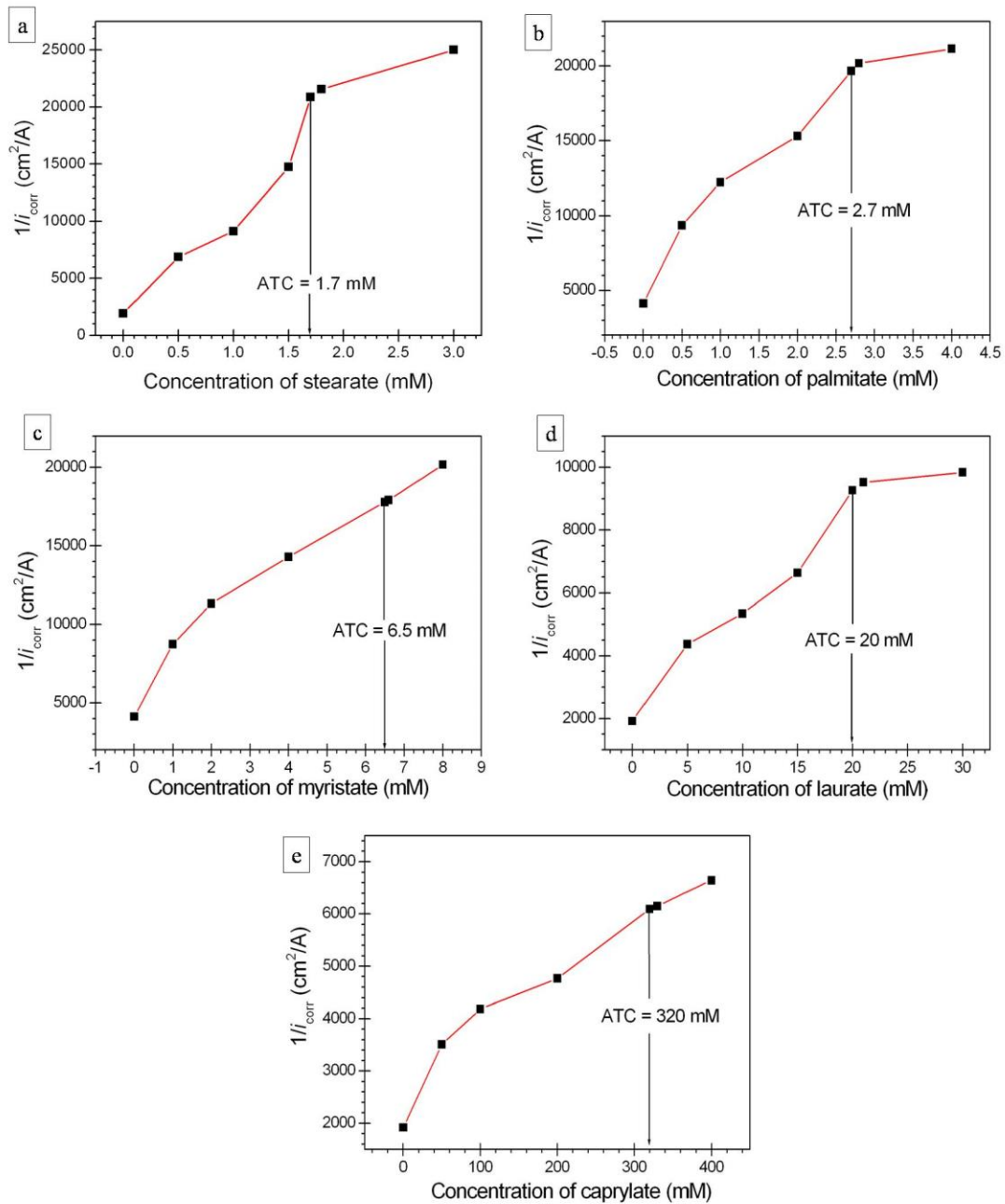
Fig. 3.49 ($1/i_{corr}$) vs. C_{inh} **plots at 30 °C for different concentrations of (a) stearate in 1.0 M Na$_2$SO$_4$, (b) palmitate in the combined medium of 0.2 M Na$_2$SO$_4$ - 0.1 M NaCl (c) myristate in the combined medium of 0.2 M Na$_2$SO$_4$ - 0.1 M NaCl and (d) laurate in 1.0 M Na$_2$SO$_4$ and (e) caprylate in 1.0 M Na$_2$SO$_4$.**

The multilayer adsorption can be validated from the plots shown in Fig. 3.50 (a), Fig. 3.50 (b), Fig. 3.50 (c), Fig. 3.50 (d) and Fig. 3.50(e), which respectively, show the change in film resistance (R_f) and film capacitance (C_f) with the concentration of stearate, palmitate, myristate, laurate and caprylate at 30 °C.
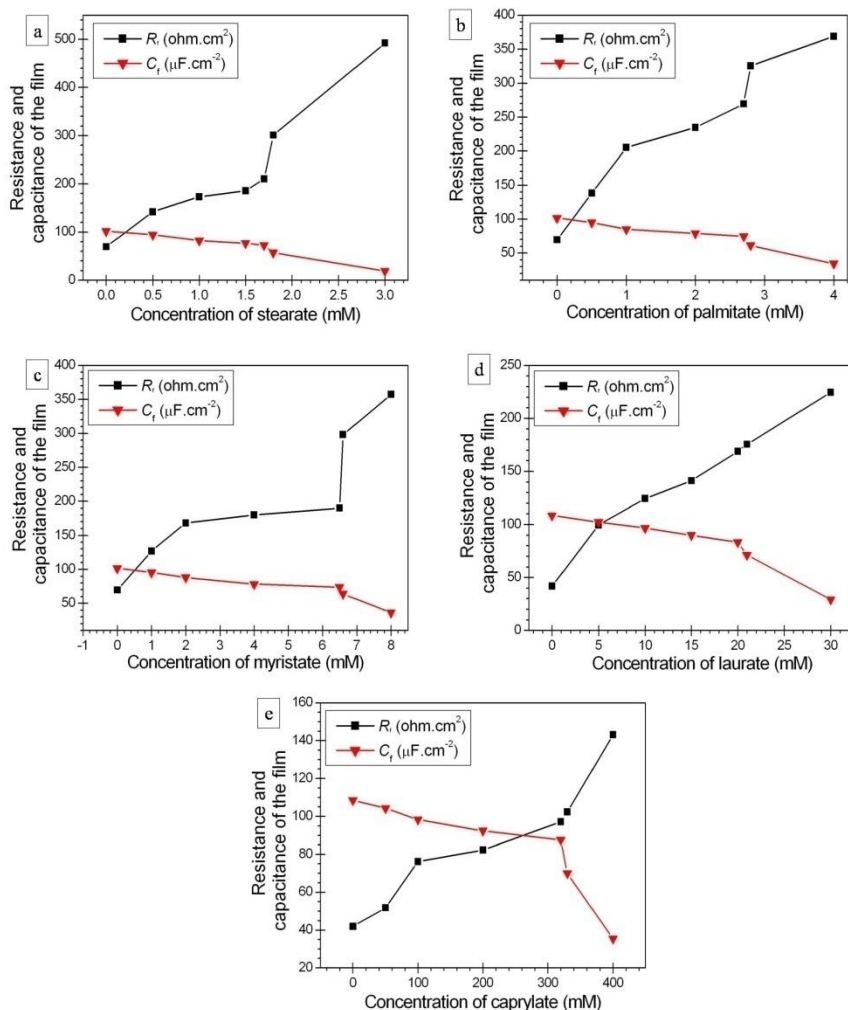
Fig. 3.50 The plots showing variation of film resistance (R_f) and film capacitance (C_f) at 30 °C for different concentrations of (a) stearate in the combined medium of 0.2 M Na_2SO_4 - 0.1 M NaCl, (b) palmitate in the combined medium of 0.2 M Na_2SO_4 - 0.1 M NaCl, (c) myristate in the combined medium of 0.2 M Na_2SO_4 - 0.1 M NaCl (d) laurate in 1.0 M Na_2SO_4 and (e) caprylate in 1.0 M Na_2SO_4.

At concentrations well above ATC (3mM for stearate, 4 mM for palmitate, 8 mM for myristate, 30 mM for laurate and 400 mM for caprylate) film resistance is remarkably high indicating a highest protection offered by the surface film and at the same time film capacitance is exceptionally low suggesting existence of a thickest surface film, both of which are the consequence of multilayer adsorption. This proposed hypothesis where the initial monolayer of the surfactants is believed to impart maximum protection has been supported by the study carried out by Xing et al. (1995) employing transferred Langmuir-Blodgett films of stearic acid on iron surface. While primary monolayer of stearic acid offered an inhibition efficiency of 65 %, the introduction of each additional monolayer increased the efficiency to a negligible extent of about 4 %.

3.7.5 Difference in inhibition efficiency among the carboxylates

The performance of the carboxylates can be compared only when the efficiency values chosen for comparison correspond to monolayer adsorption at the optimum concentration (C_{max}). For convenience the highest efficiency at optimum concentration is denoted as η_{max}. The highest efficiency at optimum concentration (η_{max}) for all the carboxylates were observed at 30 ºC in the combined medium containing 1.0 M each of sodium sulfate and sodium chloride and the values were 93.7 % for stearate, 91.1 % for palmitate, 86.6 % for myristate, 82.4 % for laurate and 72.0 % for caprylate. Interestingly the values of the optimum concentrations (C_{max}) were 1.7 mM for stearate, 2.7 mM for palmitate, 6.5 mM for myristate, 20 mM for laurate and 320 mM for caprylate. Hence stearate exhibited highest η_{max} equal to 93.7 % at a lowest C_{max} of 1.7 mM. On the other hand a very high concentration of 320 mM of caprylate is required to establish a monolayer and to achieve η_{max} equal to 72.0 %, which in comparison with the η_{max} of stearate is pretty low.

This trend in both η_{max} and C_{max} is most likely the consequence of the difference in the aliphatic chain length of the carboxylates which influences both the solubility product of the magnesium salts of the carboxylates as well as their optimum concentration (C_{max}). Since the inhibition by carboxylates is supposed to be accomplished

primarily through the compaction and densification of the porous surface film by the precipitated magnesium carboxylates, the solubility product of the magnesium salts is also a decisive factor. C_{max} is equivalent to CMC. For surfactants both CMC and the solubility product of the salts (say magnesium carboxylate) are known to vary inversely with the chain length. Hence a longer alkyl chain of carboxylates facilitates easier precipitation of magnesium carboxylates, leading to higher efficiencies at lower concentrations. Among the studied carboxylates stearate $(CH_3(CH_2)_{16}COO^-)$ has the longest alkyl chain followed by palmitate $(CH_3(CH_2)_{14}COO^-)$, myristate $(CH_3(CH_2)_{12}COO^-)$, laurate $(CH_3(CH_2)_{10}COO^-)$ and caprylate $(CH_3(CH_2)_6COO^-)$. Hence η_{max} decreases on going from stearate to caprylate, whereas C_{max} increases.

3.7.6 The influence of ionic concentration of the media

The results of the electrochemical studies collectively indicated an improved efficiency at higher ionic concentrations of the media. All the tested carboxylates showed better inhibition efficiency in chloride containing combined medium than in sulfate medium and in both the media the inhibition efficiency increased with the increase in ionic concentration. This trend can be explained by taking into account the tendency of the anions like chloride and sulfate to destabilize the magnesium hydroxide surface film by dissolution (Zucchi. et al. 2006). Such film dissolution generates magnesium ions, which function as the sites for the physisorption of carboxylate inhibitor. The increased ionic concentration thus results in increased extent of carboxylate adsorption which in turn brings about an increase in inhibition efficiency.

3.8 SURFACE MORPHOLOGY: SEM AND EDX ANALYSES

The proposed mechanism which accredits the inhibition to compaction and thickening of the surface film was further validated by examining the surface topography of the specimen exposed to carboxylate containing electrolytes. The surface studies were carried out utilizing SEM and EDX techniques. SEM images of ZE41 specimen surface after 1 hour immersion in the medium 1.0 M Na_2SO_4 containing 1.7 mM of stearate, 2.7

mM of palmitate, 6.5 mM of myristate, 20 mM of laurate and 320 mM of caprylate are shown in Fig. 3.51 (a), Fig. 3.51 (b), Fig. 3.51 (c), Fig. 3.51 (d) and Fig. 3.51 (e), respectively. The EDX spectra for the same are presented in Fig. 3.52 (a), Fig. 3.52 (b), Fig. 3.52 (c), Fig. 3.52 (d) and Fig. 3.52 (e), respectively. Fig. 3.53 (a), Fig. 3.53 (b), Fig. 3.53 (c), Fig. 3.53 (d) and Fig. 3.53 (e), respectively, are SEM images of ZE41 specimen surface after 1 hour immersion in the medium 1.0 M Na_2SO_4 - 1.0 M NaCl, containing optimum concentrations of stearate, palmitate, myristate, laurate and caprylate. The EDX spectra for the same are shown in Fig. 3.54 (a), Fig. 3.54 (b), Fig. 3.54 (c), Fig. 3.54 (d) and Fig. 3.54 (e), respectively.

In comparison with the SEM images of the corroded surface, the SEM images shown in Fig. 3.51 and Fig. 3.53 showcase a much uniform and compact surface film. The high vacuum maintained inside the SEM chamber dries out the surface film, as an outcome of this dehydration the SEM images display a "mud cracking" appearance. The EDX spectra given in Fig. 3.52 and Fig. 3.54, further substantiate the modification of the surface film brought about by the carboxylates. Besides the peaks for Mg, Zn, Zr and O, an additional peak for carbon is obtained in all the EDX spectra, which signify the presence of some organic moieties on the alloy surface, which in all probability are the surface adsorbed carboxylate molecules.
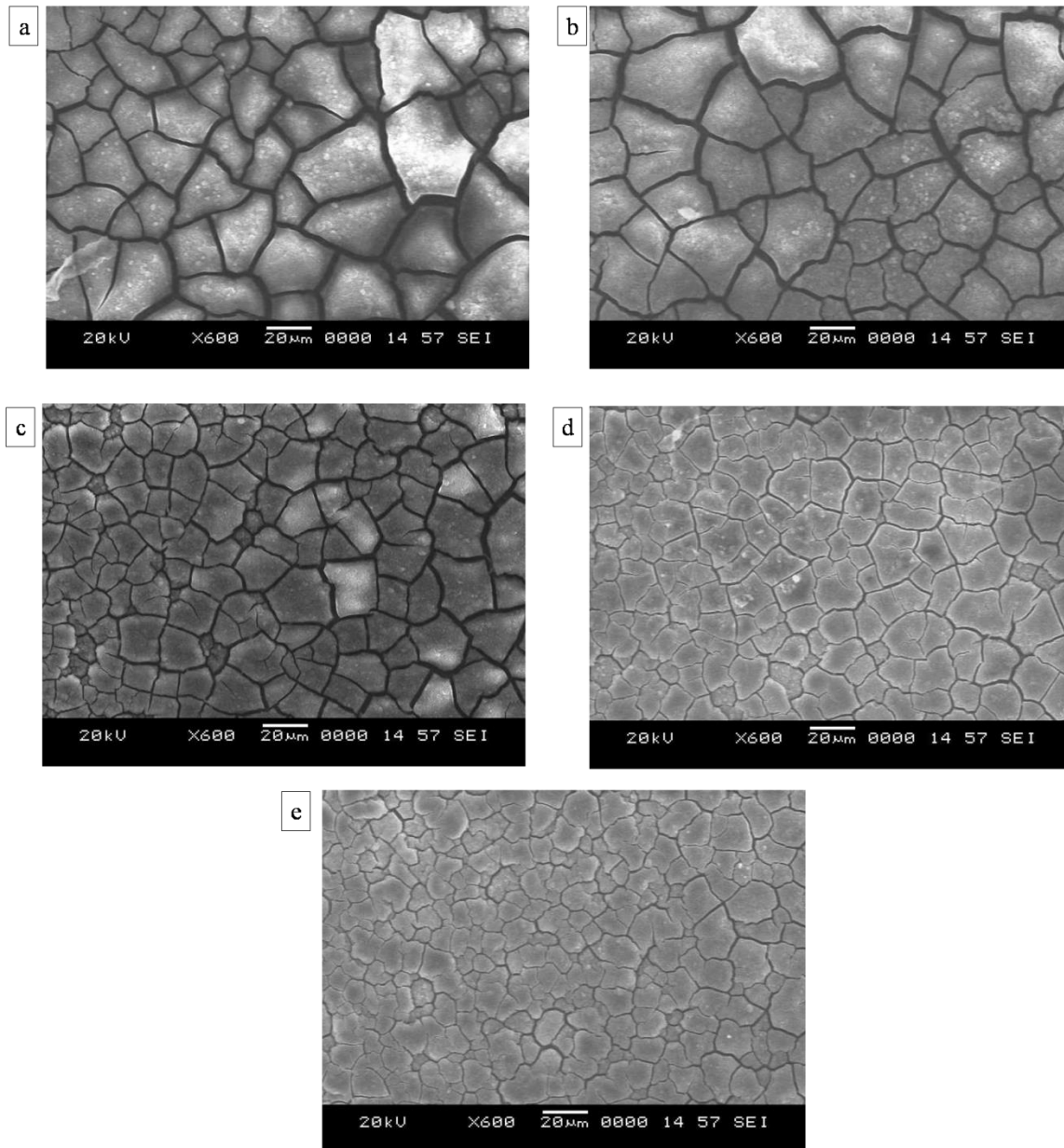
Fig. 3.51 SEM image of ZE41 specimen surface after 1 hour immersion in the medium of 1.0 M Na$_2$SO$_4$ solutions containing, (a) 1.7 mM of stearate, (b) 2.7 mM of palmitate, (c) 6.5 mM of myristate, (d) 20 mM of laurate and (e) 320 mM of caprylate.
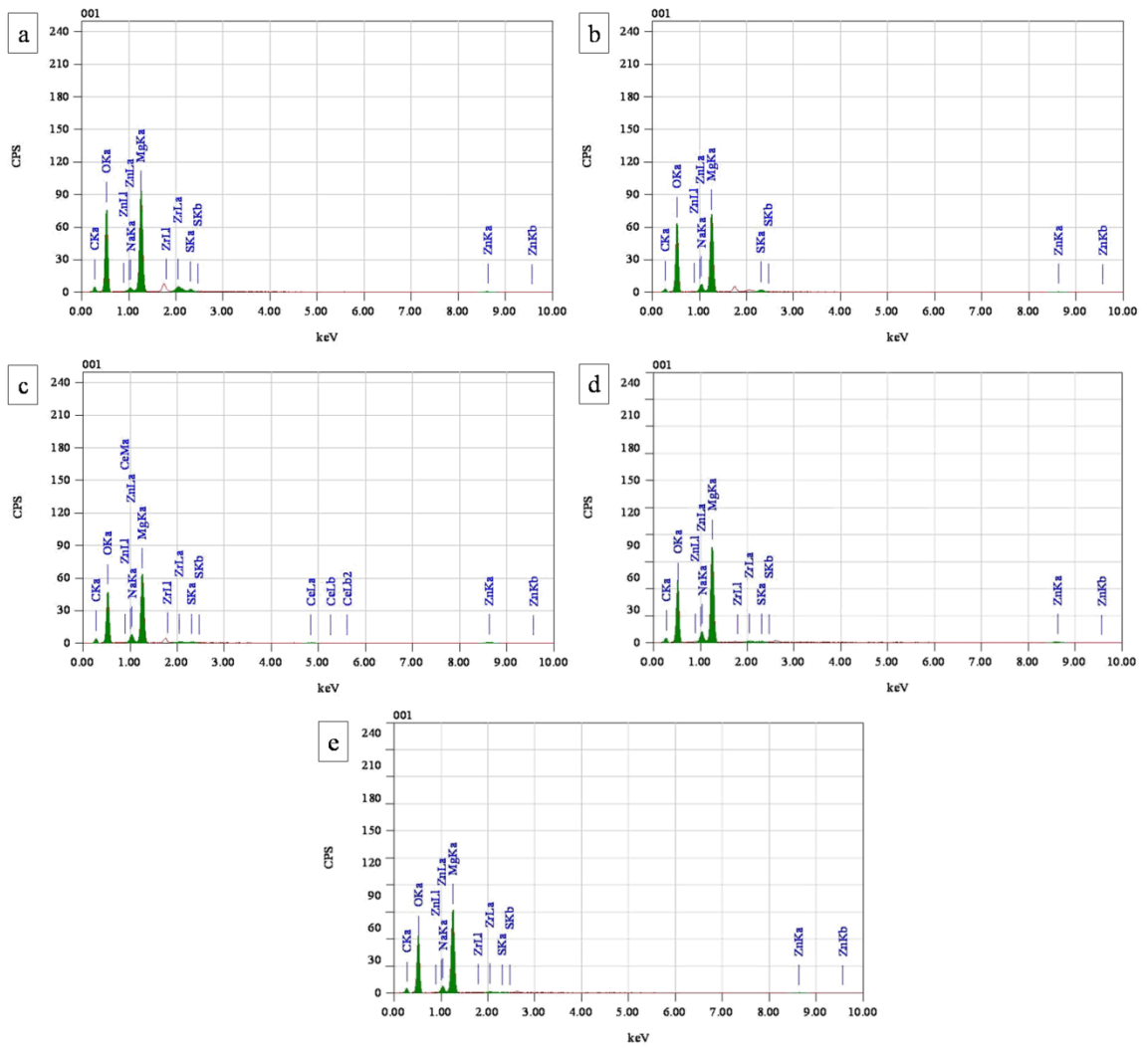
Fig. 3.52 EDX spectra of ZE41 specimen surface after 1 hour immersion in the medium of 1.0 M Na₂SO₄ solutions containing, (a) 1.7 mM of stearate, (b) 2.7 mM of palmitate, (c) 6.5 mM of myristate, (d) 20 mM of laurate and (e) 320 mM of caprylate.
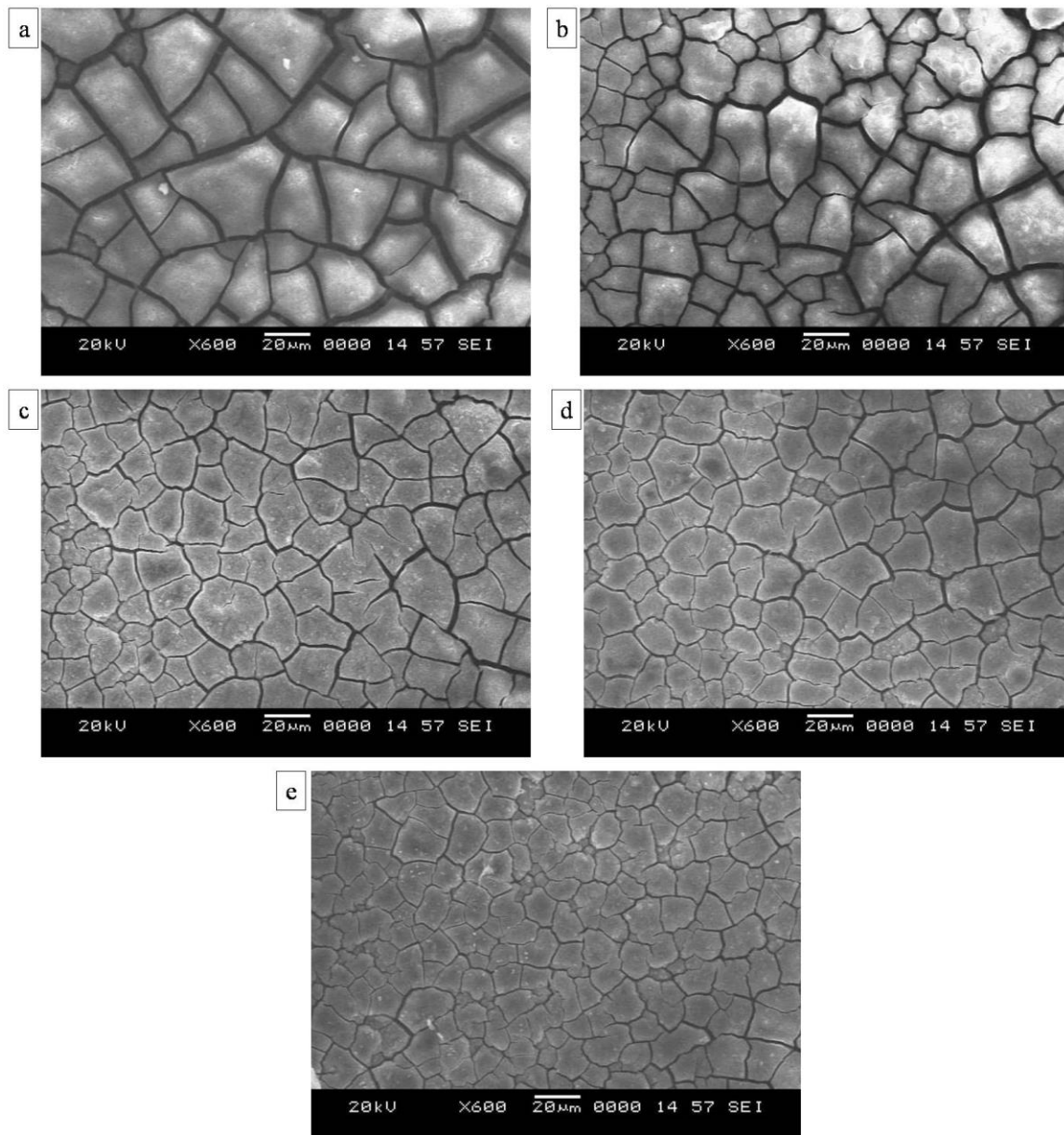
Fig. 3.53 SEM image of ZE41 specimen surface after 1 hour immersion in the combined medium of 1.0 M Na$_2$SO$_4$ - 1.0 M NaCl solutions containing, (a) 1.7 mM of stearate, (b) 2.7 mM of palmitate, (c) 6.5 mM of myristate, (d) 20 mM of laurate and (e) 320 mM of caprylate.
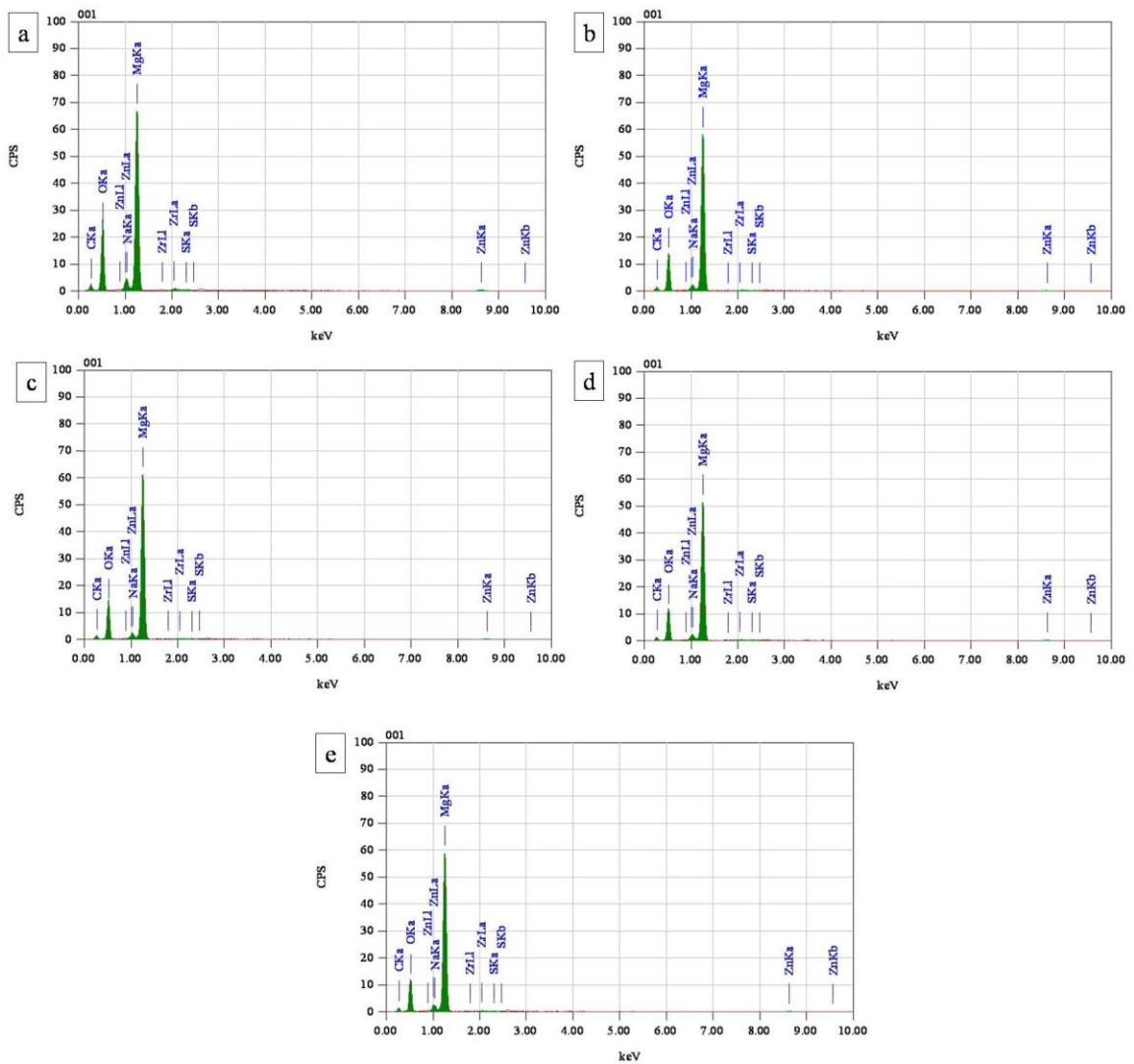
Fig. 3.54 EDX spectra of ZE41 specimen surface after 1 hour immersion in the combined medium of 1.0 M Na_2SO_4 - 1.0 M NaCl solutions containing, (a) 1.7 mM of stearate, (b) 2.7 mM of palmitate, (c) 6.5 mM of myristate, (d) 20 mM of laurate and (e) 320 mM of caprylate.

4.1 SUMMARY

The corrosion behavior of the magnesium alloy ZE41 in aqueous salt solutions like sodium sulfate and in a mixture of sodium sulfate - sodium chloride was established. The comprehensive investigation was an electrochemical approach which basically employed potentiodynamic polarization and electrochemical impedance techniques for understanding the overall phenomenon. The environmental factors like ionic concentration of the medium, solution temperature and pH were varied so as to apprehend the influence of each of these factors on the anodic dissolution of ZE41. Furthermore, studying the ZE41 corrosion at various temperatures was instrumental for the evaluation of the activation parameters. The existence of a partly protective corrosion product surface film, having a remarkable impact on the corrosion behavior of ZE41 alloy was affirmed from the results of electrochemical and surface analyses studies.

Five long chain alkyl carboxylates; stearate, palmitate, myristate, laurate and caprylate were examined for their efficacy to mitigate corrosion of magnesium alloy ZE41 in aqueous salt solutions. The inhibition tests were conducted at various medium concentrations and solution temperatures to ascertain the effect of ionic concentration of the media and that of temperature on the inhibition efficiency of the carboxylates. At every particular medium concentration and temperature, the study was further extended by varying the carboxylate concentration in a range so as to establish the optimum concentration for inhibition. The examination involving different inhibitors eventuated in to productive results which helped to comprehend the impact of molecular structure of the inhibitor on the inhibition efficiency. The activation and thermodynamic parameters were evaluated to support a complete apprehension of alloy dissolution and interfacial adsorption, respectively. The trends in variation of all the electrochemical, activation and thermodynamic parameters reported in the study have been accounted in a compendious manner.

The electrochemical results along with SEM and EDX analyses were taken into consideration for proposing a plausible mechanism for inhibition of ZE41 corrosion by

alkyl carboxylates. The chemisorption of the carboxylates at the cathodic phases was surmised to block the active reaction sites on the alloy surface, there by resulting in cathodic inhibition. The anodic inhibition was considered to ensue as a consequence of compaction and thickening of the porous surface film at anodic phases through precipitation of magnesium carboxylates. Such densification was presumed to augment the barrior effect of the surface film against the electrolyte ingress. The slight deviation from ideal Langmuir behavior was observed and was attributed to intermolecular forces like van der Waals interactions existing between the long alkyl chains of the adsorbed carboxylate molecules. Such mutual interactions were believed to further contribute towards the densification the film. The initial surfactant monolayer was predicted to impart maximum protection to the underlying alloy and the contribution from the supplementary layers towards inhibition efficiency was assumed to be minimal. Furthermore, the difference in the inhibition efficiency and the aggregate transition concentration of the carboxylates was inferred to be the consequence of difference in the aliphatic chain length which is known to predominantly control the solubility product of the corresponding magnesium salts.

4.2 CONCLUSIONS

From the comprehensive results of the investigation, following conclusions have been drawn:

1. A higher ionic concentration, higher temperature and acidic pH bring about destabilization and dissolution of the corrosion product surface film; hence accelerate the rate of ZE41 corrosion.

2. The corrosion kinetics follow Arrhenius law.

3. The results of polarization studies point out the carboxylates to be mixed-type inhibitors which predominantly impede the anodic reaction of metal dissolution.

4. For all the carboxylates, the increase in inhibition efficiency with the increase in the carboxylate concentration is pronounced up to an optimum concentration above which the increase in inhibition efficiency is negligible. This optimum concentration is equivalent to aggregate transition concentration of the carboxylate surfactants.

5. The increase temperature is unfavorable and lessons the inhibition efficiency of the carboxylates.

6. The inhibition efficiency increases with the increase in ionic concentration of the media, thus the carboxylates show a better efficiency in more concentrated corrosives.

7. The adsorption of the carboxylates on alloy surface is principally physisorption and complies with the Langmuir adsorption isotherm.

8. At aggregate transition concentration, stearate exhibits highest inhibition efficiency followed by palmitate, myristate, laurate and finally caprylate. The aggregate transition concentration increases on going from stearate to caprylate.

4.3 SCOPE FOR FUTURE WORK

1. The ZE41 alloy on isothermal heat treatment and rapid quenching is known to develop a microstructure with more homogenous zirconium distribution, which is expected to bring down the corrosion susceptibility of the alloy. The corrosion behavior and inhibition of such heat-treated ZE41 alloy can be explored.

2. The electrochemical studies can be carried out by varying the immersion time so as to comprehend the efficiency of the surface film during long exposure periods.

3. The negative difference effect (NDE) can be experimentally verified by comparing the results of the present electrochemical study with those derived from weight loss or hydrogen evolution measurements.

References

Abbasov, V.M., Abd El-Lateef, H.M., Aliyeva, L.I., Qasimov, E.E., Ismayilov, I.T., Tantawy, A.H. and Mamedxanova, S.A. (2013). "Applicability of novel anionic surfactant as a corrosion inhibitor of mild steel and for removing thin petroleum films from water surface." *Am. J. Mater. Sci. Eng*., 1, 18-23.

Abd El-Lateef, H.M., Abbasov, V.M., Aliyeva, L.I., Ismayilov, T.I., Qasimov, E.E. and Ahmadov, T.U. (2012). "Novel anionic surfactants based on cottonseed oil and their corrosion inhibition efficiency for carbon steel in CO_2 saturated solution." *Global J. Phys. Chem*., 3, 14-20.

Abdennabi, A.M.S., Abdulhadi, A.I. and Abu-Orabi, S. (1998). "Relationship between the molecular structure and the inhibition performance of triazole compounds using electrochemical methods." *Anti-Corros. Methods Mater*., 45, 103 – 108.

Afshari, V. and Dehghanian, C. (2010). "Inhibitor effect of sodium benzoate on the corrosion behavior of nanocrystalline pure iron metal in near-neutral aqueous solutions." *J. Solid State Electrochem*., 14, 1855-1861.

Agnew, S.R. (2004). "Wrought magnesium: A 21st century outlook." *JOM*, 56, 20-21.

Ambat, R., Aung, N.N. and Zhou, W. (2000). "Evaluation of microstructural effects on corrosion behaviour of AZ91D magnesium alloy." *Corros. Sci*., 42, 1433-1455.

Amin, M.A., Ahmed, M.A., Arida, H.A., Arslan, T., Saracoglu, M. and Kandemirli, F. (2011). "Monitoring corrosion and corrosion control of iron in HCl by non-ionic surfactants of the TRITON-X series – Part II, temperature effect, activation energies and thermodynamics of adsorption." *Corros. Sci*., 53, 540-548.

Ansari, F.A. and Quraishi, M.A. (2011). "Inhibitive effect of some gemini surfactants as corrosion inhibitors for mild steel in acetic acid media." *Arab. J. Sci. Eng*., 36, 11-20.

Aouniti, A., Khaled, K.F. and Hammouti, B. (2013). "Correlation between inhibition efficiency and chemical structure of some amino acids on the corrosion of armco iron in molar HCl." *Int. J. Electrochem. Sci*., 8, 5925 – 5943.

Aramaki, K. (2002). "Synergistic inhibition of zinc corrosion in 0.5 M NaCl by combination of cerium(III) chloride and sodium silicate." *Corros. Sci*., 44, 871-886.

Ardelean, H., Frateur, I. and Marcus, P. (2008). "Corrosion protection of magnesium alloys by cerium, zirconium and niobium-based conversion coatings." *Corros. Sci*., 50, 1907-1918.

Arrabal, R., Pardo, A., Merino, M.C., Mohedano, M., Casajús, P., Paucar, K. and Garcés, G. (2012). "Effect of Nd on the corrosion behaviour of AM50 and AZ91D magnesium alloys in 3.5 wt.% NaCl solution." *Corros. Sci*., 55, 301-312.

ASTM Standard G102, 1989(1999). "Standard practice for calculation of corrosion rates and related information from electrochemical measurements." *ASTM International*, West Conshohocken, PA.

Ashassi-Sorkhabi, H., Ghasemi, Z. and Seifzadeh, D. (2005) "The inhibition effect of some amino acids towards the corrosion of aluminum in 1 M HCl + 1 M H_2SO_4 solution." *Appl. Surf. Sci*., 249, 408-418.

Atrens, A. and Dietzel, W. (2007). "The negative difference effect and unipositive Mg^+." *Adv. Eng. Mater*., 9, 292–297.

Badawi, A.M., Hegazy, M.A., El-Sawy, A.A., Ahmed, H.M. and Kamel, W.M. (2010). "Novel quaternary ammonium hydroxide cationic surfactants as corrosion inhibitors for carbon steel and as biocides for sulfate reducing bacteria (SRB)." *Mater. Chem. Phys*., 124, 458-465.

Badawy, W.A., Hilal, N.H., El-Rabiee, M. and Nady, H. (2010). "Electrochemical behavior of Mg and some Mg alloys in aqueous solutions of different pH." *Electrochim. Acta*, 55, 1880-1887.

Baghni, M., Wu, Y., Li, J. and Zhang, W. (2004). "Corrosion behavior of magnesium and magnesium alloys." *T. Nonferr. Metal. Soc.*, 14, 1-10.

Balbo, A., Frignani, A., Grassi, V. and Zucchi, F. (2013). "Corrosion inhibition by anionic surfactants of AA2198 Li-containing aluminium alloy in chloride solutions." *Corros. Sci.*, 73, 80-88.

Banerjee, P.C. and Raman, R.K.S. (2011). "Electrochemical impedance spectroscopic investigation of the role of alkaline pre-treatment in corrosion resistance of a silane coating on magnesium alloy." *Electrochim. Acta*, 56, 3790-3798.

Banerjee, P.C., Raman, R.K.S., Durandet, Y. and Mcadam, G. (2013). "Influence of laser processing parameters on microstructure and corrosion kinetics of laser-treated ZE41 magnesium alloy." *Metall. Mater. Trans. A*, 44, 2346-2357.

Baril, G. and Pebere, N. (2001). "The corrosion of pure magnesium in aerated and deaerated sodium sulphate solutions." *Corros. Sci.*, 43, 471-484.

Barnartt, S. (1977). "Electrochemical nature of corrosion." *Electrochemical techniques for corrosion*, R. Baboian, eds., National Association of Corrosion Engineers, Houston, 1–10.

Ben-Hamu, G., Eliezer, D., Shin, K.S. and Cohen, S. (2007). "The relation between microstructure and corrosion behavior of Mg-Y-Zr-RE alloys." *J. Alloy. Compd.*, 431, 269-276.

Bentiss, F., Lebrini, M. and Lagrenee, M. (2005). "Thermodynamic characterization of metal dissolution and inhibitor adsorption processes in mild steel/ 2,5-bis(n-thienyl)-1,3,4-thiadiazoles/hydrochloric acid system." *Corros. Sci.*, 47, 2915–2931.

Blawert, C., Hort, N. and Kainer, K.U. (2004). "Automotive applications of magnesium and its alloys." *Trans. Indian Inst. Met*., 57, 397-408.

Boisier, G., Portail, N. and Pebere, N. (2010). "Corrosion inhibition of 2024 aluminium alloy by sodium decanoate." *Electrochim. Acta*, 55, 6182-6189.

Bradford, S.A. (2001). *Corrosion control*, second edition, CASTI, Alberta, Canada.

Brown, R.E. (2000). "Magnesium industry growth in the 1990 period" *Magnesium technology 2000*, H.I. Kaplan, J.N. Hryn and B.B. Clow, eds., TMS, *Tennessee,* 3-12.

Cai, S., Lei, T., Li, N. and Feng, F. (2012). "Effects of Zn on microstructure, mechanical properties and corrosion behavior of Mg–Zn alloys." *Mat. Sci. Eng. C–Mater*., 32, 2570–2577.

Cao, F., Shi, Z., Hofstetter, J., Uggowitzer, P.J., Song, G., Liu, M. and Atrens, A. (2013). "Corrosion of ultra-high-purity Mg in 3.5% NaCl solution saturated with $Mg(OH)_2$." *Corros. Sci*., 75, 78-99.

Carboneras, M., López, M.D., Rodrigo, P., Campo, M., Torres, B., Otero, E. and Rams, J. (2010). "Corrosion behavior of thermally sprayed Al and Al/SiCp composite coatings on ZE41 magnesium alloy in chloride medium." *Corros. Sci*., 52, 761-768.

Cheng, Y., Qin, T., Wang, H. and Zhang, Z. (2009). "Comparison of corrosion behaviors of AZ31, AZ91, AM60 and ZK60 magnesium alloys." *T. Nonferr. Met. Soc*., 19, 517-524.

Cole, G. (2007). "Summary of magnesium vision 2020: A North American automotive strategic vision for magnesium." *Magnesium technology 2007*, R.S. Beals., A.A. Luo., N.R. Neelameggham and M.O. Pekguleryuz, eds., TMS, *Florida,* 35.

Correa, P.S., Malfatti, C.F. and Azambuja, D.S. (2011). "Corrosion behavior study of AZ91 magnesium alloy coated with methyltriethoxysilane doped with cerium ions." *Prog. Org. Coat*., 72, 739-747.

Coy, A.E., Viejo, F., Skeldon, P. and Thompson, G.E. (2010). "Susceptibility of rare-earth-magnesium alloys to micro-galvanic corrosion." *Corros. Sci*., 52, 3896-3906.

Daloz, D., Rapin, C., Steinmetz, P. and Michot, G. (1998). "Corrosion inhibition of rapidly solidified Mg–3%Zn–15%Al magnesium alloy with sodium carboxylates." *Corrosion*, 54, 444–450.

Damaskin, B.B., Petrii, O.A., Batrakov, V.V., Uvarov, E.B., Parsons, R. and Barradas, R.G. (1972). "Adsorption of organic compounds on electrodes." *J. Electrochem. Soc.*, 119, 279-280.

De Béthune, A.J. and Loud, N.A.S. (1965). "Standard aqueous electrode potentials and temperature coefficients at 25°C." *J. Electrochem. Soc*., 112, 107-108.

Deyab, M.A. (2014). "Adsorption and inhibition effect of ascorbyl palmitate on corrosion of carbon steel in ethanol blended gasoline containing water as a contaminant." *Corros. Sci*., 80, 359-365.

Dodson, B. (2013). "Stainless magnesium breakthrough bodes well for manufacturing industries." *Monash University*, http://www.gizmag.com/stainless-magnesium-corrosion-monash/28856/ (Nov. 07, 2013).

Dunn, D.S., Yang, L., Wu, C. and Cragnolino, G.A. (2004). "Effect of inhibiting oxyanions on the localized corrosion susceptibility of waste package container materials." *Scientific basis for nuclear waste management XXVIII*, Materials Research Society, Boston, CC1.7.1–CC1.7.6.

Ebenso, E.E., Obot, I.B. and Murulana, L.C. (2010). "Quinoline and its derivatives as effective corrosion inhibitors for mild steel in acidic medium." *Int. J. Electrochem. Sci.*, 5, 1574 – 1586.

El Bribri, A., Tabyaoui, M., Tabyaoui, B., El Attari, H. and Bentiss, F. (2013). "The use of *Euphorbia falcata* extract as eco-friendly corrosion inhibitor of carbon steel in hydrochloric acid solution." *Mater. Chem. Phy.*, 141, 240-247.

Elewady, G.Y., El-Said, I.A. and Fouda, A.S. (2008). "Anion surfactants as corrosion inhibitors for aluminium dissolution in HCl solutions.", *Int. J. Electrochem. Sci.*, 3, 111–190.

Fan, Y., Wu, G. and Zhai, C. (2006). "Influence of cerium on the microstructure, mechanical properties and corrosion resistance of magnesium alloy." *Mat. Sci. Eng. A-Struct.*, 433, 208-215.

Fang, J. and Lie, J. (2002). "Quantum chemistry study on the relationship between molecular structure and corrosion inhibition efficiency of amides." *J. Mol. Struct.*, 593, 179-185.

Fekry, A.M. and Ameer, M.A. (2010). "Corrosion inhibition of mild steel in acidic media using newly synthesized heterocyclic organic molecules." *Int. J. Hydrogen Energy*, 35, 7641-7651.

Feliu Jr, S., Samaniego, A., Barranco, V., El-Hadad, A.A., Llorente, I. and Adeva. P. (2014). "The effect of low temperature heat treatment on surface chemistry and corrosion resistance of commercial magnesium alloys AZ31 and AZ61 in 0.6 M NaCl solution." *Corros. Sci.*, 80, 461-472.

Flick, E.W. (1993). *Corrosion inhibitors: An industrial guide*, second edition, Noyes Publications, Park Ridge, New Jersey.

Fontana, M. G. (2005). *Corrosion engineering*. third edition, McGraw-Hill, New York.

Forsyth, M., Forsyth, C.M., Wilson, K., Behrsing, T. and Deacon, G.B. (2002). "ATR characterization of synergistic corrosion inhibition of mild steel surfaces by cerium salicylate." *Corros. Sci.*, 44, 2651-2656.

Frankel, G.S., Samaniego, A. and Birbilis, N. (2013). "Evolution of hydrogen at dissolving magnesium surfaces." *Corros. Sci.*, 70, 104-111.

Free, M. (2002). "Understanding the effect of surfactant aggregation on corrosion inhibition of mild steel in acidic medium." *Corros. Sci.*, 44, 2865-2870.

Free, M. (2004). "A new corrosion inhibition model for surfactants that more closely accounts for actual adsorption than traditional models that assume physical coverage is proportional to inhibition." *Corros. Sci.*, 46, 3101-3113.

Frignani, A., Trabanelli, G., Wrubl, C. and Mollica, A. (1996). "N-Lauroyl sarcosine sodium salt as a corrosion inhibitor for type 1518 carbon steel in neutral saline environments." *Corrosion*, 52, 177-182.

Frignani, A., Grassi, V., Zanotto, F. and Zucchi, F. (2012). "Inhibition of AZ31 Mg alloy corrosion by anionic surfactants." *Corros. Sci.*, 63, 29-39.

Froes, F.H., Eliezer, D. and Aghion, E. (1998). "The science, technology, and applications of magnesium." *JOM*, 50, 30-34.

Gadag, R.V. and Shetty, A.N. (2010). "Corrosion and its control." *Engineering chemistry*, second edition, IK International, New Delhi, 54-77.

Gandel, D.S., Easton, M.A., Gibson, M.A., Abbott, T. and Birbilis, N. (2014). "The influence of zirconium additions on the corrosion of magnesium." *Corros. Sci.*, 81, 27-35.

Gao, H., Li, Q., Dai, Y., Luo, F. and Zhang, H.X. (2010). "High efficiency corrosion inhibitor 8-hydroxyquinoline and its synergistic effect with sodium dodecylbenzenesulphonate on AZ91D magnesium alloy." *Corros. Sci*., 52, 1603-1609.

Gao, H., Li, Q., Chen, F.N., Dai, Y., Luo, F. and Li, L.Q. (2011). "Study of the corrosion inhibition effect of sodium silicate on AZ91D magnesium alloy." *Corros. Sci*., 53, 1401-1407.

Ghareba, S. and Omanovic, S. (2010). "Interaction of 12-aminododecanoic acid with a carbon steel surface: Towards the development of 'green' corrosion inhibitors." *Corros. Sci*., 52, 2104-2113.

Gräfen, H., Horn, E.-M., Schlecker, H. and Schindler, H. (2000). "Corrosion." *Ullmann's encyclopedia of industrial chemistry,* Wiley-VCH, Weinheim.

Greenblatt, J.H. (1956). "A mechanism for the anodic dissolution of magnesium." *J. Electrochem. Soc.*, 103, 539-543.

Gu, X.-N. and Zheng, Y.-F. (2010). "A review on magnesium alloys as biodegradable materials." *Front. Mater. Sci. China*, 4, 111-115.

Gulbrandsen, E. (1992). "Anodic behavior of Mg in HCO_3^-/CO_3^{2-} buffer solutions: Quasi-steady measurements." *Electrochim. Acta*, 37, 1403-1412.

Gulbrandsen, E., Taftø, J. and Olsen, A. (1993). "The passive behaviour of Mg in alkaline fluoride solutions: Electrochemical and electron microscopical investigations." *Corros. Sci*., 34, 1423-1440.

Gupta, M. and Sharon, N.M.L. (2011). "Introduction to magnesium." *Magnesium, magnesium alloys and magnesium composites*, John Wiley & Sons, New Jersey, 1-11.

Ha, H.-Y., Kang, J.-Y., Yang, J., Yim, C.D. and You, B.S. (2013). "Limitations in the use of the potentiodynamic polarisation curves to investigate the effect of Zn on the corrosion behaviour of as-extruded Mg–Zn binary alloy." *Corros. Sci.*, 75, 426-433.

Hackerman, N. (1993). "A view of the history of corrosion and its control." *Corrosion 93 planery and keynote lectures*, R.D. Gundry, eds., National Association of Corrosion Engineers, Houston, 1–5.

Hamdy, A.S., Doench, I. and Möhwald, H. (2012). "Vanadia-based coatings of self-repairing functionality for advanced magnesium Elektron ZE41 Mg–Zn–rare earth alloy." *Surf. Coat. Technol.*, 206, 3686-3692.

Heakal, F.E., Shehata, O.S. and Tantawy, N.S. (2012). "Enhanced corrosion resistance of magnesium alloy AM60 by cerium(III) in chloride solution." *Corros. Sci.*, 56, 86-95.

Hegazy, M.A. (2009). "A novel Schiff base-based cationic gemini surfactants: Synthesis and effect on corrosion inhibition of carbon steel in hydrochloric acid solution." *Corros. Sci.*, 51, 2610-2618.

Helal, N.H. (2011). "Corrosion inhibition and adsorption behavior of methionine on Mg-Al-Zn alloy." *J. Chem. Eng. Mater. Sci.*, 2, 28-38.

Helal, N.H. and Badawy, W.A. (2011). "Environmentally safe corrosion inhibition of Mg-Al-Zn alloy in chloride free neutral solutions by amino acids." *Electrochim. Acta*, 56, 6581-6587.

Hu, J., Huang, D., Song, G.-L. and Guo, X. (2011). "The synergistic inhibition effect of organic silicate and inorganic Zn salt on corrosion of Mg-10Gd-3Y magnesium alloy." *Corros. Sci.*, 53, 4093-4101.

Hu, J., Huang, D., Zhang, G., Song, G.-L. and Guo, X. (2012). "Research on the inhibition mechanism of tetraphenylporphyrin on AZ91D magnesium alloy." *Corros. Sci.*, 63, 367-378.

Hu, J., Zeng, D., Zhang, Z., Shi, T., Song, G.-L. and Guo, X. (2013). "2-Hydroxy-4-methoxy-acetophenone as an environment-friendly corrosion inhibitor for AZ91D magnesium alloy." *Corros. Sci.*, 74, 35-43.

Huang, D., Hu, J., Song, G.-L. and Guo, X. (2011). "Inhibition effect of inorganic and organic inhibitors on the corrosion of Mg–10Gd–3Y–0.5Zr alloy in an ethylene glycol solution at ambient and elevated temperatures." *Electrochim. Acta*, 56, 10166–10178.

Ivanou, D.K., Starykevich, M., Lisenkov, A.D., Zheludkevich, M.L., Xue, H.B., Lamaka, S.V. and Ferreira, M.G.S. (2013). "Plasma anodized ZE41 magnesium alloy sealed with hybrid epoxy-silane coating." *Corros. Sci.*, 73, 300-308.

Jackson, J. (2011) "Cost of corrosion estimated to exceed $1 trillion in the United States in 2013." *G2MT Laboratories*, http://www.g2mtlabs.com (Oct.18, 2013).

Jiang, J., Ma, A., Saito, N., Shen, Z., Song, D., Lu, F., Nishida, Y., Yang, D. and Lin, P. (2009). "Improving corrosion resistance of RE-containing magnesium alloy ZE41A through ECAP." *J. Rare Earth.*, 27, 848-852.

John, S. and Joseph, A. (2013). "Quantum chemical and electrochemical studies on the corrosion inhibition of aluminium in 1 N HNO_3 using 1,2,4-triazine." *Mater. Corros.*, 64, 625-632.

Jüttner, K. (1990). "Electrochemical impedance spectroscopy (EIS) of corrosion processes on inhomogeneous surfaces." *Electrochim. Acta*, 35, 1501-1508.

Kannan, M.B., Dietzel, W., Blawert, C., Atrens, A. and Lyon, P. (2008). "Stress corrosion cracking of rare-earth containing magnesium alloys ZE41, QE22 and Elektron 21 (EV31A) compared with AZ80." *Mat. Sci. Eng. A-Struct.*, 480, 529-539.

Kannan, M.B., Blawert, C. and Dietzel, W. (2011). "*Electrochemical corrosion behaviour of ZE41 and QE22 magnesium alloys.*" *Mater. Sci. Forum*, 690, 385-388.

Kara, Y.S., Sagdinc, S.G. and Esme, A. (2012). "Theoretical study on the relationship between the molecular structure and corrosion inhibition efficiency of long alkyl side chain acetamide and isoxazolidine derivatives." *Prot. Met. Phys. Chem. Surf.*, 48, 710-721.

Karavai, O.V., Bastos, A.C., Zheludkevich, M.L., Taryba, M.G., Lamaka, S.V. and Ferreira, M.G.S. (2010). "Localized electrochemical study of corrosion inhibition in microdefects on coated AZ31 magnesium alloy." *Electrochim. Acta*, 49, 456-462.

Kellou-Kerkouche, F., Benchettara, A. and Amara, S.-E. (2013). "Anionic surfactant as a corrosion inhibitor for synthesized ferrous alloy in acidic solution." *J. Mater.*, 2013, 1-11.

Khalfaoui, W., Valerio, E., Masse, J.E. and Autric, M. (2010). "Excimer laser treatment of ZE41 magnesium alloy for corrosion resistance and microhardness improvement." *Opt. Laser. Eng.*, 48, 926-931.

King, A.D., Birbilis, N. and Scully, J.R. (2014). "Accurate electrochemical measurement of magnesium corrosion rates; a combined impedance, mass-loss and hydrogen collection study." *Electrochim. Acta*, 121, 394-406.

Knag, M. (2006). "Fundamental behavior of model corrosion inhibitors." *J. Dispers. Sci. Technol.*, 27, 587-597.

Koch, G.H., Brongers, M.P.H., Thompson, N.G., Virmani, Y.P. and Payer, J.H. (2001). *Corrosion costs and preventive strategies in the United States*, Federal Highway Administration, Washington DC.

Kramer, D.A. (2013). "Magnesium metal." *Mineral commodity summaries*, U.S. Geological Survey, Virginia, 98-99.

Lambertin, D., Frizon, F. and Bart, F. (2012). "Mg–Zr alloy behavior in basic solutions and immobilization in Portland cement and Na-geopolymer with sodium fluoride inhibitor." *Surf. Coat. Technol.*, 206, 4567-4573.

Lasia, A. (1999). "Electrochemical impedance spectroscopy and its applications." *Modern aspects of electrochemistry*, B.E. Conway., J. Bockris and R.E. White, eds., Kluwer Academic/ Plenum Publishers, New York, 143-248.

Lee, D.Y., Kim, W.C. and Kim, J.G. (2012). "Effect of nitrite concentration on the corrosion behavior of carbon steel pipelines in synthetic tap water." *Corros. Sci*., 64, 105-114.

Li, L.-J., Yao, Z.-M., Lei, J.-L., Xu, H., Zhang, S.-T. and Pang, F.-S. (2009). "Adsorption and corrosion behaviour of sodium dodecylbenzenesulfonate on AZ31 magnesium alloy." *Acta Phys-Chim. Sin*., 25, 1332–1336.

Liao, J., Hotta, M. and Yamamoto, N. (2012). "Corrosion behavior of fine-grained AZ31B magnesium alloy." *Corros. Sci*., 61, 208-214.

Liu, Q., Cheng, W., Zhang, H., Xu, C. and Zhang, J. (2014). "The role of Ca on the microstructure and corrosion behavior of Mg–8Sn–1Al–1Zn–Ca alloys." *J. Alloy. Compd*., 590, 162-167.

Liu, W., Cao, F., Chang, L., Zhang, Z. and Zhang, J. (2009). "Effect of rare earth element Ce and La on corrosion behavior of AM60 magnesium alloy." *Corros. Sci*., 51, 1334-1343.

Liu, Y.F., Yang, W., Qin, Q.L., Wu, Y.C., Wen, W., Zhai, T., Yu, B., Li, D.Y., Luo, A. and Song, G.-L. (2014). "Microstructure and corrosion behavior of die-cast AM60B magnesium alloys in a complex salt solution: A slow positron beam study." *Corros. Sci*., 81, 65-74.

Logan, S.D. (2007). "Lightweight automobile body concept featuring ultra-large, thin-wall structural magnesium castings." *Magnesium technology*, R.S. Beals, A.A. Luo, N.R. Neelameggham and M.O. Pekguleryuz, eds., TMS, Warrendale, *Pennsylvania,* 41.

López, A.J., Otero, E. and Rams, J. (2010). "Sol–gel silica coatings on ZE41 magnesium alloy for corrosion protection." *Surf. Coat. Technol.*, 205, 2375-2385.

Lopez, M.G. and Natta, B. (2001). "Evidence of two anodic processes in the polarization curves of magnesium in aqueous media." *Corrosion*, 712, 712-720.

Lukovits, I., Kalman, E. and Zucchi, F. (2001). "Corrosion inhibitors-correlation between chemical structure and efficiency." *Corrosion*, 57, 3-8.

Luo, A.A. (2002). "Magnesium: current and potential automotive applications." *JOM*, 54, 42-48.

Lyndon, J.A., Gupta, R.K., Gibson, M.A. and Birbilis, N. (2013). "Electrochemical behaviour of the β-phase intermetallic (Mg_2Al_3) as a function of pH as relevant to corrosion of aluminium–magnesium alloys." *Corros. Sci.*, 70, 290-293.

Malik, M.A., Hashim, M.A., Nabi, F., AL-Thabaiti., S.A. and Khan, Z. (2011). "Anti-corrosion ability of surfactants: A review." *Int. J. Electrochem. Sci.*, 6, 1927-1948.

Mandal, M., Moon, A.P., Deo, G., Mendis, C.L. and Mondal, K. (2014). "Corrosion behavior of Mg–2.4 Zn alloy micro-alloyed with Ag and Ca." *Corros. Sci.*, 78, 172-182.

Mansfeld, F. (1990). "Electrochemical impedance spectroscopy (EIS) as a new tool for investigating methods of corrosion protection." *Electrochim. Acta*, 35, 1533-1544.

Mansfeld, F., Tsai, C.H. and Shih, H. (1992). "Software for simulation and analysis of electrochemical impedance spectroscopy (EIS) data." *Computer modeling in corrosion*, R.S. Munn, eds., ASTM, Philadelphia, 186-196.

Makar, G.L. and Kruger, J. (1990). "Corrosion studies of rapidly solidified magnesium alloys." *J. Electrochem. Soc.*, 137, 414–421.

Martinez, S. and Stern, I. (2002). "Thermodynamic characterization of metal dissolution and inhibitor adsorption processes in the low carbon steel/mimosa tannin/sulfuric acid system." *Appl. Surf. Sci.*, 199, 83-89.

Masel, R.I. (1996). "Adsorption II – Adsorption isotherms." *Principles of adsorption and reaction on solid surfaces*, Wiley Interscience, New York, 235-302.

Mathaudhu, S. and Nyberg, E. A. (2010). "Magnesium technology: Magnesium alloys in U.S. military applications: Past, current and future solutions." *Magnesium technology 2010*, S.R. Agnew, eds., TMS, *Warrendale, Pa., 27-33.*

Mathieu, S., Rapin, C., Hazan, J. and Steinmetz, P. (2002). "Corrosion behavior of high pressure die-cast and semi-solid cast AZ91D alloys." *Corros. Sci.*, 44, 2737-2756.

Mathieu, S., Rapin, C., Steinmetz, J. and Steinmetz, P. (2003). "A corrosion study of the main constituent phases of AZ91 magnesium alloys." *Corros. Sci.*, 45, 2741-2755.

Matsubara, H., Ichige, Y., Fujita, K., Nishiyama, H. and Hodouchi, K. (2013). "Effect of impurity Fe on corrosion behavior of AM50 and AM60 magnesium alloys." *Corros. Sci.*, 66, 203-210.

McCafferty, E. (2010). *Introduction to corrosion science*, Springer, New York.

Mesbah, A., Juers, C., Lacouture, F., Mathieu, S., Rocca, E., Francois, M. and Steinmetz, J. (2007). "Inhibitors for magnesium corrosion: Metal-organic frameworks." *Solid. State. Sci.*, 9, 322-328.

Migahed, M.A. and Al-Sabagh, A.M. (2009). "Beneficial role of surfactants as corrosion inhibitors in petroleum industry: a review article." *Chem. Eng. Commun.*, 196, 1054-1075.

Montemor, M. and Ferreira, M.G.S. (2008). "Analytical characterization and corrosion behaviour of bis-aminosilane coatings modified with carbon nanotubes activated with

rare-earth salts applied on AZ31 Magnesium alloy." *Surf. Coat. Technol*., 202, 4766-4774.

Negm, N.A. and Zaki, M.F. (2008). "Corrosion inhibition efficiency of nonionic Schiff base amphiphiles of p-aminobenzoic acid for aluminum in 4N HCL." *Colloid. Surface A*, 322, 97-102.

Negm, N.A., Kandile, N.G., Aiad, I.A. and Mohammad, M.A. (2011). "New eco-friendly cationic surfactants: Synthesis, characterization and applicability as corrosion inhibitors for carbon steel in 1 N HCl." *Colloid. Surface A*, 391, 224-233.

Neil, W.C., Forsyth, M., Howlett, P.C., Hutchinson, C.R. and Hinton, B.R.W. (2009). "Corrosion of magnesium alloy ZE41- The role of microstructural features." *Corros. Sci*., 51, 387-394.

Neil, W.C., Forsyth, M., Howlett, P.C., Hutchinson, C.R. and Hinton, B.R.W. (2011). "Corrosion of heat treated magnesium alloy ZE41." *Corros. Sci*., 53, 3299-3308.

Niu, J. and Lee, J.Y. (2000). "A new approach for the determination of fish freshness by electrochemical impedance spectroscopy." *J. Food. Sci*., 65, 780-785.

Nordlien, J.H., Ono, S., Masuko, N. and Nisancioglu, K. (1997). "A TEM investigation of naturally formed oxide films on pure magnesium." *Corros. Sci*., 39, 1397-1414.

Ortíz, M.R., Rodríguez, M.A., Carranza, R.M. and Rebak, R.B. (2013). "Oxyanions as inhibitors of chloride-induced crevice corrosion of Alloy 22." *Corros. Sci*., 68, 72-83.

Papavinasam, S. (2011). "Evaluation and selection of corrosion inhibitors." *Uhlig's corrosion handbook*, R.W. Revie, eds., John Wiley & Sons, New Jersey, 1169-1178.

Pardo, A., Merino, M.C., Coy, A.E., Viejo, F., Arrabal, R. and FeliúJr, S. (2008). "Influence of microstructure and composition on the corrosion behavior of Mg/Al alloys in chloride media." *Electrochim. Acta*, 53, 7890-7902.

Pardo, A., Feliu, S., Merino, M.C., Arrabal, R. and Matykina, E. (2010). "Electrochemical estimation of the corrosion rate of magnesium/aluminium alloys." *Int. J. Corros.*, 2010, 1-8.

Pebere, N., Riera, C. and Dabosi, F. (1990). "Investigation of magnesium corrosion in aerated sodium sulfate solution by electrochemical impedance spectroscopy." *Electrochim. Acta*, 35, 555-561.

Peng, L.-M., Chang, J.-W., Guo, X.-W., Atrens, A., Ding, W.-J. and Peng, Y.-H. (2009). "Influence of heat treatment and microstructure on the corrosion of magnesium alloy Mg-10Gd-3Y-0.4Zr." *J. Appl. Electrochem.*, 39, 913-920.

Peng, Z.-K., Zhang, X.-M., Chen, J.-M., Xiao, Y. and Jiang, H. (2005). "Grain refining mechanism in Mg–9Gd–4Y alloys by zirconium." *Mater. Sci. Technol.*, 21, 722-726.

Pilling, N.B. and Bedworth, R.E. (1923). "The oxidation of metals at high temperatures." *J. Inst. Met.*, 29, 529-591.

Pokhmurskii, V.I., Zin, I.M., Vynar, V.A. and Bily, L.M. (2011). "Contradictory effect of chromate inhibitor on corrosive wear of aluminium alloy." *Corros. Sci.*, 53, 904-908.

Pourbaix, M. (1974). "Pourbaix diagram for the system of magnesium and water at 25 ℃." *Atlas of electrochemical equilibria aqueous solutions*, National Association of Corrosion Engineers, Houston, 139.

Prasad, A., Uggowitzer, P.J., Shi, Z. and Atrens, A. (2012). "Production of high purity magnesium alloys by melt purification with Zr." *Adv. Eng. Mater.*, 14, 477-490.

Qian, M., StJohn, D.H. and Frost, M.T. (2003). "Zirconium alloying and grain refinement of magnesium alloys." *Magnesium technology 2003*, H.I. Kaplan, eds., TMS, *Tennessee,* 209-214.

Qiao, Z., Shi, Z., Hort, N., Zainal-Abidin, N.I. and Atrens, A. (2012). "Corrosion behaviour of a nominally high purity Mg ingot produced by permanent mould direct chill casting." *Corros. Sci*., 61, 185-207.

Railsback, L.B. (2006). "Some fundamentals of mineralogy and geochemistry." *University of Georgia*, http://www.gly.uga.edu/railsback/FundamentalsIndex.html (Nov. 07, 2013).

Rammelt, U., Koehler, S. and Reinhard, G. (2008). "Synergistic effect of benzoate and benzotriazole on passivation of mild steel." *Corros. Sci*., 50, 1659-1663.

Rammelt, U., Koehler, S. and Reinhard, G. (2011). "Electrochemical characterisation of the ability of dicarboxylic acid salts to the corrosion inhibition of mild steel in aqueous solutions." *Corros. Sci*., 53, 3515-3520.

Roberge, P.R. (2008). *Corrosion engineering: Principles and practice*, McGraw-Hill, New York.

Rosalbino, F., Angelini, E., DeNegri, S., Saccone, A. and Delfino, S. (2006). "Electrochemical behavior assessment of novel Mg-rich Mg-Al-RE alloys (RE = Ce, Er)." *Intermetallics*, 14, 1487-1492.

Rosen, G.I., Segal, G. and Lubinsky, A. (2005). "Large profile magnesium alloy extrusions for automotive applications." *Magnesium technology 2005*, N.R. Neelameggham, H.I. Kaplan and B.R. Powell, eds., TMS, *California,* 61.

Rzychoń, T. and Kiełbus, A. (2006). "Effect of rare earth elements on the microstructure of Mg-Al alloys." *JAMME*, 17, 1-2.

Saji, V.S. (2010). "A review on recent patents in corrosion inhibitors." *Recent Patent. Corros. Sci*., 2, 6-12.

Sastri, V.S. (1998). *Corrosion inhibitors: Principles and applications*, Wiley, New York.

Sastri, V.S., Ghali, E. and Elboujdaini, M. (2007). *Corrosion prevention and protection: Practical solutions*, John Wiley & Sons, New York.

Sastri, V.S. (2012). *Green corrosion inhibitors: Theory and practice*, Wiley, New York.

Schweitzer, P.A. (2010). *Fundamentals of corrosion: Mechanisms, causes and preventive methods*, CRC Press, Yew York.

Senthilkumar, A.N., Tharini, K. and Sethuraman, M.G. (2011). "Studies on a few substituted piperidin-4-one oximes as corrosion inhibitor for mild steel in HCl." *J. Mater. Eng. Perform.*, 20, 969-977.

Sherif, E.M. and Almajid, A.A. (2011). "Corrosion of magnesium/manganese alloy in chloride solutions and its inhibition by 5-(3-aminophenyl)-tetrazole." *Int. J. Electrochem. Sci.*, 6, 2131-2148.

Shi, H., Han, E.-H. and Liu, F. (2011). "Corrosion protection of aluminium alloy 2024-T3 in 0.05 M NaCl by cerium cinnamate." *Corros. Sci.*, 53, 2374-2384.

Shi, Z., Liu, M. and Atrens, A. (2010). "Measurement of the corrosion rate of magnesium alloys using Tafel extrapollation." *Corros. Sci.*, 52, 579-588.

Shi, Z., Jia, J.X. and Atrens, A. (2012a). "Galvanostatic anodic polarization curves and galvanic corrosion of AZ31B in 0.01 M Na_2SO_4 saturated with $Mg(OH)_2$." *Adv. Eng. Mater.*, 14, 324-334.

Shi, Z., Jia, J.X. and Atrens, A. (2012b). "Galvanostatic anodic polarization curves and galvanic corrosion of high purity Mg in 3.5% NaCl saturated with $Mg(OH)_2$." *Corros. Sci.*, 60, 296-308.

Shi, Z., Cao, F., Song, G.-L., Liu, M. and Atrens, A. (2013). "Corrosion behaviour in salt spray and in 3.5% NaCl solution saturated with $Mg(OH)_2$ of as-cast and solution heat-treated binary Mg–RE alloys: RE = Ce, La, Nd, Y, Gd." *Corros. Sci.*, 76, 98-118.

Song, G., Atrens, A., StJohn, D., Nairn, J. and Li, Y. (1997a). "The electrochemical corrosion of pure magnesium in 1N NaCl." *Corros. Sci.*, 39, 855-875.

Song, G., Atrens, A., StJohn, D., Wu, X. and Nairn, J. (1997b). "Anodic dissolution of magnesium in chloride and sulphate solutions." *Corros. Sci.*, 39, 1981-2004.

Song, G., Atrens, A., Wu, X. and Zhang, B. (1998). "Corrosion behavior of AZ21, AZ501 and AZ91 in sodium chloride." *Corros. Sci.*, 40, 1769-1791.

Song, G., Atrens, A. and Dargusch, M. (1999). "Influence of microstructure on the corrosion of diecast AZ91D." *Corros. Sci.*, 41, 249-273.

Song, G. and StJohn, D. (2002). "The effect of zirconium grain refinement on the corrosion behavior of magnesium-rare earth alloy MEZ." *J. Light. Met.*, 2, 1-16.

Song, G. and Atrens, A. (2003). "Understanding magnesium corrosion–A framework for improved alloy performance." *Adv. Eng. Mater.*, 5, 837-858.

Song, G. and StJohn, D. (2004). "Corrosion behavior of magnesium in ethylene glycol." *Corros. Sci.*, 46, 1381-1399.

Song, G., Bowles, A.L. and StJohn, D. (2004). "Corrosion resistance of aged die cast magnesium alloy AZ91D." *Mat. Sci. Eng. A- Struct.*, 366, 74-86.

Song, G. and StJohn, D. (2005). "Corrosion of magnesium alloys in commercial engine coolants." *Mater. Corros.*, 56, 15-23.

Song, G.-L. (2009). "An irreversible dipping sealing technique for anodized ZE41 Mg alloy." *Surf. Coat. Technol.*, 203, 3618-3625.

Song, G.-L. and Xu, Z. (2012). "Effect of microstructure evolution on corrosion of different crystal surfaces of AZ31 Mg alloy in a chloride containing solution." *Corros. Sci.*, 54, 97-105.

Song, W., Martin, H.J., Hicks, A., Seely, D., Walton, C.A., Lawrimore II, W.B., Wang, P.T. and Horstemeyer, M.F. (2014). "Corrosion behaviour of extruded AM30 magnesium alloy under salt-spray and immersion environments." *Corros. Sci.*, 78, 353-368.

Song, Y., Han, E.-H., Shan, D., Yim, C.D. and You, B.S. (2012). "The effect of Zn concentration on the corrosion behavior of Mg–*x*Zn alloys." *Corros. Sci.*, 65, 322-330.

Song, Y.L. (2007). "Effect of cerium addition on microstructure and corrosion resistance of die cast AZ91 magnesium alloy." *Mater. Corros.*, 58, 189–192.

Srinivasan, S. (2006). "Electrode/electrolyte interfaces: structure and kinetics of charge transfer." *Fuel cells: from fundamentals to applications*, Springer, New York, 28.

Südholz, A.D., Birbilis, N., Bettles, C.J. and Gibson, M.A. (2009). "Corrosion behavior of Mg-alloy AZ91E with atypical alloying additions." *J. Alloy. Copmd.*, 471, 109-115.

Sudholz, A.D., Gusieva, K., Chen, X.B., Muddle, B.C., Gibson, M.A. and Birbilis, N. (2011). "Electrochemical behaviour and corrosion of Mg–Y alloys." *Corros. Sci.*, 53, 2277-2282.

Sun, M., Wu, G., Wang, W. and Ding, W. (2009). "Effect of Zr on the microstructure, mechanical properties and corrosion resistance of Mg–10Gd–3Y magnesium alloy." *Mat. Sci. Eng. A-Struct.*, 523, 145-151.

Tamar, Y. and Mandler, D. (2008). "Corrosion inhibition of magnesium by combined zirconia silica sol–gel films." *Electrochim. Acta*, 53, 5118-5127.

Takenaka, T., Ono, T., Narazaki, Y., Naka, Y. and Kawakami, M. (2007). "Improvement of corrosion resistance of magnesium metal by rare earth elements." *Electrochim. Acta*, 53, 117–121.

Thomaz, T.R., Weber, C.R., Pelegrini Jr., T, Dick, L.F.P. and Knörnschild, G. (2010). "The negative difference effect of magnesium and of the AZ91 alloy in chloride and stannate-containing solutions." *Corros. Sci.*, 52, 2235-2243.

Thompson, N,G. and Payer, G.H. (1998). "DC electrochemical test methods." *Corrosion testing made easy*, National Association of Corrosion Engineers, Houston.

Tunold, R., Holtan, H., Berge, M.H., Lasson, A. and Steen-Hansen, R. (1977). "The corrosion of magnesium in aqueous solution containing chloride ions." *Corros. Sci.*, 17, 353-365.

Turgoose, S. (1990). "Mechanism of corrosion inhibition in neutral environments." *Chemical inhibitors for corrosion control*, B.G. Clubley, eds., Royal Society of Chemistry, Cambridge.

Udhayan, R. and Bhatt, D.P. (1996). "On the corrosion behavior of magnesium and its alloys using electrochemical techniques." *J. Power Sources*, 63, 103-107.

Uhlig, H.H and Revie, R.W. (1991). *Corrosion and corrosion control*, third edition, John Wiley & Sons, New York.

Valcarce, M.B. and Vázquez, M. (2010). "Phosphate ions used as green inhibitor against copper corrosion in tap water." *Corros. Sci.*, 52, 1413-1420.

Volovitch, P., Masse, J.E., Fabre, A., Barrallier, L. and Saikaly, W. (2008). "Microstructure and corrosion resistance of magnesium alloy ZE41 with laser surface cladding by Al–Si powder." *Surf. Coat. Technol.*, 202, 4901-4914.

Wagner, D. (2006). "Chemische Fabrik Griesheim – pioneer of electrochemistry." *J. Bus. Chem.*, 3, 31-38.

Wang, L., Shinohara, T. and Zhang, B.-P. (2010a). "Influence of chloride, sulfate and bicarbonate anions on the corrosion behavior of AZ31 magnesium alloy." *J. Alloy. Compd.*, 496, 500-507.

Wang, N., Wang, R., Peng, C., Feng, Y. and Zhang, X. (2010b). "Corrosion behavior of Mg-Al-Pb and Mg-Al-Pb-Zn-Mn alloys in 3.5% NaCl solution." *T. Nonferr. Met. Soc.*, 20, 1936-1943.

Wang, W. and Free, M.L. (2004). "Prediction and measurement of corrosion inhibition of mild steel using nonionic surfactants in chloride media." *Corros.Sci.*, 46, 2601-2611.

Wendt, A. (2005). "Magnesium castings in aeronautics applications – Special requirements." *Magnesium technology 2005*, N.R. Neelameggham, H.I. Kaplan and B.R. Powell, eds., TMS, *California*, 269-273.

Williams, G., McMurray, H.N. and Grace, R. (2010). "Inhibition of magnesium localized corrosion in chloride containing electrolyte." *Electrochim. Acta*, 55, 7824-7833.

Xing, W., Shan, Y., Guo, D., Lu, T. and Xi, S. (1995). "Mechanism of iron inhibition by stearic acid langmuir-blodgett monolayers." *Corrosion*, 51, 45-49.

Yamasaki, M., Hayashi, N., Izumi, S. and Kawamura, Y. (2007). "Corrosion behavior of rapidly solidified Mg–Zn–rare earth element alloys in NaCl solution." *Corros. Sci.*, 49, 255-262.

Yang, X., Pan, F.-S. and Zhang, D.F. (2009). "A study on corrosion inhibitor for magnesium alloy." *Mater. Sci. Forum*, 610, 920-926.

Yohai, L., Vázquez, M. and Valcarce, M.B. (2011). "Brass corrosion in tap water distribution systems inhibited by phosphate ions." *Corros. Sci.*, 53, 1130-1136.

Yin, D.-S., Zhang, E.-L. and Zeng, S.-Y. (2008). "Effect of Zn on mechanical property and corrosion property of extruded Mg–Zn–Mn alloy." *T. Nonferr. Met. Soc*., 18, 763–768.

Yuan, M. and Zheng, Z. (2014). "Effects of Zn on the microstructures and mechanical properties of Mg–3Sm–0.5Gd–xZn–0.5Zr ($x = 0$, 0.3 and 0.6) alloy." *J. Alloy. Compd*., 590, 355-361.

Zeng, R.-C., Sun, L., Zheng, Y.-F., Cui, H.-Z. and Han, E.-H. (2014). "Corrosion and characterization of dual phase Mg–Li–Ca alloy in Hank's solution: The influence of microstructural features." *Corros. Sci*., 79, 69-82.

Zhang, E., Hea, W., Duc, H. and Yanga, K. (2008). "Microstructure, mechanical properties and corrosion properties of Mg–Zn–Y alloys with low Zn content." *Mat. Sci. Eng. A-Struct*., 488, 102-111.

Zhang, J. and Wu, C. (2010). "Corrosion and protection of magnesium alloys- A review of the patent literature." *Recent Patent. Corros. Sci*., 2, 55-68.

Zhang, Q., Gao, Z., Xu, F. and Zou, X. (2011a). "Adsorption and corrosion inhibitive properties of gemini surfactants in the series of hexanediyl-1,6-bis-(diethyl alkyl ammonium bromide) on aluminium in hydrochloric acid solution." *Colloid. Surface A*, 380, 191-200.

Zhang, S., Zhang, X., Zhao, C., Li, J., Song, Y., Xie, C., Tao, H., Zhang, Y., He, Y., Jiang, Y., Bian, Y. (2010). "Research on an Mg–Zn alloy as a degradable biomaterial." *Acta Biomater*., 6, 626–640.

Zhang, T., Shao, Y., Meng, G., Cui, Z. and Wang, F. (2011b). "Corrosion of hot extrusion AZ91 magnesium alloy: I-relation between the microstructure and corrosion behavior." *Corros. Sci*., 53, 1960-1968.

Zhao, M.-C., Liu, M., Song, G. and Atrens, A. (2008a). "Influence of the β-phase morphology on the corrosion of the Mg alloy AZ91." *Corros. Sci.*, 50, 1939-1953.

Zhao, M.-C., Liu, M., Song, G.-L. and Atrens, A. (2008b). "Influence of pH and chloride ion concentration on the corrosion of Mg alloy ZE41." *Corros. Sci.*, 50, 3168-3178.

Zhao, L., Liu, Q., Gao, R., Wang, J., Yang, W. and Liu, L. (2014a). "One-step method for the fabrication of superhydrophobic surface on magnesium alloy and its corrosion protection, antifouling performance." *Corros. Sci.*, 80, 177-183.

Zhao, S., Peng, Q., Li, H. and Liu, B. (2014b). "Effects of super-high pressure on microstructures, nano-mechanical behaviors and corrosion properties of Mg–Al alloys." *J. Alloy. Compd.*, 584, 56-62.

Zucchi, F., Grassi, V., Frignani, A., Monticelli, C. and Trabanelli, G. (2006). "Electrochemical behavior of magnesium alloy containing rare earth elements." *J. Appl. Electrochem.*, 36, 195-204.

LIST OF PUBLICATIONS

a) In journals

1. Nandini, D. and Shetty, A.N. (2013). "Electrochemical investigations of the corrosion behavior of magnesium alloy ZE41 in a combined medium of chloride and sulphate." *J. Magnesium Alloy.*, 1(3), 201-209.

2. Nandini, D. and Shetty, A.N. (2013). "Investigation of influence of medium pH and sulfate ion concentrations on corrosion behavior of magnesium alloy ZE41." *Surf. Eng. Appl. Electrochem.*, 50(2), 149-156.

3. Nandini, D. and Shetty, A.N. (2013). "Stearate as a green corrosion inhibitor of magnesium alloy ZE41 - Study on efficiency, adsorption behavior and influence on hydrogen evolution." *Arab. J. Chem.* [Communicated].

4. Nandini, D. and Shetty, A.N. (2013). "Alkyl carboxylates as efficient and green inhibitors of magnesium alloy ZE41 corrosion in aqueous salt solution." *Corros. Sci.* [Communicated].

5. Nandini, D. and Shetty, A.N. (2014). "Laurate and caprylate as inhibitors of magnesium alloy ZE41 corrosion: An electrochemical investigation." *J. Solid State Electrochem.* [Communicated].

b) In Conferences.

1. Nandini, D. and Shetty, A.N. (2013). "Environmentally safe corrosion inhibition of magnesium alloy ZE41 by anionic surfactant stearate." International Conference on Recent Advances in Material Science and Technology (ICRAMST - 13), January 17-19, 2013, National Institute of Technology, Surathkal, India.

2. Nandini, D. and Shetty, A.N. (2013). "Corrosion of magnesium alloy ZE41- Influence of medium pH and sulfate ion concentrations." The International Corrosion Prevention Symposium for Research Scholars (CORSYM 2013), February 28 - March 2, 2013, Chennai, India.

3. Nandini, D. and Shetty, A.N. (2013). "Corrosion behavior of magnesium alloy ZE41 in sulfate medium: An electrochemical investigation." Scope of Advanced Materials in Energy and Environment (SAMEE 2013), August 7-8, 2013, CMR Institute of Technology, Bangalore, India.

4. Nandini, D. and Shetty, A.N. (2013). "Corrosion inhibition of light-weight magnesium alloy ZE41 by anionic surfactant laurate: An ecofriendly and economic approach." International Conference in Asia (ICA-IUMRS 2013), December 16-20, 2013, Indian Institute of Science, Bangalore, India.

5. Nandini, D. and Shetty, A.N. (2014). "Myristate as corrosion inhibitor for magnesium alloy ZE41: An electrochemical examination." 16th National Symposium in Chemistry (CRSI-NSC 2014), February 07-09, 2014, Indian Institute of Technology, Mumbai, India.

BIODATA

PERSONAL INFORMATION

Name   : Nandini K

DOB   : 14-July-1988

Place of birth   : Sringeri, Karnataka

Languages known   : English, Hindi, Kannada

Gender   : Female

Marital status   : Married

Contact number   : +918095990005

Email id   : nandinidindody@gmail.com

Address   : #334, 4th C cross

3rd phase, 5th block

BSK 3rd stage, Bangalore - 560085.

EDUCATION DETAILS

Qualification	Year	Institution	University
PhD	Submitted the thesis in April 2014	NITK, Surathkal	NITK, Surathkal
M Sc Chemistry	2010-11	NITK, Surathkal	NITK, Surathkal
B Sc	2008-09	Alva's College, Moodbidri, Karnataka	Mangalore University
II PUC	2005-06	Jawhar Navodaya Vidyalaya, Balehonnur, Karnataka	-
SSLC	2003-04	Jawhar Navodaya Vidyalaya, Balehonnur, Karnataka	-

RESEARCH POSITIONS

1. Assisted with the research project on 'Tannin Assay' at Central Coffee Research Institute, Chikamagalore, May - July 2008.

2. Worked as a Summer Research Fellow at Jawaharlal Nehru Centre for Advanced Scientific Research (JNCASR) Jakkur, Bangalore, May - July 2010.

RESEARCH PUBLICATIONS

a) In international journals

1. Nandini, D. and Shetty, A.N. (2013). "Electrochemical investigations of the corrosion behavior of magnesium alloy ZE41 in a combined medium of chloride and sulphate." *J. Magnesium Alloy.*, 1(3), 201-209.

2. Nandini, D. and Shetty, A.N. (2013). "Investigation of influence of medium pH and sulfate ion concentrations on corrosion behavior of magnesium alloy ZE41." *Surf. Eng. Appl. Electrochem.*, 50(2), 149-156.

3. Nandini, D. and Shetty, A.N. (2013). "Alkyl carboxylates as efficient and green inhibitors of magnesium alloy ZE41 corrosion in aqueous salt solution." *Corros. Sci.* [Communicated].

4. Nandini, D. and Shetty, A.N. (2013). "Stearate as a green corrosion inhibitor of magnesium alloy ZE41 corrosion- Study on efficiency, adsorption behavior and influence on hydrogen evolution." *Arab. J. Chem.* [Communicated].

5. Nandini, D. and Shetty, A.N. (2014). "Laurate and caprylate as inhibitors of magnesium alloy ZE41 corrosion: An electrochemical investigation." *J. Solid State Electrochem.* [Communicated].

b) In conference proceedings

1. Nandini, D. and Shetty, A.N. (2013). "Environmentally safe corrosion inhibition of magnesium alloy ZE41 by anionic surfactant stearate." International Conference on Recent Advances in Material Science and Technology (ICRAMST - 13), January 17-19, 2013, National Institute of Technology, Surathkal, India.

2. Nandini, D. and Shetty, A.N. (2013). "Corrosion of magnesium alloy ZE41- Influence of medium pH and sulfate ion concentrations." The International Corrosion Prevention Symposium for Research Scholars (CORSYM 2013), February 28 - March 2, 2013, Chennai, India.

3. Nandini, D. and Shetty, A.N. (2013). "Corrosion behavior of magnesium alloy ZE41 in sulfate medium: An electrochemical investigation." Scope of Advanced Materials in Energy and Environment (SAMEE 2013), August 7-8, 2013, CMR Institute of Technology, Bangalore, India.

4. Nandini, D. and Shetty, A.N. (2013). "Corrosion inhibition of light-weight magnesium alloy ZE41 by anionic surfactant laurate: An ecofriendly and economic approach." International Conference in Asia (ICA-IUMRS 2013), December 16-20, 2013, Indian Institute of Science, Bangalore, India.

5. Nandini, D. and Shetty, A.N. (2014). "Myristate as corrosion inhibitor for magnesium alloy ZE41: An electrochemical examination." 16th National Symposium in Chemistry (CRSI-NSC 2014), February 07-09, 2014, Indian Institute of Technology, Mumbai, India.